PACIFIC EARTHQUAKE ENGINEERING
RESEARCH CENTER

Empirical Evaluation of Inertial Soil-Structure Interaction Effects

Jonathan P. Stewart
Raymond B. Seed
Gregory L. Fenves
University of California, Berkeley

PEER 1998/07
NOV. 1998

EMPIRICAL EVALUATION OF INERTIAL SOIL-STRUCTURE INTERACTION EFFECTS

by

Jonathan P. Stewart
Civil & Environmental Engineering Department, University of California, Los Angeles

Raymond B. Seed and Gregory L. Fenves
Department of Civil & Environmental Engineering, University of California, Berkeley

Research supported by the U.S. Geological Survey (USGS), Department of the Interior, under USGS award number 1434-HQ-97-GR-02995. The views and conclusions contained in this document are those of the authors and should not be interpreted as necessarily representing the official policies, either expressed or implied, of the U.S. Government.

Report No. PEER-98/07

Pacific Earthquake Engineering Research Center
University of California
Berkeley, California

November 1998

ABSTRACT

Award No. 1434-HQ-97-GR-02995

EMPIRICAL EVALUATION OF INERTIAL
SOIL-STRUCTURE INTERACTION EFFECTS

PI: Raymond B. Seed
Civil and Environmental Engineering Dept.
University of California
Berkeley, CA 94720-1710
tel: 510-642-8438 fax: 510-642-7476
cegeot@ce.berkeley.edu

Co - PI: Jonathan P. Stewart
Civil and Environmental Engineering Dept.
University of California
Los Angeles, CA 90095-1593
tel: 310-206-2990 fax: 310-206-2222
jstewart@seas.ucla.edu

Strong motion data obtained over the last decade from sites with instrumented structures and free-field accelerographs has provided an unprecedented opportunity to evaluate empirically the effects of soil-structure interaction (SSI) on the seismic response of structures. Strong motion data were gathered for 58 sites encompassing a wide range of structural systems, geotechnical conditions, and ground shaking levels. System identification analyses were employed with these records to quantify the effects of inertial interaction on modal parameters of structures. Simple indices of free-field and foundation-level ground motions were also compared. From these results, the conditions under which significant SSI effects occur were identified, and simplified analytical techniques for predicting these effects were calibrated.

For each site, system identification analyses were used to evaluate first-mode periods and damping ratios for a flexible-base case which incorporates SSI effects, and a fixed-base case in which only the structural flexibility is represented. Inertial interaction effects were evaluated from variations between fixed- and flexible-base parameters (i.e. the lengthening of first-mode fixed-base period due to foundation translation and rocking, and the damping attributable to foundation-soil interaction). These inertial interaction effects were found to be significant at some sites (e.g. period lengthening ratios of 4, and 30% foundation damping), and negligible at others (no period lengthening and zero foundation damping).

Analytical formulations similar to procedures in contemporary building codes were used to predict inertial interaction effects at the sites for comparison with the “empirical” results. A collective examination of the empirical and predicted results revealed a pronounced influence of structure-to-soil stiffness ratio on inertial interaction, as well as secondary influences from structure aspect ratio and foundation embedment ratio, type, shape, and non-rigidity. The analytical predictions were generally found to be reasonably accurate, with some limitations for deeply embedded and long-period structures.

NON-TECHNICAL PROJECT SUMMARY

Recent improvements in seismological source modeling and the analysis of travel path and site response effects have led to significant advances in both code-based and more advanced procedures for evaluating seismic demand for structural design. A missing link, however, has been an improved and empirically verified treatment of soil-structure interaction (SSI) effects on both strong motions transmitted to structures and structural response to these motions. This research employed system identification analysis with earthquake strong motion recordings to quantify the effects of soil-structure interaction on seismic structural response, and used these observations to calibrate simplified analysis procedures for predicting these effects.

TABLE OF CONTENTS

LIST OF FIGURES

LIST OF TABLES

LIST OF SYMBOLS

a, b	Halfwidth of foundation in direction normal and perpendicular to horizontal projection of inclined incident wave ray path, respectively
$a_1 \ldots a_{2J}$, $b_1 \ldots b_{2J}$	Parameters describing discrete-time parametric transfer function
a_0	Normalized frequency, $= \omega r/V_S$
$\tilde{a}_0$	Normalized frequency a_0 adjusted for incoherence and wave inclination effects, Eq. 2.16
A_f	Area of foundation
c	Internal damping of single degree-of-freedom structure
c	Damping matrix of multi degree-of-freedom structure
c_u, c_θ	Coefficients of foundation translational and rotational dashpots
c_{rx}, c_{ry}	Dimensionless dashpot coefficients for foundation rocking radiation damping in longitudinal and transverse directions of foundation, Fig. 2.6
d	Delay between x(t) and y(t), used in parametric system identification
d_S	Depth of finite soil layer
D	Flexural rigidity of foundation, Eq. 2.9
e	Foundation embedment
E_f	Young's modulus of foundation
f_i, $\tilde{f}_i$, $\tilde{f}_i$*	Fixed-, flexible-, and pseudo flexible-base frequencies for mode *i*. Parameters are for the first mode if index *i* is not shown.
f	Frequency in Hz
f_{eq}	Predominant frequency of earthquake shaking, in Hz
f_{Nyq}	Nyquist frequency, $=1/(2 \cdot \Delta t)$
G	Shear modulus of soil

h	Effective height of structure, i.e. distance above foundation-level at which a building's mass can be concentrated to yield the same base moment that would occur in the actual structure assuming a linear first mode shape
H	Total height of structure from base to roof
H(s), H(s)	Complex-valued transfer function determined from parametric system identification for single input-multiple output and single input-single output motion pairs, respectively
H(iω), H(iω)	Complex-valued transmissibility function for single input-multiple output and single input-single output motion pairs, respectively
H(z)	Discrete time transfer function for single input-single output model
$\lvert H_u(\omega) \rvert$, $\lvert H_\theta(\omega) \rvert$	Analytical transfer function amplitude for foundation input motion (FIM) in translation and rocking
i	$\sqrt{-1}$, also occasionally used as modal index
I	Rotational inertia of structure
I_f	Moment of inertia of foundation
J	Number of modes used to model *n* degree-of-freedom structure in system identification analysis (J < *n*)
k	Lateral stiffness of single degree-of-freedom structure
k	Stiffness matrix of multi degree-of-freedom structure
$\bar{k}_u$, $\bar{k}_\theta$	Complex-valued dynamic foundation impedance for translation and rocking deformations
k_u, K_u	Dynamic and static translational stiffnesses for foundation on halfspace
k_θ, K_θ	Dynamic and static rotational stiffnesses for foundation on halfspace
$(K_u)_{FL}$,$(K_u)_{FL/E}$	Static translational stiffnesses for foundation on finite soil layer and foundation embedded into finite soil layer, Eqs. 2.6 and 2.7
$(K_\theta)_{FL}$,$(K_\theta)_{FL/E}$	Static rotational stiffnesses for foundation on finite soil layer and foundation embedded into finite soil layer, Eqs. 2.6 and 2.7

L/B	Aspect ratio of foundation in plan view, used in context of discussion of shape effects on foundation impedance, Section 2.2.2(d)
L_i*	Generalized influence factor of structure for mode *i*
m_i*	Generalized mass of structure for mode *i*
m	Mass matrix of multi degree-of-freedom structure
M	Base moment in structure
n	Number of structural degrees-of-freedom
N	Number of points in time history used for system identification analysis
r_1, r_2	Radii which match the area and moment of inertia, respectively, of assumed circular foundation in impedance function formulations to the actual foundation area and moment of inertia, Eq. 2.3
r	Radius of circular foundation
$R_x(\tau)$, $R_{xy}(\tau)$	Autocorrelation function, cross correlation function
s	Variable for Laplace-transformed functions, units of frequency
$S_x(\omega)$, $S_{xy}(\omega)$	Power spectral density function, cross power spectral density function (also used as S_g, S_ϕ, and S_{cir} for free-field torsional, and circumferential motions, respectively)
t	Variable for time-dependent functions
t_f	Thickness of foundation slab
Δt	Data sampling interval of strong motion data
T_{eq}	Predominant period of earthquake shaking
T_i, $\tilde{T}_i$, $\tilde{T}_i$*	Fixed-, flexible-, and pseudo flexible-base periods for mode *i*. Parameters are for the first mode if index *i* is not shown.
u, **u**	Displacement of single degree-of-freedom and multi degree-of-freedom structure relative to its base

u^t, $\mathbf{u}^t$	Total displacement of structure, = $u_g + u_f + h\theta + u$, total displacement vector of multi degree-of-freedom structure
u_{FIM}	Translation of foundation due to kinematic interaction effects
u_g	Free-field ground displacement
u_f	Horizontal displacement of foundation relative to free-field
V	Base shear in structure
V_S	Shear wave velocity of soil
$V(\Theta)$	Measure of cumulative error between model and recorded output in parametric system identification analysis
x(t)	Input time history used in system identification analyses
$X_j(t)$	Generalized coordinate used to express structural deformations, Eq. 3.3
y(t)	Output time history used in system identification analyses
z	Variable for Z-transformed functions, dimensionless
α_u, β_u	Dimensionless parameters expressing the frequency-dependence of foundation translational stiffness and damping, respectively, Eq. 2.4
α_θ, β_θ	Dimensionless parameters expressing the frequency-dependence of foundation rocking stiffness and damping, respectively, Eq. 2.4
α_V	Inclination angle of incident seismic waves
β	Soil hysteretic damping ratio
$\varepsilon(t, \Theta)$	Error between model and recorded output in parametric system identification analysis, Eq. 3.20
γ	Ratio of structure-to-soil mass, Eq. 2.13
$\gamma^2(i\omega)$	Coherence function for single input/single output motion pair, Eq. 3.12
$\gamma(\omega)$	Coherency function for single input/single output motion pair, Eq. 4.1
η	Ratio of foundation-to-soil rigidity, Eq. 2.8

κ	Dimensionless incoherence parameter
λ	Forgetting factor for exponential window used in parametric system identification analyses by the Recursive Prediction Error Method
μ	Ratio of structure/structure-plus-foundation mass
θ	Base rocking of foundation slab
θ_{FIM}	Base rocking of foundation slab due to kinematic interaction effects
ρ	Mass density of soil
σ	Ratio of soil-to-structure stiffness, Eq. 2.12
υ	Soil Poisson ratio
υ_f	Poisson ratio of foundation
ω	Angular frequency in radians/sec.
ω_i, $\tilde{\omega}_i$, $\tilde{\omega}_i$ *	Fixed-, flexible-, and pseudo flexible-base angular frequencies for mode *i*. Parameters are for the first mode if index *i* is not shown.
ω_u, ω_θ	Foundation dynamic translational and rotational stiffnesses expressed in units of frequency, Eq. 3.41
ζ_i, $\tilde{\zeta}_i$, $\tilde{\zeta}_i$ *	Fixed-, flexible-, and pseudo flexible-base damping ratios for mode *i*. Parameters are for the first mode if index *i* is not shown.
ζ_u, ζ_θ	Foundation dynamic translational and rotational damping expressed in units of damping ratio, Eq. 3.41
$\tilde{\zeta}_0$	Foundation damping factor, defined in Eq. 2.11
Φ_i	Mode shape of structure for mode *i*
Γ	Function representing the effects of ground motion incoherence, Eq. 2.15
$\Gamma(t)$	Vector of input and output motions, Eq. 3.17
Θ	Vector of parameters in parametric system identification, Eq. 3.18

ACKNOWLEDGMENTS

A number of individuals and organizations contributed greatly to this study by providing structural and geotechnical data for the sites which were considered. They are far too numerous to completely acknowledge here, however, we would like to extend special thanks to Martin Hudson and Paul Schade of Law/Crandall, Inc., Paul Boddi and Lelio Mejia of Woodward-Clyde Consultants, Robert Darragh of the California Strong Motion Instrumentation Program (CSMIP), Walt Jungblut and John Tinsley of the U.S. Geological Survey, and David Hsu of the City of Los Angeles.

The gathering of strong motion data for this study would not have been possible without the help of Robert Darragh of CSMIP, Gerald Brady (retired) and Ron Porcella of the U.S. Geological Survey, Maria Todorovska of the University of Southern California, and H.T. Tang of the Electrical Power Research Institute. Thanks are also extended to Doug Dreger of the University of California, Berkeley Seismographic Station for providing access to seismograph-digitization equipment, and to Walter Silva of Pacific Engineering and Analysis for his assistance in the processing of seismic data.

Support for this project was provided by the U.S. Geological Survey, National Earthquake Hazards Reduction Program, Award No. 1434-HQ-97-GR-02995. Support for closely related research focusing on data gathering for this project was provided by the California Department of Transportation under Contract No. RCA-59A130 and by the Earthquake Engineering Research Institute/Federal Emergency Management Agency 1995-96 NEHRP Fellowship in Earthquake Hazard Reduction. This support is gratefully acknowledged.

CHAPTER 1

INTRODUCTION

1.1 Introduction

Assessments of seismic loading for structures must appropriately characterize a number of factors including the earthquake source, travel path effects, local site effects, and Soil-Structure Interaction (SSI) effects (Fig. 1.1). For the purpose of engineering design, source effects generally refer to the earthquake magnitude, rupture mechanism, and location relative to the site, while travel path effects refer to the attenuation of seismic waves as they travel from the source through bedrock towards the site. Site effects refer to the frequency-dependent amplification or attenuation experienced by seismic waves propagating towards the surface through soil. The end result of these first three effects is a "free-field" seismic ground motion at the ground surface, where "free-field" refers to the lack of any influence from structural vibrations on the motion. Finally, SSI effects account for the flexibility of the foundation support beneath the structure and potential variations between foundation and free-field motions. In effect, SSI determines the actual loading experienced by the structure-foundation-soil system resulting from the free-field seismic ground motions.

Recent major advances have been made in the treatment of site effects in the National Earthquake Hazards Reduction Program (NEHRP) seismic design code (BSSC, 1997) and the Uniform Building Code (ICBO, 1997). These advances have emerged largely as a result of clearly documented examples of significant site effects in major earthquakes such as the 1985 Mexico City and 1989 Loma Prieta earthquakes (Seed et al., 1988 and 1990), and

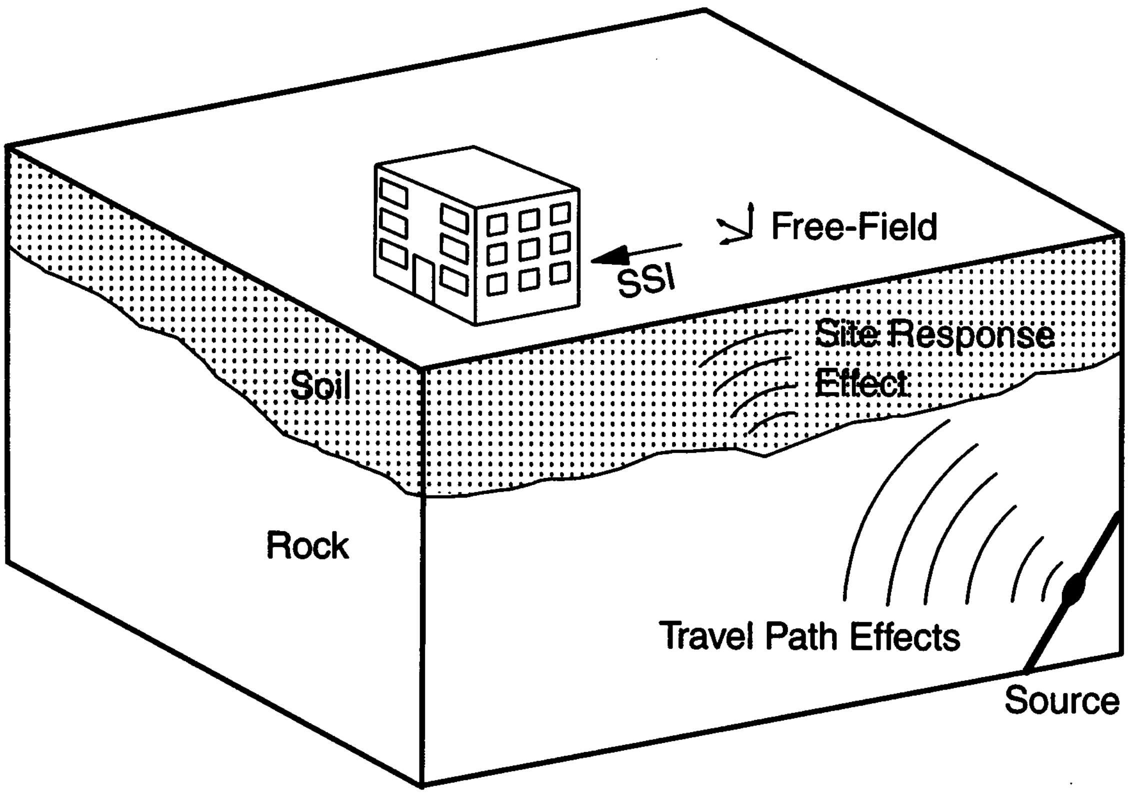

Fig. 1.1: Schematic showing context of SSI in an engineering assessment of seismic loading for a structure

subsequent studies which have calibrated simplified analytical formulations against this "field" data (e.g. Borcherdt, 1994 and Seed et al., 1992).

The state-of-practice for engineering characterization of SSI effects for routine structures has not undergone recent similar advancement, though the state-of-the-art in SSI analyses has evolved steadily over the last three decades. As described in detail in Chapter 2, available SSI analysis procedures include direct approaches in which the soil and structure are modeled together and analyzed in a single step, and substructure approaches where the analysis is broken down into several relatively simple steps. Simplified substructure-based SSI provisions are included in the NEHRP (BSSC, 1997) and Applied Technology Council (ATC, 1978) codes, but these provisions have not been calibrated against field performance data as has been done for site effects. Due to the common perception that to ignore SSI effects is conservative (a situation likely fueled by the lack of well-documented field performance data), the SSI provisions in the NEHRP and ATC codes are voluntary and are often neglected in practice.

The objectives of this study are to make use of strong motion data from recent earthquakes to evaluate the effects of SSI on structural response for a range of site and structural conditions, and then to use these results to calibrate simplified analytical formulations similar to those in the NEHRP and ATC codes. This project is timely in that a wealth of strong motion data has become available in recent years from sites which are sufficiently instrumented to enable empirical assessments of SSI effects (these sites have an instrumented structure and, in most cases, a free-field accelerograph). The locations of some of the most significant earthquakes contributing to this data set are indicated in Fig. 1.2, along with the locations of sites incorporated into this study. As other major advances

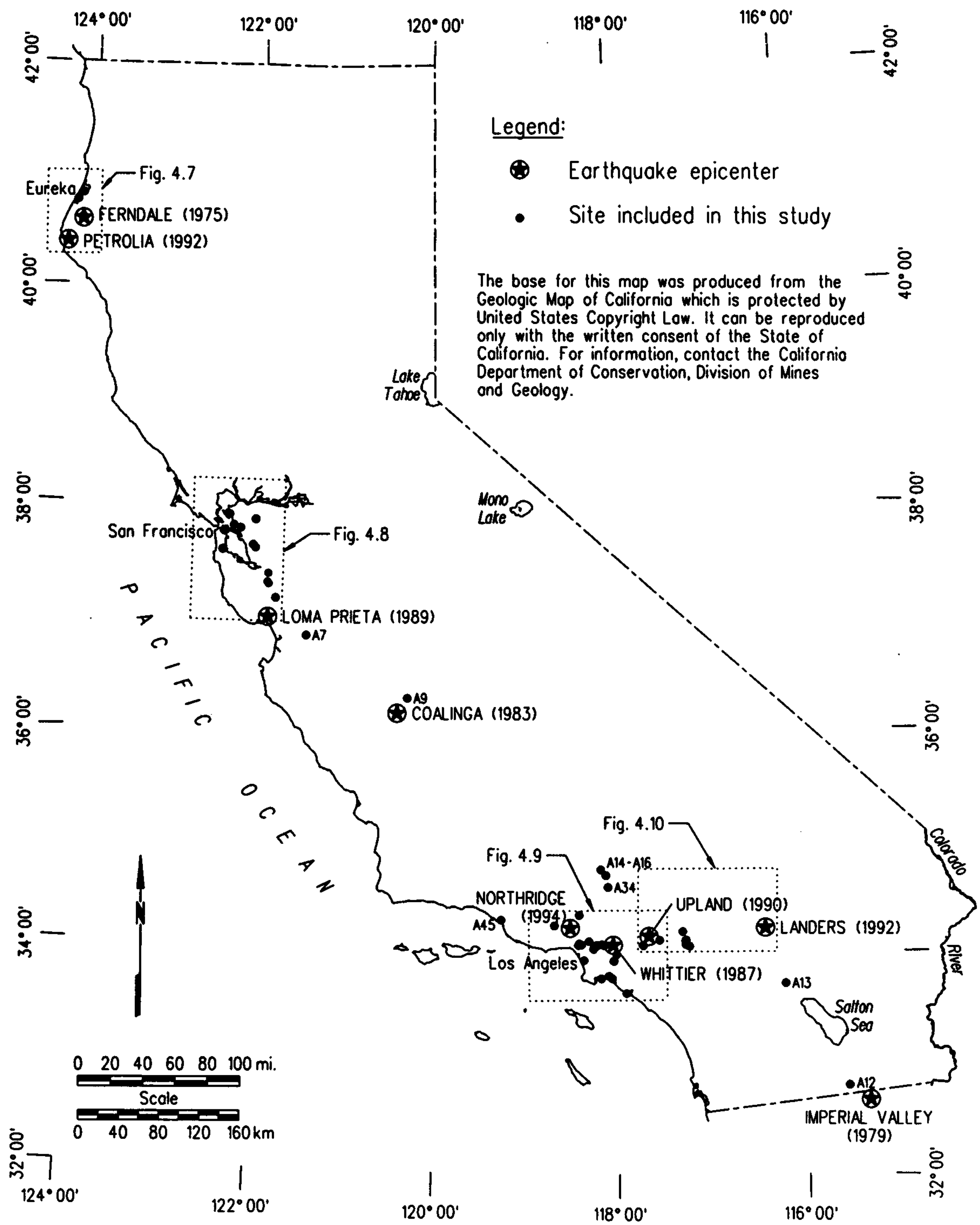

Fig. 1.2: Map of California showing locations of sites and selected earthquakes considered in this study

ssites.dgn[100]

in U.S. seismic design practice are made in the wake of these earthquakes, it is important that SSI effects also be clearly understood by the profession and suitably incorporated into routine practice. This study is intended to contribute towards achieving this goal.

1.2 Organization of the Report

This study involved the collection and analysis of data from 58 sites so that insights into SSI effects could be obtained for a wide range of conditions. A companion report (Stewart, 1997) presents the data collected for the individual sites and the site-specific analytical results. This report presents background information relevant to the study, the compiled results for the sites, and recommendations for engineering design characterization of SSI effects.

In Chapter 2 the key physical processes associated with SSI are described (i.e. inertial and kinematic interaction), and simplified analytical formulations to predict SSI effects are presented. The emphasis is on substructuring methods for SSI analysis in which the evaluation of free-field ground motions, foundation input motions, and inertial interaction effects are performed separately. The analyses performed in this study for inertial interaction effects are generally consistent with the methodologies outlined in the NEHRP and ATC codes. In these analyses, inertial interaction effects are quantified in terms of (1) the lengthening of “fixed” base first-mode period due to the flexibility of the foundation-soil system and (2) a foundation damping factor which expresses the damping attributable to foundation-soil interaction. The fixed-base case includes only the flexibility of the structure (i.e. no SSI), while the flexible-base case includes the flexibility of the foundation-soil system (in translation and rocking) as well as the structural flexibility. The principal source of uncertainty in these analyses, and the main focus of the discussion, is on the evaluation of impedance functions describing the stiffness and damping characteristics of foundation-soil interaction. Analyses of kinematic effects are discussed separately for surface foundations where the primary consideration is base-slab averaging effects, and embedded foundations where the reduction of ground motion amplitude with depth must also be considered. These effects are quantified by transfer function amplitudes which express the frequency-dependent ratio of base-slab to free-field motions.

The focus of Chapter 3 is on system identification techniques used to evaluate modal parameters of instrumented structures. Single-output/single-input methods for nonparametric and parametric analyses of multi degree-of-freedom systems are presented, and the evaluation of fixed- and flexible-base modal parameters from results for different output/input pairs are discussed. Both fixed- and flexible-base modal parameters can be directly evaluated when free-field motions, foundation and roof translations, and structural base rocking are measured. For cases where free-field or base rocking motions are missing, procedures were developed to estimate fixed-base parameters (for missing base rocking) or flexible-base parameters (for missing free-field motions). The results of these analyses for individual sites are presented in the companion report (Stewart, 1997).

In Chapter 4, the criteria used for site selection are discussed, and the range of geotechnical, structural, and earthquake shaking conditions represented in the database are presented. There are two classes of site instrumentation: (1) ‘A’ sites having both a free-field accelerograph and an instrumented structure (45 sites), and (2) ‘B’ sites having a structure instrumented to record base rocking and base and roof translations, but no free field recordings (13 sites). Criteria for determining when free-field accelerographs at 'A' sites are too close or too far from structures are discussed.

Chapter 5 presents a compilation of the inertial interaction effects (i.e. period lengthening and foundation damping factors) determined from site-specific studies, and compares these "empirical" effects to "predictions" from the analytical formulations described in Chapter 2. The compiled empirical and predicted results are examined to illustrate the strong influence of structure-to-soil stiffness ratio, as well as secondary influences from structure aspect ratio and foundation embedment ratio, type, shape, and non-rigidity.

Chapter 6 presents a summary of the significant SSI effects observed from these studies and recommendations for simplified modeling techniques appropriate for earthquake-resistant design. Suggestions for future research and ways to improve instrumentation configurations for buildings are also provided.

CHAPTER 2

SIMPLIFIED ANALYTICAL PROCEDURES FOR PREDICTING SOIL-STRUCTURE INTERACTION EFFECTS

2.1 Introduction and Problem Definition

2.1.1 Components of the Soil-Structure Interaction Problem

The deformations of a structure during earthquake shaking are affected by interactions between three linked systems: the structure, the foundation, and the geologic media underlying and surrounding the foundation. A seismic Soil-Structure Interaction (SSI) analysis evaluates the collective response of these systems to a specified free-field ground motion.

Two physical phenomena comprise the mechanisms of interaction between the structure, foundation, and soil:

- *Inertial Interaction*: Inertia developed in the structure due to its own vibrations gives rise to base shear and moment, which in turn cause displacements of the foundation relative to the free-field.
- *Kinematic Interaction*: The presence of stiff foundation elements on or in soil will cause foundation motions to deviate from free-field motions. Three mechanisms can potentially contribute to such deviations: (a) Base-Slab Averaging; free-field motions associated with inclined and/or incoherent wave fields are "averaged" within the footprint area of the base-slab due to the kinematic constraint of essentially rigid-body motion of the slab, (b) Embedment effects; the reduction of seismic ground motion

with depth for embedded foundations, and (c) Wave Scattering; scattering of seismic waves off of corners and asperities of the foundation.

The effects of these phenomena are often described by a complex-valued transfer function relating free-field and foundation motions, and a complex-valued impedance function which quantifies the stiffness and damping characteristics of foundation-soil interaction. The damping represented by the imaginary part of the impedance function is a consequence of hysteretic damping in the soil and foundation, and radiation of seismic energy away from the foundation through the soil.

Both the transfer and impedance functions are dependent on the finite stiffness and damping characteristics of the soil medium. For the fictional condition of an infinitely stiff soil, the amplitude of the transfer function for translational motion is unity and the phase is zero (i.e. the foundation and free-field motions are identical), and the impedance function has infinite real parts and zero imaginary parts. It is of some practical significance that this unrealistic assumption of rigid soil is made when SSI effects are ignored (which is common practice in structural design).

2.1.2 Methodologies for Soil-Structure Interaction Analysis

The general methods by which SSI analyses are performed can be categorized as direct and substructure approaches. In a direct approach, the soil and structure are included within the same model and analyzed in a single step. The soil is often discretized with solid finite elements and the structure with finite beam elements. Because assumptions of superposition are not required, true nonlinear analyses are possible (e.g. Borja et al., 1992 and Weidlinger Assoc., 1978). However, results from nonlinear analyses can be quite sensitive to poorly-defined parameters in the soil constitutive model, and the analyses remain quite expensive from a computational standpoint. Hence, direct SSI analyses are more commonly performed using equivalent-linear methods to approximate the effects of soil nonlinearity (e.g. FLUSH, Lysmer et al., 1975).

In a substructure approach, the SSI problem is broken down into three distinct parts which are combined to formulate the complete solution. The superposition inherent to this approach requires an assumption of linear soil and structure behavior. Referring to Fig. 2.1, the three steps in the analysis are as follows:

1. Evaluation of a Foundation Input Motion (FIM), which is the motion that would occur on the base-slab if the structure and foundation had no mass. The FIM is dependent on the stiffness and geometry of the foundation and soil. Since inertial effects are neglected, the FIM represents the effects of kinematic interaction only.
2. Determination of the impedance function. The impedance function describes the stiffness and damping characteristics of foundation-soil interaction. It should account for the soil stratigraphy and foundation stiffness and geometry, and is computed using equivalent-linear soil properties appropriate for the in situ dynamic shear strains.
3. Dynamic analysis of the structure supported on a compliant base represented by the impedance function and subjected to a base excitation consisting of the FIM.

The principal advantage of the substructure approach is its flexibility. Because each step is independent of the others, the analyst can focus resources on the most significant aspects of the problem.

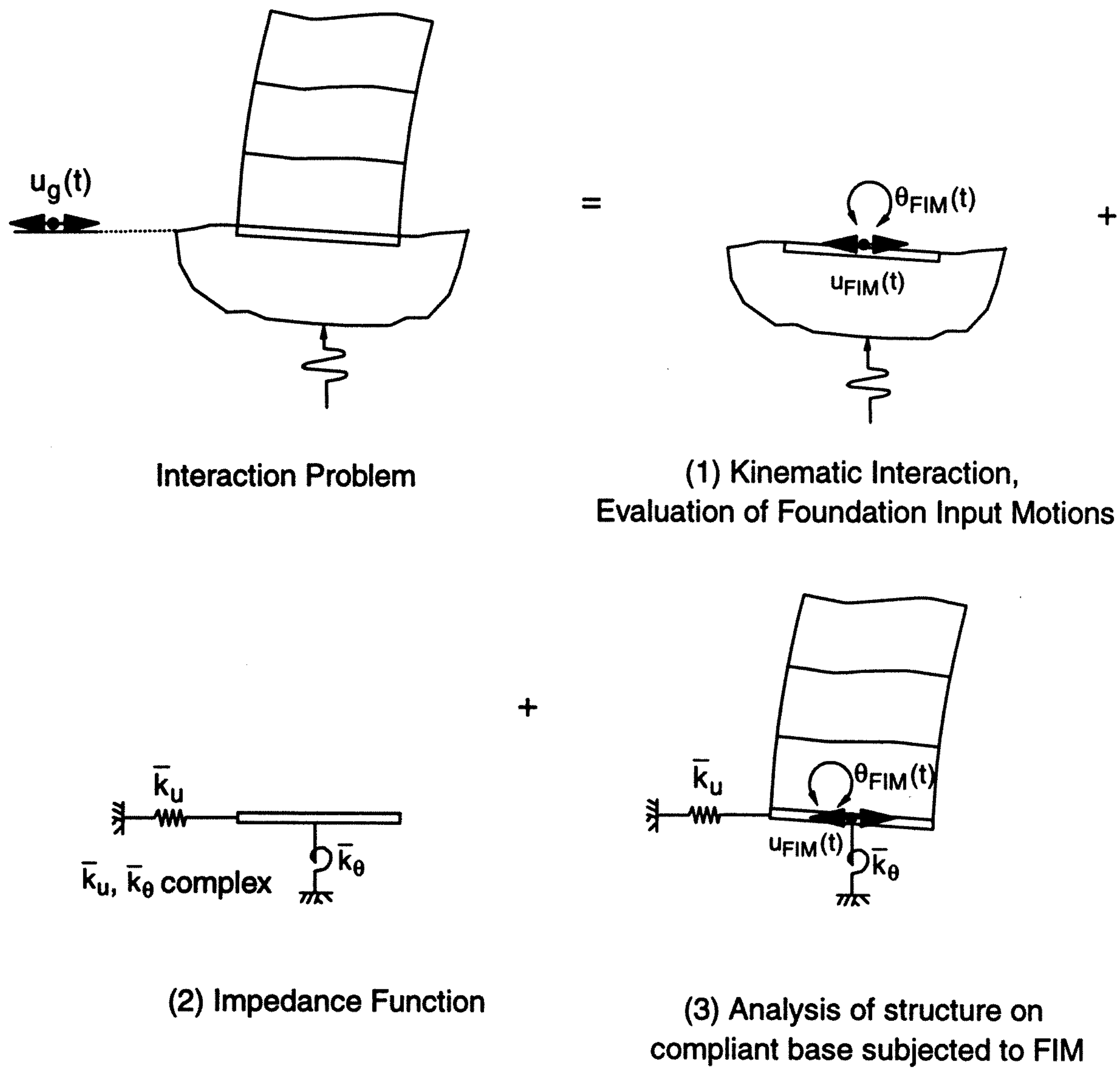

Fig. 2.1: Substructure approach to analysis of the SSI problem

The simplified analytical formulations which are calibrated in this study against "empirical" data are based on the substructure approach. Analyses of inertial interaction effects predict the variations of first-mode period and damping ratio between the actual "flexible-base" case (which incorporates the flexibility of both the foundation-soil system and the structure) and a fictional "fixed-base" case (which incorporates only the flexibility of the structure). The flexible-base modal parameters can be used with a free-field response spectrum to evaluate design base shear forces for the structure. Hence, these analyses correspond to Steps 2 and 3 of the substructure approach. The analyses for kinematic interaction (Step 1 of the substructure approach) predict frequency-dependent transfer function amplitudes relating foundation and free-field motions.

SSI provisions in the Applied Technology Council (ATC, 1978) and the National Earthquake Hazards Reduction Program (NEHRP) (BSSC, 1997) seismic design codes are similar to portions of the inertial interaction analysis procedures described in this chapter. Kinematic interaction effects are neglected in the code provisions, meaning that free-field motions and FIMs are assumed to be identical.

The literature on SSI analytical techniques is extensive, and it is not the purpose of this chapter to review it comprehensively. Rather, the emphasis is on providing background for the analysis procedures used to predict SSI effects at the sites considered in this study. Inertial and kinematic interaction analyses are discussed in Sections 2.2 and 2.3, respectively.

2.2 Inertial Interaction

2.2.1 System Considered

A system commonly employed in simplified analyses of inertial interaction is shown in Fig. 2.2. The system consists of a single degree-of-freedom structure with height h, mass m, stiffness k, and viscous damping coefficient c. The base of the structure is allowed to translate relative to the free-field an amount u_f and rotate an amount θ. The impedance function is represented by lateral and rotational springs with complex stiffnesses $\bar{k}_u$ and $\bar{k}_\theta$, respectively. The imaginary components of the foundation stiffness terms represent the effects of damping.

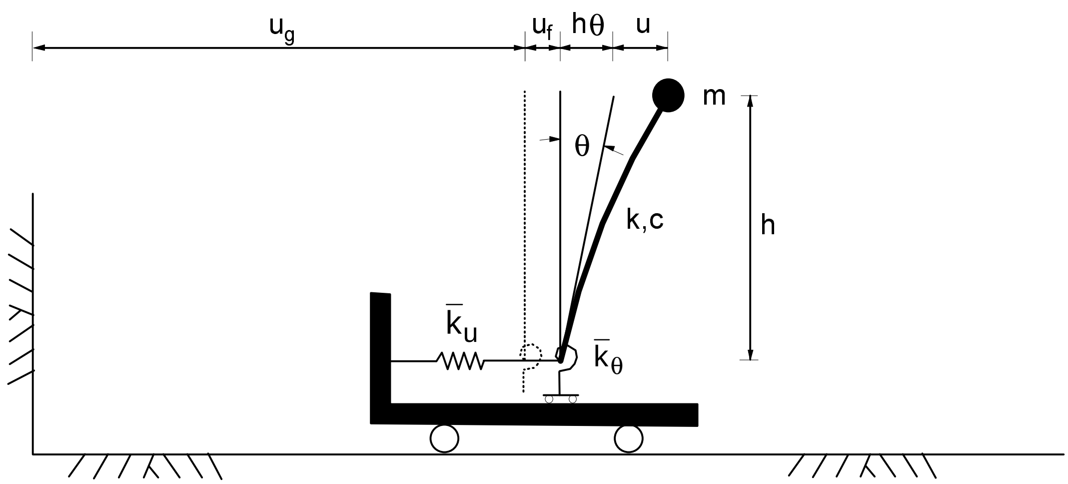

Fig. 2.2: Simplified model for analysis of inertial interaction

The simple system in Fig. 2.2 can be viewed as a direct model of a single-story building or, more generally, as an approximate model of a multi-mode, multi-story structure which is dominated by first-mode response. In the latter case, h is interpreted as the distance from the base to the centroid of the inertial forces associated with the first vibration mode.

2.2.2 Impedance Function

In general, the impedance function is the most poorly defined component of the model in Fig. 2.2. As described previously, the impedance function represents the dynamic stiffness and damping characteristics of foundation-soil interaction. Mathematically, an impedance function is a matrix which relates the forces (e.g. base shear and moment) at the base of the structure to the displacements and rotations of the foundation relative to the free-field. The terms in the impedance function are complex-valued and frequency dependent. When values of impedance parameters at a single frequency must be used (as is the case for the model in Fig. 2.2), values at the predominant frequency of the soil-structure system are selected.

(a) *Basic case*

In the most general case, six degrees of freedom would be necessary for each support point on the foundation. In practice, however, the foundation is often assumed to be rigid, which reduces the total degrees of freedom to six. When considering the lateral response of a structure on a rigid foundation in a particular direction, as is the case for the model in Fig. 2.2, only two impedance terms are generally necessary (Eq. 2.1). In Eq. 2.1, off-diagonal terms are neglected as they are usually small. It should be noted that vertical excitation and torsion are neglected in the simple impedance function in Eq. 2.1.

$$\begin{bmatrix} V \\ M \end{bmatrix} = \begin{bmatrix} \bar{k}_u & 0 \\ 0 & \bar{k}_\theta \end{bmatrix} \begin{bmatrix} u_f \\ \theta \end{bmatrix} \tag{2.1}$$

A number of analytical procedures are available for the computation of impedance functions, many of which are summarized in Luco (1980b) and Roesset (1980). Perhaps the most widely used solution is that for a rigid circular foundation on the surface of a visco-elastic halfspace (Veletsos and Wei, 1971 and Veletsos and Verbic, 1973). This solution accounts for the three-dimensional nature of the problem and the frequency dependence of the stiffness and damping parameters.

In the solution for a rigid disk on a halfspace, terms in the impedance function are expressed in the form

$$\bar{k}_j = k_j(a_0, \upsilon) + i\omega c_j(a_0, \upsilon) \tag{2.2}$$

where *j* denotes either deformation mode u or θ, ω is angular frequency (radians/sec.), a_0 is a dimensionless frequency defined by $a_0 = \omega r/V_S$, r = foundation radius, V_S = soil shear wave velocity, and υ = soil Poisson ratio. Foundation radii are computed separately for translational and rotational deformation modes to match the area (A_f) and moment of inertia (I_f) of the actual foundation, as follows,

$$r_1 = \sqrt{\frac{A_f}{\pi}} \qquad r_2 = \sqrt[4]{\frac{4 \cdot I_f}{\pi}} \tag{2.3}$$

There are corresponding different values of $(a_0)_1$ and $(a_0)_2$ as well.

The real stiffness and damping of the translational and rotational springs and dashpots are expressed, respectively, by

$$k_u = \alpha_u K_u \tag{2.4a}$$

$$c_u = \beta_u \frac{K_u r_1}{V_S} \tag{2.4b}$$

$$k_\theta = \alpha_\theta K_\theta \tag{2.4c}$$

$$c_\theta = \beta_\theta \frac{K_\theta r_2}{V_S} \tag{2.4d}$$

The quantities α_u, β_u, α_θ, and β_θ are dimensionless parameters expressing the frequency dependence of the results, while K_u and K_θ represent the static stiffness of a disk on a halfspace, defined by

$$K_u = \frac{8}{2-\upsilon} G r_1 \tag{2.5a}$$

$$K_\theta = \frac{8}{3(1-\upsilon)} G r_2^3 \tag{2.5b}$$

where G = soil dynamic shear modulus. Presented in Fig. 2.3 are the frequency-dependent values of α_u, β_u, α_θ, and β_θ for $\upsilon = 0.4$ based on closed form expressions in Veletsos and Verbic (1973). These results are similar to those obtained by Luco and Westmann (1971) for the case of a circular foundation on the surface of an elastic halfspace.

Values of soil shear stiffness G and hysteretic damping β used in the formulation of impedance functions should be appropriate for the in situ shear strains. For this study, these parameters were established from deconvolution analyses performed with the one-dimensional site response program SHAKE (Schnabel et al., 1972). In these analyses, nonlinear soil behavior is simulated by the equivalent-linear technique. Details on soil modeling and profile depths used in these analyses are provided in Stewart (1997). When

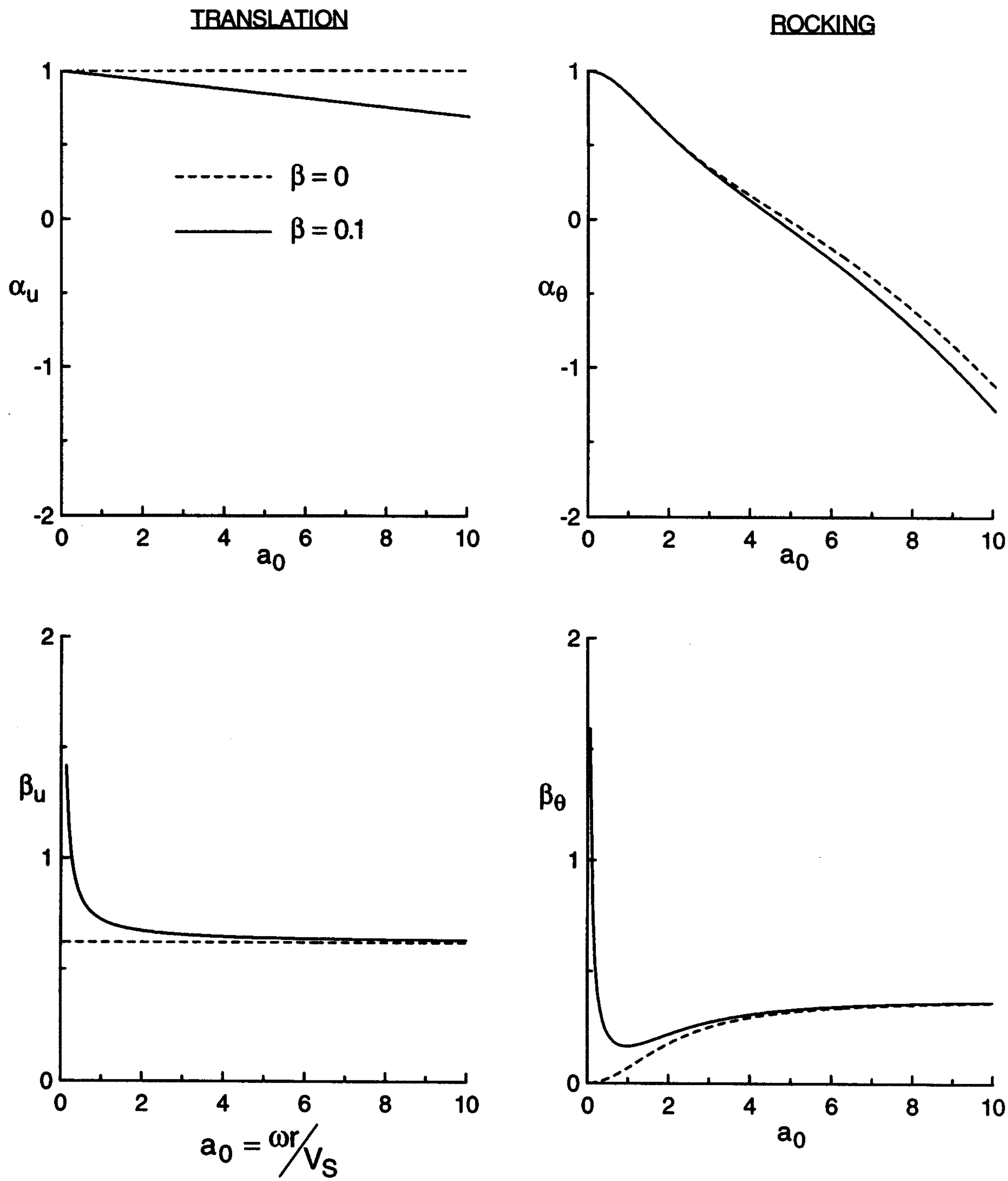

Fig. 2.3: Foundation stiffness and damping factors for elastic and viscoelastic halfspaces, $\upsilon = 0.4$ (after Veletsos and Verbic, 1973)

compared to recorded motions, results obtained from SHAKE deconvolution analyses have generally been well verified at shallow depths (i.e. 50 to 100 feet, e.g. Chang et al., 1985 and Geomatrix, 1991). Although shear strains resulting from SSI are not modeled by these deconvolution analyses, such strains are generally small relative to the strains associated with the free-field ground response.

Validation studies for the above and similar impedance function formulations have been conducted by Lin and Jennings (1984) and Crouse et al. (1990) for small surface foundations. In the Lin and Jennings study, a 10 x 10-foot specimen structure was subjected to sinusoidal ground vibrations generated in an excitation structure located about 50 feet away. The foundation impedance at the resonant frequency of the specimen structure was derived from the experimental results, and was consistent with theoretical predictions by Veletsos and Wei (1971). In the Crouse et al. (1990) study, two 4 x 4-foot slabs (one founded essentially at the ground surface and the other having 1.5 to 2.0-foot deep piers at the corners) were subjected to sinusoidal forced vibration testing across a range of frequencies from 10 to 60 Hz with a shaker mounted on the slabs. Impedance functions evaluated from these test results were compared to theoretical functions for layered media derived from integral equations (Apsel and Luco, 1987). The experimental and theoretical frequency-dependent impedances agreed reasonably well given the uncertainty in near-surface V_S data at the two sites, though the agreement was considerably better for the slab without corner piers. Theoretical results from Apsel and Luco (1987) and Veletsos and Verbic (1973) are nearly identical for surface foundations, hence these experimental results effectively validate both formulations.

Despite the demonstrated utility of the impedance function formulation by Veletsos and Verbic, commonly encountered conditions such as nonuniform soil profiles, embedded, non-circular, or flexible foundations, and the presence of piles or piers are not directly modeled by these procedures. The effects of such conditions (except piles or piers) on foundation impedance can be approximately simulated with adjustments to the basic solution, as discussed in Parts (b) through (e) below.

(b) *Nonuniform soil profiles*

Nonuniform soil profiles can often be characterized by gradual increases in stiffness with depth, or by a very stiff layer underlying relatively soft, surficial layers. For profiles having gradual increases in stiffness with depth, Roesset (1980) found that using soil properties from a depth of about $0.5 \cdot r$ gave halfspace impedances which reasonably simulated the impedance of the variable profile. In this study, equivalent halfspace velocities were computed as $V_S = r_1/t_{r\text{-}0}$, where $t_{r\text{-}0}$ is the travel time for vertically propagating shear waves to travel from a depth r_1 to the ground surface. These equivalent halfspace velocities are often similar to the actual V_S at a depth of $0.5 \cdot r_1$. Details on the calculation of V_S for individual sites are presented in Stewart (1997).

For the case of a finite soil layer overlying a much stiffer material, the key considerations are an increase in the static stiffness and changes in the frequency dependent variations of stiffness and damping. The increased static stiffnesses can be estimated as follows (Kausel, 1974),

$$
\begin{aligned}
(K_u)_{FL} &= K_u\left(1+\frac{1}{2}\frac{r_1}{d_s}\right)\\
(K_\theta)_{FL} &= K_\theta\left(1+\frac{1}{6}\frac{r_2}{d_s}\right)
\end{aligned}
\tag{2.6}
$$

where $(K_u)_{FL}$ and $(K_\theta)_{FL}$ are the static horizontal and rocking stiffnesses of the foundation on finite soil layer, and d_S is the depth of the layer. The frequency dependent variations of stiffness terms follow the general trends for a halfspace in Fig. 2.3, but have oscillations associated with the natural frequency of the stratum at low levels of soil damping. For hysteretic damping exceeding about 7%, Roesset (1980) found that the oscillations can be neglected. With regard to damping, the key issue is a lack of radiation damping at frequencies less than the fundamental frequency of the finite soil layer. Halfspace damping ratios can be used for frequencies greater than the soil layer frequency, and a transition to zero radiation damping at smaller frequencies can be defined per Elsabee and Morray (1977).

(c) *Foundation embedment*

Foundation embedment effects were investigated by Elsabee and Morray (1977) for the case of a circular foundation embedded to a depth e into a homogeneous soil layer of depth d_S (Fig. 2.4). It was found that the static horizontal and rocking stiffness for such foundations [$(K_U)_{FL/E}$ and $(K_\theta)_{FL/E}$] is approximated as follows for $r/d_S < 0.5$ and $e/r < 1$:

$$
\begin{aligned}
(K_u)_{FL/E} &= K_u\left(1+\frac{2}{3}\frac{e}{r}\right)\left(1+\frac{5}{4}\frac{e}{d_s}\right)\left(1+\frac{1}{2}\frac{r}{d_s}\right)\\
(K_\theta)_{FL/E} &= K_\theta\left(1+2\frac{e}{r}\right)\left(1+0.7\frac{e}{d_s}\right)\left(1+\frac{1}{6}\frac{r}{d_s}\right)
\end{aligned}
\tag{2.7}
$$

Coupling impedance terms were found to be small relative to $(K_u)_{FL/E}$ and $(K_\theta)_{FL/E}$ for small embedment ratios (i.e. e/r < 0.5). Elsabee and Morray suggested that the frequency dependence of the foundation stiffness and damping terms could be approximated as per Eqs. 2.4a-d (which strictly apply only for a rigid, circular surface foundation on a halfspace). These recommendations have been adopted into the NEHRP (BSSC, 1997) code provisions, with the exception of the frequency dependence stiffness terms (α) which are assumed to be unity.

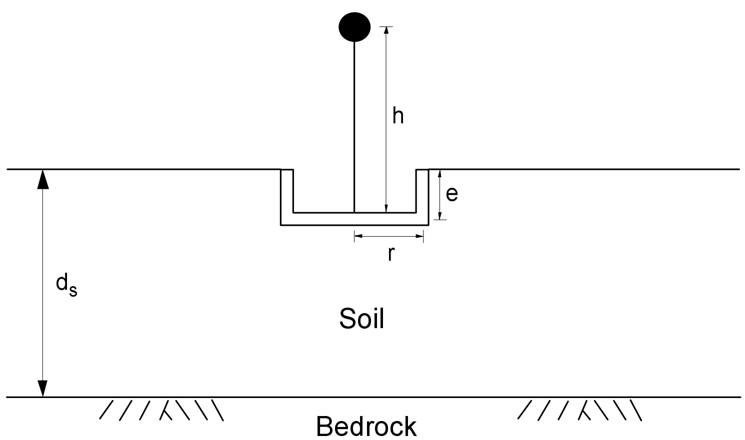

Fig. 2.4: Embedded soil-foundation-structure system on finite soil layer

Approximate normalized impedance factors for a cylindrical foundation embedded in a halfspace obtained from Eq. 2.7 are compared to a more rigorous analytical solution derived from integral equations (Apsel and Luco, 1987) in Fig. 2.5. The approximate curves were computed as the product of dimensionless impedance factors α_u, α_θ, β_u, and β_θ and the first modifier on the right hand side of Eq. 2.7. Both solutions apply for a uniform visco-elastic halfspace with β=1%, ν = 0.25, and perfect bonding between the soil and foundation. The comparisons are generally poor, with the exception of stiffness

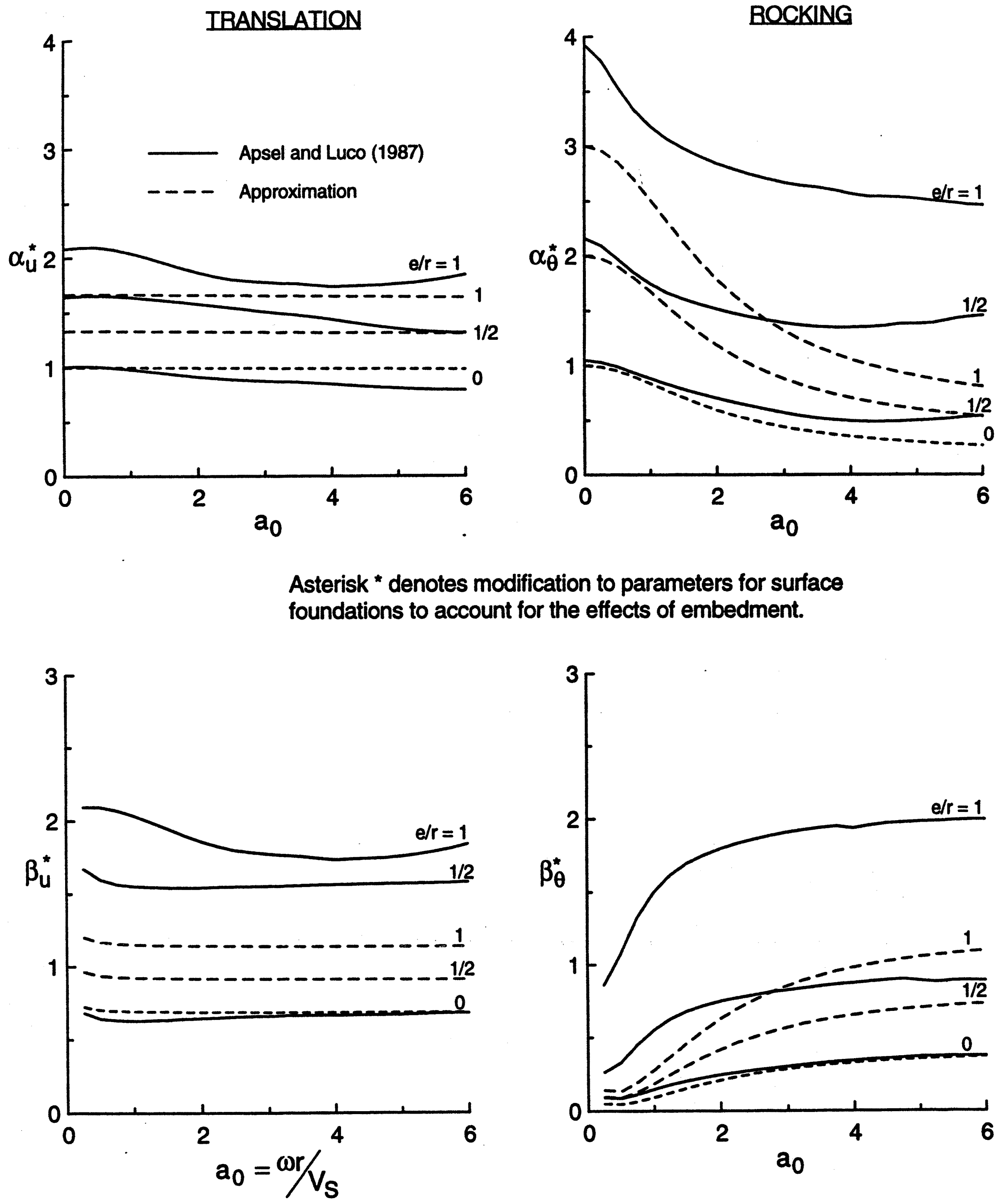

Fig. 2.5: Foundation stiffness and damping factors for rigid cylindrical foundations embedded in a halfspace; approximation vs. solution by Apsel and Luco (1987)

terms α_u and α_θ, which are reasonably well predicted for $e/r \leq 0.5$, and in the case of α_θ, for $a_0 < 1.5$ as well. In the case of damping, the comparison in Fig. 2.5 is essentially one of radiation damping effects due to the low β value in this example. The approximation grossly underpredicts radiation damping effects even at moderate embedments (e.g. e/r = 0.5) at all frequencies. However, this underprediction of radiation damping may be tolerable in some situations, because at the low frequencies typical of many structures (a_0<1), radiation damping effects are small relative to hysteretic soil damping, and consequently estimates of total foundation damping may be reasonable.

Field vibration testing of a small (10 x 10 ft) embedded structure (Lin and Jennings, 1984) found that Elsabee and Morray's predictions of the embedment effect on rocking stiffness and damping were fairly accurate, especially for low embedment ratios (e/r = 0.44). However, translational stiffness and damping were significantly underpredicted for both embedment ratios tested (0.44 and 0.90). Forced vibration testing of a nine-story reinforced concrete building with a single-level basement (e/r = 13/45 ft = 0.29) by Wong et al. (1988) revealed low frequency ($a_0 \approx 0.2$ to 0.4) impedance function ordinates for rocking that were in excellent agreement with the Apsel and Luco theoretical predictions (and, by inference, the approximate solution as well). Horizontal stiffness was found to be overpredicted by the Apsel and Luco theory by about 20 to 40%, while damping comparisons were inconclusive.

In this study, embedment effects on foundation impedance were evaluated with two separate analyses. The first analysis is based on static foundation stiffnesses established per Eq. 2.7 (with coupling terms assumed to be zero) and frequency dependent modifications to stiffness and damping terms with the α_u, α_θ, β_u, and β_θ factors in Eq.

2.4a-d. The second analysis, formulated by Bielak (1975), more rigorously incorporates soil/basement-wall interaction effects into the foundation impedance function, and hence is similar to Apsel and Luco (1987). This second formulation is discussed further in Section 2.2.3.

(d) *Foundation shape*

Conventional practice has been that foundations of arbitrary shape are analyzed as equivalent circular mats, provided that the foundation aspect ratio in plan (L/B) is less than 4:1 (Roesset, 1980). As noted in Eq. 2.3, an equivalent radius for translational stiffness is derived by equating the area of the mats, while an equivalent radius for rocking stiffness is derived by equating the moment of inertia of the mats. These criteria have been adopted into the NEHRP (BSSC, 1997) code.

Dobry and Gazetas (1986) reviewed the literature for impedance function solutions for foundations of various shapes including circles and rectangles with aspect ratios of 1 to ∞. Their results generally confirmed that the use of equivalent circular mats is an acceptable practice for aspect ratios < 4:1, with the notable exception of dashpot coefficients in the rocking mode. As shown in Fig. 2.6, dimensionless radiation damping coefficients c_{rx} and c_{ry} (for longitudinal and transverse rocking, respectively) are seen to be underestimated by the equivalent disk assumption at low frequencies. This is a consequence of the tendency for rocking vibrations to be dissipated into the soil primarily via the ends of the foundation. Hence, as L/B increases, the two ends act increasingly as independent wave sources with reduced destructive interference between waves emanating from the foundation. For the case of longitudinal rocking, damping can be

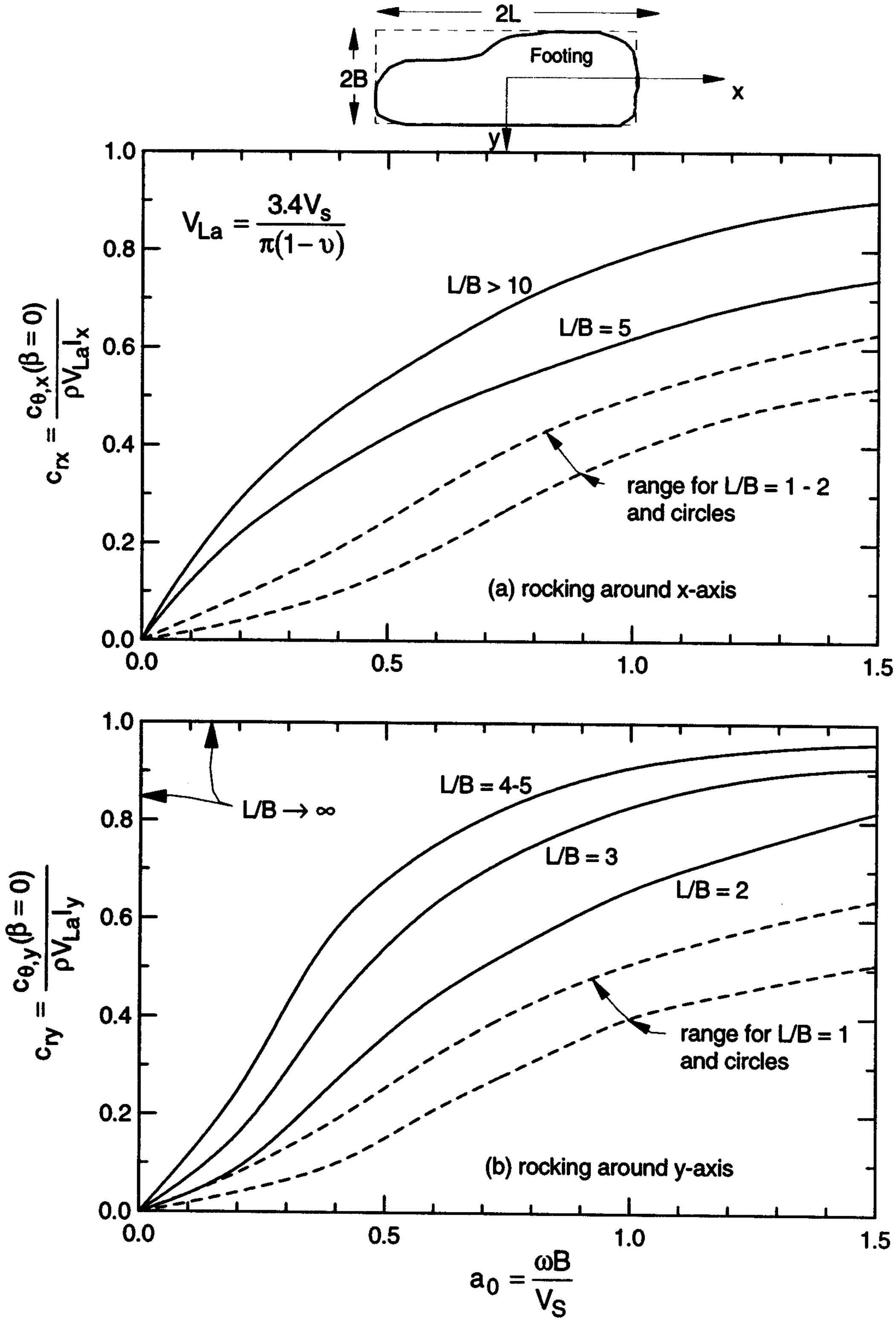

Fig. 2.6: Dashpot coefficients for rocking radiation damping vs. frequency for different foundation shapes (Dobry and Gazetas, 1986)

underpredicted by more than 100% for aspect ratios of L/B ≈ 4. For higher frequencies (a_0 > 3 - 4, not shown), the results for the various aspect ratios converge to c_{rx}, c_{ry} ~ 1. This occurs because these high frequency waves have short wavelengths, so destructive interference between the waves decreases.

In this study, radiation dashpot coefficients for oblong, non-circular foundations were corrected according to the results in Fig. 2.6. This correction was made by multiplying the radiation damping component of the disk dashpot coefficients from Part (a) by $(c_r)_{L/B}/(c_r)_{L/B=1}$, where the c_r values were determined at the a_0 value corresponding to the structure's fundamental frequency.

(e) *Foundation flexibility*

The effects of foundation flexibility on impedance functions for surface disk foundations have been investigated by Iguchi and Luco (1982) for the case of loading applied through a rigid central core, Liou and Huang (1994) for the case of thin perimeter walls, and Riggs and Waas (1985) for the case of rigid concentric walls (Fig. 2.7). These studies have generally focused on foundation flexibility effects on rocking impedance; the horizontal impedance of non-rigid and rigid foundations are similar (Liou and Huang, 1994).

A key parameter in the evaluation of foundation flexibility effects on rocking impedance is the ratio of the soil-to-foundation rigidity,

$$\eta = \frac{Gr^3}{D} \tag{2.8}$$

in which G is the soil dynamic shear modulus and D is the foundation's flexural rigidity,

$$D = \frac{E_f t_f^3}{12\left(1-\upsilon_f^2\right)} \tag{2.9}$$

where E_f, t_f, and ν_f are the Young's modulus, thickness, and Poisson's ratio of the foundation, respectively. For the case of rocking impedance, the significance of foundation flexibility effects depends on the wall configuration on the disk. As shown in Fig. 2.8, these effects are most important for the rigid central core case, for which significant reductions in stiffness and damping are possible. The reductions are greatest for narrow central cores and large values of relative soil/foundation rigidity (i.e. η = 10 to 1000). For the case of thin perimeter walls, the foundation impedances are reasonably close to rigid base values for $a_0 < 3$. For the concentric wall case considered by Riggs and Waas (1985), it was similarly found that flexible foundations behave similarly to rigid foundations at low frequencies.

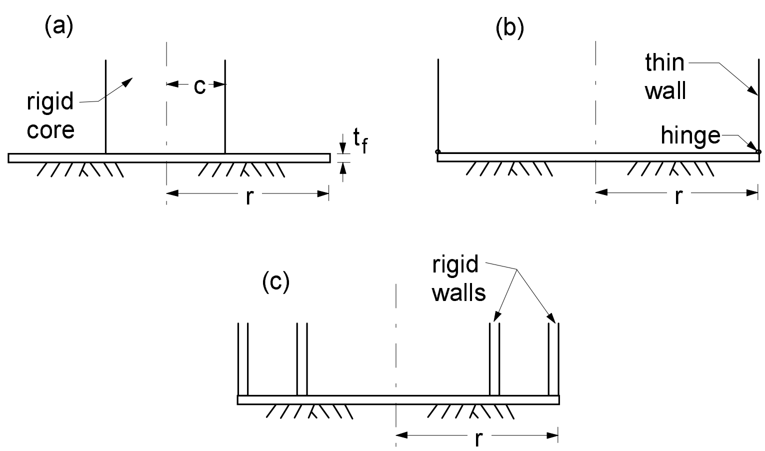

Fig. 2.7: Disk foundations with (a) rigid core considered by Iguchi and Luco (1982) (b) thin perimeter walls considered by Liou and Huang (1994), and (c) rigid concentric walls considered by Riggs and Waas (1985)

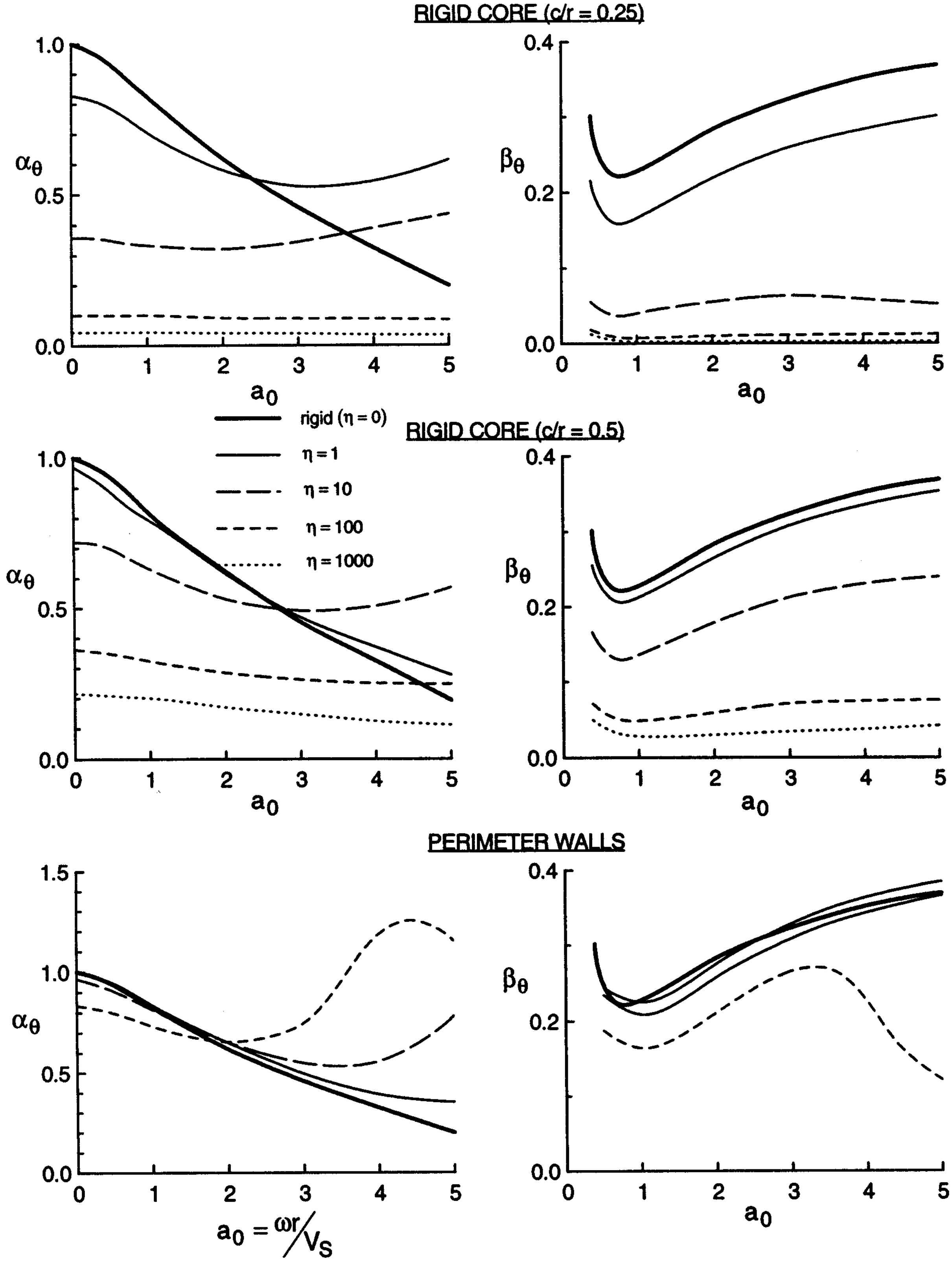

Fig. 2.8: Rocking stiffness and damping factors for flexible foundations; rigid core cases (Iguchi and Luco, 1982) and perimeter wall case (Liou and Huang, 1994)

In this study, corrections for foundation flexibility effects were made to rocking impedance terms for structures having central core shear walls using the curves in Fig. 2.8. This correction was made by multiplying the disk rocking stiffness and dashpot coefficients from Part (a) by $(\alpha_\theta)_{flex}/(\alpha_\theta)_{rigid}$ and $(\beta_\theta)_{flex}/(\beta_\theta)_{rigid}$, respectively, where the α_θ and β_θ values were determined at the a_0 value corresponding to the structure frequency. No corrections to rocking impedance terms were made for other wall configurations, nor were corrections applied to horizontal impedance terms.

(f) *Piles or piers*

The influence of pile foundations on impedance functions cannot easily be accounted for with simplified analyses. Many analytical techniques are available for evaluating the impedance of pile supported foundations (e.g. Novak, 1991 and Gohl, 1993), but a review of such techniques is beyond the scope of this chapter. The effects of piles/piers were not explicitly accounted for in the development of impedance functions for the analyses in this study. Instead, the influence of foundation type on the final results was evaluated empirically, as discussed in Chapter 5.

2.2.3 Results

Veletsos and Meek (1974) found that the maximum seismically induced deformations of the oscillator in Fig. 2.2 could be predicted accurately by an equivalent fixed-base single degree-of-freedom oscillator with period $\tilde{T}$ and damping ratio $\tilde{\zeta}$. These are referred to as "flexible-base" parameters, as they represent the properties of an oscillator which is allowed to translate and rotate at its base (i.e. Fig. 2.2). The flexible-base period is evaluated from (Veletsos and Meek, 1974),

$$\frac{\tilde{T}}{T} = \sqrt{1 + \frac{k}{k_u} + \frac{kh^2}{k_\theta}} \tag{2.10}$$

where T is the fixed-base period of the oscillator in Fig. 2.2 (i.e. the period that would occur in the absence of base translation or rocking). The flexible-base damping ratio has contributions from the viscous damping in the structure as well as radiation and hysteretic damping in the foundation. Jennings and Bielak (1973) and Veletsos and Nair (1975) expressed the flexible-base damping $\tilde{\zeta}$ as

$$\tilde{\zeta} = \tilde{\zeta}_0 + \frac{\zeta}{\left(\tilde{T}/T\right)^3} \tag{2.11}$$

where $\tilde{\zeta}_0$ is referred to as the foundation damping factor and represents the damping contributions from foundation-soil interaction (with hysteretic and radiation components). A closed form expression for $\tilde{\zeta}_0$ is presented in Veletsos and Nair (1975).

The relationships between the fixed- and flexible-base oscillator properties depend on aspect ratio h/r_2, soil Poisson Ratio υ, soil hysteretic damping ratio β, and the following dimensionless parameters:

$$\sigma = V_S T/h \tag{2.12}$$

$$\gamma = \frac{m}{\rho \pi r_1^2 h} \tag{2.13}$$

Parameters σ and γ represent the ratio of the soil-to-structure stiffness and structure-to-soil mass, respectively. For conventional building structures, $\sigma > 2$ and $\gamma \approx 0.1$ to 0.2 [a representative value of $\gamma = 0.15$ is recommended by Veletsos and Meek (1974)]. Both $\tilde{T}/T$ and $\tilde{\zeta}_0$ are sensitive to σ, while the sensitivity to γ is modest for $\tilde{T}/T$ (± 10 to 15% error), and low for $\tilde{\zeta}_0$ (Aviles and Perez-Rocha, 1996).

For the case of a rigid circular foundation on the surface of a visco-elastic halfspace (impedance defined in Section 2.2.2), analytical results from Veletsos and Nair (1975) for $\tilde{T}/T$ and $\tilde{\zeta}_0$ vs. $1/\sigma$ are shown in Figs. 2.9 and 2.10, respectively. The results show that $\tilde{T}$ is always lengthened relative to T, and that the period lengthening ratio ($\tilde{T}/T$) increases with $1/\sigma$ and h/r for h/r > 1. This implies that the ratio of structure-to-soil stiffness ($1/\sigma$) is a critical factor controlling the period lengthening, and that for a given value of $1/\sigma$, period lengthening increases for taller structures (i.e. higher h/r) with more overturning moment. The flexible base damping $\tilde{\zeta}$ can actually increase or decrease relative to ζ depending on the period lengthening in the structure and the foundation damping factor $\tilde{\zeta}_0$. In Fig. 2.10, $\tilde{\zeta}_0$ is seen to increase with $1/\sigma$ and decrease with h/r, indicating that lateral movements of the foundation (which dominate at low h/r) dissipate energy into soil more efficiently than foundation rocking (which dominates at high h/r). The contributions to foundation damping from radiation and hysteretic damping are compared in Fig. 2.10; the significance of hysteretic damping is seen to increase with increasing h/r due to the decreased radiation damping effect.

For the case of a rigid circular foundation embedded into a visco-elastic soil, analytical results for $\tilde{T}/T$ and $\tilde{\zeta}_0$ vs. $1/\sigma$ are shown in Fig. 2.11 for the analytical formulation presented above (i.e. the Veletsos and Nair (V & N) model) as well as two

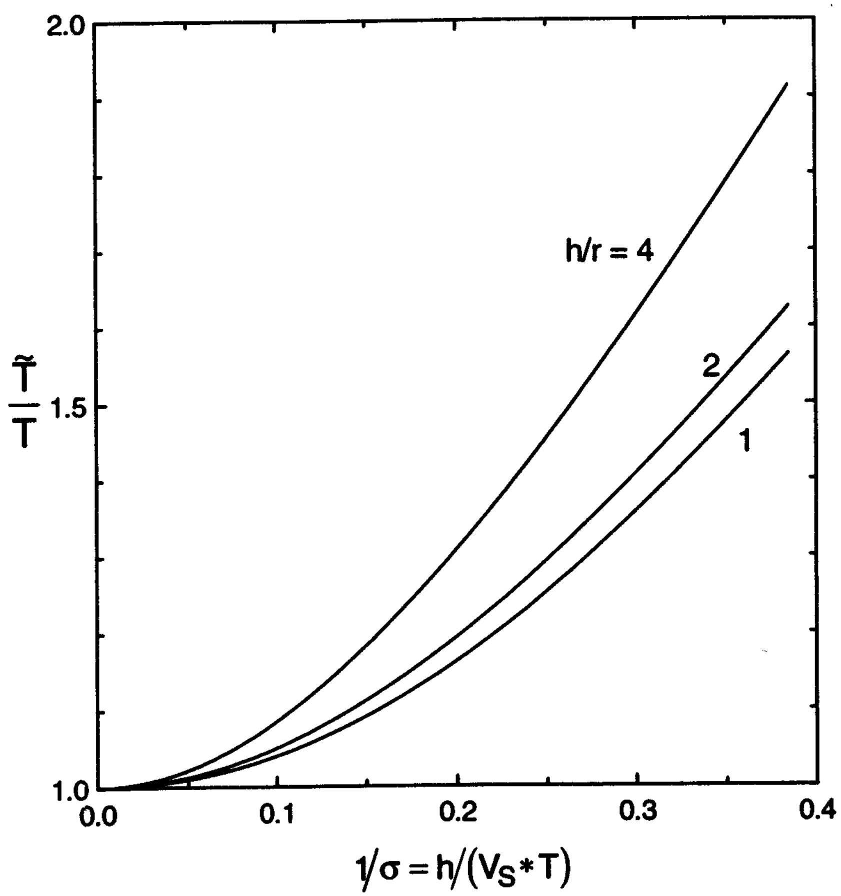

Fig. 2.9: Period lengthening ratios for single degree-of-freedom structure with rigid circular foundation on viscoelastic halfspace ($\upsilon = 0.4, \gamma = 0.15$) [Veletsos and Nair, 1975]

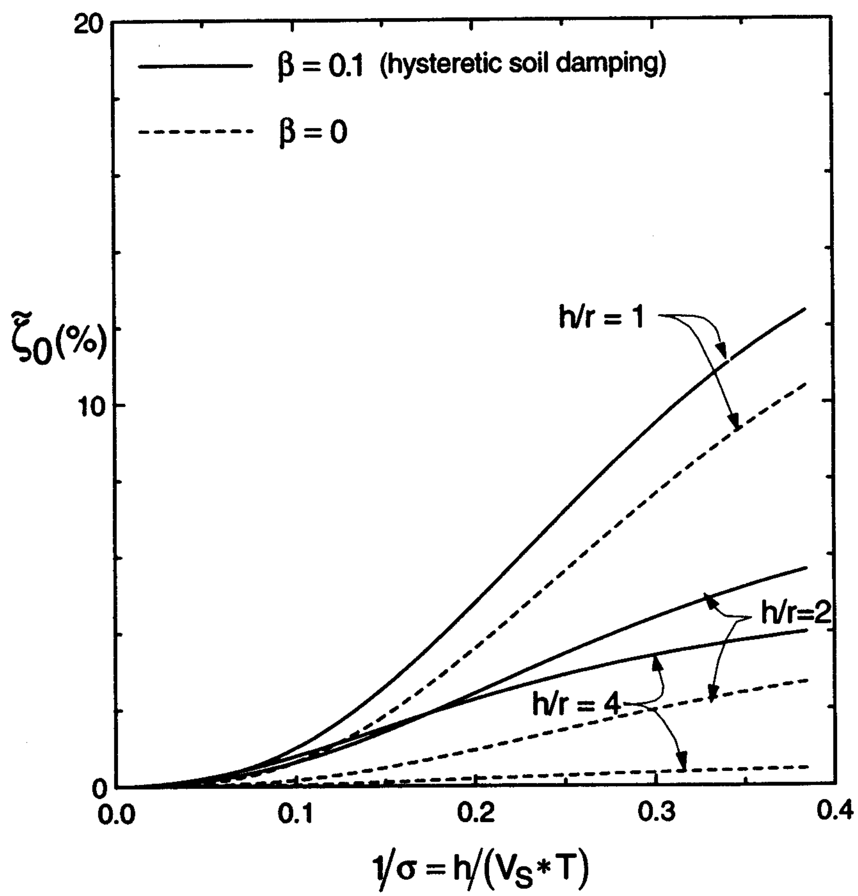

Fig. 2.10: Foundation damping factors for single degree-of-freedom structure with rigid circular foundation on elastic and viscoelastic half-space ($\upsilon = 0.4, \gamma = 0.15$) [Veletsos and Nair, 1975]

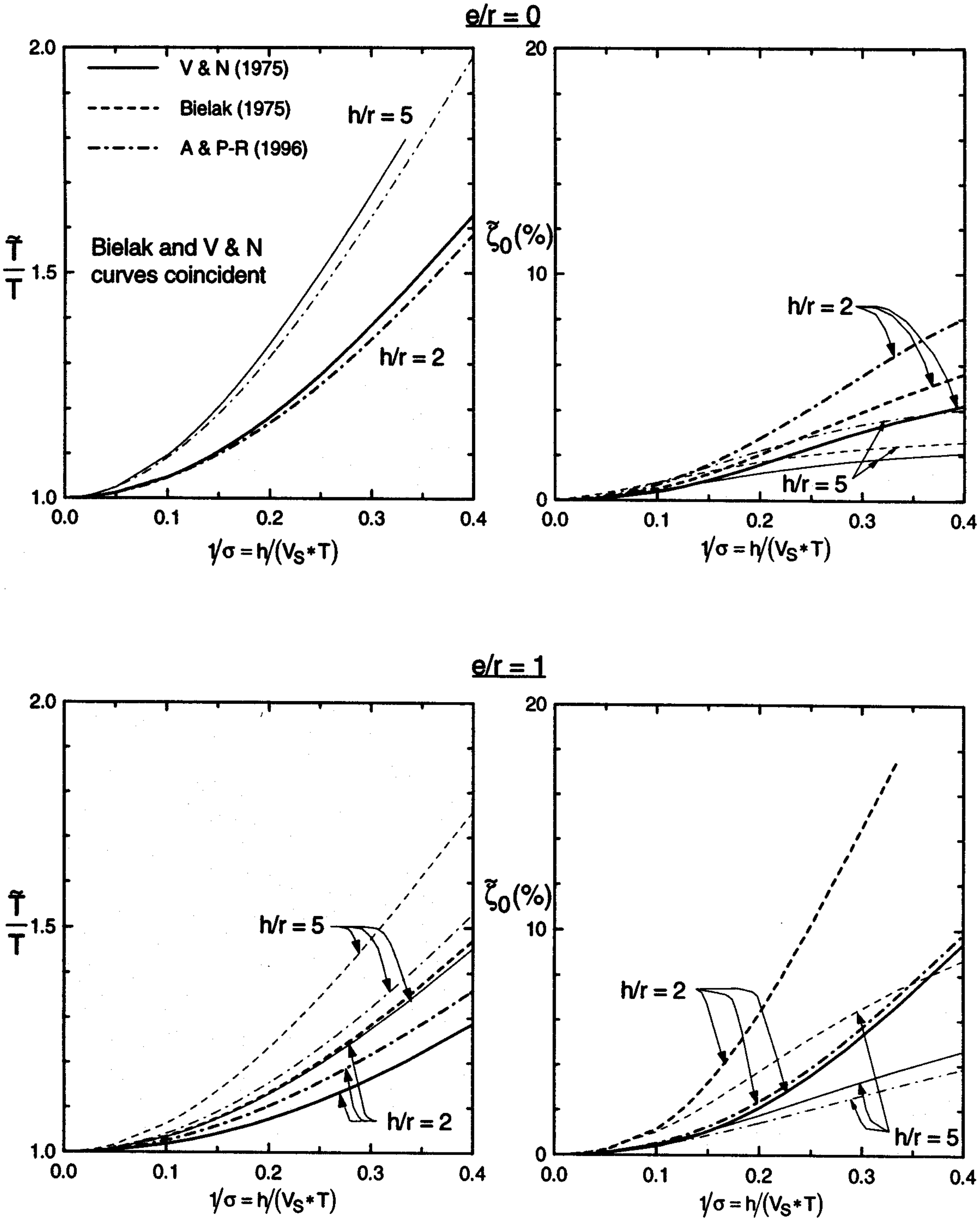

Fig. 2.11: Comparison of period lengthening ratios and foundation damping factors for single degree-of-freedom structure with surface and embedded foundations ($\upsilon = 0.45, \beta = 5\%, \gamma = 0.15, \zeta = 5\%$)
[Veletsos and Nair, 1975; Bielak, 1975; Aviles and Perez-Rocha, 1996]

others [Bielak (1975) and Aviles and Perez-Rocha (A & P-R), 1996]. The V & N and Bielak solutions are for a foundation embedded into a halfspace, while the A & P-R solution is for a thick finite layer ($d_S/r = 10$). The SSI models solved in the Bielak and V & N approaches are similar, except that dynamic soil/basement-wall interaction effects on foundation impedance are incorporated into the Bielak formulation. Similarly, the only significant difference between the A & P-R and Bielak models is the finite soil layer used by A & P-R. For the plots in Fig. 2.11, embedment corrections for the V & N approach were made according to Eq. 2.7. For the case of zero embedment ($e/r = 0$), the three formulations yield essentially identical results with the exception of relatively high damping from the A & P-R model. For the case of $e/r = 1$, increases in damping and decreases in period lengthening are predicted by all three models. The Bielak model yields the highest damping predictions. V & N and A & P-R indicate smaller damping due to the lack of a dynamic basement wall-soil interaction model (V & N) and the finite soil layer (A & P-R). It should be noted that the embedment ratio $e/r = 1$ is approaching the limit of validity for the expression in Eq. 2.7, and results from the three formulations are more consistent for lower e/r.

In this study, the analysis by Veletsos and Nair (1975) was generally used with appropriate modifications to the foundation impedance for nonuniform soil profiles, foundation embedment (i.e. Eq. 2.7), foundation shape, and foundation flexibility effects. To more accurately model the stiffness and damping of embedded foundations, analyses were also performed using the Bielak (1975) approach with appropriate modifications for nonuniform soil profiles and foundation shape and flexibility effects. For subsequent reference, these analyses are termed the "modified Veletsos" and "modified Bielak" formulations.

2.2.4 Calibration of Analysis Results with Field Performance Data

Research efforts have been undertaken to calibrate analytical techniques for SSI using seismic field performance data from the Humboldt Bay Nuclear Power Plant (Valera et al., 1977) and the Lotung 1/4-scale containment model (Bechtel Power Corporation, 1991). Several test structures have also been examined by Japanese researchers (e.g. a 12.5 m tower, Ganev et al., 1994, and a 31 m scaled containment structure, Hanada et al., 1988). The objectives of these studies were generally to compare recorded structural motions with predicted analytical motions.

The instrumented structure at the Humboldt site essentially consists of a deep caisson (there is no significant above-ground structure), so the simplified analytical techniques discussed above are not applicable. Fixed- and flexible-base structural periods and damping ratios were evaluated for the Lotung site, though these parameters were not compared to analytical predictions of $\tilde{T}/T$ and $\tilde{\zeta}_0$. However, relatively sophisticated analyses of the soil-structure system using the SASSI (Lysmer et al., 1981) and CLASSI (Luco, 1980b) programs were successful at reasonably accurately reproducing the overall structural response, and hence by inference the flexible-base modal parameters. The analytical formulation in the CLASSI program is based on a substructure procedure similar to that outlined in this section. The accuracy of the CLASSI analyses relative to the Lotung data reinforces the validity of these substructure procedures. Similar confirmation of simple SSI models was obtained in back-analyses of data from the

Japanese test structures. It should be noted that the Humboldt and Lotung sites were included in this study as sites A3 and A46. Data from the Japanese sites could not be obtained for this study.

A number of studies have developed two- or three-dimensional frame models of instrumented structures, verified the model's accuracy using periods identified from recorded data, and investigated SSI effects by varying the base fixity condition (e.g. Wallace and Moehle, 1990 and Fenves and Serino, 1992). The study by Wallace and Moehle examined the response of a 22-story shear wall building in Chilé under forced vibration testing, low-level (0.05g) earthquake shaking, and moderate-level (0.18g) shaking. From three-dimensional frame analyses, the period lengthening was found to be 15%, 22%, and 43% in the forced vibration and earthquake shaking conditions, respectively. For the moderate-level shaking condition, the ATC (1978) procedure predicted 37% period lengthening, which is in good agreement with the 43% from frame analyses. Comparisons were not made for the lower-level shaking conditions. Fenves and Serino examined the response of a 14-story concrete-frame warehouse structure (site A29 in this study) during the 1987 Whittier Earthquake. Fixed-base periods were not reported, but changes in base shear resulting from SSI effects were found to be reasonably predicted by the ATC procedure (using smoothed free-field spectra).

Poland et al. (1994) analyzed the effects of SSI on base shear in four buildings using two simple analytical techniques (FLUSH and ATC code provisions) and compared these results to reductions in the base shear calculated using a single degree-of-freedom structural model subjected to recorded free-field and foundation motions (so-called "time history" analyses). Poor agreement between the analytical and "time history" results was found. However, it is not clear how to interpret these results as the modal parameters used in the "time history" analyses are not reported. SSI effects on structural response can be more rationally assessed by comparing fixed- and flexible-base modal parameters. It should be noted that the four buildings studied by Poland et al. are also examined in this study (sites A6, A10, A12, and A29).

In addition to the above research efforts, a number of calibration studies for impedance functions have been performed (see Section 2.2.2), and modal parameters of several structures have been evaluated using various system identification techniques with some inferences made about SSI effects (see Stewart, 1997 for references). However, fixed- and flexible-base modal parameters were seldom directly compared in these studies.

It appears that no previous studies have attempted to evaluate on a large scale the fixed- and flexible-base modal parameters of structures subjected to significant levels of seismic excitation for the purpose of calibrating simplified analytical procedures such as those in the ATC and NEHRP codes. This is the principle objective of this study.

2.3 Kinematic Interaction

As noted in Section 2.1, kinematic interaction generally results from base-slab averaging, deconvolution/embedment effects, and wave scattering effects. At present, relatively little is known about the effects of wave scattering on base-slab motions, as its effects are almost invariably combined with more significant base-slab averaging and embedment effects, which are the focus of this section.

2.3.1 Base-Slab Averaging

For vertically incident, coherent wave fields, the motion of a rigid surface foundation is identical to the free-field motion. Base-slab averaging effects result from wave fields which have an angle of incidence relative to the vertical, α_V, or which are incoherent in time and space. Incoherence of seismic waves results from different wave ray paths (i.e. due to laterally traveling seismic waves in the underlying bedrock) and local heterogeneities in the geologic media through which the seismic waves have traveled.

In the presence of incoherent or non-vertically incident wave fields, translational base-slab motions are reduced relative to the free-field, and torsional rotation of the base-slab is introduced. Rocking of the base-slab can also occur in the presence of inclined SV or P waves, but is negligible for SH waves. The reduction of base-slab translation, and the introduction of torsion and rocking, are all effects which tend to become more significant with increasing frequency. The frequency-dependence of these effects is primarily associated with the increased effective size of the foundation relative to the seismic wavelengths at higher frequencies. In addition, incoherence effects are greater at higher frequencies.

Veletsos and Prasad (1989) and Veletsos et al. (1997) evaluated the response of a rigid, massless disk of radius r and a rectangle of dimension 2a by 2b on the surface of an elastic halfspace to incoherent SH waves propagating either vertically or at an angle α_V to the vertical (Fig. 2.12). The incident motions are assumed to be polarized in the x-direction, and the effective horizontal propagation of inclined waves is in the y-direction. A result of the analyses is transfer functions relating the horizontal and torsional motions

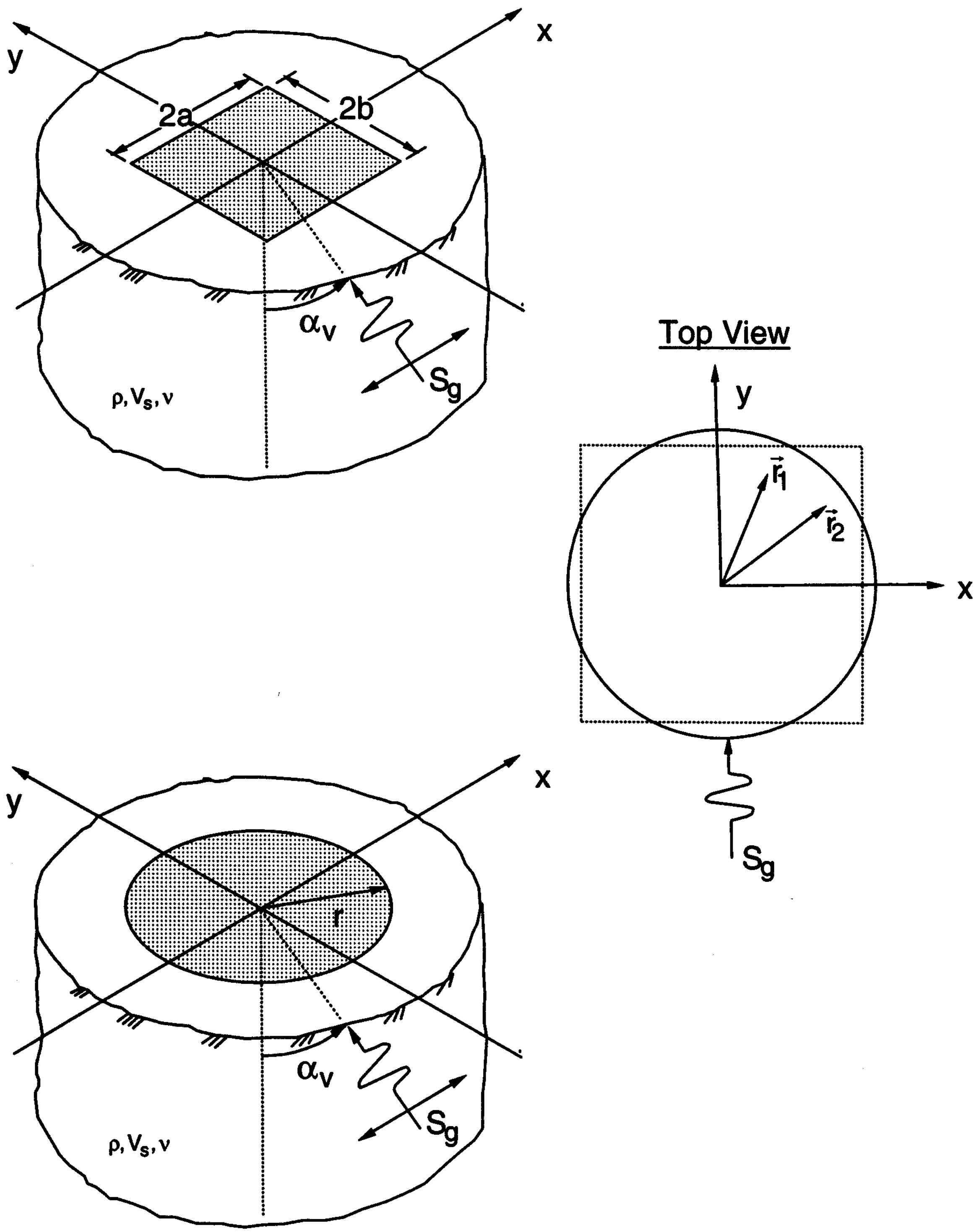

Fig. 2.12: System considered for kinematic interaction analyses (Veletsos and Prasad, 1989 and Veletsos et al., 1997)

of the foundation to the free-field motions, thus providing a quantification of base-slab averaging effects. Similar analytical formulations were developed by Luco and Wong (1986) for rectangular foundations and Luco and Mita (1987) for circular foundations. The Veletsos approach is presented here because of the relative simplicity of its formulation.

A key step in the development of the transfer functions is the numerical modeling of the spatial variation of the free-field ground motions. The temporal variation of these motions is specified by a space invariant power spectral density (psd) function, $S_g(\omega)$. The spatial variation of the incoherent free-field motions is defined by a cross spectral density function,

$$S_{xy}(\omega) = \Gamma\left(\left|\mathbf{r}_1 - \mathbf{r}_2\right|, \omega\right) e^{-\left(\frac{i\omega}{(V_S)_H}\left|\mathbf{r}_1 - \mathbf{r}_2\right|\right)} S_g(\omega) \tag{2.14}$$

where $\mathbf{r}_1$ and $\mathbf{r}_2$ are position vectors for two points, and $(V_S)_H$ is the apparent horizontal velocity of the wave front, $(V_S)_H = V_S/\sin\alpha_V$. In Eq. 2.14, the exponential term represents the wave passage effect (due to nonvertically incident waves), and the Γ term represents the ground motion incoherence effect. The coherence function used in the Veletsos formulations is,

$$\Gamma\left(\left|\mathbf{r}_1 - \mathbf{r}_2\right|, \omega\right) = e^{-\left(\frac{\kappa\omega}{V_S}\left|\mathbf{r}_1 - \mathbf{r}_2\right|\right)^2} \tag{2.15}$$

where κ is a dimensionless incoherence factor which reportedly can be quantified by κ/V_S ~ $(2\text{-}3)\times10^{-4}$ sec/m (Luco and Wong, 1986).

Coherence functions have been modeled using exponential functions similar to Eq. 2.15 by a number of researchers (Luco and Wong, 1986; Somerville et al., 1991; Novak, 1987). More refined coherence functions defined using five parameters in the regression have been developed by Abrahamson (1988, 1992), who also performed the regression using $\tanh^{-1}(\Gamma)$ instead of Γ. Abrahamson cautions that functional forms of coherence not using $\tanh^{-1}(\Gamma)$ may not be appropriate because Γ is not normally distributed but $\tanh^{-1}(\Gamma)$ is approximately normally distributed. Nevertheless, the exponential coherence function in Eq. 2.15 was retained for this study due to the relative simplicity of its algebraic form and its ability to capture the decay in coherence with increasing separation and frequency (though not in the mathematically ideal form). The primary errors introduced by the use of Eq. 2.15 are overpredictions of coherence at large distances (i.e. > 100 m) and low frequencies (i.e. < 1 Hz) (Novak, 1987).

Using spatial averaging procedures with the cross spectral density function in Eq. 2.14 and the coherence function in Eq. 2.15, Veletsos and Prasad (1989) and Veletsos et al. (1997) developed expressions for the psds of the horizontal (S_x) and torsional (S_ϕ) motions of the base-slab in terms of $S_g(\omega)$ for circular and rectangular foundation geometries, respectively. In the presentation of results, the torsional motions were represented by circumferential motions of the base-slab in the x-direction (i.e. $S_{cir}=r\cdot S_\phi$ for circular foundations and $b\cdot S_\phi$ for rectangular foundations).

The transfer function amplitudes associated with base slab averaging are presented in Fig. 2.13 for circular and rectangular foundations subject to vertically incident incoherent waves, and Fig. 2.14 for nonvertically incident coherent waves. These transfer functions are plotted against the dimensionless frequency parameter $\tilde{a}_0$, which is defined as follows for circular and rectangular footings, respectively,

$$\tilde{a}_0 = a_0\sqrt{\kappa^2 + \sin^2 \alpha_v}$$
$$\tilde{a}_0 = \frac{\omega b}{V_S}\sqrt{\kappa^2 + \sin^2 \alpha_v} \tag{2.16}$$

where $a_0 = \omega r/V_S$. The definition of the $\tilde{a}_0$ factor given in Eq. 2.16 for rectangular foundations applies for identical wave incoherence factors κ in the x and y directions.

Figs. 2.13 and 2.14 indicate that the lateral transfer functions ($\sqrt{S_x/S_g}$) for circular and various rectangular geometries are similar, regardless of the type of wave field. The near equivalence of the results for different aspect ratios (a/b) of rectangular foundations suggests that the lateral transfer function primarily depends on the total area of the foundation. This result is a product of the model formulation in which spatial variations of ground motion only result from random incoherence (which is assumed to be identical in both horizontal directions) or nonvertically incident waves. That is, the effects of "traveling waves," which might result in a temporal incoherence of incident waves across a foundation, has not been considered. Such effects would be sensitive to the plan angle of propagation of the traveling waves relative to the foundation and the aspect ratio of the foundation (but might only be significant for very large foundations).

The torsional transfer function results show a relatively high degree of sensitivity to a/b and the type of wave field. Higher torsional motions occur for lower a/b and nonvertically incident coherent wave fields.

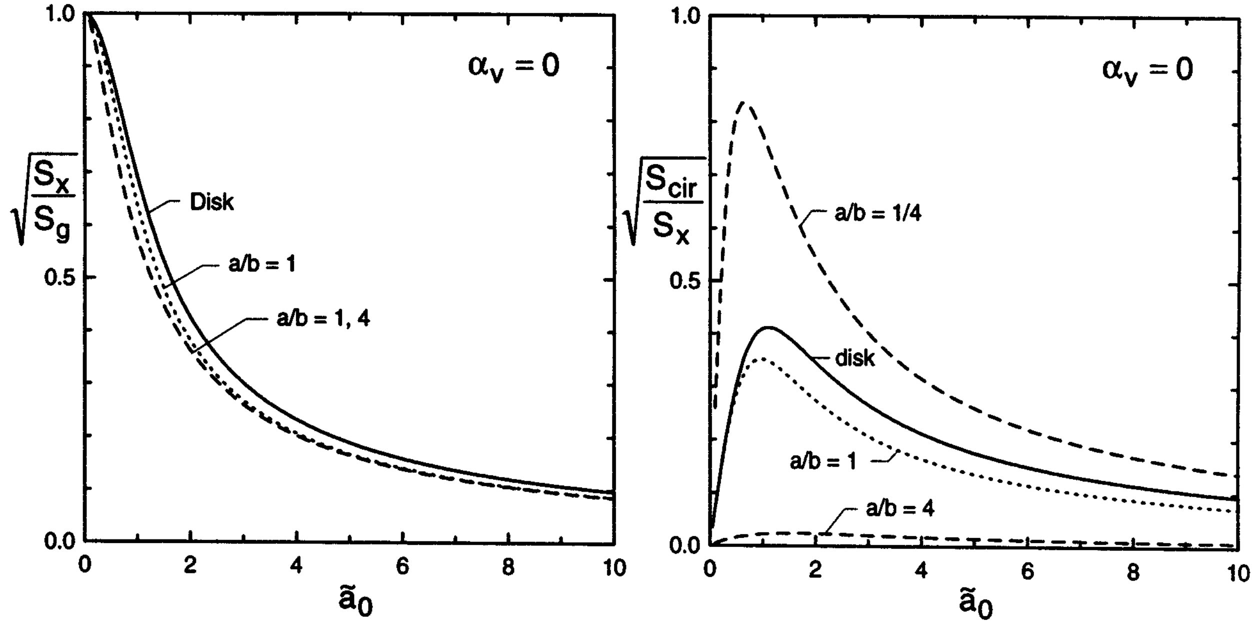

Fig. 2.13: Magnitudes of transfer functions between free-field ground motion and FIM for vertically incident incoherent waves (Veletsos et al., 1997 and Veletsos and Prasad, 1989)

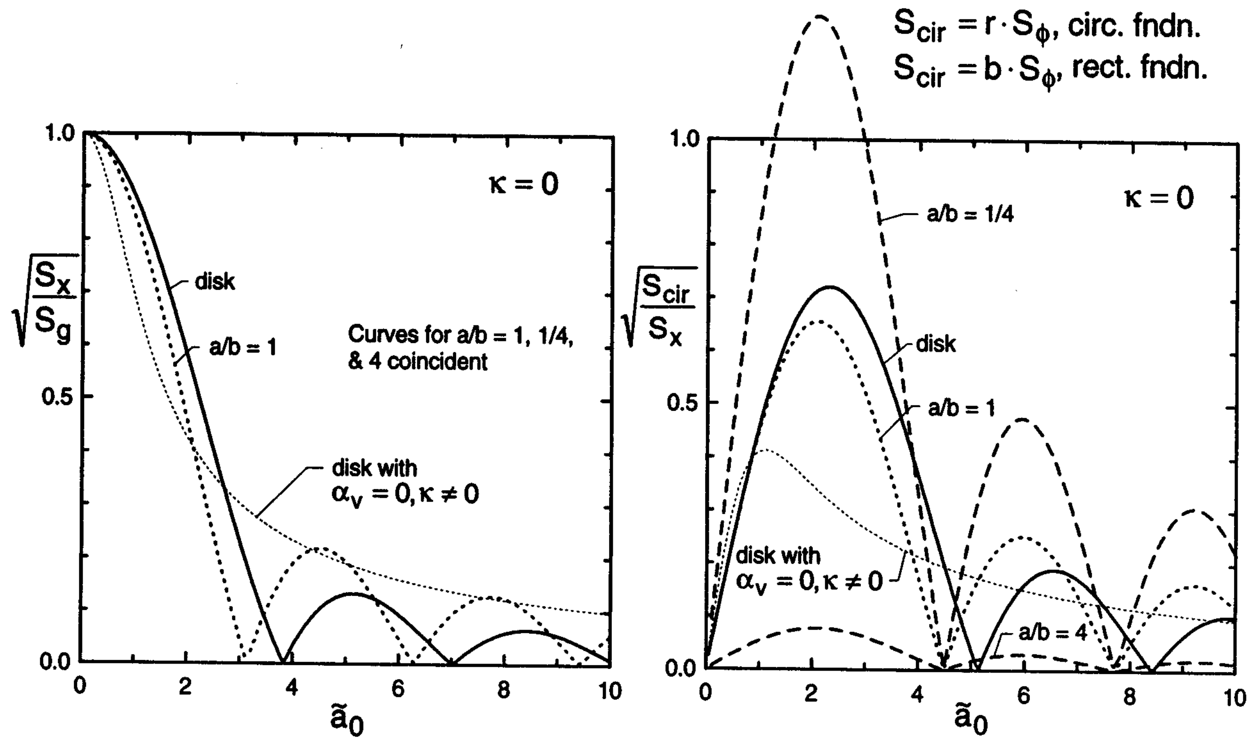

Fig. 2.14: Magnitudes of transfer functions between free-field ground motion and FIM for obliquely incident coherent waves. Curves for disk and vertically incident incoherent waves also shown for comparison (Veletsos et al., 1997 and Veletsos and Prasad, 1989)

2.3.2 Embedment

When subjected to vertically propagating coherent SH waves, embedded foundations experience a reduction in base-slab translational motions relative to the free-field, and rocking motions are introduced. This rocking is not a product of base moment associated with structural inertia, as structure and foundation masses are neglected in the analysis of kinematic interaction. Rather, the rocking is caused by incompatible shear strains along the sides of the excavation and the free-field. Roesset (1980) suggests that these embedment effects are likely to be significant for e/r greater than about 0.15. Analytical and empirical studies have been performed to examine embedment effects on foundation input motions (FIMs), the results of which are presented in the following sections.

(a) *Analytical studies*

Analytical studies of embedment effects have focused on the evaluation of transfer functions expressing the amplitude ratio of base-slab translational and rocking motions to free-field motions (e.g. Elsabee and Morray, 1977 and Day, 1977). These formulations are generally based on assumed vertically propagating coherent waves, so that the base-slab averaging effects discussed in Section 2.3.1 are negligible.

Day (1977) used finite element analyses to evaluate the base motions of a rigid cylindrical foundation embedded in a uniform elastic half space ($\beta = 0$, $\nu = 0.25$) and subjected to vertically incident, coherent SH waves. Elsabee and Morray (1977) performed similar studies but for the case of a visco-elastic soil layer of finite depth over a rigid base ($\beta = 0.05$ and $\nu = 0.33$). The amplitude of the transfer functions for translation and rocking are shown in Fig. 2.15 for the halfspace and Fig. 2.16 for the

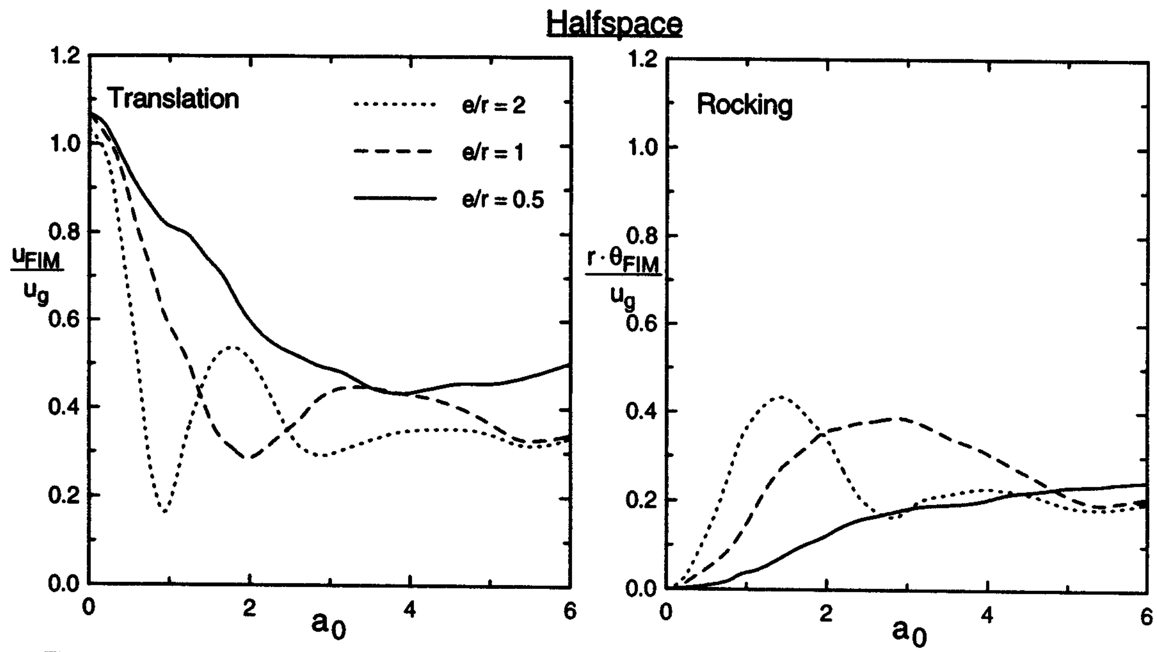

Fig. 2.15: Amplitudes of transfer functions between free-field ground motion and FIM for rigid cylindrical foundation embedded in elastic halfspace and subjected to vertically incident coherent waves (Day, 1977)

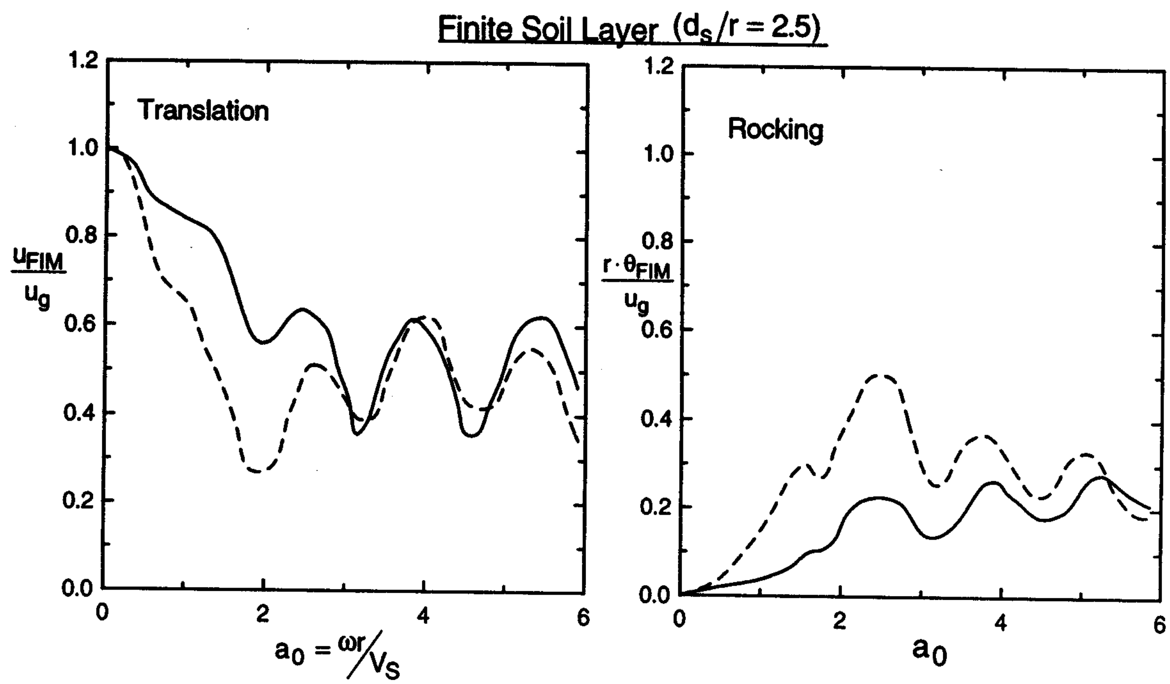

Fig. 2.16: Amplitudes of transfer functions between free-field ground motion and FIM for rigid cylindrical foundation embedded in finite soil layer over rigid base and subjected to vertically incident coherent waves (Elsabee and Morray, 1977)

finite soil layer. The only significant differences between the finite soil layer and halfspace results are high frequency ($a_0 > 1.5$) oscillations in the finite soil layer case. The results for embedment ratios e/r = 0.5, 1.0, and 2.0 (halfspace) and 0.5 and 1.0 (finite soil layer) indicate significant filtering of translational motions for $a_0 > 0.5$ and the development of significant rocking for $a_0 > 1$. At low frequencies ($a_0 < 1.5$), the filtering of foundation motions and the magnitude of rocking motions increases with increasing embedment ratio, while at higher frequencies there is little sensitivity to embedment ratio. These results can be contrasted with the behavior of a surface foundation which would have no reduction of translational motions and no rocking motions when subjected to vertically incident coherent shear waves.

As part of the work by Elsabee and Morray, approximate transfer functions were proposed for the translation and rocking motions of the circular foundation as follows,

$$\text{translation:} \qquad \left|H_u(\omega)\right| = \begin{cases} \cos\left(\frac{e}{r} a_0\right) & a_0 \le 0.7 \cdot \bar{a}_0 \\ 0.453 & a_0 > 0.7 \cdot \bar{a}_0 \end{cases} \tag{2.17}$$

$$\text{rocking:} \qquad \left|H_\theta(\omega)\right| = \begin{cases} \frac{0.257}{r}\left(1 - \cos\left(\frac{e}{r} a_0\right)\right) & a_0 \le \bar{a}_0 \\ \frac{0.257}{r} & a_0 > \bar{a}_0 \end{cases} \tag{2.18}$$

where $\bar{a}_0 = \pi/2 \cdot r/e$. Normalized frequency $\bar{a}_0$ corresponds to the fundamental frequency of the soil from the surface to depth e ($\bar{a}_0 = 2\pi f_1 r/V_S$ where $f_1 = V_S/4e$). In Fig. 2.17, these approximate transfer functions are compared to the halfspace (Day, 1977) and finite soil layer (Elsabee and Morray, 1977) solutions for embedment ratios of e/r = 0.5, 1.0, and 2.0. The approximation is reasonable for each embedment ratio and both profiles.

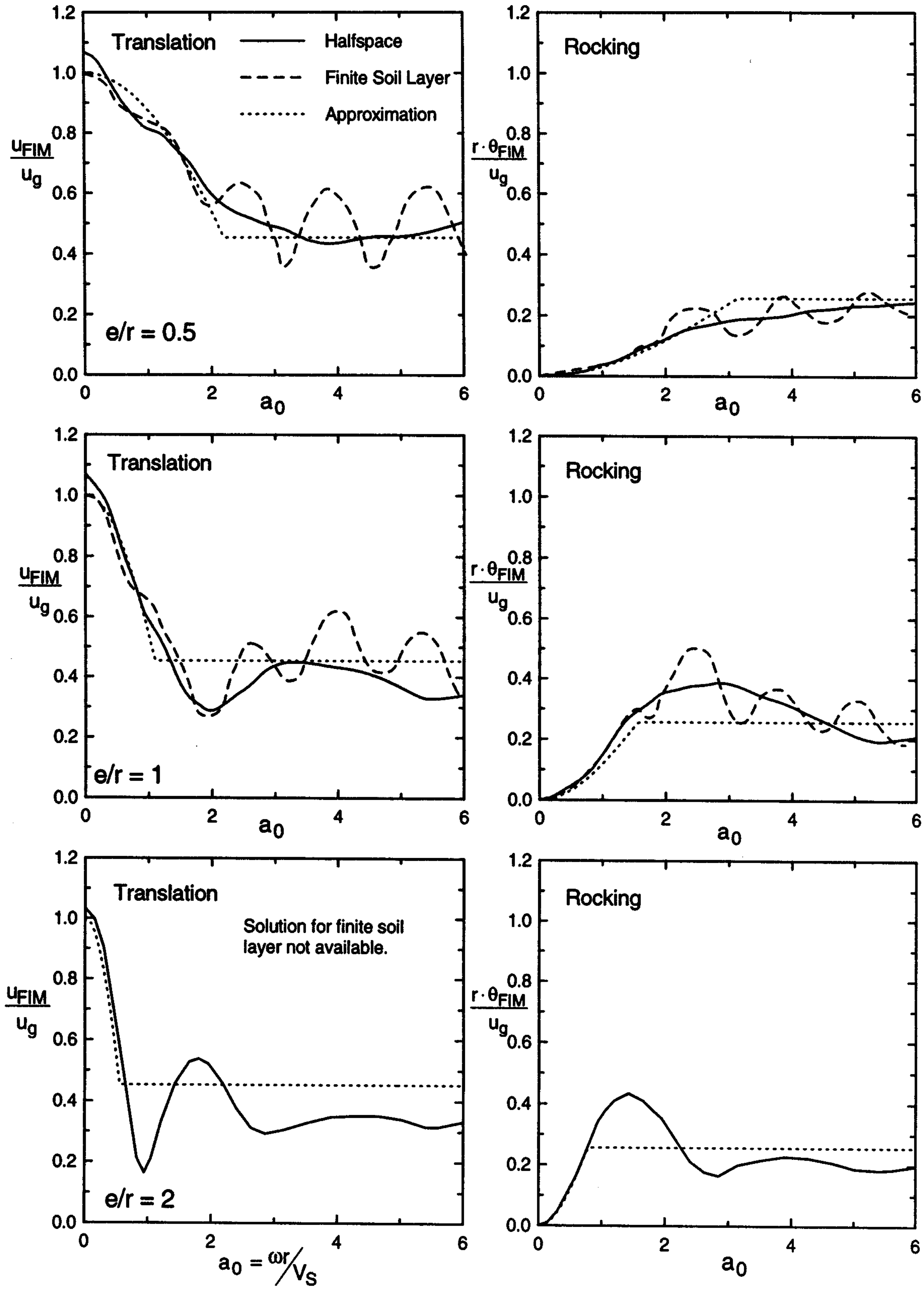

Fig. 2.17: Comparison of transfer function amplitudes for cylinders embedded in a halfspace and finite soil layer and approximation by Elsabee and Morray (Day, 1977 and Elsabee and Morray, 1977)

These results for an embedded rigid cylinder subjected to vertically incident coherent SH waves have been extended for cases of (1) soil properties varying with depth (Elsabee and Morray, 1977), (2) horizontally propagating coherent SH waves (Day, 1977), and (3) non-circular foundations (Mita and Luco, 1989) as follows:

- For soil properties which vary with depth, Elsabee and Morray found that the approximate transfer functions in Eq. 2.17-2.18 remain valid provided an averaged V_S across the embedment depth is used.
- For the case of horizontally propagating coherent SH waves, Day found that the base rocking was practically negligible, the filtering of horizontal motions was significant but was relatively insensitive to e/r, and a significant torsional response was induced at high frequencies ($a_0 > 1.5$). It should be noted, however, that horizontally propagating shear waves are generally of negligible engineering significance in SSI problems because components of ground motion with frequencies above about 1 Hz tend to attenuate rapidly with distance (Chen et al., 1981).
- Mita and Luco found that an embedded square foundation could be replaced by an equivalent cylinder without introducing significant error. The radius of the equivalent cylinder was defined as the average of the radii necessary to match the area and moment of inertia of the square base.

(b) *Empirical studies*

Studies by Seed and Lysmer (1980), Chang et al. (1985), and Johnson and Asfura (1993) have documented reductions in ground motion with depth using both downhole free-field arrays and comparisons of basement and free-field motions. These data are not repeated here; however, it is noted that both data sets (free-field/downhole and free-field/basement) consistently indicated reductions of peak ground acceleration and high frequency spectral ordinates with depth. It was also concluded by Seed and Lysmer that deconvolution analytical procedures which assume vertically propagating shear waves (e.g. the computer program SHAKE, Schnabel et al., 1972) simulate these effects reasonably well.

Ishii et al. (1984) developed empirical transfer functions for translational motions using earthquake recordings from 18 partially buried tanks in Japan. However, the regression analyses did not include e/r as a variable. Hence the results are likely of limited value as e/r appears to be significant based on the analytical studies discussed in Part (a).

Most structures are not instrumented sufficiently at the foundation-level to measure base rocking, so relatively little data on this effect is available. Even for structures which are instrumented to record base rocking, separation of the kinematic and inertial rocking effects would be impossible without making assumptions about the foundation impedance and wave field, so purely empirical transfer functions for kinematic base rocking are difficult to formulate and have not been developed to date.

2.4 Summary

In this chapter, a number of simplified analytical techniques have been presented for performing both inertial and kinematic SSI analyses. The intent of these analysis procedures is to predict period lengthening ratios and foundation damping factors (inertial interaction) and foundation/free-field transfer functions (kinematic interaction). Key aspects of these analytical procedures are summarized below.

2.4.1 Inertial Interaction

For analyses of inertial interaction effects, the objectives are predictions of first-mode period lengthening $\tilde{T}/T$ and foundation damping factor $\tilde{\zeta}_0$. The necessary input parameters are:

- Soil conditions: characterization of the site as a halfspace or finite soil layer over rigid base; shear wave velocity V_S and hysteretic damping ratio β which are representative of the site stratigraphy and the level of ground shaking; representative soil Poisson's ratio ν.
- Structure/Foundation Characteristics: effective height of structure above foundation level, h; embedment, e; foundation radii which match the area and moment of inertia of the actual foundation, r_1 and r_2; appropriate corrections to the foundation impedance for embedment, shape, and flexibility effects.
- Fixed Base 1st Mode Parameters: period and damping ratio, T and ζ.

Using these data, the following steps are carried out:

1. Evaluate the foundation impedance function at an assumed period for the flexible-base structure $\tilde{T}$. Static foundation stiffnesses are computed first according to Eq. 2.5 with appropriate modifications for finite soil layer and embedment effects (Eqs. 2.6 and 2.7). Dynamic coefficients α_u, α_θ, β_u, and β_θ are then evaluated for the assumed $\tilde{T}$ using equations in Veletsos and Verbic (1973) with appropriate

modifications to β_θ to account for foundation shape effects, and to α_θ and β_θ to account for flexible foundation effects.

2. Calculate dimensionless parameters σ and γ using Eqs. 2.12 and 2.13. For most structures, it is assumed that γ= 0.15.
3. Estimate the period lengthening and damping using Eqs. 2.10 and 2.11, calculate a new estimate of $\tilde{T}$.
4. Repeat steps 1 to 3 until the dynamic coefficients α_u, α_θ, β_u, and β_θ are estimated at the actual system period.
5. For embedded foundations, repeat the analyses for $\tilde{T}/T$ and $\tilde{\zeta}_0$ using the formulation by Bielak (1975).

The procedures in steps 1 to 4 are referred to as the "modified Veletsos" formulation. The "modified" term refers to the extension of the basic model considered in Veletsos and Nair (1975) to account for embedded, non-circular, and flexible foundations, and non-uniform soil profiles. Similarly, the Bielak (1975) procedure applied in Step 5 to embedded structures is referred to as the "modified Bielak" formulation.

2.4.2 Kinematic Interaction

For surface foundations, analytical predictions of base-slab averaging effects are made using the transfer functions in Figs. 2.13 and 2.14. A topic of recommended future study is to compare these analytical transfer functions with transfer functions computed from recordings of surface foundation and free-field motion. From such a comparison, the effects of ground motion incoherence and incident wave inclination could be approximately quantified. Similarly, for embedded structures, the analytical transfer functions in Eqs. 2.17 and 2.18 should be validated against field performance data.

CHAPTER 3

SYSTEM IDENTIFICATION PROCEDURES FOR EVALUATING SOIL-STRUCTURE INTERACTION EFFECTS

3.1 Introduction

This chapter presents the methods of system identification used to evaluate dynamic properties of soil-structure systems from recordings of earthquake shaking at the sites included in this study. A review of relevant structural dynamics theory is initially presented in Section 3.2 to establish the framework within which these analyses were performed. Two system identification techniques, parametric and nonparametric analyses, are discussed in Sections 3.3 and 3.4. In Section 3.5, the specific system identification procedures used in this study are summarized, while the interpretation of results for different input-output pairs is discussed in Section 3.6.

3.1.1 Objectives

As illustrated schematically in Fig. 3.1(a), the fundamental objective of any system identification analysis is to evaluate the properties of an unknown system given a known input into, and output from, that system. For applications in this study, the system is generally associated with structural flexibility alone, or the structural flexibility coupled with foundation flexibility in rocking and/or translation. The inputs and outputs are various combinations of free-field, foundation, and roof-level recordings (Fig. 3.1b). The input-output pairs used to evaluate modal parameters for various cases of base fixity are discussed in Section 3.6.

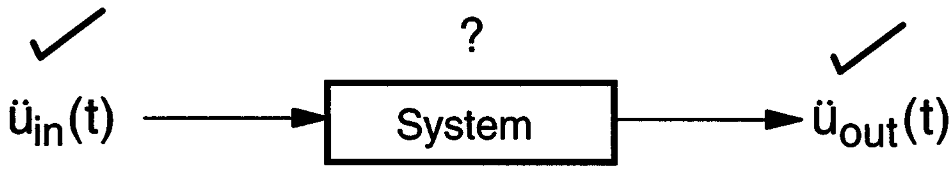

Fig. 3.1(a): Schematic of the system identification problem

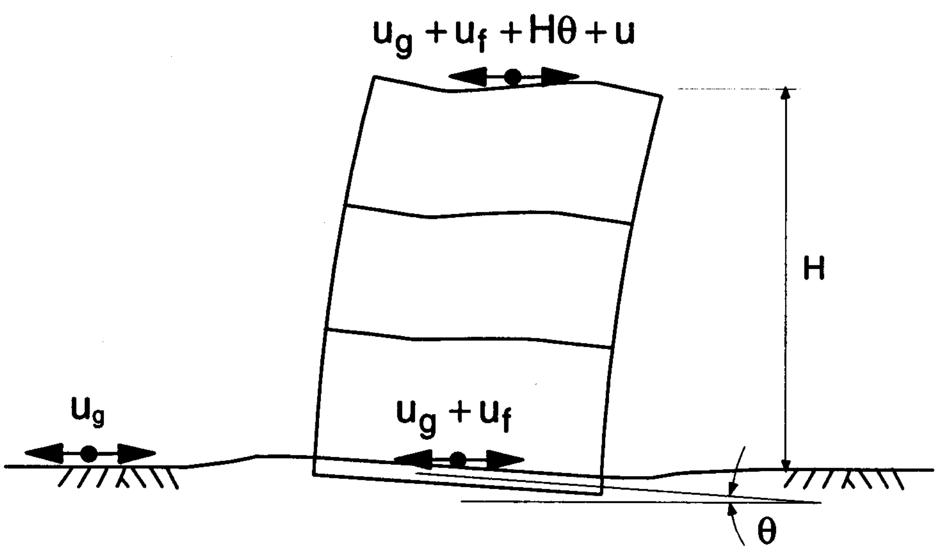

Fig. 3.1(b): Motions used as inputs and outputs for system identification of structures

The desired results from these system identification procedures are the following system properties:

1. Modal frequencies and damping ratios of the structures for the fixed- and flexible-base cases.
2. Transmissibility functions describing the frequency-dependent variations between input and output motions.

3.1.2 Fundamental Assumptions

A significant assumption made in the system identification analyses described in this chapter is that the dynamic response of soil-structure systems can be described by linear dynamic models with proportional damping. The validity of this assumption is suspect when structures are damaged or yield, or when pronounced soil degradation occurs. However, nonlinear systems generally can be modeled by linear systems with time-dependent parameters (Priestly, 1980). Hence, recursive analyses were employed in this study to track time-dependent changes of linear system parameters. These recursive results provide insight into possible structural damage during strong shaking, and serve as a "check" on simpler analyses assuming linear, time-invariant response.

It was also assumed that input and output motions used for system identification analyses were representative of their respective domains. For foundation motions, this implies that lateral and rocking motions at the same elevation are uniform, which strictly holds only for rigid foundation slabs. Roof motions are assumed to be not influenced by torsional deformations in the structure. Perhaps most significantly, recordings at free-field accelerographs are assumed to be representative of the free-field at large, which is seldom correct due to spatial incoherence effects. Although a given recorded motion (roof, foundation, or free-field) is unlikely to be perfectly representative of its domain, repeated identifications for sites with multiple input or output recordings generally revealed that identification results were relatively insensitive to the specific output or input motion chosen to represent a given domain.

3.2 Derivation of Transfer Functions from Modal Equations

Transfer functions describe the changes which occur to input signals as they pass though a system and emerge as output signals. In particular, as used here, transfer functions describe the modification of motions between single input and output points. Equations describing transfer functions for structures are derived in this section.

The properties of a linear structure with *n* degrees of freedom include its mass matrix **m**, stiffness matrix **k**, and damping matrix **c**. The damping matrix is intended to model energy dissipation in the structure, and is assumed to be "proportional" (i.e. a linear combination of the mass and stiffness matrices).

The dynamic displacements of the structure relative to its base are described by the *n*x1 vector $\mathbf{u}$, with corresponding velocity and acceleration vectors $\dot{\mathbf{u}}$ and $\ddot{\mathbf{u}}$, respectively. The total displacement vector $\mathbf{u}^t$ is the sum of the ground displacement u_g and the dynamic displacement of the structure,

$$\mathbf{u}^t(t) = \mathbf{u}(t) + \mathbf{1}^T u_g(t) \tag{3.1}$$

where **1**=a 1xn vector of 1's. The equation of motion for the structure is (Clough and Penzien, 1993):

$$\mathbf{m}\ddot{\mathbf{u}}(t) + \mathbf{c}\dot{\mathbf{u}}(t) + \mathbf{k}\mathbf{u}(t) = \mathbf{-m1}^{T}\ddot{u}_{g}(t) \tag{3.2}$$

The undamped eigenvalue problem for the structure, $\mathbf{k\Phi}_i=\omega_i^2\mathbf{m\Phi}_i$, gives the vibration frequencies, ω_i, and vibration mode shapes, $\mathbf{\Phi}_i$, for each mode *i*. The generalized mass of mode *i* is defined as $m_i^*=\mathbf{\Phi}_i^T\mathbf{m\Phi}_i$, and the generalized influence factor as $L_i^*=\mathbf{1}^T\mathbf{m\Phi}_i$.

The solution to Eq. 3.2 is exactly represented by superposition of all *n* vibration modes using generalized coordinates $X_i(t)$, but can also be reliably approximated by J<<n modes:

$$\mathbf{u}(t) \cong \sum_{i=1}^{J} \mathbf{\Phi}_i X_i(t) \tag{3.3}$$

Inserting Eq. 3.3 into Eq. 3.2, multiplying both sides by $\mathbf{\Phi}_j^T$, and taking advantage of mode orthogonality, the equation of motion for mode *j* can be expressed in terms of generalized coordinates as:

$$\ddot{X}_j(t) + 2\zeta_j\omega_j\dot{X}_j(t) + \omega_j^2 X(t) = -\frac{L_j^*}{m_j^*}\ddot{u}_g(t) \tag{3.4}$$

where ζ_j is the damping ratio for mode *j*. The solution to Eq. 3.4 is obtained through the use of Laplace transforms. The Laplace transform of a time-dependent function is expressed here as $f(t) = f(s)e^{st}$, where *s* is the operator in the Laplace domain. Using Laplace transforms, the solution of Eq. 3.4 is:

$$X_j(s) = \frac{-1}{s^2 + 2\zeta_j\omega_j s + \omega_j^2} \cdot \frac{L_j^*}{m_j^*}\ddot{u}_g(s) \tag{3.5}$$

Since strong motion recordings are of total acceleration, Eq. 3.1 is applied to Eq. 3.3 before taking its Laplace transform. The result, after differentiating twice with respect to time to convert to acceleration, is:

$$\ddot{\mathbf{u}}^{t}(s) = \sum_{j=1}^{J} \boldsymbol{\Phi}_j \ddot{X}_j(s) + \mathbf{1}^{T} \ddot{u}_g(s) \tag{3.6a}$$

where $\ddot{X}_j(s) = s^2 \cdot X_j(s)$. Making use of a relation modified from Fenves and Desroches (1994) to substitute into Eq. 3.6(a),

$$\mathbf{1}^{T} \approx \sum_{j=1}^{J} \frac{L_j{}^{*}}{m_j{}^{*}} \cdot \boldsymbol{\Phi}_j \tag{3.6b}$$

and substituting Eq. 3.5 into Eq. 3.6(a), the total structure accelerations can be related to the ground acceleration as follows:

$$\ddot{\mathbf{u}}^{t}(s) = \left[\sum_{j=1}^{J} \frac{L_j{}^{*}}{m_j{}^{*}} \cdot \boldsymbol{\Phi}_j \left(1 - \frac{s^2}{s^2 + 2\zeta_j \omega_j s + \omega_j{}^2} \right) \right] \ddot{u}_g(s) \tag{3.6c}$$

To simplify this expression, the total acceleration vector can be written as

$$\ddot{\mathbf{u}}^{t}(s) = \mathbf{H}(s) \ddot{u}_g(s) \tag{3.7a}$$

where,

$$\begin{aligned} \mathbf{H}(s) &= \sum_{j=1}^{J} \frac{L_j{}^{*}}{m_j{}^{*}} \cdot \boldsymbol{\Phi}_j \cdot H_j(s) \\ H_j(s) &= \frac{2\zeta_j \omega_j s + \omega_j{}^2}{s^2 + 2\zeta_j \omega_j s + \omega_j{}^2} \end{aligned} \tag{3.7b}$$

Element *j* of the vector quantity **H**(s) in Eq. 3.7(a) represents the transfer function between the ground (input) and degree-of-freedom *j* (output) in the superstructure.

Different recording locations within a structure exhibit the same poles, so generally it is adequate to consider only the output at the roof for identifying parameters for the lower, most significant modes. Hence, single-output system identification analyses were used in this study, which reduces the vector **H**(s) to a scalar function for the roof response. It should be noted that contributions from all *J* modes are represented in the single-output solution, although only fundamental-mode parameters are significantly affected by SSI (Jennings and Bielak, 1973).

The amplitude of a particular component of **H**(s) is a continuous surface with peaks located at poles which can be related to modal frequencies and damping ratios. When a component of **H**(s) is evaluated along the imaginary axis, the transmissibility function H(iω) is obtained, which gives the ratio of output-to-input acceleration as a function of frequency ω. The roof component of **H**(s) for an example structure is presented in Section 3.5.2(c).

3.3 Nonparametric System Identification

Nonparametric system identification is used to examine the dynamic response of structural systems by estimating the transmissibility function H(iω) for a given input-output pair. Transfer functions **H**(s) cannot be directly estimated by nonparametric techniques. Calculation of transmissibility functions and smoothing procedures for these functions are the subject of this section.

3.3.1 Transmissibility Functions

Transmissibility functions are useful for identifying vibration frequencies and frequency ranges over which amplification or de-amplification occurs. This section will describe how transmissibility functions are computed from an input x(t) and output y(t) accelerogram pair. The formulations are based on a single input, single output model, meaning that **H**(s) in Eq. 3.7 is a scalar quantity denoted as H(s); similarly **H**(iω) is denoted here as H(iω).

Fundamentally, the transmissibility function H(iω) represents the ratio of the Fourier transform of the output signal to that of the input signal. However, since the input signal is random, its Fourier transform may not exist (i.e. zero amplitude) at some frequencies, causing the H(iω) ratio to be undefined. For this reason, H(iω) is usually computed from power spectral density functions (S_x, S_y) and cross spectral density functions (S_{xy}) of the input and output signals, which always exist (Pandit, 1991).

For an ergodic and random process with zero mean, power spectra and cross power spectral density functions are Fourier transforms of the auto-correlation functions $R_x(\tau)$ and $R_y(\tau)$ and the cross-correlation function $R_{xy}(\tau)$ for processes x and y (Clough and Penzien, 1993):

$$\begin{aligned} S_x(\omega) &= \frac{1}{2\pi}\int_{-\infty}^{\infty} R_x(\tau)e^{-i\omega\tau}d\tau \\ S_y(\omega) &= \frac{1}{2\pi}\int_{-\infty}^{\infty} R_y(\tau)e^{-i\omega\tau}d\tau \\ S_{xy}(\omega) &= \frac{1}{2\pi}\int_{-\infty}^{\infty} R_{xy}(\tau)e^{-i\omega\tau}d\tau \end{aligned} \tag{3.8}$$

The functions S_x and S_y are real-valued, while S_{xy} is a complex-valued Hermitian function $S_{xy}=S^*_{yx}$ (where * denotes complex conjugation). The auto-correlation and cross-correlation functions are, in turn, defined from the discrete input and output signals as:

$$\begin{aligned} R_x(\tau) &= \sum_{t=0}^{N-|\tau|} x(t)x^*(t+\tau) \\ R_y(\tau) &= \sum_{t=0}^{N-|\tau|} y(t)y^*(t+\tau) \\ R_{xy}(\tau) &= \sum_{t=0}^{N-|\tau|} x(t)y^*(t+\tau) \end{aligned} \tag{3.9}$$

where, as before, * denotes complex conjugation and N = number of data points in the time histories x(t) and y(t).

Using the spectral density functions defined in Eq. 3.8, $H(i\omega)$ can be computed two ways (Ljung, 1987 and Pandit, 1991):

$$\begin{aligned} S_{yx}(\omega) &= H(i\omega)S_x(\omega) \\ S_y(\omega) &= H(i\omega)S_{xy}(\omega) \end{aligned} \tag{3.10}$$

Hence, two estimates of the complex-valued $H(i\omega)$ are possible:

$$\begin{aligned} H_1(i\omega) &= \frac{S_{yx}(\omega)}{S_x(\omega)} \\ H_2(i\omega) &= \frac{S_y(\omega)}{S_{xy}(\omega)} \end{aligned} \tag{3.11}$$

The two estimates of $H(i\omega)$ should theoretically be equal, but generally are not due to noise in the signals and other errors associated with the discrete Fourier transform. The $H_1(i\omega)$ estimate is less sensitive to output noise, while $H_2(i\omega)$ is less sensitive to input noise (Fenves and Desroches, 1994). The quality of the transmissibility function in the presence of noise and other errors can be assessed using the coherence function, which is defined as the ratio of the two estimates of H(iω) (Ljung, 1987 and Pandit, 1991):

$$\gamma^2(i\omega) = \frac{H_1(i\omega)}{H_2(i\omega)} = \frac{\left|S_{xy}(\omega)\right|^2}{S_x(\omega)S_y(\omega)} \tag{3.12}$$

The coherence varies between zero and one, and provides insight into the noise spectrum which is proportional to $1-\gamma^2(i\omega)$. The transmissibility function H(iω) is well estimated when the coherence is near unity because the signal to noise ratio is large. However, estimates of H(iω) with coherencies less than one are common in practice, indicating that the absolute value of $H_2(i\omega)$ exceeds the absolute value of $H_1(i\omega)$. Hence, $H_2(i\omega)$ gives larger peaks than $H_1(i\omega)$, and for this reason $H_2(i\omega)$ was used as the estimator of the transmissibility functions in order to illustrate the modal frequencies as clearly as possible.

3.3.2 Smoothing of Frequency Response Functions

Unsmoothed power spectral density, cross spectral density, and coherence functions computed using the procedures in Section 3.3.1 have a spiky appearance which can make the interpretation of these frequency response functions difficult. For this reason, some smoothing was performed using periodograms as estimates of spectral density functions (Oppenheim and Schafer, 1989). Periodograms employ an averaging procedure which smoothes the spectra by reducing the randomness associated with the estimation procedures.

The averaging procedure is based on the method by Welch (1967). The records are divided into equal length segments in time which may overlap. The Fast Fourier Transform (FFT) of each segment with a data window is computed. The periodogram is the average of the square of the FFT amplitudes for all the segments. In the case of the coherence functions, the averaging procedure is performed on each spectral density function in Eq. 3.12 before computing the coherence.

There is a tradeoff between the smoothness of a periodogram and error, or bias, relative to the true, unsmoothed spectrum (Pandit, 1991). As the number of segments used to compute the periodogram is increased, the results become smoother, but the frequency resolution is decreased and the peaks are flattened. In this study, periodograms were generally computed using four equal-length segments without overlap.

Tapering windows were used for each segment in a periodogram to reduce the statistical dependence between sections due to overlap and to diminish side lobe interference or "spectral leakage" while increasing the width of spectral peaks (Krauss et al., 1994). A Kaiser window with a factor of 15.7 was used for this purpose.

3.4 Parametric System Identification

3.4.1 Introduction

Problems can arise in identifying vibration properties of a structure solely by spectral analysis. In essence, recovery of the general transfer function surface $\mathbf{H}(s)$ from a discrete estimate of $\mathbf{H}(i\omega)$ with limited frequency resolution by the FFT can be problematic (Pandit, 1991). For this reason, it is desirable to identify a parameterized model of the structure in the discrete time domain from which a more robust estimate of the structure's vibration properties can be computed.

The model of the structure represented in continuous time by Eq. 3.7 must initially be converted to an equivalent model in the discrete time domain. The parameters describing this discrete time model are then estimated by least squares procedures to minimize the error between the model and the recorded output. This section will describe how these steps were performed for this study. As in Section 3.3.1, these formulations are based on a single input, single output model, so the transfer function is denoted as H(s).

3.4.2 Representation of Continuous Transfer Functions in Discrete Time

The equation of motion employed in Section 3.2 (Eq. 3.2) was based on a continuous time representation of a linear structural system. However, earthquake recordings of ground and structure motion are digital, and hence are data in the discrete time domain. In this section, the continuous time transfer function in Eq. 3.7 is modified to develop an equivalent discrete time representation.

A number of methodologies are presented in the literature for conversion from the continuous to discrete domain; these are summarized by Safak (1988 and 1991), Franklin and Powell (1980), and Åström and Wittenmark (1984). The methodology employed in this study is to approximate the transfer function by the hold-equivalence technique (Franklin and Powell, 1980). The continuous input is approximated by piece-wise constants (zero-order hold), and is passed through the continuous system to calculate the corresponding discrete output. The discrete transfer function is then determined by taking the ratio of the Z-transforms of the discrete output to that of the input. The result of this procedure is (Franklin and Powell, 1980),

$$H(z) = \left(1 - \frac{1}{z}\right) Z\left[\frac{H(s)}{s}\right] \tag{3.13}$$

where H(z) is the discrete time transfer function, z is the complex Z-transform operator, and Z[f] denotes the Z-transform of the function f. Applying Eq. 3.13 to Eq. 3.7(b),

$$H(z) = \sum_{j=1}^{J} \frac{\beta_{1j} z^{-1} + \beta_{2j} z^{-2}}{\alpha_{2j} z^{-2} + \alpha_{1j} z^{-1} + 1} \tag{3.14}$$

where the α and β parameters are related to the parameters in Eq. 3.7(b) by equations given in Åström and Wittenmark (1984). According to Safak (1991), the result in Eq. 3.14 can also be obtained using several other continuous-to-discrete conversion methodologies such as pole-zero mapping and covariance equivalence techniques.

The expression in Eq. 3.14 can be expanded as a rational polynomial (Safak, 1991),

$$H(z) = \frac{b_1 z^{-1} + b_2 z^{-2} + \ldots + b_{2J} z^{-2J}}{1 + a_1 z^{-1} + a_2 z^{-2} + \ldots + a_{2J} z^{-2J}} \tag{3.15}$$

which represents a discrete time filter of order 2J (the filter order is the highest power in the denominator). Note that the order of the filter, and hence the order of the model, is twice the number of modes being included in the structural idealization.

The model represented by the discrete time transfer function in Eq. 3.15 can be described as a linear difference equation which relates the input x(t) and output y(t),

$$\begin{aligned} &y(t) + a_1 y(t-1) + \ldots + a_{2J} y(t-2J) = \\ &b_1 x(t-d-1) + b_2 x(t-d-2) + \ldots + b_{2J} x(t-d-2J) \end{aligned} \tag{3.16}$$

where *d* is the time delay between the input and output (i.e. an input at time *t* creates an output at time t+d). The specific representation in Eq. 3.16 of the general model in Eq. 3.15 is referred to as an ARX model, for autoregressive model with extra input (Ljung, 1987).

3.4.3 Solution Procedures

Least squares techniques were used to solve for the parameters a_j and b_j in Eq. 3.16 which describe the discrete time transfer function. Two approaches were generally used for these analyses. First, a single set of a_j and b_j parameters was determined which minimizes the sum of the errors between the model and recorded output over all N time steps. This procedure is referred to as the cumulative error method (CEM), and its results are only accurate if the system properties are time invariant. In the second approach, separate sets of a_j and b_j parameters are determined for each time step. Referred to as the recursive prediction error method (RPEM), this approach enables the time variation of linear system properties to be tracked.

The solution procedures for the CEM and RPEM are summarized in Parts (a) and (b) of this section. Procedures for extracting modal frequencies and damping ratios from the a_j and b_j parameters are presented in Part (c), while uncertainty in the estimated model is discussed in Part (d). The CEM as employed here was originally presented in Safak (1991), while the RPEM was presented in Safak (1988) and Ghanem et al. (1991).

(a) *Model parameter estimation by the cumulative error method (CEM)*

To simplify the notation of the solution procedure, Eq. 3.16 is re-written by defining the following vectors:

$$\Gamma(t) = \left[-y(t-1) \quad -y(t-2) \quad \cdots \quad -y(t-2J) \quad x(t-d-1) \quad x(t-d-2) \quad \cdots \quad x(t-d-2J)\right]^T \tag{3.17}$$

and

$$\Theta = \left(a_1 \quad a_2 \quad \cdots \quad a_{2J} \quad b_1 \quad b_2 \quad \cdots \quad b_{2J}\right)^T \tag{3.18}$$

With these substitutions, Eq. 3.16 can be re-written as

$$y(t) = \Gamma^T(t)\Theta \tag{3.19}$$

Since x(t) and y(t) are the recorded time histories, $\Gamma(t)$ is known. The objective of the identification is then to determine the unknown vector Θ.

For a given Θ and time *t*, the error between the model and recorded output, $\varepsilon(t, \Theta)$, can be written as

$$\varepsilon(t,\Theta) = y(t) - \Gamma^T(t)\Theta \tag{3.20}$$

A measure of the cumulative error $V(\Theta)$ can then be taken as the sum of the squares of the errors for each time step as follows:

$$V(\Theta) = \frac{1}{N}\sum_{t=2J+d+1}^{N}\varepsilon^2(t,\Theta) = \frac{1}{N}\sum_{t=2J+d+1}^{N}\left(y(t) - \Gamma^T\Theta\right)^2 \tag{3.21}$$

The summation starts from t=2J+d+1 to prevent a negative time step from occurring in the formation of the Γ^T vector. The optimum set of parameters is determined by minimizing $V(\Theta)$ as,

$$\frac{dV(\Theta)}{d\Theta} = 0 \tag{3.22}$$

which leads to the following equation for Θ:

$$\Theta = \left[\sum_{t=2J+d+1}^{N} \Gamma(t)\Gamma^T(t) \right]^{-1} \left[\sum_{t=2J+d+1}^{N} \Gamma(t)y(t) \right] \tag{3.23}$$

With the vector Θ known, the discrete time transfer function for the system is completely determined.

(b) *Model parameter estimation by the recursive prediction error method (RPEM)*

The notation used here is similar to that in Part (a), namely, **Γ**(t) and **Θ** are defined by Eqs. 3.17 and 3.18, respectively, and the error, ε(t, Θ), at time step *t* is defined as

$$\varepsilon(t,\Theta) = y(t) - \Gamma^T(t)\Theta(t-1) \tag{3.24}$$

Note that the vector of estimated parameters Θ is now time dependent. The fundamental difference between the RPEM and CEM is that the total error is defined at each time step *t* by,

$$V(t,\Theta) = \frac{1}{2}\gamma(t) \sum_{\tau=2J+d+1}^{t} \beta(t,\tau)\varepsilon^2(\tau,\Theta) \tag{3.25}$$

where β(t, τ) is a weighting factor and γ(t) is the normalization factor for β(t, τ) defined by

$$\gamma(t) = \frac{1}{\sum_{\tau=2J+d+1}^{t} \beta(t,\tau)} \tag{3.26}$$

The $\beta(t, \tau)$ and $\gamma(t)$ factors define a window of time within which incremental errors $\varepsilon(\tau,\Theta)$ are included in the computation of total error $V(t, \Theta)$ for time step *t*. In this study, an exponential window was used with a constant forgetting factor λ (Ljung, 1987). For these conditions, the weighting factor is defined as,

$$\beta(t,\tau) = \lambda^{t-\tau} \tag{3.27}$$

The smaller the value of λ, the shorter is the window, and the more sensitive are the results to time dependent changes in the system properties. However, small data windows can be more susceptible to noise in the input and output signals. Hence, a tradeoff exists between the time-tracking ability of the analysis and the sensitivity of the solution to noise. In most cases, values of λ=0.98 to 0.99 were found to be appropriate.

As with the CEM, it is required with the RPEM to minimize the total error according to least squares criteria,

$$\frac{\partial V(t,\Theta)}{\partial \Theta} = \mathbf{V}'(t,\Theta) = 0 \tag{3.28a}$$

where $\mathbf{V'}$ is a vector of length 4J. Due to the randomness of the signals resulting from the noise in the system, the condition in Eq. 3.28(a) is met in an average sense by requiring,

$$E[\mathbf{V}'(t,\Theta)] = 0 \tag{3.28b}$$

where E denotes the expected value operator. The solution of Eq. 3.28(b) is obtained using stochastic approximation techniques (Safak, 1988). The result is the following recursive relationship for $\Theta(t)$:

$$\Theta(t) = \Theta(t-1) + \alpha_t\left[\mathbf{V}''(t,\Theta(t-1))\right]^{-1}\mathbf{V}'(t,\Theta(t-1)) \tag{3.29}$$

where α_t is a series of positive constants generally taken as α_t=1 (Safak, 1988).

The solution of Eq. 3.29 requires the estimation of the total error derivatives $\mathbf{V}''(t, \Theta)$ and $\mathbf{V}'(t, \Theta)$. The development of recursive relations for these derivatives is detailed in Safak (1988) and will not be repeated here. The final form of the recursion relation for the RPEM algorithm is (Safak, 1988 and Ljung, 1987),

$$\Theta(t) = \Theta(t-1) + \gamma(t)\mathbf{R}^{-1}(t)\Psi(t)\varepsilon(t,\Theta) \tag{3.30}$$

where α_t was taken as 1, $\mathbf{\Psi}(t)$ is defined for the case of an ARX model as

$$\Psi(t) = \begin{bmatrix} -y(t-1) & \cdots & -y(t-2J) & y(t-d-1) & \cdots & y(t-d-2J) \end{bmatrix}^T \tag{3.31}$$

and $\mathbf{R}(t, \Theta)$, a 4Jx4J matrix, is estimated as follows:

$$\mathbf{R}(t) = \mathbf{R}(t-1) + \gamma(t)\left[\Psi(t)\Psi^T(t) - \mathbf{R}(t-1)\right] \tag{3.32}$$

Numerical inversion procedures for $\mathbf{R}^{-1}(t)$ are discussed in Safak (1988). In order to start the recursion, initial values of the vectors $\Theta(0)$ and $\mathbf{\Psi}(0)$ and matrix $\gamma(0)\mathbf{R}^{-1}(0)$ are taken as

$$\Theta(0) = 0 \quad \Psi(0) = 0 \quad \gamma(0)\mathbf{R}^{-1}(t) = 10^4 \times \mathbf{I} \tag{3.33}$$

The initial conditions cause the results for $\Theta(t)$ early in the time history to be erratic and unreliable, though a stable solution is usually achieved subsequently. When erratic results extend through more than a few seconds of the time history as a result of the initial conditions in Eq. 3.33, a second RPEM analysis can be performed using initial conditions derived from parameters associated with an appropriate time step from the first analysis.

(c) *Evaluation of modal frequencies and damping ratios*

Once the parameters describing the discrete time transfer function (i.e. the Θ or Θ(t) vectors) have been determined, the frequencies and damping ratios corresponding to the *J* modes included in the analysis can be estimated. The poles of the discrete time transfer function are first identified as the roots of the denominator from Eq. 3.15,

$$1 + a_1 z^{-1} + a_2 z^{-2} + \ldots + a_{2J} z^{-2J} = 0 \tag{3.34}$$

The roots $z_1, z_2, \ldots, z_{2J}$ are complex numbers which lie within a unit circle in the complex plane for stable systems.

The poles of the discrete time transfer function are related to the poles in the Laplace domain by (Safak, 1991),

$$s_j = \frac{1}{\Delta t} \ln z_j \tag{3.35}$$

where Δt = the data sampling interval. The poles s_j are the roots of the transfer function denominator in Eq. 3.7(b), which can be expressed as the complex conjugate pair (Fenves and Desroches, 1994),

$$s_j, s^*_j = -\zeta_j \omega_j \pm i \omega_j \sqrt{1 - \zeta_j^2} \tag{3.36}$$

from which the modal frequencies and damping ratios can be computed as follows:

$$\begin{aligned} \omega_j &= \sqrt{s_j s^*_j} \\ \zeta_j &= -\frac{\mathrm{Re}(s_j)}{\omega_j} \end{aligned} \tag{3.37}$$

where $\mathrm{Re}(s_j)$ means to take the real part of the complex number s_j.

(d) *Uncertainty in the estimated model*

There is always uncertainty in models identified from parametric analyses due to imperfect model structures and disturbances in the output data (Ljung, 1995). Systematic errors can result from inadequate model structure (i.e. poor selection of the d or J parameters) which cannot be readily quantified. In this study, such errors were minimized through careful selection of the d and J parameters as described in Section 3.5.2(c). A second type of model variability results from random disturbances in the data. This variability is associated with how the model would change if the identification were repeated with the same model structure and input, but with a different realization of the output. This uncertainty can be readily quantified as part of the estimation of an ARX model.

3.5 Summary of System Identification Analysis Procedures

3.5.1 Data Preprocessing

Strong motion data must be preprocessed to provide satisfactory identifications of soil-structure systems. Preprocessing of data consists of baseline correction, removal of outliers, filtering, decimation, and synchronization and alignment of input and output. Many of these operations were performed by the agencies which provided much of the strong motion data used in this study (California Strong Motion Instrumentation Program, CSMIP, and United States Geological Survey, USGS).

Non-zero mean values in strong motion data represent static components of the system and low frequency drifts (Safak, 1991). These are removed via baseline correction, which is typically accomplished by subtracting the mean or using high-pass filters. Outliers in the data are erroneous peaks typically associated with instrument failure or accidental impact against the accelerograph. Baseline correction and removal of outliers from accelerograms is performed as part of the digitization process by CSMIP and USGS.

The objective of filtering is to remove the frequency components of data dominated by noise. These frequencies are at the low and high end of the spectrum, and are usually not of interest in system identification because they are far removed from the modal frequencies of typical soil-structure systems. The cutoff frequencies used in filtering vary somewhat from site to site due to variable accelerograph sensitivities, though typical high-pass cutoff frequencies are about 0.1 to 0.5 Hz and typical low-pass cutoff frequencies are about 15 to 50 Hz. Both CSMIP and USGS typically perform low- and high-pass filtering on accelerograms during processing (though much of the USGS data from the Northridge Earthquake was not low-pass filtered). The frequency cutoffs used for each site are indicated in Stewart (1997).

Decimation refers to a process by which the sampling rate of the time histories is decreased. Most accelerograms are originally digitized at a sampling interval of $\Delta t=0.005$ sec, and are decimated during processing to $\Delta t=0.01$ or 0.02 sec. An accelerogram contains information up to its Nyquist frequency, which is half the sampling rate in Hz (e.g. for $\Delta t=0.01$ sec, $f_{Nyq}=50$ Hz). In most buildings, the highest modal frequency of interest is much less than the Nyquist frequency, and hence the accelerograms can be further decimated without losing relevant information. In such cases, decimation was performed by first low-pass filtering the data with a corner at the desired new f_{Nyq} (8th order low-pass Chebyshev type I filter), and then re-sampling the resulting smoothed signal at the specified lower rate. The analysis summaries in Stewart (1997) indicate whether decimation was performed for a given set of records and the order of decimation (i.e. the factor by which the sampling rate was decreased).

Synchronization of accelerograms used in system identification analysis was necessary to ensure a constant start time. Sensors within a structure are usually connected to a central recorder, and hence are triggered simultaneously. At some recently instrumented sites, free-field instruments are also connected to the central recorder, so no synchronization was necessary. If any synchronization was required, it was generally between free-field and structural data. The required time shift was typically determined by maximizing the cross correlation between the vertical free-field and foundation accelerations. The cross correlations and associated time shifts are provided with the site data in Stewart (1997) for sites where synchronization was necessary.

At some sites, the azimuths of free-field and structural recordings were different. In such cases, the horizontal free-field data was rotated to align it with structural sensors.

3.5.2 Analysis Procedures

Key aspects of the analyses performed for each site are outlined in this section. Considerations in the selection of structural instruments are described, and the nonparametric and parametric system identification techniques are summarized. In general, the analyses were performed using routines written for the Matlab programming environment (Krauss et al., 1994 and Ljung, 1995). The results compiled for each site are not listed here, but are provided in Stewart (1997).

(a) *Instrument selection*

A given instrumented level of a structure typically had several sensors at different locations. Sensors were selected for use in system identification analysis by considering the following: (1) sensors should be located within the planes of lateral force resisting elements such as frames or shear walls, (2) for irregular structures, sensors should be located near the centers of mass and rigidity so that torsional contributions to the recorded motions are minimized, and (3) sensors at different elevations should be located directly over each other. Specific instruments used for each structure are listed in Stewart (1997).

(b) *Nonparametric system identification*

Transfer and coherence functions were computed for the transverse and longitudinal directions of the structure using roof/free-field, roof/foundation, and foundation/free-field output/input pairs. The amplitude and phase of the transmissibility function were examined to provide rough estimates of modal frequencies. Coherence functions were also computed to assess the reliability of the transmissibility function amplitudes. Each of these functions was smoothed according to the criteria in Section 3.3.2.

(c) *Parametric system identification*

The steps below were performed for input-output pairs of interest. The procedure is discussed using the example of the roof/free-field pair at Site A23 (Northridge Earthquake). These time histories are shown in the top two plots of Fig. 3.2.

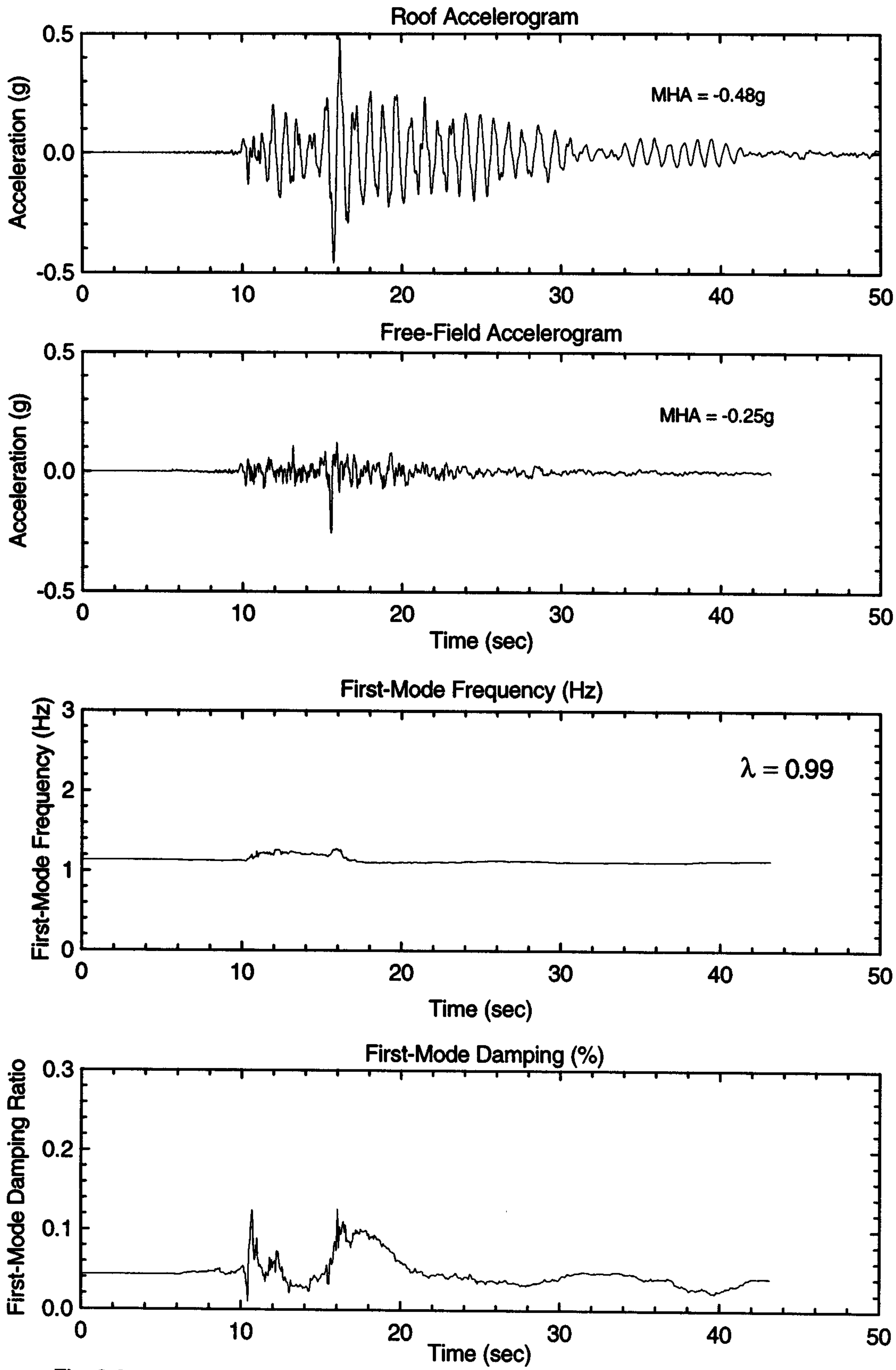

Fig. 3.2: Time variation of first-mode, flexible-base parameters for Site A23, transverse direction, 1994 Northridge Earthquake

1. Two user-defined parameters are needed to define the parametric model: the time delay, *d*, between the input and output motions, and the number of modes necessary to optimize the response, *J*. The delay is evaluated by examining the variation of cumulative error between the recorded output and model output as a function of *d* using a single mode, i.e. J=1. The value that minimizes the error for the example structure is d=2 time steps, as shown in Fig. 3.3. Using this delay, the model order is estimated by calculating the variation of error with *J*. Fig. 3.4 shows that the error initially decreases rapidly with *J*, but stabilizes beyond a value of J=4, which is the selected model order.

2. Using these *d* and *J* values, parameters describing the transfer function surface are calculated by the CEM. These parameters are used to define a transfer function surface with "poles" (high points) and "zeros" (low points). Fig. 3.9 presents the roof/free-field transfer function surface for the example structure with the axes on the horizontal plane scaled according to Eq. 3.37 to match the modal frequency and damping at the poles. The modal frequencies (ω_j) and damping ratios (ζ_j) computed from the complex-valued pole locations are indicated in Table 3.1. Standard deviations arising from random disturbances in the data are reported along with the mean values in Table 3.1. Coefficients of variation for first-mode parameters are usually about 0.5 to 1.5% for frequency and 5 to 15% for damping.

Table 3.1: Results of CEM parametric analyses for roof/free-field pair at Site A23, transverse direction, 1994 Northridge Earthquake

Mode	$\tilde{f}$ (Hz)	$\tilde{\zeta}$ (%)
1	1.12 ± 0.01	5.5 ± 0.5
2	3.85 ± 0.05	8.4 ± 1.0

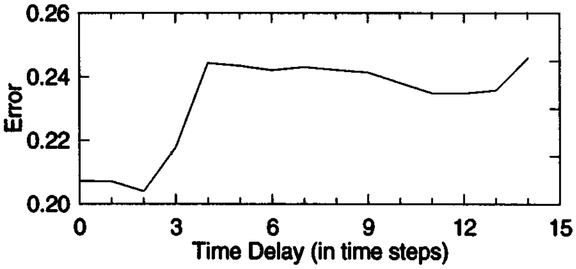

Fig. 3.3: Variation of Error with Time Delay

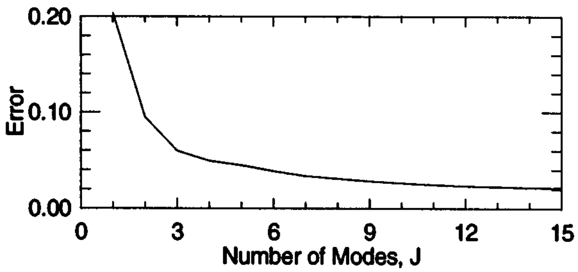

Fig. 3.4: Variation of Error with Number of Modes

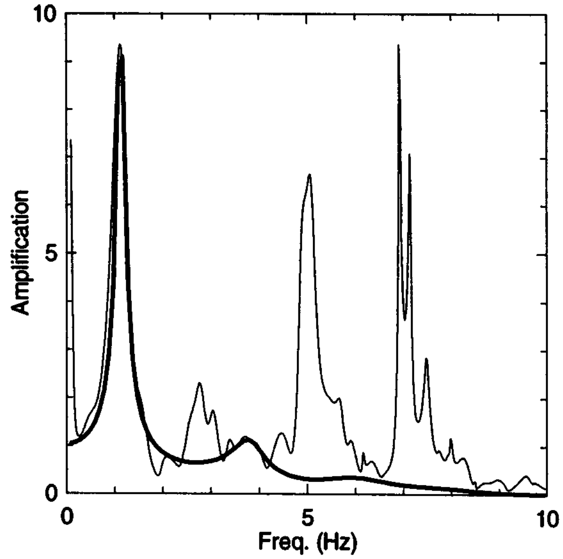

Fig. 3.5: Comparison of transmissibility functions from nonparametric analysis (light line) and parametric model (heavy line)

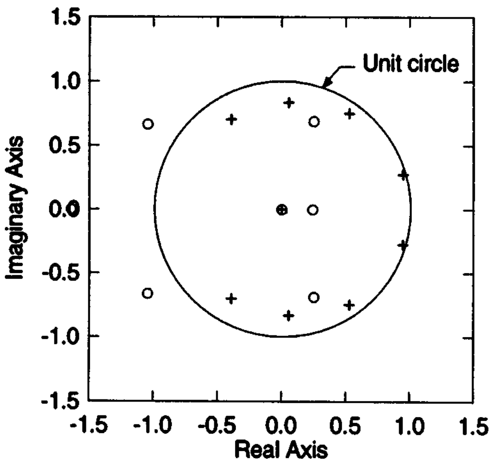

Fig. 3.6: Zeros (o) and poles (+) of the discrete-time transfer function

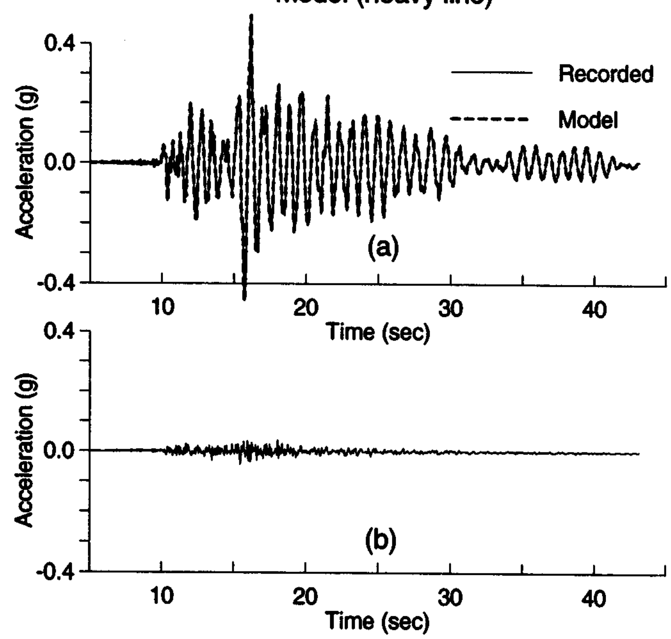

Fig. 3.7: (a) Comparison of model and recorded output, and (b) residual of identification for roof motions

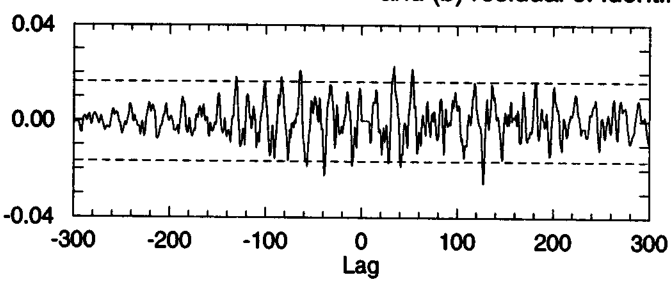

Fig. 3.8: Cross-correlation function between input and residual and 99% confidence limits of independence

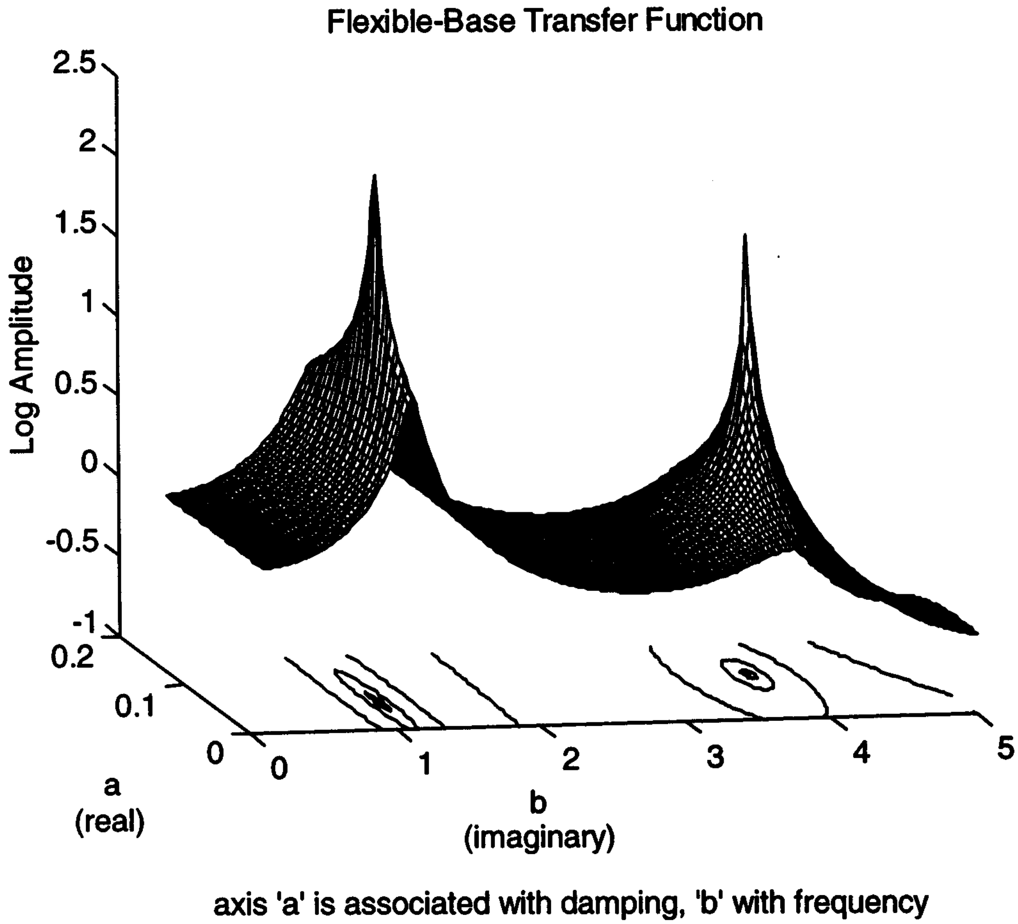

Fig. 3.9: Flexible-base transfer function surface identified by parametric system identification, Site A23, 1994 Northridge earthquake

3. The intersection of the model transfer function surface with the imaginary plane is compared to the nonparametric transmissibility function amplitude to check the model. Major peaks of the curves should occur at similar frequencies, but the amplitude match is not always good because nonparametric transmissibility functions are somewhat arbitrary due to their dependence on the smoothing technique used and the number of points in the FFT. As shown in Fig. 3.5, a good match is obtained near the first-mode frequency. The match is poor at higher frequencies, indicating the limited ability of transmissibility functions to capture higher mode responses containing relatively little seismic energy.

4. Additional checks on the parametric identification are performed as follows: (a) The unscaled poles and zeros of the transfer function are plotted in the complex plane to check for pole-zero cancellation (Fig. 3.6). The pole locations (s_j) in Fig. 3.6 are the unscaled counterparts to the pole locations on the horizontal plane in Fig. 3.9. The unscaled poles should always plot inside the unit circle, whereas zeros can be inside or outside the circle. If poles and zeros are found to overlap, the model is over-constrained and J is decreased. (b) The model and recorded outputs are compared, and the residual is computed (e.g. Fig. 3.7). This check is made to confirm that the residual is small compared to the recorded output, and that the residual has no dominant frequencies. (c) The cross-correlation of the residual with the input is computed to determine if there are components common to these time series (e.g. Fig. 3.8). The dashed lines in Fig. 3.8 are the 99% confidence intervals of independence, meaning that there is a 99% probability that the cross correlation will be contained within these limits if the residual and input are truly independent. Significant cross-correlation indicates that the model order should be

increased to better define the transfer function (Safak, 1988). However, high cross-correlation at negative lags is common and indicates output feedback in the input (Ljung, 1987). This is a product of SSI, and does not imply a problem with the model.

5. The nonlinearity of the structural response can be investigated using the time variability of first-mode parameters calculated by recursive parametric identification (Safak, 1988). These analyses are performed using the *d* and *J* values from Step 1. Plots of the time dependent first-mode frequencies and damping ratios for the example pair are presented in Fig. 3.2, from which an essentially time invariant first-mode response is observed.

3.6 Interpretation of Results

In system identification analysis of structural systems, the physical meaning of the results depends on the input and output motions used. The purpose of this section is to derive the input and output pairs used to evaluate fixed- and flexible-base modal parameters, and to describe how these parameters can be estimated when a direct identification is impossible as a result of insufficient instrumentation at a site.

3.6.1 Base Fixity Conditions for Different Input-Output Pairs

In this section, transfer functions and corresponding pole descriptions for different input-output pairs are derived in terms of soil, foundation, and structure properties. Expressions for the frequencies and damping ratios associated with the poles are then derived so that relationships between these modal parameters and the system properties can be defined.

The interpretation of the modal parameters that are identified from different input-output pairs is made with respect to the simple SSI model shown in Fig. 2.2. Single degree-of-freedom structural models are commonly employed in SSI analyses because inertial interaction effects are most pronounced in the first mode. As noted in Section 2.2.1, if this simple system represents an approximate model of a multi-mode, multi-storey structure, the height *h* is the distance from the base to the centroid of the intertial forces associated with the first vibration mode, and displacement *u* is that of the centroid. The effective displacement in Fig. 2.2 is different than the roof displacement used for single-output system identification. This use of different displacements in the single degree-of-freedom model and the system identification does not affect the location of the poles, and fundamental mode parameters derived from the system identification procedures in Section 3.4 can be used in conjunction with the simple model in Fig. 2.2.

As shown in Fig. 2.2, the displacement of mass *m* has contributions from structural deformation u, free-field motion u_g, and foundation translation and rocking, u_f and $h\theta$, respectively. The equations of motion describing the simple system in Fig. 2.2 are as follows (Chopra and Gutierrez, 1973),

lateral at m: $$m(\ddot{u}_f + h\ddot{\theta} + \ddot{u}) + c\dot{u} + ku = -m\ddot{u}_g \tag{3.38a}$$

total lateral: $$m(\ddot{u}_f + h\ddot{\theta} + \ddot{u}) + m_f\ddot{u}_f + c_u\dot{u}_f + k_u u_f = -(m + m_f)\ddot{u}_g \tag{3.38b}$$

total rotation: $$mh(\ddot{u}_f + h\ddot{\theta} + \ddot{u}) + I\ddot{\theta} + c_\theta\dot{\theta} + k_\theta\theta = -mh\ddot{u}_g \tag{3.38c}$$

where I is the rotational moment of inertia of the structure, and k_u, c_u, k_θ, and c_θ are foundation impedance values (Eq. 2.4) evaluated at the frequency of the soil-structure system. Eq. 3.38a-c are divided through by m, m+m_f, and mh, respectively, and the time-dependent functions are transformed to the Laplace domain according to $f(t) = \hat{f}e^{st}$.

With this transformation, the quantities $\hat{k}_u$, $\hat{c}_u$, $\hat{k}_\theta$, and $\hat{c}_\theta$ are interpreted as foundation impedance values in the Laplace domain evaluated at the pole of the transfer function being sought. With these substitutions, Eqs. 3.38a-c can be re-written as,

$$s^2\hat{u}_f + s^2 h\hat{\theta} + A\hat{u} = -s^2\hat{u}_g \tag{3.39a}$$

$$A_u\hat{u}_f + s^2\mu h\hat{\theta} + s^2\mu\hat{u} = -s^2\hat{u}_g \tag{3.39b}$$

$$s^2\hat{u}_f + A_\theta h\hat{\theta} + s^2\hat{u} = -s^2\hat{u}_g \tag{3.39c}$$

where μ = m/(m+m_f). Neglecting the rotational inertia of the structure and the mass of the foundation (i.e. I = 0, μ = 1), the A coefficients are defined as

$$A = s^2 + 2\zeta\omega s + \omega^2 \tag{3.40a}$$

$$A_u = s^2 + 2\zeta_u\omega_u s + \omega_u^2 \tag{3.40b}$$

$$A_\theta = s^2 + 2\zeta_\theta\omega_\theta s + \omega_\theta^2 \tag{3.40c}$$

where the frequencies and damping ratios in Eqs. 3.40a-c describe the dynamic behavior of the structure (ω, ζ) or soil-foundation system (ω_u, ζ_u and $\omega_\theta, \zeta_\theta$). These parameters are related to the system properties in Fig. 2.2 as follows,

$$\omega^2 = \frac{\hat{k}}{m} \qquad \zeta = \frac{\hat{c}}{2m\omega} \tag{3.41a}$$

$$\omega_u^2 = \frac{\hat{k}_u}{m} \qquad \zeta_u = \frac{\hat{c}_u}{2m\omega_u} \tag{3.41b}$$

$$\omega_\theta^2 = \frac{\hat{k}_\theta}{mh^2} \qquad \zeta_\theta = \frac{\hat{c}_\theta}{2mh^2\omega_\theta} \tag{3.41c}$$

In Eqs. 3.39a-c, there are three unknown response functions (u, u_f, and θ) and three equations. Hence, the deformations can be solved for directly in terms of the system properties, with the results that follow:

$$\frac{\hat{u}}{\hat{u}_g} = \frac{-B_\theta B_u s^2}{s^2\left(B_u B + B_u B_\theta + B_\theta B\right) + B_u B B_\theta} = -\frac{B_\theta B_u s^2}{C_s} \tag{3.42a}$$

$$\frac{\hat{u}_f}{\hat{u}_g} = -\frac{B_\theta B s^2}{C_s} \tag{3.42b}$$

$$\frac{h\hat{\theta}}{\hat{u}_g} = -\frac{B B_u s^2}{C_s} \tag{3.42c}$$

where $B = A - s^2$, $B_u = A_u - s^2$, $B_\theta = A_\theta - s^2$, and $C_s = s^2\left(B_u B + B_u B_\theta + B_\theta B\right) + B_u B B_\theta$.

Eqs. 3.42a-c represent the complete solution for the simple structure in Fig. 2.2, so any transfer function of interest can be directly evaluated from these results. Three specific input-output pairs are considered in the following Parts (a) to (c).

(a) *Flexible-base*

For the flexible-base case, the input is the free-field ground motion (u_g) and the output is the total motion at the roof level ($u_g + u_f + h\theta + u$). The transfer function is defined as the ratio of these two motions,

$$H_a(s) = \frac{\hat{u}_g + \hat{u}_f + h\hat{\theta} + \hat{u}}{\hat{u}_g} = \frac{\hat{u}_g\left(1 + \hat{u}_f/\hat{u}_g + h\hat{\theta}/\hat{u}_g + \hat{u}/\hat{u}_g\right)}{\hat{u}_g} \tag{3.43}$$

Substituting Eqs. 3.42 into Eq. 3.43 and simplifying,

$$H_a(s) = \frac{B_u B B_\theta}{C_s} \tag{3.44}$$

The poles for the flexible-base case are defined as those values of *s* for which $C_S = 0$. Expanding C_S in terms of the system properties and ignoring small terms which are the product of two damping ratios, a 3rd order polynomial in *s* is found as follows,

$$\begin{aligned} C_s = \; & 2s^3\left[\zeta\omega\left(\omega_u^2 + \omega_\theta^2\right) + \zeta_u\omega_u\left(\omega^2 + \omega_\theta^2\right) + \zeta_\theta\omega_\theta\left(\omega_u^2 + \omega^2\right)\right] + \cdots \\ & s^2\left(\omega^2\omega_u^2 + \omega_\theta^2\omega_u^2 + \omega^2\omega_\theta^2\right) + \cdots \\ & 2s\left(\zeta\omega\omega_u^2\omega_\theta^2 + \zeta_u\omega_u\omega^2\omega_\theta^2 + \zeta_\theta\omega_\theta\omega_u^2\omega^2\right) + \omega_\theta^2\omega_u^2\omega^2 \end{aligned} \tag{3.45a}$$

which can be re-written as

$$C_S = A_1 s^3 + A_2 s^2 + A_3 s + A_4 \tag{3.45b}$$

where

$$\begin{aligned} A_1 &= 2\left[\zeta\omega\left(\omega_u^2 + \omega_\theta^2\right) + \zeta_u\omega_u\left(\omega^2 + \omega_\theta^2\right) + \zeta_\theta\omega_\theta\left(\omega_u^2 + \omega^2\right)\right] \\ A_2 &= \left(\omega^2\omega_u^2 + \omega_\theta^2\omega_u^2 + \omega^2\omega_\theta^2\right) \\ A_3 &= 2\left(\zeta\omega\omega_u^2\omega_\theta^2 + \zeta_u\omega_u\omega^2\omega_\theta^2 + \zeta_\theta\omega_\theta\omega_u^2\omega^2\right) \\ A_4 &= \omega_\theta^2\omega_u^2\omega^2 \end{aligned} \tag{3.45c-f}$$

Finding the roots of the third-order polynomial in Eq. 3.45(a) is a non-trivial algebraic problem, though it is known from the factors in Eqs. 3.45c-f that the discriminant is positive and hence there are one real and two complex conjugate roots. Of these, only the complex conjugate roots are physically meaningful. The complex conjugate roots were found to be well approximated by an expression with the same form as Eq. 3.36, but with system frequency and damping ($\tilde{\omega}$ and $\tilde{\zeta}$) defined as,

$$\tilde{\omega}^2 = \frac{A_4}{A_1} = \frac{\omega_\theta^2 \omega_u^2 \omega^2}{\omega^2 \omega_u^2 + \omega_\theta^2 \omega_u^2 + \omega^2 \omega_\theta^2} = \frac{1}{\frac{1}{\omega_\theta^2} + \frac{1}{\omega^2} + \frac{1}{\omega_u^2}} \qquad (3.46a)$$

and

$$\frac{\tilde{\zeta}}{\tilde{\omega}} = \frac{A_2 A_3 - A_4 A_1}{2 A_2 A_4} \qquad (3.46b)$$

which simplifies to,

$$\tilde{\zeta} = \left(\frac{\tilde{\omega}}{\omega_u}\right)^3 \zeta_u + \left(\frac{\tilde{\omega}}{\omega}\right)^3 \zeta + \left(\frac{\tilde{\omega}}{\omega_\theta}\right)^3 \zeta_\theta \qquad (3.46c)$$

Eqs. 3.46a-c are an approximate representation of the roots to Eq. 3.45(a) because terms which are the product of damping ratios are neglected.

These results indicate that flexible-base parameters are dependent on the foundation impedance in translation and rocking and the structural parameters.

(b) *Pseudo flexible-base*

The pseudo flexible-base case applies for a condition of partial base flexibility, representing base rocking only. This condition is important because actual flexible-base parameters are often well-approximated by pseudo flexible-base parameters. Furthermore, pseudo flexible-base parameters can be used in procedures to estimate either fixed- or flexible-base parameters (see Section 3.6.2). For the pseudo flexible-base case, the input is the total base translation (u_g+u_f) and the output is the total motion at the roof level ($u_g + u_f + h\theta + u$). Proceeding as in Part (a), the transfer function is,

$$H_b(s) = \frac{\hat{u}_g + \hat{u}_f + h\hat{\theta} + \hat{u}}{\hat{u}_g + \hat{u}_f} = \frac{\hat{u}_g\left(1 + \hat{u}_f/\hat{u}_g + h\hat{\theta}/\hat{u}_g + \hat{u}/\hat{u}_g\right)}{\hat{u}_g\left(1 + \hat{u}_f/\hat{u}_g\right)} = \frac{B_u B B_\theta}{C_s - s^2 B_\theta B} \tag{3.47}$$

The denominator is again a 3rd order polynomial in *s*,

$$\begin{aligned} & C_s - s^2 B_\theta B = \\ & 2s^3\left[\zeta\omega\omega_u^2 + \zeta_u\omega_u\left(\omega^2 + \omega_\theta^2\right) + \zeta_\theta\omega_\theta\omega_u^2\right] + \cdots \\ & s^2\left(\omega^2\omega_u^2 + \omega_\theta^2\omega_u^2\right) + \cdots \\ & 2s\left(\zeta\omega\omega_u^2\omega_\theta^2 + \zeta_u\omega_u\omega^2\omega_\theta^2 + \zeta_\theta\omega_\theta\omega_u^2\omega^2\right) + \omega_\theta^2\omega_u^2\omega^2 \end{aligned} \tag{3.48}$$

from which the system frequency and damping ratio can be evaluated as,

$$\left(\tilde{\omega}^2\right)^* = \frac{\omega_\theta^2\omega_u^2\omega^2}{\omega^2\omega_u^2 + \omega_\theta^2\omega_u^2} = \frac{1}{\dfrac{1}{\omega_\theta^2} + \dfrac{1}{\omega^2}} \tag{3.49a}$$

$$\left(\tilde{\zeta}\right)^* = \left(\frac{\tilde{\omega}^*}{\omega}\right)^3 \zeta + \left(\frac{\tilde{\omega}^*}{\omega_\theta}\right)^3 \zeta_\theta \tag{3.49b}$$

From Eqs. 3.49a-b, pseudo flexible-base parameters are seen to be dependent on the rocking impedance of the foundation and the structural properties. It may be noted that flexible- and pseudo flexible-base parameters are numerically similar when base rocking dominates the SSI (which, excepting broad, short structures, is often true).

(c) *Fixed-base*

For the fixed-base case, the input is the sum of the total base translation and the contribution of base rocking to roof translation (u_g+u_f+$h\theta$), and the output is the total motion at the roof level ($u_g + u_f + h\theta + u$). Proceeding as with Parts (a) and (b), the transfer function is,

$$H_c(s) = \frac{\hat{u}_g + \hat{u}_f + h\hat{\theta} + \hat{u}}{\hat{u}_g + \hat{u}_f + h\hat{\theta}} = \frac{\hat{u}_g\left(1+ \hat{u}_f/\hat{u}_g + h\hat{\theta}/\hat{u}_g + \hat{u}/\hat{u}_g\right)}{\hat{u}_g\left(1+ \hat{u}_f/\hat{u}_g + h\hat{\theta}/\hat{u}_g\right)} = \frac{B_u B B_\theta}{C_s - s^2\left(B_\theta B + B B_u\right)} \tag{3.50}$$

The denominator in this case can be reduced to the product of a first- and second-order polynomial in *s*,

$$\begin{gathered} C_s - s^2\left(B_\theta B + B B_u\right) = \\ \left[2s\left(\zeta_u\omega_u\omega_\theta^2 + \zeta_\theta\omega_\theta\omega_u^2\right) + \omega_\theta^2\omega_u^2\right]\left(s^2 + 2\zeta\omega s + \omega^2\right) \end{gathered} \tag{3.51}$$

The second-order polynomial in Eq. 3.51 is the same as the denominator of Eq. 3.7(b). Hence, by analogy to that solution, the fixed-base parameters identified from this analysis are simply ω and ζ, respectively.

(d) *Summary*

The results presented in parts (a)-(c) show that a component of system flexibility is absent from the parametric system identification results when its associated motion is added to u_g in the input. For example, in Part (b), when the base translation motion is added to u_g in the input, the results represent only the structural flexibility and rocking foundation flexibility (i.e. base translation effects are “removed”). Similarly, when base rocking and translation are added to u_g for the input in Part (c), the only remaining system flexibility is that of the structure.

The input and output required to evaluate system parameters for various conditions of base fixity are summarized in Table 3.2. These same results were derived by Luco (1980a), who solved the equations of motion (i.e. Eqs. 3.38a-c) in the frequency domain to determine the input-output pairs necessary for evaluations of flexible-, pseudo flexible-, and fixed-base modal parameters using nonparametric identification procedures. The advantage of the present approach is that the more accurate estimates of transfer functions from parametric identification can be used to derive fundamental mode vibration parameters for various conditions of base fixity.

Table 3.2: Required input and output to evaluate system parameters for various conditions of base fixity

	System	Input	Output
a	Flexible-Base	u_g	$u_g + u_f + h\theta + u$
b	Pseudo Flexible-Base	$u_g + u_f$	$u_g + u_f + h\theta + u$
c	Fixed-Base	$u_g + u_f + h\theta$	$u_g + u_f + h\theta + u$

3.6.2 Estimation of Fixed and Flexible-Base Modal Parameters

Based on the results in Table 3.2, it is necessary to have recordings of free-field, foundation and roof translations as well as base rocking to evaluate directly both fixed- and flexible-base modal parameters of structures. If no recordings of roof translation are available, no modal parameters can be identified. However, if one of the other three motions is missing, the set of modal parameters not directly evaluated can be estimated. The two specific cases that will be considered here are missing base rocking motions (in which case fixed-base parameters are estimated), and missing free-field motions (in which case flexible-base parameters are estimated). The derivations in this section are made with respect to the single degree-of-freedom model in Fig. 2.2. For multi-mode structures, the quantities *m* and *h* are the effective mass and height, respectively. Although *m* and *h* are functions of participation factors (which are not identified), the fundamental frequency and damping ratio are generally insensitive to reasonable estimates of *m* and *h*.

Verification of these parameter estimation procedures is presented in Section 5.3.2 using results from sites where all three sets of modal parameters were directly evaluated from system identification analyses.

(a) *Estimation of fixed-base modal parameters (missing base rocking motions)*

It will be shown in this section that fixed-base modal parameters for a structure can be estimated from "known" flexible- and pseudo flexible-base parameters. Hence, it is assumed that $\tilde{\omega}$, $\tilde{\zeta}$, $\tilde{\omega}^*$, and $\tilde{\zeta}^*$ have been determined from system identification analyses [Cases (a) and (b) in Table 3.2]. Considering frequency first, Eqs. 3.46(a) and 3.49(a) are re-written as,

$$\begin{aligned} \frac{1}{\tilde{\omega}^2} &= \frac{1}{\omega^2} + \frac{1}{\omega_\theta^2} + \frac{1}{\omega_u^2} \\ \frac{1}{\left(\tilde{\omega}^2\right)^*} &= \frac{1}{\omega^2} + \frac{1}{\omega_\theta^2} \end{aligned} \tag{3.52}$$

from which ω_u can be readily determined as

$$\frac{1}{\omega_u^2} = \frac{1}{\tilde{\omega}^2} - \frac{1}{\left(\tilde{\omega}^2\right)^*} \tag{3.53}$$

The ratio of ω_θ to ω_u is then taken using Eq. 3.41 to evaluate ω_θ as follows,

$$\left(\frac{\omega_\theta}{\omega_u}\right)^2 = \frac{\hat{k}_\theta / mh^2}{\hat{k}_u / m} = \frac{K_\theta \cdot \hat{\alpha}_\theta(s) \cdot \frac{1}{h^2}}{K_u \cdot \hat{\alpha}_u(s)} \tag{3.54}$$

where $\hat{\alpha}_u$ and $\hat{\alpha}_\theta$ are modifiers to the static foundation impedance defined in the Laplace domain (similar to the frequency dependent α factors defined in Eq. 2.4).

For surface foundations, Eq. 3.54 can be simplified using the impedance for a rigid circular disk foundation on the surface of a homogeneous, isotropic halfspace. In this case, the static stiffnesses are as indicated in Eq. 2.5, and the ratio of ω_θ to ω_u can be expressed as,

$$\left(\frac{\omega_\theta}{\omega_u}\right)^2 = \left(\frac{r_2^3}{r_1 h^2}\right)\left(\frac{2-\upsilon}{3(1-\upsilon)}\right)\left(\frac{\hat{\alpha}_\theta(s)}{\hat{\alpha}_u(s)}\right) \tag{3.55}$$

where r_2 and r_1 are defined in Eq. 2.3. Assuming the effective structure height, foundation geometry, and soil Poisson's ratio are known, the only unknown quantity in Eq. 3.55 is the ratio of dynamic factors $\hat{\alpha}_\theta / \hat{\alpha}_u$. In the frequency domain, the factors α_u and α_θ are commonly evaluated as functions of both frequency and soil hysteretic damping. Hence, such solutions may also be considered valid in the Laplace domain. As an approximation, the ratio $\hat{\alpha}_\theta / \hat{\alpha}_u$ can be computed for surface foundations using the frequency dependent impedance factors for a circular foundation on a uniform viscoelastic half-space derived by Veletsos and Verbic (1973). As shown in Fig. 2.3, both factors are nearly unity for the low frequencies of most structures ($a_0 < 1$), so the $\hat{\alpha}_\theta / \hat{\alpha}_u$ ratio should not significantly affect the results.

For embedded foundations, Eq. 3.54 can be simplified using the impedance for a rigid circular disk foundation embedded into a homogeneous, isotropic halfspace. Using the solution by Elsabee and Morray (1977) for shallowly embedded (e/r < 1) foundations discussed in Section 2.2.2(d), the solution of Eq. 3.54 is reduced to

$$\left(\frac{\omega_\theta}{\omega_u}\right)^2 = \left(\frac{r_2^3}{r_1 h^2}\right)\left(\frac{2-\upsilon}{3(1-\upsilon)}\right)\left(\frac{\hat{\alpha}_\theta(s)}{\hat{\alpha}_u(s)}\right)\left(\frac{1+2(e/r)}{1+0.67(e/r)}\right) \tag{3.56}$$

where $\hat{\alpha}_\theta$ and $\hat{\alpha}_u$ are derived for surface foundations.

Obviously, use of Elsabee and Morray's approximate solution for embedded foundation impedance increases the expected error in estimates of the ratio ω_θ / ω_u. However, for the moderate embedment ratios of many building structures (e/r < 0.5), this error is expected to be small.

Once ω_θ is computed from Eqs. 3.55 or 3.56, the fixed-base frequency can be readily computed from Eq. 3.49(a) as,

$$\frac{1}{\omega^2} = \frac{1}{\left(\tilde{\omega}^2\right)^*} - \frac{1}{\omega_\theta^2} \tag{3.57}$$

The evaluation of fixed-base damping involves slightly more algebra, but the same principles apply. Eqs. 3.46(c) and 3.49(b) are used in conjunction with the ratio of the damping definitions for ζ_u and ζ_θ (Eq. 3.41) to evaluate the unknown damping quantities ζ_u, ζ_θ, and ζ. The result is as follows,

$$\zeta = \frac{1}{C_1} \cdot \tilde{\zeta} - \frac{C_2}{C_1} \tilde{\zeta}^* \tag{3.58a}$$

where

$$C_1 = \left(\frac{\tilde{\omega}}{\omega}\right)^3 - C_3 \frac{\left(\tilde{\omega}^* / \omega\right)^3}{\left(\tilde{\omega}^* / \omega_\theta\right)^3} \qquad C_2 = \frac{C_3}{\left(\tilde{\omega}^* / \omega_\theta\right)^3}$$

$$C_3 = C_4 \left(\frac{\tilde{\omega}}{\omega_u}\right)^3 + \left(\frac{\tilde{\omega}}{\omega_\theta}\right)^3 \qquad C_4 = \frac{\omega_\theta}{\omega_u} \cdot \frac{\hat{\beta}_u}{\hat{\beta}_\theta} \cdot \frac{r_1^2 h^2}{r_2^4} \cdot \frac{3(1-\upsilon)}{2-\upsilon} \tag{3.58b-e}$$

The terms $\hat{\beta}_u$ and $\hat{\beta}_\theta$ in C_4 are dimensionless dashpot coefficients similar to the β_u and β_θ terms in Eq. 2.4. The only assumption made in this analysis is that the ratio of soil damping factors $\hat{\beta}_u / \hat{\beta}_\theta$ can be computed from the formulation in Veletsos and Verbic (1973), with appropriate corrections for foundation embedment, shape, and non-rigidity effects. Even for surface foundations and low frequencies, these factors can be quite sensitive to frequency and hysteretic soil damping (e.g. Fig. 2.3), so the evaluation of $\hat{\beta}_u / \hat{\beta}_\theta$ may be subject to significant errors. These errors are compounded for embedded foundations because radiation damping from basement-wall/soil interaction is not rigorously accounted for in the estimation of $\hat{\beta}_u$ and $\hat{\beta}_\theta$. Hence, estimates of fixed-base damping are subject to greater uncertainty than estimates of fixed-base frequency.

(b) *Estimation of flexible-base modal parameters (missing free-field motions)*

For the derivation of flexible-base modal parameters, it is assumed that fixed- and pseudo flexible-base system identification analyses have been performed [Cases (b) and (c) in Table 3.2]. Hence, parameters $\tilde{\omega}^*$, $\tilde{\zeta}^*$, ω, and ζ are assumed known. The derivation follows the same steps as in Part (a). Using Eq. 3.49(a), ω_θ is evaluated as

$$\frac{1}{\omega_\theta^2} = \frac{1}{\left(\tilde{\omega}^2\right)^*} - \frac{1}{\omega^2} \tag{3.59}$$

Frequency ω_u is computed from the ratio ω_θ/ω_u in Eqs. 3.55 or 3.56, and the flexible-base frequency is determined directly from Eq. 3.46(a).

For the case of damping, the algebra is less lengthy than Part (a). The first step is the calculation of ζ_θ from Eq. 3.49(b),

$$\zeta_\theta = \frac{\tilde{\zeta}^* - \left(\tilde{\omega}^* / \omega\right)^3 \zeta}{\left(\tilde{\omega}^* / \omega_\theta\right)^3} \tag{3.60}$$

Damping ζ_u is then evaluated from the following,

$$\zeta_u = \zeta_\theta \frac{\omega_\theta}{\omega_u} \cdot \frac{\hat{\beta}_u}{\hat{\beta}_\theta} \cdot \frac{r_1^2 h^2}{r_2^4} \cdot \frac{3(1-\upsilon)}{2-\upsilon} \tag{3.61}$$

and the flexible-base damping is determined directly from Eq. 3.46(c).

The same limitations on solution accuracy that were stated in Part (a) apply here as well. Namely, the accuracy of estimated flexible-base frequency is generally better than the accuracy of flexible-base damping, especially for embedded foundations.

CHAPTER 4

SELECTION OF SITES AND CONDITIONS CONSIDERED

Two general classes of sites were used in this study for empirical evaluations of SSI effects. The first, denoted as 'A' sites, have a free-field accelerograph and a structure instrumented to record base and roof translations. A few of the structures at 'A' sites are also instrumented to record base rocking. The second class of sites ('B' sites) have structures instrumented to record base rocking as well as base and roof translations, but have no free-field accelerographs. This chapter presents the criteria employed for the selection of 'A' sites. Criteria for the selection of 'B' sites are relatively trivial, as structures at these sites merely needed the appropriate instrumentation. This chapter is concluded with a summary of the geotechnical, structural, and ground shaking conditions at the 'A' and 'B' sites.

4.1 Site Selection Criteria: 'A' Sites

The key consideration for the selection of 'A' sites was the degree to which "free-field" motions recorded near a building are likely to remain pure of contamination from structural vibrations or excessive spatial incoherence. For most sites, the suitability of "free-field" recordings was evaluated based on the distance separating the structure and free-field instrument, with due consideration of the structure's fundamental frequency and the site conditions. This section presents criteria for evaluating conditions for which "free-field" instruments are too close or too far from a structure.

4.1.1 Effects of Building Vibrations on Ground Motions

A number of studies have sought to quantify ground motions induced by structural vibrations. Analytical studies have examined (a) two-dimensional shear walls on both an undamped elastic halfspace (Trifunac, 1972) and a soil layer overlying a halfspace (Wirgin and Bard, 1996), and (b) three-dimensional lumped mass structures on a soil layer overlying a halfspace (Bard et al., 1996). Empirical studies have examined ground motions induced by forced vibration tests in structures (Jennings, 1970 and Kobori and Shinozaki, 1982) and coherencies between foundation and “free-field” earthquake motions (Celebi, 1995).

(a) *Analytical studies*

Several studies have evaluated ground motions induced by vibrations of two-dimensional shear walls. Trifunac (1972) analyzed the response of an elastic wall with a rigid semi-cylindrical foundation resting on an undamped elastic halfspace subjected to plane SH waves of variable incidence angles (Fig. 4.1a). It was found that the presence of the wall significantly influenced the amplitude of ground displacements to a distance one order of magnitude greater than the characteristic foundation dimension (i.e. to about 10×a or 5×building width). Fig. 4.2 shows the Fourier amplitude of the surface motion near the wall normalized by the amplitude of free-field motion (i.e. the surface motion in the absence of the wall) for vertically incident SH waves. The zero amplitude at the wall is a result of these curves being computed at frequencies matching the fixed-base natural frequencies of the elastic shear wall. If the wall-soil system were damped, a finite base-

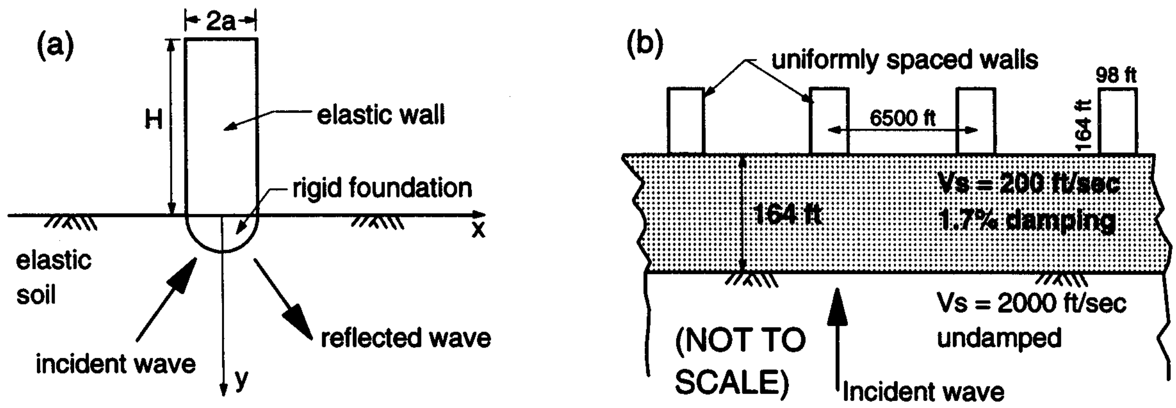

Fig. 4.1: Systems considered by (a) Trifunac (1972) and (b) Wirgin and Bard (1996)

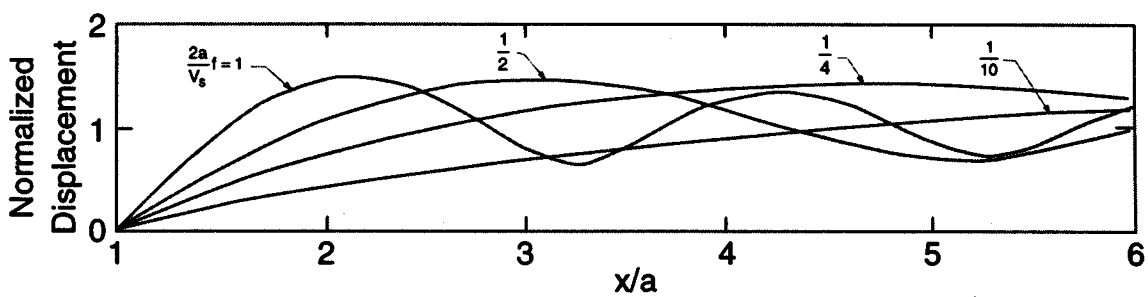

Fig. 4.2: Fourier amplitude of ground surface displacement adjacent to shear wall for vertically incident SH waves (Trifunac, 1972)

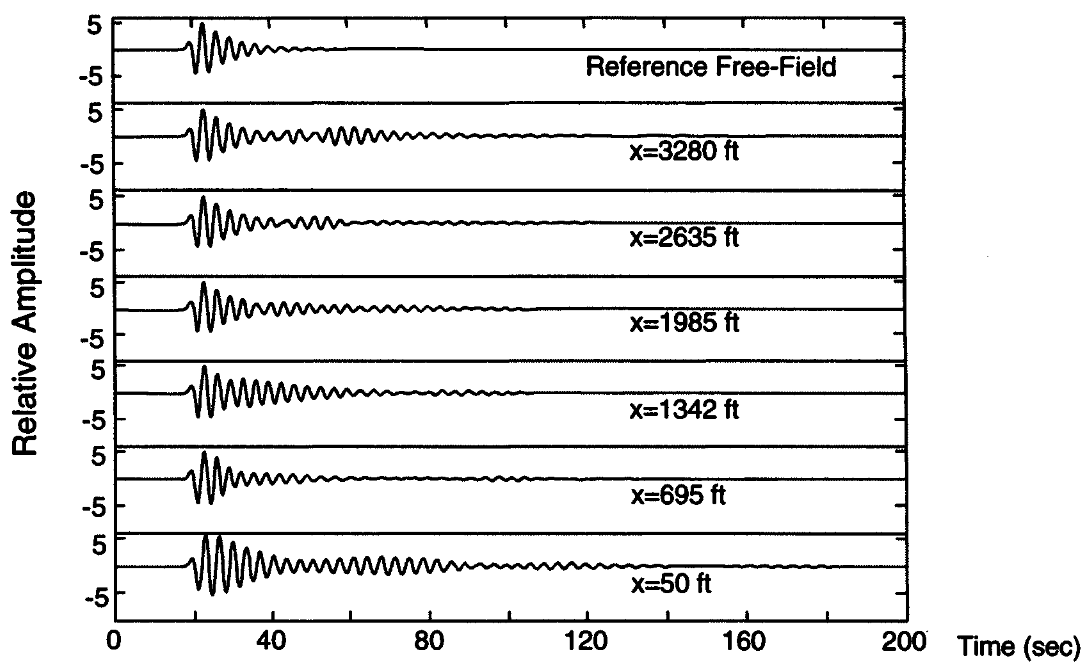

Fig. 4.3: Synthetic seismograms for ground sites and reference free-field; f(bldg)=0.5 Hz, f(site)=0.3 Hz, f(input)=0.25 Hz (Wirgin and Bard, 1996)

of-wall displacement would occur, but the general trends of ground surface displacements near the wall would be similar (Trifunac, 1972).

Two-dimensional shear walls were also studied by Wirgin and Bard (1996), who analyzed uniformly spaced viscoelastic walls with flat foundations resting on a layered viscoelastic halfspace subjected to vertically incident SH waves (Fig. 4.1b). Analyzed were cases of lightly damped soft soils (V_s = 200 ft/sec, β = 1.7%) overlying a relatively stiff base (V_s = 2000 ft/sec). The ground vibrations induced by the walls were found to be substantial when the soil layer frequencies were close to, but less than, the wall's fundamental frequency. Results for such a case are shown in Fig. 4.3. The vertical scale on these time histories is the surface motion amplitude relative to the motion that would occur in the free-field if the soil were a uniform halfspace (e.g. the amplification that results from the soil layering alone is indicated on the free-field plot). Though the amplitude of the ground surface motions are only slightly increased by the structural vibrations, the duration was considerably lengthened.

Bard et al. (1996) extended Wirgin and Bard's analysis to encompass three-dimensional lumped mass structures with and without foundation embedment. Base rocking was found to generate more significant ground waves than base translation, and the most efficient transmission of ground waves occurred when the structure and site were in resonance and the structure was embedded. For a particular ground instrument in Mexico City located 164 feet from an embedded structure which is resonant with the site, Bard et al. predicted 31% amplification of peak ground acceleration due to structural vibrations. This situation effectively represents a worst case scenario for these effects.

(b) *Empirical studies*

Ground motions resulting from structural vibrations can only be directly examined on an empirical basis when the true free-field motions that would occur in the absence of the structure are known. Such is the case with forced vibration testing of structures, as the free-field motions are zero (ignoring noise). Such ground motions have been examined by Jennings (1970) for forced vibration testing of a 9-story building (69 by 75 feet in plan) and Kobori and Shinozaki (1982) for forced vibration testing of a 6.5 x 6.5-ft. test footing. Jennings recorded ground motions dominated by the first-mode period of the structure that had about 11 to 22% of the base-of-structure amplitude 30 to 60 ft. from the structure, and 0.0015% amplitude 6.7 miles from the structure. The testing involved a low foundation-level peak acceleration of 0.0019g. The site examined by Kobori and Shinozaki (1982) had cut and fill areas, and the variation of ground motion amplitude with distance away from the structure had some minor peaks. Nonetheless, a general trend of degradation of velocity Fourier amplitude with distance was observed, with relative velocity amplitudes at 26 and 184 feet separations of about 2 to 6% and 0.04 to 0.08%, respectively.

Ground motions associated with earthquake-induced structural vibrations can be approximately examined by comparing foundation and "free-field" recordings. Celebi (1995) examined potential correlations between these motions using spectral and coherence functions. Four sites were examined, each of which was also considered in this study (A4, A11, A32, A33). Celebi argued that high coherencies at the structure's modal frequencies provide evidence for contamination of "free-field" recordings from structural vibrations. As shown in Fig. 4.4, at site A4, the motions are fairly coherent near the second and third modal frequencies; at site A11, the motions are coherent near the first-modal frequency; and at sites A32 and A33, the motions are coherent near the first two modal frequencies. However, the high coherencies only directly indicate a similarity in the respective motions, and do not constitute proof of structural vibrations affecting "free-field" motions. In fact, it is expected that "free-field" and foundation motions would be fairly coherent at sites with relatively uniform geologic conditions and with soil-structure systems not prone to significant inertial interaction effects (which is generally the case for the sites examined by Celebi).

The uncertainty associated with the interpretation of high coherencies between foundation and ground motions can be illustrated by further examination of sites A4 and A33. At site A4, coherencies computed from the north ground instrument (130 feet from the structure) are nearly unity for $f < 2.2$ Hz, whereas coherencies using the south ground instrument (530 feet from the structure) have substantial fluctuations. In this case, the relatively high coherencies obtained using the north ground data clearly indicate the strong influence of structural vibrations on recordings at this instrument. On the other hand, at site A33, coherencies computed from three ground instruments (located 662, 125, and 502 feet from the structure) are near unity for $f < 2$ Hz for each pair. As there is no significant variation in coherence with structure-ground instrument separation at this site, it appears that the high coherencies are a result of uniform site conditions and minimal SSI and not structural vibrations. Hence, as illustrated by these examples, high coherencies between foundation and ground motions must be interpreted with caution.

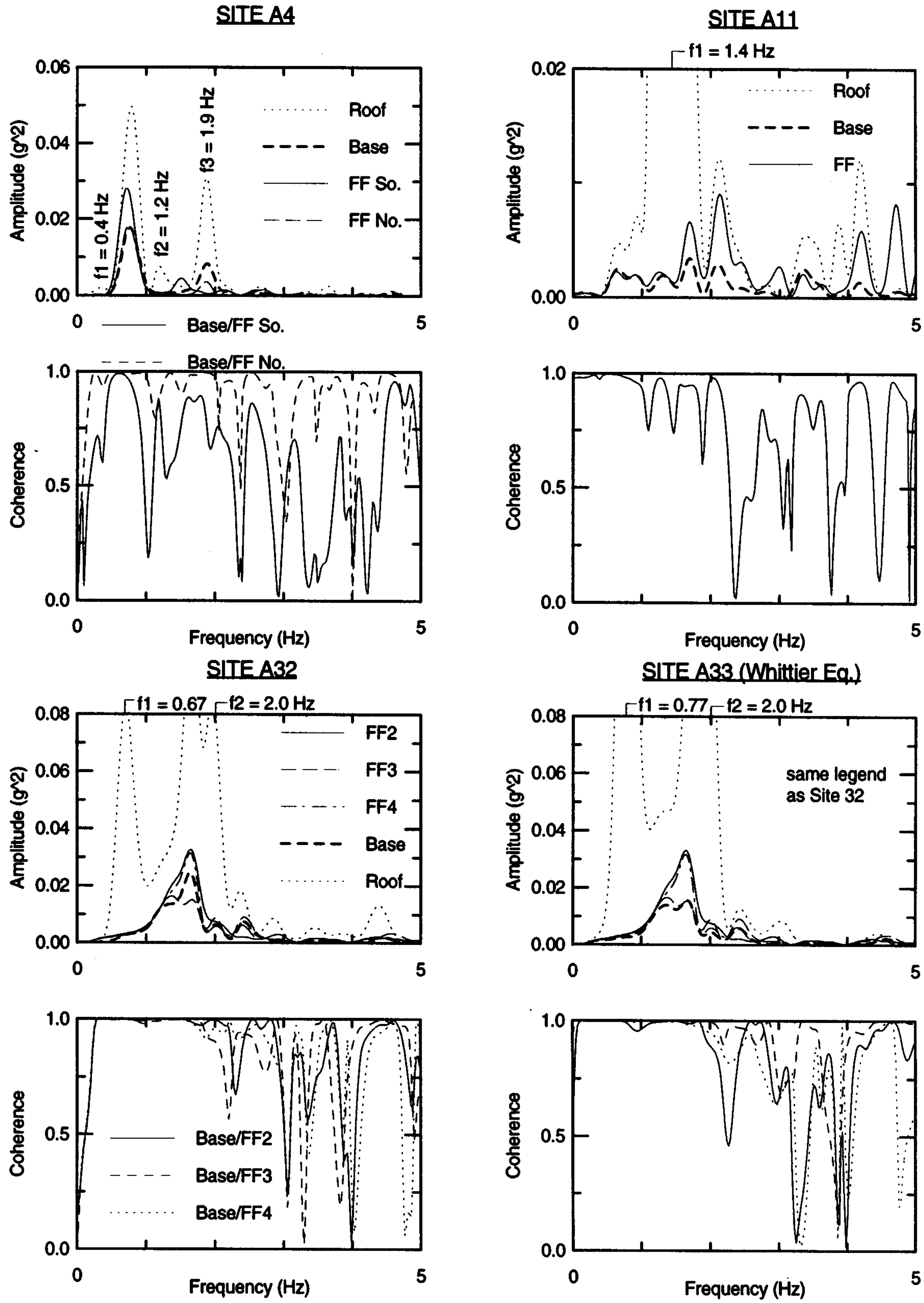

Fig. 4.4: Power spectral density and coherence functions for sites A4, 11, 32, and 33, NS direction

(c) *Summary*

The key observations from the above-cited studies are as follows: (1) at low soil damping (i.e. < 2%), the analytical studies indicate a significant influence of structural vibrations on ground motions to a distance of about 5×building width for a halfspace, and to much greater distances for a soft soil layer overlying a stiff material, provided the frequency of the soil layer is nearly equal to or less than the structural frequency, (2) structural vibrations often affect the duration of nearby ground motions more than the amplitude, (3) structures induce ground vibrations most efficiently when they are embedded, and when there is significant base rocking, and (4) high coherencies between seismic ground and foundation motions at modal frequencies can be associated with structural vibrations affecting the ground instrument, but do not provide proof of such interaction. Since the analytical studies and forced vibration test data are only applicable for low hysteretic soil damping, results from these studies may not be applicable to earthquake loading conditions involving strong shaking. To the extent that high coherencies between foundation and ground motion recordings indicate at least a potential influence of structural vibrations on ground motions, such analyses can provide insight. However, unless multiple ground recordings from the site are available, the true cause of such high coherencies is difficult to ascertain.

In this study, the potential influence of structural vibrations on “free-field” motions was examined as follows: (1) using power spectral density functions, “free-field” spectra were examined for peaks at the modal frequencies of the adjacent structure, especially if such peaks were also present in the spectra of foundation motions, (2) coherencies between foundation and “free-field” motions were examined for values near unity at modal frequencies, and (3) “free-field” motions were checked for unusually long durations if significant free vibrations occurred in the structure following the conclusion of strong ground shaking. For the sites in this study, the influence of structural vibrations on “free-field” motions was generally estimated to be minor or negligible, with a few exceptions noted below.

The only cases where a significant influence of structural vibrations was evident in the “free-field” data was at sites A26 and A29. Fig. 4.5 shows power spectral density and coherence functions for these sites, from which contamination is suspected based on unusually large spectral amplitudes at the frequencies noted. At both sites, the spurious vibrations likely originated from another structure unusually close to the “free-field” accelerograph (i.e. about 50 feet from a parking garage at site A26 and about 6 feet from a 3-story storage building at site A29). However, these vibrations occurred at frequencies far removed from the lower-mode frequencies of the instrumented structure, so the “free field” motions were still used in system identification analyses of the flexible-base structural response.

4.1.2 Effects of Spatial Incoherence on the Compatibility of Foundation and Free-Field Motions

Even at uniform sites, earthquake ground motions recorded at different locations are spatially incoherent as a result of different wave ray paths and local heterogeneities in the geologic media. These effects have been studied empirically using data from dense arrays of strong motion instrumentation at sites in Lotung, Taiwan (e.g. Abrahamson et al., 1991 and Abrahamson, 1988), Parkfield, California (e.g. Schneider et al., 1990),

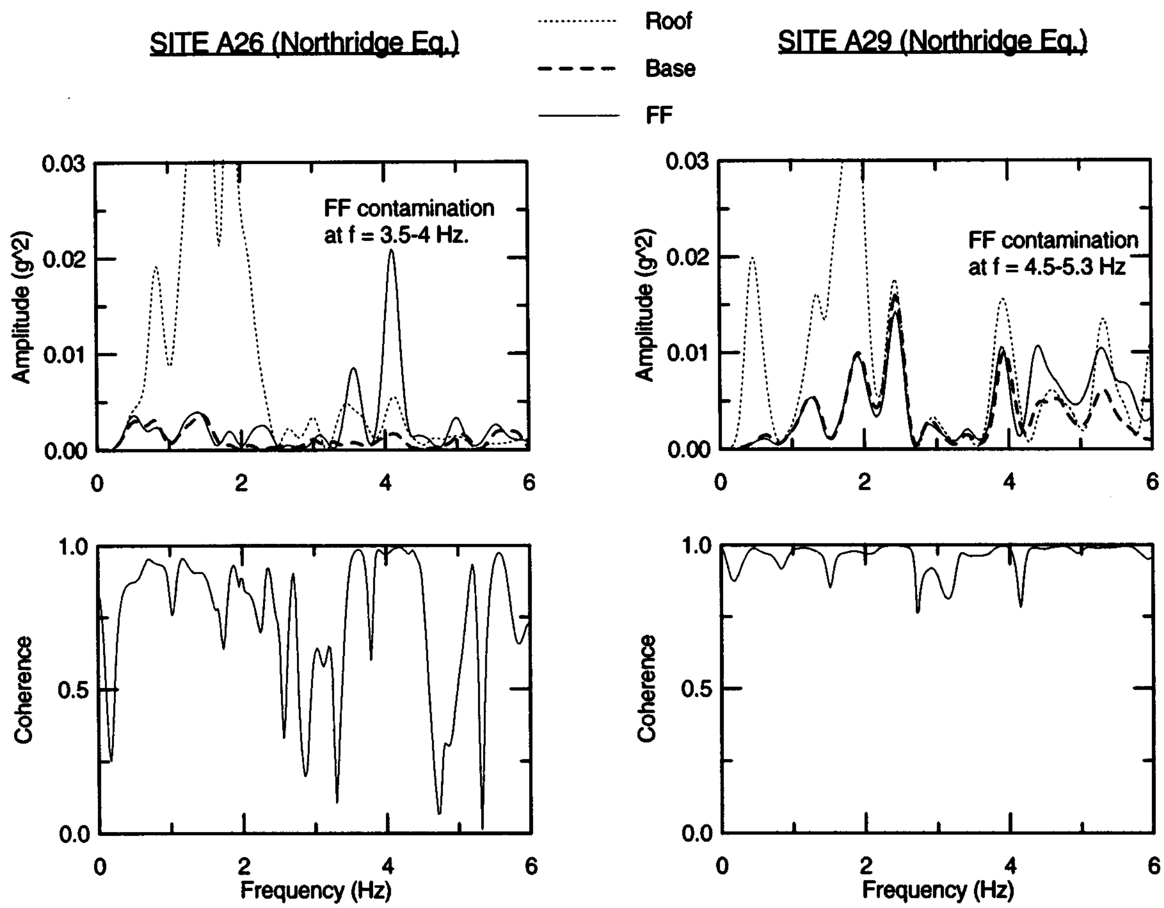

Fig. 4.5: Power spectral density and coherence functions for sites with "free-field" motions influenced by vibrations of structures near the accelerograph

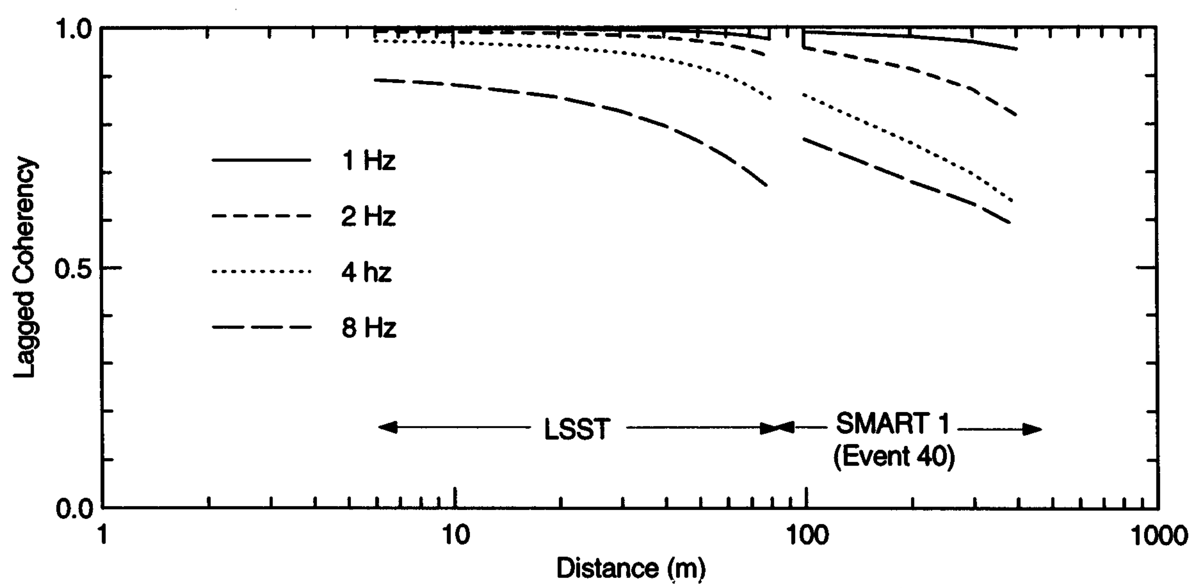

Fig. 4.6: Comparison of coherencies computed from regression equations in Abrahamson et al., 1991 for LSST array (all events) and Abrahamson, 1988 for SMART1 array (Event 40)

Coalinga, California (e.g. Somerville et al., 1991), and Imperial Valley, California (e.g. Smith et al., 1982).

Spatial incoherence effects are generally quantified in terms of a coherency function which is the square root of the coherence function defined in Eq. 3.12,

$$\gamma(\omega) = \frac{S_{xy}(\omega)}{\left[S_x(\omega)S_y(\omega)\right]^{1/2}} \tag{4.1}$$

Coherency is a complex-valued function with the real part describing the similarity of two ground motions without correction for passage of inclined plane waves. The modulus, $|\gamma(\omega)|$, removes the wave passage effect. Abrahamson et al. (1991) defined Re(γ) as unlagged coherency and $|\gamma(\omega)|$ as lagged coherency, and these definitions are retained here.

In the selection of 'A' sites, the key issue with regard to spatial incoherence is deciding when free-field instruments are located too far from a structure. Incoherence resulting from wave passage effects alone are correctable with synchronization (Section 3.5.1), so the principle concern here is the lagged coherency.

Abrahamson (1988) performed regression analyses on $\tanh^{-1}|\gamma(\omega)|$, which is approximately normally distributed, using 13 stations in the SMART 1 array in Lotung, Taiwan. The station separations ranged from 87 to 411 m. Separate regressions were performed for four events ranging in magnitude from M_S = 5.6 to 7.8, and in epicentral distance from 6 to 79 km. Abrahamson et al. (1991) also performed regression analyses on $\tanh^{-1}|\gamma(\omega)|$ using 15 closely spaced stations within the SMART 1 array known as the LSST array. Station separations in the LSST array range from 6 to 85 m. The regression was performed using data from 15 events ranging in magnitude from 3.7 to 7.8 and in epicentral distance from 5 to 80 km.

The results from the LSST regression are shown in Fig. 4.6 together with the SMART 1 regression results for a specific event (Event 40, M_S = 6.4, epicentral distance = 68 km). Event 40 regression results were similar to results for other events for frequencies < 2 Hz. In Fig. 4.6, the coherency is seen to decrease more rapidly with frequency than with distance in the motions recorded at both arrays.

The results in Fig. 4.6 were based on data from the Lotung site which has a relatively uniform near-surface geologic profile. Regression results from the Parkfield array, which also has a relatively uniform soil profile, were found to be similar to those for the Lotung array (Schneider et al., 1990). In contrast, spatial incoherence in highly heterogeneous media, such as folded sedimentary rock at the Coalinga array, does not show the strong dependence on distance and frequency evident in Fig. 4.6 (Somerville et al., 1991). Further, the coherence for such heterogeneous sites is lower at close distances and low frequencies than at uniform sites.

Many of the sites considered for this study had relatively uniform soil profiles, and it was assumed that the regression curves in Fig. 4.6 provide a reasonable quantification of spatial incoherence effects. It was decided to maintain coherencies greater than about 0.8 at the predominant period of the building. For the majority of sites in this study, this required free-field-structure separations less than about 2600 ft (800 m) for 1 Hz structures, 1500 ft (450 m) for 2 Hz structures, and 500 feet (150 m) for 4 Hz structures. Since the likelihood of geologic uniformity decreases for large separations, an effective maximum separation of about 1500 ft was used for low frequency ($f_1 < 2$ Hz) structures. These guidelines were used for the initial screening of sites for this study.

The sites considered in this study are listed in Table 4.1 along with their first-mode period and the separation distance between the free-field instrument and structure. Almost all of the sites meet the above guidelines for separation distance, and for most sites, spatial incoherence is not believed to have significantly contaminated the free-field recordings. Several sites which narrowly meet the above separation distance guidelines (A20 and A36) have fairly uniform geologic profiles, and incoherence effects were not excessive. Several rock sites are quite geologically heterogeneous (sites A5, A6, and A11); of these, the separations at sites A5 and A11 are relatively small (about 500 ft.) and significant incoherence was not encountered. Spatial incoherence was a problem at sites A6 and A22. At site A6, the combination of a 1260 ft. separation and heterogeneous geologic media resulted in significant incoherence which essentially invalidated the analytical results. At site A22, the 1700 ft. separation for this 2 Hz structure slightly exceeds the maximum separation distance guidelines. The free-field and base-of-structure motions were fairly dissimilar in this case, hence the analytical results were tagged with a "low confidence" designation (see Section 5.3.3).

4.2 Conditions Examined

The purpose of this section is to provide a brief overview of the range of conditions represented by the sites considered in this study. All of the sites are listed in Table 4.1. As noted above, there are two classes of sites: 'A' sites which have an instrumented

Table 4.1: Site and structural data for sites included in this study

Site*	Station	No. Eqs.	Rock/Soil	Avg. Vs (ft./sec)	Piles (Y/N)	Embed. (ft.)	No. Stories	Structural System**	Period (sec)	FF-Str. Sep. (ft.)
'A' Sites										
1	Eureka Silvercrest Apts.	1	S	800	N	0	5	SW	0.2	340
2	Fortuna 1-St. Supermarket	2	S	*915*	N	0	1	SW	0.4	350
3	Humboldt Bay Power Plant	2	S	980	N	86	1	SW	na	240
4	Emeryville Pacific Pk. Plaza	1	S	620	Y	0	31	CF	2.5	530/130
5	Hayward City Hall	1	R	2210	Y	0	11	DWF	1.2	470/500
6	Hayward 13-St. School Bldg.	1	R	1350	Y	0	13	DWF	1.3	1260
7	Hollister 1-St. Warehouse	1	S	*670*	N	0	1	SW	0.7	400
8	Piedmont Jr. High School	1	R	1830	N	0	3	SW	0.2	120
9	Pleasant Valley Pump. Plant	2	S	*1010*	N	32	1	DWF	0.5	300
10	Richmond City Hall	1	S	830	N	10	3	DWF	0.3	650
11	San Jose 3-St. Offc. Bldg.	1	R	2690	N	0	3	SF	0.7	510
12	El Centro Imp. Co. Ser. Bldg.	1	S	580	Y	0	6	DWF	0.7	340
13	Indio 4-St. Gov't Offc. Bldg.	1	S	*760*	Y	16	4	DWF	0.7	240
14	Lancaster 3-St. Offc. Bldg.	1	S	*920*	Y	0	3	SW	0.2	250
15	Lancaster 5-St. Hospital	1	S	*1030*	Y	0	5	SF	0.7	360
16	Lancaster Fox Airfield	1	S	*1000*	N	0	5	SF	0.3	160
17	Loma Linda VA Hos.	1	S	1520	Y	0	4	SW	0.3	400/400
18	Long Beach Har. Ad. Bldg.	1	S	*700*	Y	0	7	SF	1.4	200
20	Long Beach VA Hospital	1	S	1210	N	23	11	SW	0.6	980
21	LA 2-St. FCCB	3	R	*1030*	N	0	2	BI	0.8	100
22	LA 3-St. Comm. Bldg.	1	S	1160	N	23	3	DWF	0.6	1700
23	LA 6-St. Offc. Bldg.	1	S	630	N	14	5	SF	0.9	830
24	LA 6-St. Pkg. Garage	1	S	870 (tr) 640 (L)	Y	0	6	SW	0.5	240
25	LA 7-St. USC Hos.	2	R	1170	N	0	7	BI	1.2	350
26	LA 7-St. UCLA Bldg	1	S	*700*	N	14	7	DWF	0.7	930
27	LA 15-St. Offc. Bldg.	2	R	*1180*	N	0	17	SF	3.1	750
28	LA 19-St. Offc. Bldg.	1	S	1160	Y	38	19	SF	3.2	940
29	LA Hollywood Storage Bldg.	4	S	960	Y	9	14	CF	2.2	140
30	LA Wadsworth VA Hospital	1	S	*1130*	Y	31	6	SF	0.9	470/1320
31	Newport Beach Hoag Hospital	2	S	*1050*	N	0	11	SW	0.9	650
32	Norwalk 12400 Imp. Hwy.	1	S	*910*	Y	14	7	SF	1.5	490-570
33	Norwalk 12440 Imp. Hwy.	2	S	*1000*	Y	15	7	SF	1.3	130-660
34	Palmdale 4-St. Hotel	1	S	1620	N	0	4	SW	0.2	240
35	Pomona 2-St. Bldg.	2	S	*1280*	Y	11	2	CF	0.3	290
36	Pomona 6-St. Bldg.	2	S	*1250*	N	13	6	CF	1.2	1270
37	Rancho Cucamonga LJC	5	S	*1190*	N	14	4	BI	0.6	330
38	San Bernardino 3-St.	1	S	*980*	N	0	3	SF	0.6	690
39	San Bernardino 5-St.	1	S	*1310*	N	13	5	SW	0.6	490
40	San Bernardino Vanir Tower	1	S	*920*	Y	0	9	SF	2	910
41	San Bernardino Co. Govt Cntr	1	S	*1060*	Y	0	5	SF	0.5	210
42	Santa Susana Bldg 462	1	R	*4500*	N	0	8	SF	0.6	160
43	Seal Beach Rockwell Bldg 80	2	S	970	Y	16	8	BI	1.3	460
44	Sylmar Olive View Med. Cen	2	S	1530	N	0	6	SW	0.3	460
45	Ventura 12-St. Hotel	1	S	*920*	Y	0	12	SW	0.7	180

46	Lotung Containment Structure	1	S	460	N	15	1	SW	0.5	100
'B' Sites										
1	Milpitas 2-St. Offc. Bldg.	1	S	*690*	N	0	2	SW	0.3	na
2	San Bruno 9-St. Offc. Bldg.	1	S	*1010*	N	0	9	SW	1.1	na
3	San Fran. 47-St. Offc. Bldg.	1	S	570	Y	39	47	SF	5.2	na
4	San Fran. Transamerica Tow.	1	S	*960*	N	51	60	SF	3.6	na
5	San Jose 10-St. Resid. Bldg.	1	S	*840*	Y	0	10	SW	0.5	na
6	San Jose 13-St. Gov't Offc.	1	S	*770*	N	14	12	SF	2.2	na
7	Walnut Creek 10-St. Offc.	1	R	1450	Y	0	10	DWF	0.8	na
9	El Segundo 14-St. Offc. Bldg.	1	S	1010	N	0	14	SF	2.1	na
10	LA 9-St. Offc. Bldg.	1	S	960	N	13	9	DWF	1.3	na
11	LA 17-St. Resid. Bldg.	2	R	1200	Y	0	17	SW	1.1	na
12	LA 32-St. Offc. Bldg.	1	R	1380	N	54	32	DWF	1.9	na
13	LA 54-St. Offc. Bldg.	1	R	1430	N	59	54	SF	5.9	na
14	Whittier 8-St. Hotel	1	S	870	N	0	8	SW	0.6	na

Shear wave velocities in *italics* are estimated.
*Sites A19 and B8 omitted
** Lateral force resisting systems:
SW = masonry or concrete shear walls
DWF = dual wall/frame system
CF = concrete frame
SF = steel frame
BI = base isolated

structure and a free-field accelerograph, and ‘B’ sites which have a structure specially instrumented to record base rocking, but no free-field accelerograph. There are 45 ‘A’ sites and 13 ‘B’ sites, with a total of 79 sets of available processed data. Sites A19 and B8 were omitted in the final compilation for reasons discussed below.

With the exception of the 1/4-scale reactor structure in Lotung, Taiwan, all of the sites are located in California. Fig. 1.2 is a map of California showing the locations of the sites and major earthquakes considered in this study. Larger scale maps for particular areas of interest are presented in Figs. 4.7 to 4.10 for the Humboldt/Arcata Bay area, San Francisco Bay area, Los Angeles area, and San Bernardino areas. The contributing earthquakes in the Humboldt/Arcata Bay area (Fig. 4.7) were the 1975 Ferndale and 1992 Petrolia events, and there are three ‘A’ sites in this vicinity. The 1989 Loma Prieta Earthquake was the key event for the San Francisco Bay area (Fig. 4.8), with six recordings at ‘A’ sites and seven recordings at ‘B’ sites. In the Los Angeles and San Bernardino areas (Figs. 4.9-10), the contributing events were the 1971 San Fernando, 1985 Redlands, 1987 Whittier, 1990 Upland, 1991 Sierra Madre, 1992 Landers, and 1994 Northridge earthquakes. There are a total of 25 ‘A’ sites and 6 ‘B’ sites in these two regions. Sites not included in the local maps (Figs. 4.7-10) are A7 in Hollister, A9 near Coalinga, A12 in El Centro, A13 in Indio, A14-16 in Lancaster, A34 in Palmdale, and A45 in Ventura. The locations of these sites are shown in Fig. 1.2.

A summary of the 15 California earthquakes which contributed data to this study is presented in Table 4.2. The magnitudes range from 4.8 to 7.4, though the events contributing the vast majority of the data were the M_W = 6.0 Whittier, M_W = 6.9 Loma Prieta, M_W = 5.6 Upland, M_W = 7.0 Petrolia, M_W = 7.3 Landers, and M_W = 6.7 Northridge

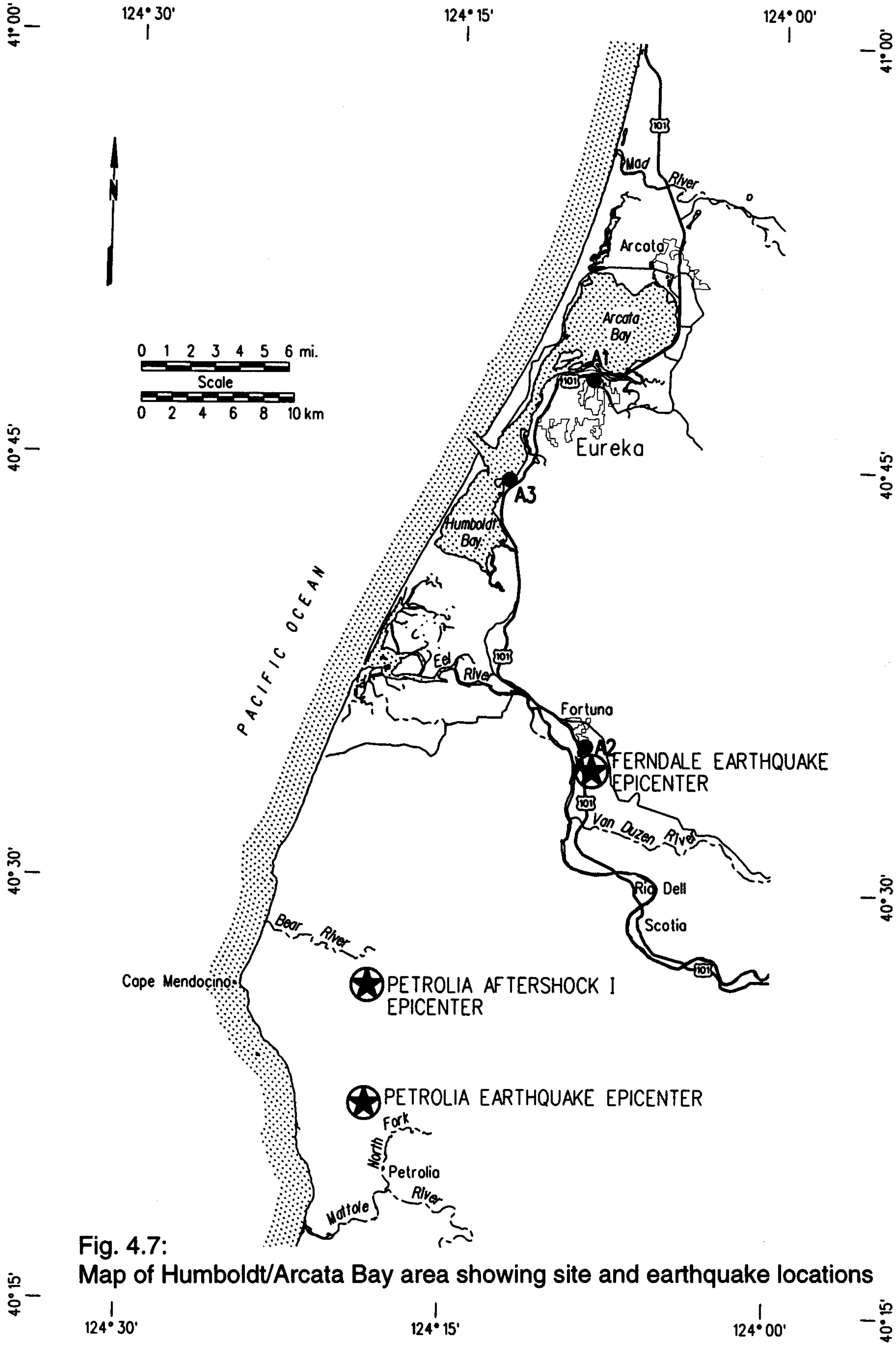

Fig. 4.7:
Map of Humboldt/Arcata Bay area showing site and earthquake locations

humarca.dgn

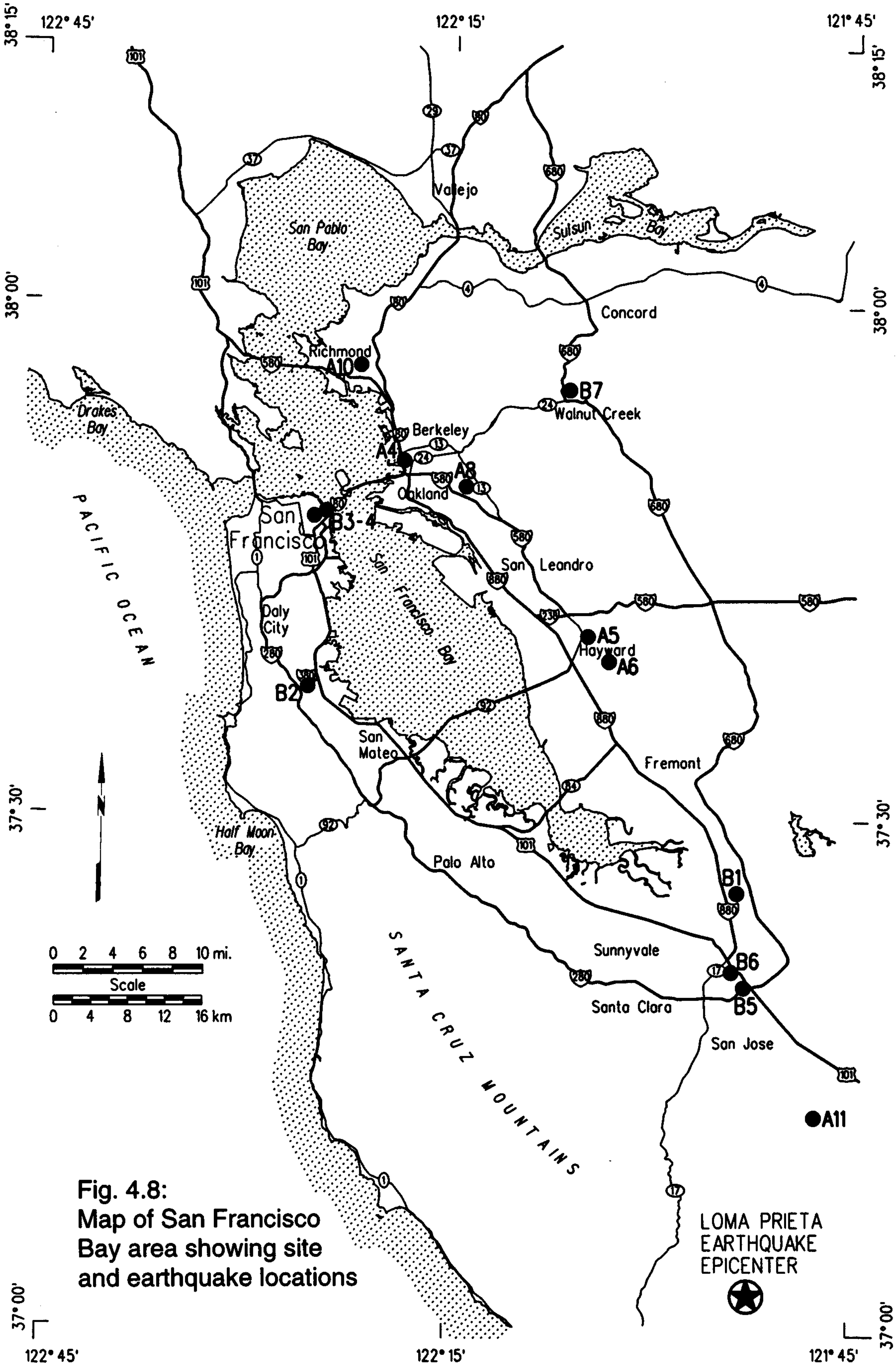

**Fig. 4.8:
Map of San Francisco
Bay area showing site
and earthquake locations**

sfbay.dgn

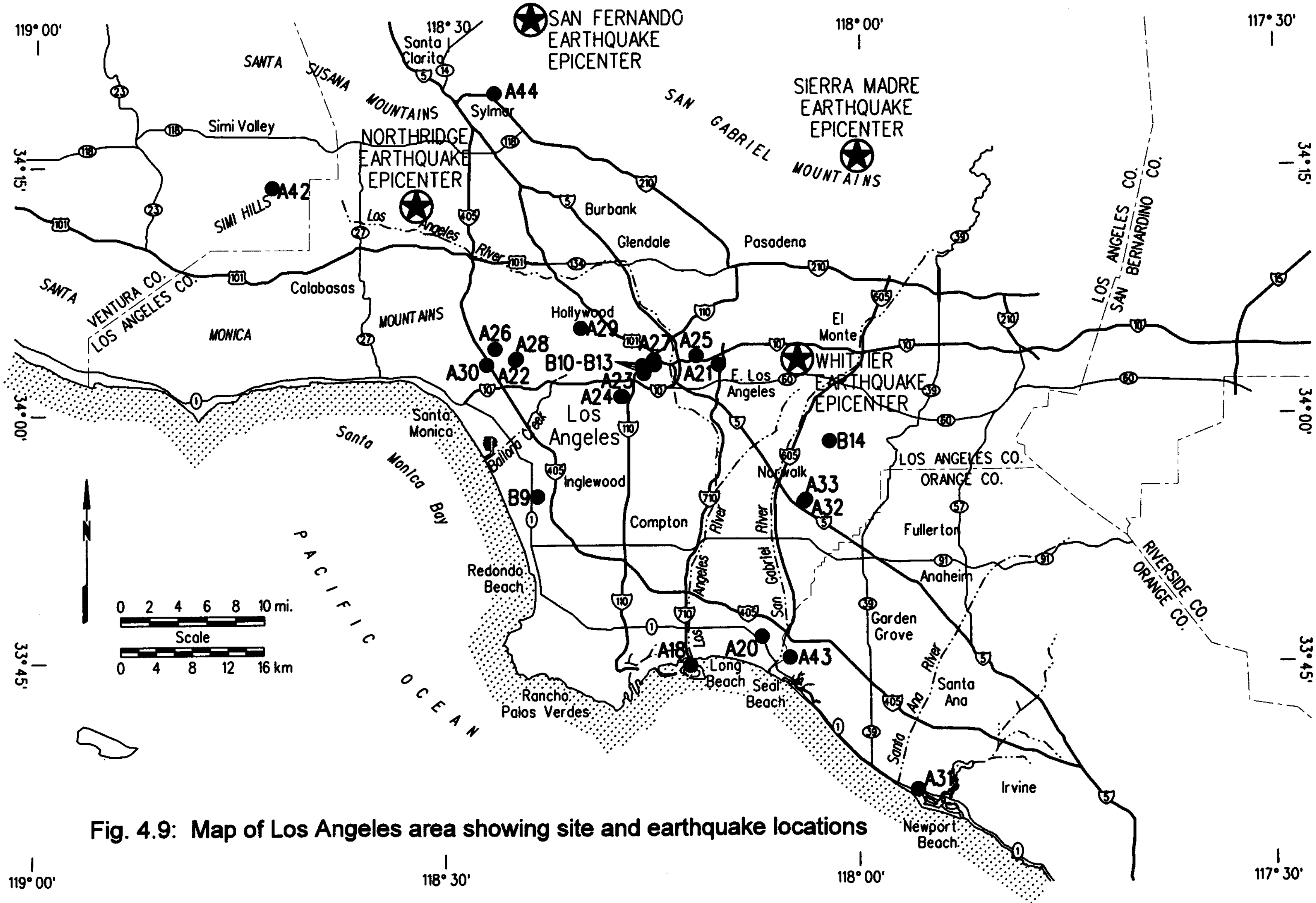

Fig. 4.9: Map of Los Angeles area showing site and earthquake locations

la.dgn

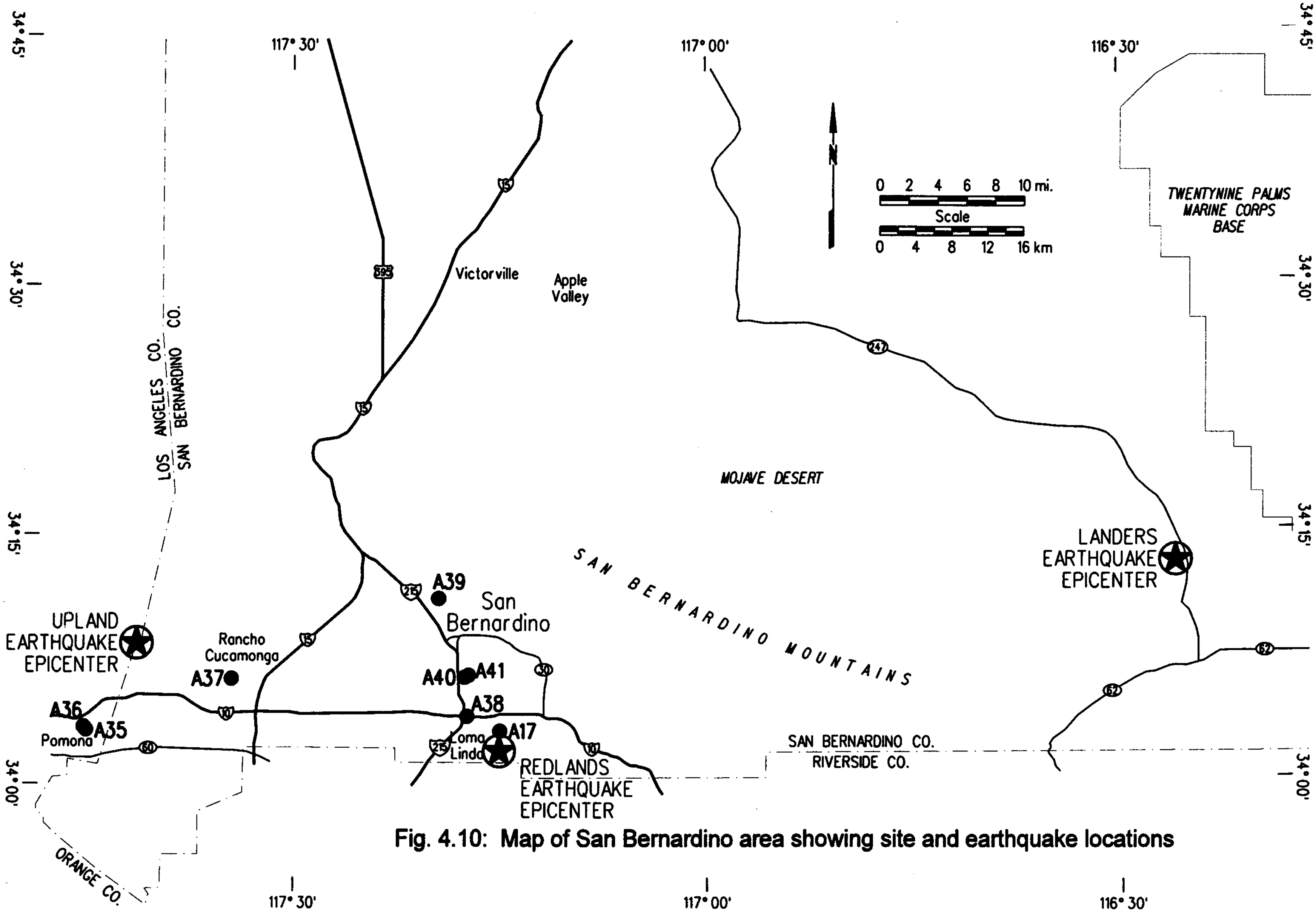

Fig. 4.10: Map of San Bernardino area showing site and earthquake locations

sanbern.dgn

earthquakes. The maximum horizontal accelerations (MHAs) produced by these earthquakes at the sites break down as,

MHA > 0.6g	1 data sets
MHA = 0.4-0.6g	4 data sets
MHA = 0.2-0.4g	23 data sets
MHA = 0.1-0.2g	17 data sets
MHA < 0.1g	34 data sets

Hence, moderate- and low-level shaking is well represented in the database, but data for intense shaking (MHA > 0.4g) is relatively sparse (only 4 data sets).

Table 4.2: Earthquakes which contributed data to this study

Earthquake	Magnitude	Recordings
1952 Kern County (kn)	$M_W = 7.4$	1
1971 San Fernando (sf)	$M_W = 6.6$	1
1975 Ferndale (fn)	$M_L = 5.2$	1
1979 Imperial Valley (imp)	$M_W = 6.5$	1
1983 Coalinga (cg)	$M_W = 6.4$	1
1983 Coalinga Aftershock (cga)	$M_W = 5.4$	1
1985 Redlands (rd)	$M_L = 4.8$	1
1987 Whittier (wt)	$M_W = 6.0$	9
1989 Loma Prieta (lp)	$M_W = 6.9$	14
1990 Upland (up)	$M_W = 5.6$	3
1991 Sierra Madre (sm)	$M_W = 5.6$	1
1992 Petrolia (pt)	$M_W = 7.0$	3
1992 Petrolia Aftershock (pta)	$M_W = 6.2$	1
1992 Landers (ld)	$M_W = 7.3$	11
1994 Northridge (nr)	$M_W = 6.7$	31

As indicated in Table 4.1, the geologic conditions at the sites break down as 46 soil sites and 12 rock sites. The average V_S indicated in the table is computed as the ratio of r_1 to the travel time for shear waves to travel to the surface from a depth of r_1 (where r_1 is the disk foundation radius defined in Eq. 2.3). These calculations were made using the small-strain shear wave velocities provided for each site in Stewart (1997), with supplementation by more recently obtained data for several sites. It may be observed from the table that shear wave velocities at many of the rock sites are sufficiently low that there is relatively little distinction between the V_S at these sites and some stiff soil sites (e.g. sites A6, A8, A21, A25, A27, B7, and B11 to B14).

Some of the structural/foundation conditions at the sites can be categorized as follows. Foundations for 23 buildings have piles or piers, while 35 have shallow foundations such as footings, mats, or grade beams. Most buildings are not embedded (36) or have shallow single-level basements (14). Only eight buildings have multi-level basements. The building heights and principle lateral force resisting systems break down as,

1 to 4 stories:	18 buildings
5 to 11 stories:	27 buildings
> 11 stories:	13 buildings

Masonry/concrete shear walls:	20 buildings
Dual wall/frame systems:	11 buildings
Concrete frames:	4 buildings
Steel frames:	19 buildings
Base isolated:	4 buildings

Lastly, it should be noted that two sites, A19 and B8, were omitted from the compilation. Data for site A19 did not become available by the time this report was prepared. There were flaws in the analytical results for site B8 that could not be resolved.

CHAPTER 5

EMPIRICAL EVALUATION OF SOIL-STRUCTURE INTERACTION EFFECTS AND CALIBRATION OF ANALYSIS PROCEDURES

5.1 Introduction

The principal objectives of this study are to make use of strong motion data from recent earthquakes to evaluate the effects of soil-structure interaction (SSI) on structural response for a range of site and structural conditions, and then to use these results to calibrate existing simplified analytical formulations intended to predict these same effects. Previous chapters have described the system identification procedures used to evaluate SSI effects from earthquake strong motion recordings (Chapter 3), and simplified analytical methodologies against which the empirical results can be compared (Chapter 2). This chapter will realize the stated project objectives by (1) empirically quantifying SSI effects of interest through an assessment of system identification results for the 58 sites considered in this research, and (2) evaluating the accuracy and limitations of the simplified analytical procedures through comparisons of the predicted and empirical SSI effects. It should be noted that the results presented here are a summary of key findings from 58 individual site studies; specific analysis results and site conditions for each site are presented in Stewart (1997).

SSI effects evaluated from site studies are collectively examined in three stages to address different aspects of the problem. The initial stage, presented in Section 5.2, examines variations between free-field and foundation motions using indices such as peak acceleration, velocity, and displacement and various spectral accelerations. These comparisons simplistically illustrate the filtering effects of kinematic interaction on foundation translational motion and the contributions of inertial interaction to foundation motion near the first-mode period of the structure.

In the second stage (Section 5.3), inertial interaction effects are investigated using fixed- and flexible-base first-mode parameters derived from system identification and related modal parameter estimation procedures. These effects are quantified by the flexible-to-fixed-base period lengthening ratio ($\tilde{T}/T$) and the foundation damping factor $\tilde{\zeta}_0$, which represents the effects of hysteretic and radiation damping in the soil and foundation.

In the third stage (Section 5.4), the “empirical” period lengthening ratios and foundation damping factors are compared to predictions from the “modified Veletsos” and “modified Bielak” analytical methodologies to calibrate these procedures. Section 5.5 goes on to compare the empirical results to evaluations of period lengthening and foundation damping from procedures in the BSSC (1997) and ATC (1978) seismic design codes.

In the following, sites are referred to by number with direction and earthquake information tagged on when necessary. For example, A25-L(nr) indicates site A25, longitudinal direction (L = longitudinal, tr = transverse), Northridge Earthquake. The shorthand for earthquakes is defined in Table 4.2. No direction is given if the tag applies to both directions or if there is only one direction for which data are available. Similarly, no earthquake tag is given if data are only available for one event at the site.

5.2 Comparison of Free-Field and Foundation-Level Structural Motions

The simplest way to evaluate basic kinematic and inertial interaction effects is to compare indices of free-field and foundation motions. The ground motion indices examined in this section are peak horizontal acceleration, velocity, and displacement, as well as 5%-damped spectral acceleration at the flexible-base period of the structure ($\tilde{T}$) and the predominant period of free-field shaking (T_{eq}). The $\tilde{T}$ values were determined from system identification analysis, while T_{eq} is defined as the period at which the power spectral density of free-field motion is maximized.

The motions examined consist of processed data from 'A' sites. A significant amount of additional unprocessed data is available for these and other sites which could have been used to supplement the database compiled for this study. However, these unprocessed data are almost entirely for low shaking levels (i.e. peak acceleration < 0.1g) which are well-represented in the database, and hence the incorporation of potentially erroneous unprocessed data is not justified.

The ground motion indices compiled for the 45 'A' sites are presented in Table 5.1. Presented in Figs. 5.1 to 5.5 are comparisons of free-field and foundation-level strong motion indices sorted by (a) rock/soil sites, (b) structures with deep/shallow foundations, (c) short/tall structures, and (d) structures with/without basements. For each of plots (a) - (d), second-order polynomials fit to the data using linear regression analyses are drawn to clarify trends for the respective conditions.

Table 5.1: Indices of free-field and foundation ground motions for 'A' sites

Site	Station	Eqk.	Rock/Soil	Piles (Y/N)	No. Stories	Bsmt. (Y/N)	Peak Acc. (g)				Peak Vel. (cm/sec)				Peak Disp. (cm)				Sa @ $\tilde{T}$ (g)				Sa @ Teq (g)			
							FF		Str		FF		Str		FF		Str		FF		Str		FF		Str	
							tr	L	tr	L	tr	L	tr	L	tr	L	tr	L	tr	L	tr	L	tr	L	tr	L
1	Eureka Apts.	PT	S	N	5	N	0.15	0.18	0.15	0.17	20.0	28.6	19.9	27.0	5.9	11.8	4.6	10.8	0.40	0.43	0.42	0.35	0.24	0.33	0.26	0.24
2	Fortuna Market	PT	S	N	1	N	0.11	0.12	0.12	0.14	20.9	28.8	17.8	17.5	12.2	19.8	4.2	4.9	0.25	0.23	0.23	0.24	0.12	0.08	0.12	0.06
		PTA	S	N	1	N	0.18	0.19	0.17	0.16	11.3	11.1	13.3	11.6	2.3	2.2	2.4	2.3	0.36	0.66	0.47	0.66	0.65	0.50	0.58	0.53
3	Humboldt PP	FN	S	N	2	Y	0.25	0.18	0.11	0.08	1.3	1.0	0.8	0.6	0.6	1.0	0.3	0.4	*	*	*	*	*	*	*	*
		PT					0.27	0.24	0.14	0.13	15.7	13.7	8.5	9.0	3.1	2.4	2.3	2.4	0.45	0.38	0.22	0.21	0.70	0.71	0.21	0.31
4	Emeryville PPP	LP	S	Y	31	N	0.21	0.25	0.18	0.21	21.2	40.6	15.6	36.5	3.7	8.1	3.4	9.2	0.04	0.11	0.03	0.09	0.60	0.40	0.38	0.26
5	Hayward City Hall	LP	R	Y	11	Y	0.05	0.05	0.05	0.04	5.6	5.7	4.7	5.0	4.0	3.9	3.7	3.8	0.04	0.05	0.04	0.05	0.06	0.07	0.06	0.06
6	Hayward 13-St.	LP	R	Y	13	N	0.09	0.07	0.07	0.08	6.2	6.3	6.2	6.9	3.5	2.2	0.9	0.8	0.08	0.05	0.05	0.04	0.10	0.08	0.06	0.05
7	Hollister 1-St.	LP	S	N	1	N	0.23	0.36	0.25	0.36	40.4	58.3	44.6	52.0	22.6	18.9	23.3	17.3	0.39	0.47	0.38	0.51	0.10	0.88	0.10	0.71
8	Piedmont Jr. HS	LP	R	N	3	N	0.07	0.08	0.09	0.07	8.7	7.7	10.1	6.2	1.3	1.5	1.6	1.1	0.12	0.12	0.19	0.11	0.09	0.13	0.10	0.14
9	PVPP	CGM	S	N	1	Y	0.59	0.52	0.30	0.27	61.4	39.1	36.7	21.7	19.8	5.0	10.4	3.8	1.94	*	1.10	*	0.79	2.91	0.52	1.19
		CGA					0.10	0.21	0.05	0.13	7.7	9.9	5.8	6.5	1.0	0.7	0.6	0.5	0.20	*	0.12	*	0.19	0.57	0.12	0.34
10	Richmond CH	LP	S	N	3	Y	0.13	0.11	0.12	0.09	18.0	13.4	15.3	12.7	2.6	2.3	2.2	2.2	0.16	0.24	0.21	0.19	0.41	0.22	0.33	0.25
11	San Jose 3-St.	LP	R	N	3	N	0.27	0.23	0.16	0.20	22.4	19.2	18.9	15.4	7.0	3.6	6.7	3.3	0.45	0.37	0.38	0.39	0.40	0.73	0.34	0.35
12	El Centro Bldg.	IMP	S	Y	6	N	0.21	0.24	0.29	0.33	36.2	64.4	42.4	64.6	16.4	28.2	16.0	27.4	0.54	0.39	0.48	0.43	0.51	0.24	0.56	0.25
13	Indio 4-St.	LD	S	Y	4	Y	0.08	0.09	0.08	0.08	14.8	30.2	12.1	23.6	6.4	14.0	4.2	13.1	0.15	0.14	0.15	0.13	0.15	0.20	0.15	0.18
14	Lancaster 3-St.	WT	S	Y	3	N	0.07	0.06	0.06	0.05	2.5	2.9	2.7	2.9	0.2	0.2	0.2	0.2	0.19	0.15	0.18	0.12	0.23	0.07	0.16	0.06
15	Lancaster 5-St.	NR	S	Y	5	N	0.06	0.07	0.05	0.07	8.9	8.9	9.2	8.0	2.6	2.3	2.7	2.6	0.09	0.17	0.09	0.13	0.15	0.26	0.16	0.20
16	Lancaster Airfield	NR	S	Y	5	N	0.08	0.06	0.08	0.09	7.0	5.4	5.7	6.9	1.5	1.2	1.0	1.8	0.12	0.15	0.12	0.18	0.17	0.20	0.18	0.21
17	Loma Linda VA	NR	S	Y	4	N	0.04	0.06	0.05	0.06	4.9	5.1	4.7	6.3	1.2	1.1	0.9	0.6	0.12	0.14	0.10	0.10	0.08	0.09	0.11	0.12
18	Long Beach 7-St.	WT	S	Y	7	N	0.07	0.05	0.07	0.04	7.9	4.6	8.7	4.4	1.1	0.6	1.2	0.6	0.04	0.08	0.05	0.08	0.22	0.10	0.22	0.09
20	Long Beach VA	NR	S	N	11	Y	0.07	0.06	0.05	0.06	5.7	5.1	5.2	4.6	1.6	1.5	1.8	1.5	0.12	0.12	0.10	0.14	0.25	0.20	0.15	0.15
21	LA 2-St. FCCB	SM	R	N	2	N	0.11	0.09	0.08	0.08	6.4	5.6	5.3	5.1	1.4	0.9	1.4	0.9	0.08	0.13	0.09	0.11	0.08	0.25	0.09	0.17
		LD					0.05	0.05	0.05	0.05	7.4	8.0	7.9	9.1	3.6	3.6	3.6	3.9	0.08	0.09	0.09	0.10	0.07	0.13	0.08	0.13
		NR					0.32	0.22	0.22	0.18	15.8	13.0	14.3	11.1	2.6	3.0	2.7	3.0	0.18	0.15	0.16	0.17	0.75	0.95	0.52	0.72
22	LA 3-St. Bldg.	NR	S	N	3	Y	0.28	0.24	0.33	0.32	21.0	26.8	16.1	29.6	4.7	5.7	4.5	4.9	0.39	0.34	0.50	0.52	0.46	0.35	0.37	0.64
23	LA 6-St. Bldg.	NR	S	N	5	Y	0.25	0.12	0.24	0.17	22.2	9.7	20.6	10.3	5.2	2.4	4.8	2.2	0.30	0.17	0.32	0.15	0.43	0.37	0.47	0.44
24	LA 6-St. Garage	NR	S	Y	6	N	0.22	0.15	0.28	0.15	17.0	15.6	19.5	18.9	3.9	3.5	4.4	3.5	0.35	0.21	0.44	0.29	0.32	0.27	0.38	0.31
25	LA 7-St. Hos.	LD	R	N	7	Y	0.04	0.04	0.03	0.04	6.1	5.8	5.6	4.8	2.2	3.1	2.5	3.0	0.08	0.04	0.07	0.05	0.08	0.09	0.07	0.08
		NR					0.21	0.49	0.16	0.37	10.7	31.1	9.0	25.9	2.5	2.4	2.2	1.7	0.08	0.15	0.10	0.12	0.70	1.37	0.45	1.00
26	LA 7-St. Bldg.	NR	S	N	7	N	0.28	0.47	0.22	0.28	22.0	21.9	24.6	24.1	4.0	7.3	5.8	5.1	0.22	0.46	0.30	0.45	0.49	0.35	0.26	0.46
27	LA 15-St. Bldg.	LD	R	N	17	N	0.03	0.03	0.03	0.03	7.0	10.4	12.1	7.5	3.5	8.6	7.2	6.2	0.03	0.02	0.03	0.02	0.06	0.09	0.06	0.10

		NR					0.17	0.19	0.13	0.21	14.5	17.1	12.3	16.2	2.9	2.7	3.2	2.9	0.02	0.02	0.03	0.02	0.35	0.28	0.24	0.32
28	LA 19-St. Bldg.	NR	S	Y	19	Y	0.28	0.25	0.20	0.32	21.3	29.3	15.0	21.8	5.0	5.6	4.8	5.2	0.06	0.06	0.06	0.07	0.49	0.33	0.32	0.27
29	LA Hollywood SB	KN	S	Y	14	Y	0.06	0.04	0.06	0.04	6.6	8.9	6.1	9.4	4.5	6.5	5.1	5.9	*	*	*	*	0.12	0.10	0.12	0.10
		SF					0.17	0.21	0.11	0.15	16.5	21.1	17.0	19.4	8.1	14.7	8.6	13.1	*	*	*	*	0.34	0.29	0.33	0.28
		WT					0.21	0.11	0.11	0.06	9.2	6.9	9.3	6.3	1.4	0.9	1.4	0.9	0.04	0.19	0.04	0.17	0.23	0.20	0.26	0.17
		NR					0.39	0.23	0.28	0.21	22.3	18.2	22.0	18.9	4.3	4.7	4.0	4.7	0.04	0.31	0.04	0.29	0.83	0.31	0.79	0.27
30	LA Wadsworth	NR	S	Y	6	Y	0.25	0.25	0.27	0.17	33.1	17.9	24.8	14.6	10.9	5.4	7.9	3.9	0.26	0.31	0.20	0.31	0.59	0.37	0.36	0.38
31	Newport Beach	NR	S	N	11	N	0.11	0.09	0.08	0.05	7.2	6.5	5.3	5.8	1.5	1.3	1.8	1.4	0.08	0.11	0.10	0.11	0.44	0.23	0.29	0.20
32	Norwalk 12400	WT	S	Y	7	Y	0.23	0.09	0.20	0.11	25.5	9.9	19.8	6.9	4.7	1.3	2.4	0.9	0.09	0.05	0.08	0.05	0.58	0.13	0.52	0.13
33	Norwalk 12440	WT	S	Y	7	Y	0.23	0.09	0.19	0.11	25.5	9.9	23.8	11.5	4.7	1.3	4.0	1.7	0.14	0.07	0.12	0.09	0.58	0.13	0.47	0.19
		NR					0.08	0.05	0.06	0.05	6.0	5.7	5.8	4.5	1.6	1.3	1.8	1.3	0.05	0.04	0.05	0.04	0.14	0.18	0.11	0.18
34	Palmdale 4-St.	NR	S	N	4	N	0.08	0.07	0.09	0.06	7.1	10.7	8.7	9.9	1.3	2.3	1.5	2.2	0.15	0.17	0.20	0.17	0.18	0.13	0.21	0.14
35	Pomona 2-St.	WT	S	Y	2	Y	0.06	0.06	0.05	0.05	2.3	2.4	2.1	2.9	0.2	0.3	0.1	0.4	0.15	0.10	0.12	0.11	0.17	0.08	0.13	0.10
		UP					0.21	0.19	0.12	0.13	8.0	10.4	8.4	10.1	1.3	1.2	1.3	1.2	0.37	0.45	0.22	0.34	0.59	0.61	0.25	0.60
36	Pomona 6-St.	UP	S	N	6	Y	0.21	0.19	0.10	0.13	8.0	10.4	7.6	10.3	1.3	1.2	1.5	1.7	0.08	0.15	0.09	0.13	0.59	0.61	0.22	0.56
		LD					0.04	0.07	0.05	0.07	8.5	12.3	9.7	11.1	2.7	5.8	2.4	3.1	0.09	*	0.10	*	0.15	0.23	0.16	0.25
37	Rancho Cuc. LJC	RD	S	N	4	Y	0.04	0.03	0.03	0.04	0.8	0.5	0.7	0.4	0.1	0.0	0.1	0.0	0.01	0.01	0.01	0.01	0.20	0.15	0.13	0.16
		WT					0.05	0.06	0.02	0.03	1.4	1.4	1.0	1.0	0.2	0.1	0.2	0.1	0.02	0.02	0.02	0.02	0.11	0.13	0.05	0.08
		UP					0.24	0.23	0.14	0.11	8.3	4.9	5.1	2.9	0.6	0.4	0.6	0.3	0.13	0.09	0.09	0.06	0.60	0.95	0.27	0.36
		LD					0.11	0.07	0.10	0.06	12.2	8.4	11.6	8.6	3.1	2.2	3.1	2.2	0.15	0.11	0.13	0.11	0.12	0.14	0.12	0.14
		NR					0.07	0.05	0.04	0.04	3.8	3.2	3.0	3.1	0.5	0.6	0.5	0.7	0.05	0.07	0.05	0.07	0.13	0.15	0.09	0.08
38	San Bern. 3-St.	LD	S	N	3	N	0.08	0.09	0.12	0.08	19.6	13.9	24.2	15.7	9.1	6.2	12.2	7.6	0.29	0.25	0.33	0.22	0.30	0.23	0.46	0.25
39	San Bern. 5-St.	NR	S	N	5	Y	0.07	0.04	0.04	0.03	4.1	2.5	3.6	2.2	0.5	0.4	0.5	0.4	0.14	0.07	0.10	0.08	0.15	0.08	0.10	0.07
40	San Bern. 9-St.	LD	S	Y	9	N	0.09	0.10	0.08	0.07	15.3	13.3	14.7	14.8	7.5	6.1	7.4	5.4	0.05	0.11	0.05	0.08	0.11	0.17	0.08	0.16
41	San Bern. CGC	NR	S	Y	5	N	0.04	0.04	0.04	0.04	3.3	3.6	4.5	4.7	0.7	0.7	0.8	0.7	0.08	0.06	0.13	0.07	0.08	0.08	0.07	0.07
42	Santa Susana	NR	R	N	8	N	0.26	0.28	0.35	0.25	17.9	16.2	18.7	14.3	6.0	3.3	6.2	3.0	0.51	0.30	0.47	0.26	0.85	1.05	0.97	0.90
43	Seal Beach 8-St.	LD	S	Y	8	Y	0.04	0.05	0.04	0.04	15.5	8.5	15.5	8.1	11.3	5.3	11.1	5.3	0.11	0.13	0.10	0.13	0.06	0.05	0.06	0.05
		NR					0.06	0.08	0.05	0.08	5.6	5.9	4.9	5.7	1.3	1.5	1.4	1.5	0.04	0.06	0.04	0.06	0.17	0.29	0.16	0.27
44	Sylmar Hos.	WT	S	N	6	N	0.06	0.05	0.06	0.06	4.0	3.5	3.1	3.7	0.6	0.5	0.5	0.6	0.13	0.13	0.17	0.18	0.06	0.07	0.08	0.07
		NR					0.84	0.60	0.80	0.38	129	76.9	112	71.1	32.6	15.2	28.3	18.4	2.72	1.01	2.04	1.11	2.81	1.19	1.79	1.01
45	Ventura 12-St.	NR	S	Y	12	N	0.05		0.07		7.8		8.2		2.6		2.5		0.15		0.26		0.13		0.12	
46	Lotung Reactor	L07	S	N	1	Y	0.21	0.16	0.13	0.15	16.9	30.3	14.1	30.9	6.4	8.4	6.5	9.7	0.11	0.11	0.12	0.11	0.44	0.34	0.31	0.32

* = flexible-base period not determined, so spectral accelerations not evaluated

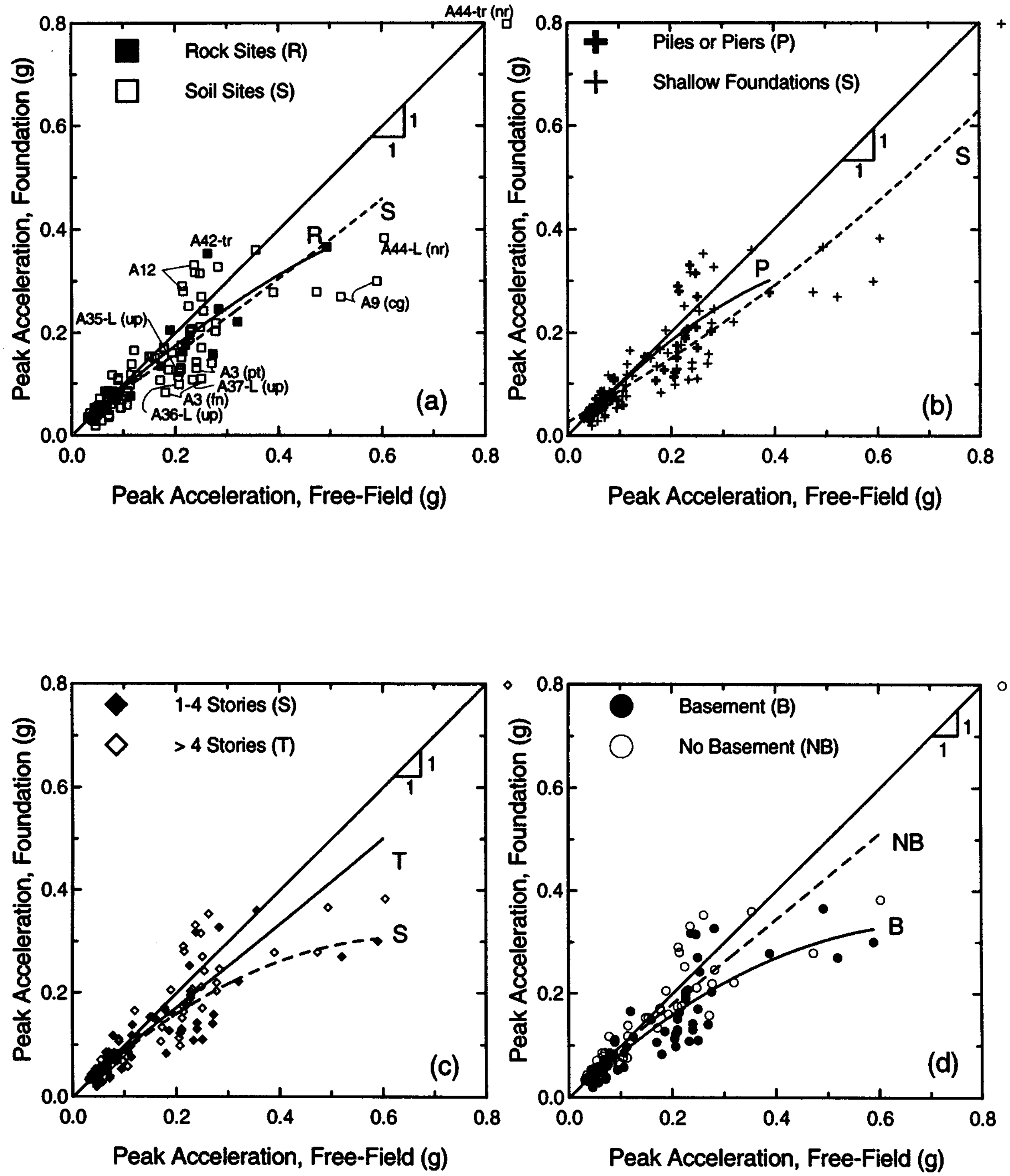

Fig. 5.1: Comparison of peak accelerations in the free-field and at the foundation-level of structures

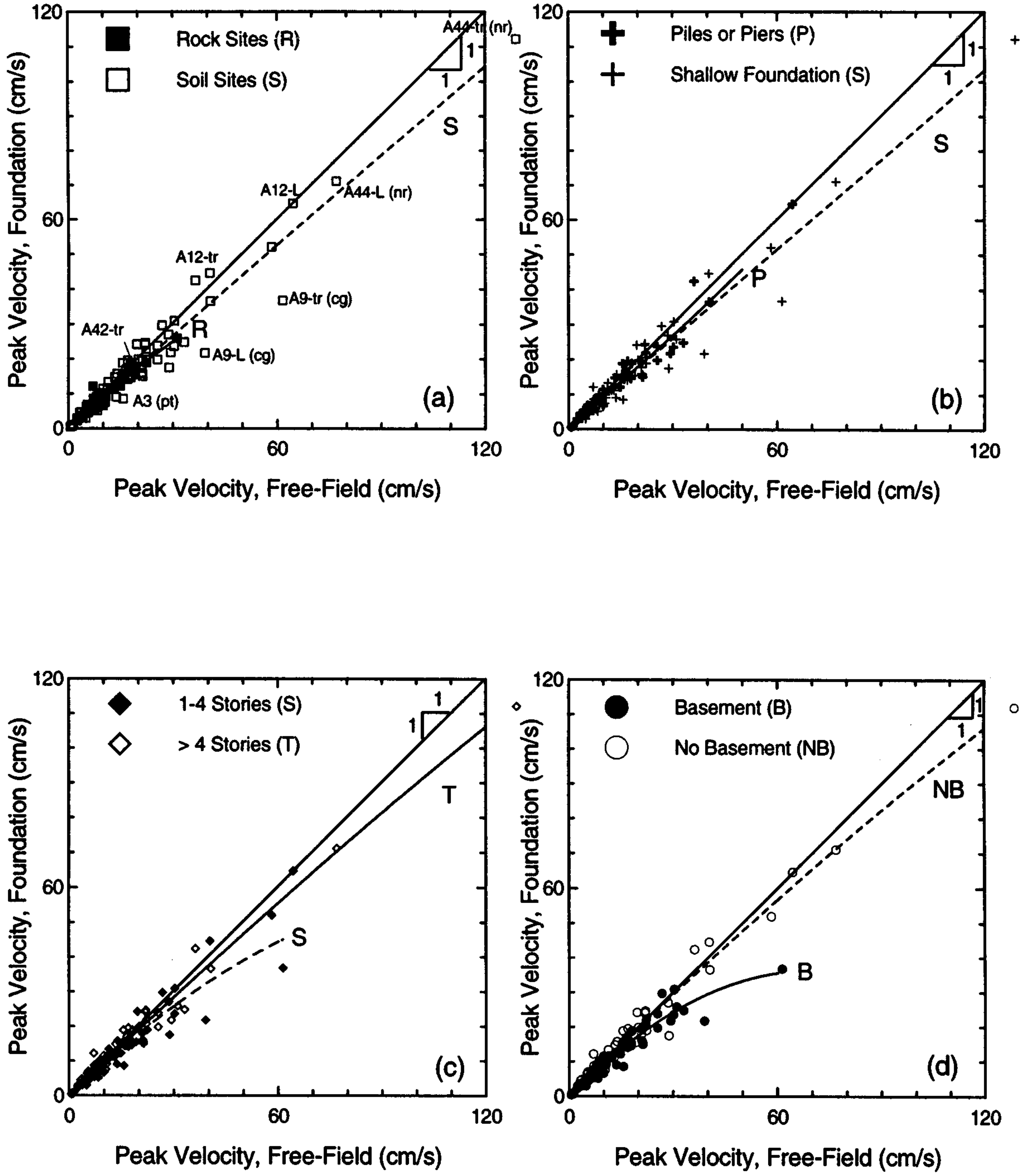

Fig. 5.2: Comparison of peak velocities in the free-field and at the foundation-level of structures

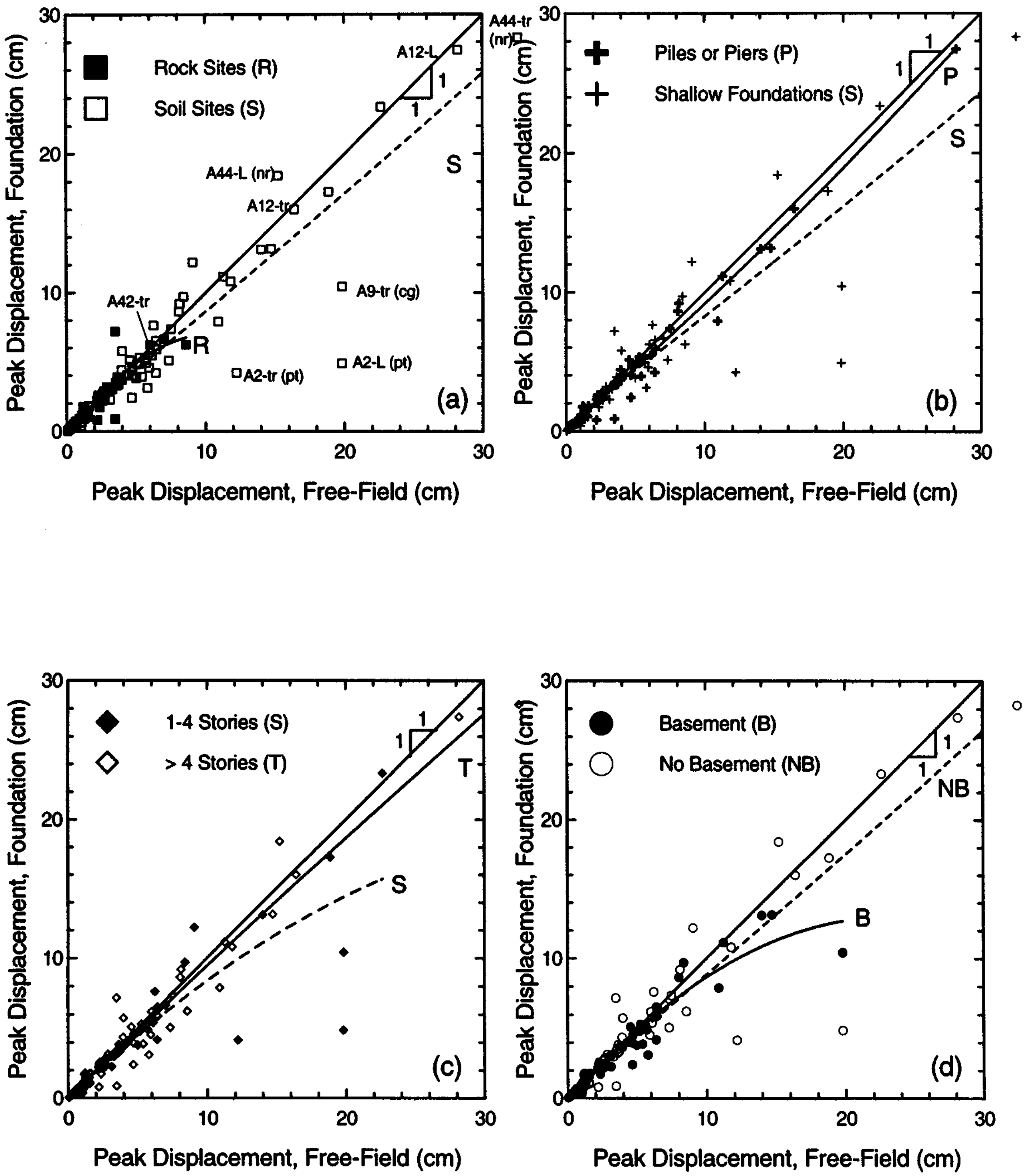

Fig. 5.3: Comparison of peak displacements in the free-field and at the foundation-level of structures

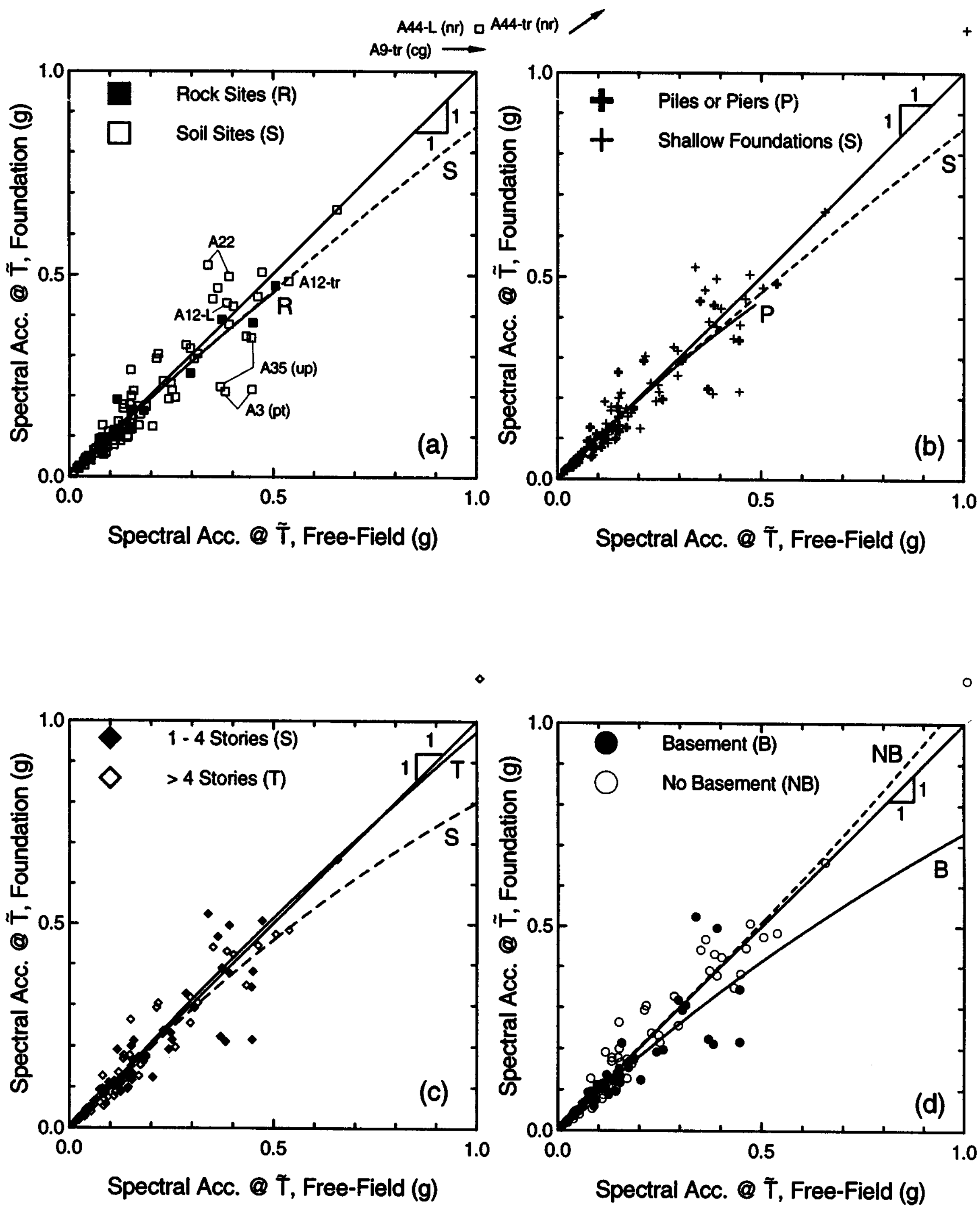

Fig. 5.4: Comparison of 5%-damped spectral accelerations at $\tilde{T}$ in the free-field and at the foundation-level of structures

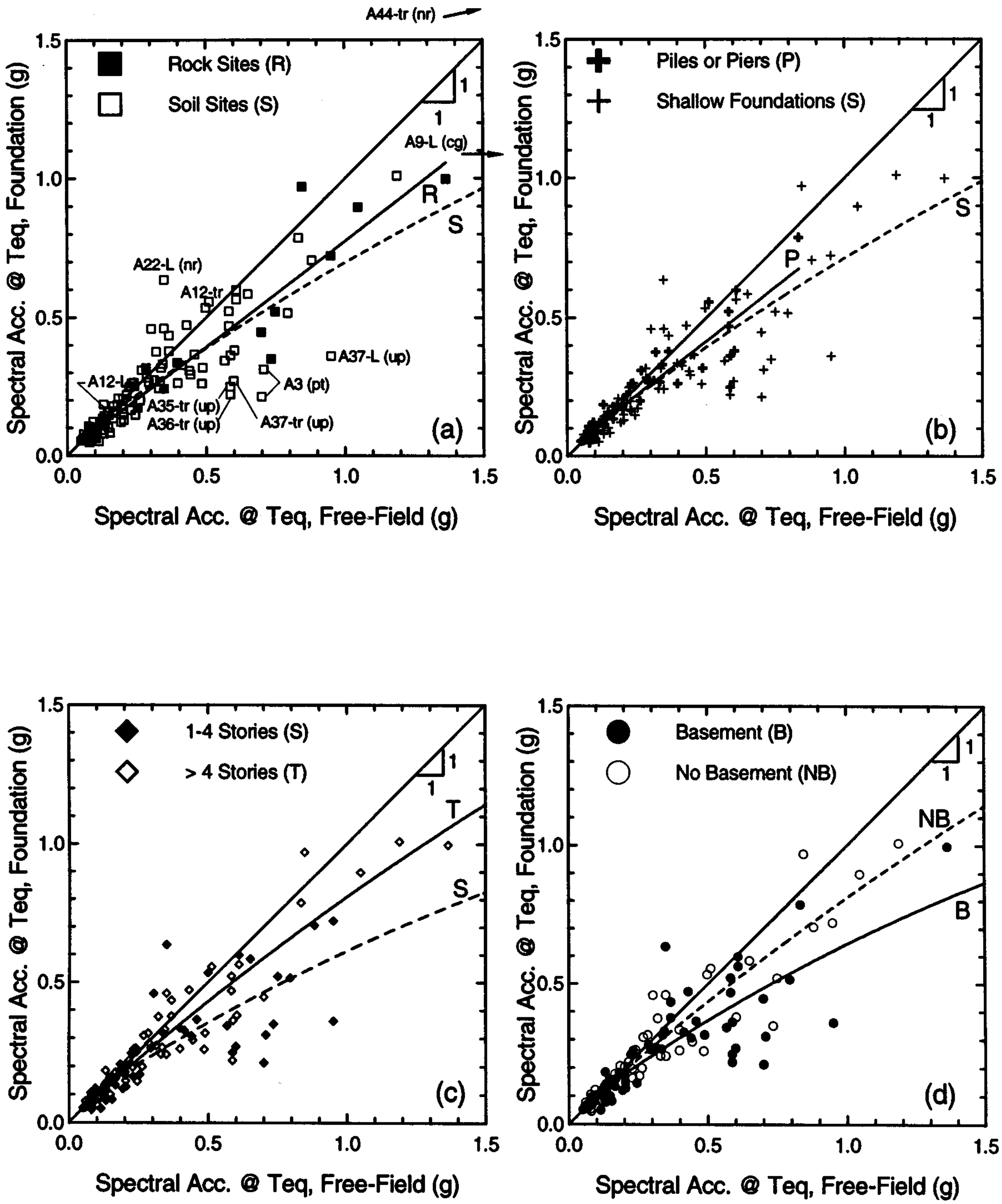

Fig. 5.5: Comparison of 5%-dampied spectral accelerations at Teq in the free-field and at the foundation-level of structures

5.2.1 Peak Accelerations, Velocities, and Displacements

The data in Fig. 5.1 indicate that peak foundation-level accelerations are generally de-amplified relative to the free-field. No significant differences are apparent between the average de-amplification of foundation motions at rock vs. soil sites or buildings with deep vs. shallow foundations. However, the de-amplification is larger in "short" structures (1-4 stories) than "tall" structures (> 4 stories), and is also larger in embedded than surface structures. The data for peak velocities and displacements in Figs. 5.2 and 5.3 generally indicate less de-amplification than was observed from the peak acceleration data. The trends in the data for rock vs. soil, deep vs. shallow foundations, short vs. tall structures, and embedded vs. surface structures are similar to those for acceleration.

The deviations between foundation and free-field motions in Figs. 5.1 to 5.3 are associated with kinematic and inertial interaction effects, as well as peculiarities of particular sites, structures, and earthquakes. Hence, it is tenuous to draw firm conclusions about a particular SSI effect from these results. However, there are some notable trends in the data which provide insights into SSI effects, and these are discussed below along with peculiar results for several sites.

(a) *Larger de-amplification of foundation peak accelerations than peak velocities or displacements*

Peak acceleration is sensitive to high frequency components of motion, whereas velocities and displacements are sensitive to lower frequency components. The de-amplification of foundation accelerations likely results from the filtering effect of kinematic interaction on high frequency components of ground motion. The smaller de-amplification of velocities and displacements likely results from both the reduced kinematic interaction at these lower frequencies and contributions to foundation motion from inertial interaction effects (which typically occur at relatively low frequencies).

(b) *Increased de-amplification of foundation-level motions in embedded structures*

The pronounced de-amplification of basement motion relative to free-field motion is a result of the tendency for ground motion amplitude to decrease with depth, and to some extent from wave scattering effects. Such de-amplification was also noted by Poland et al. (1994).

(c) *Reduced de-amplification of foundation-level motions in >4-story structures*

Inertial interaction effects in tall structures can enhance their foundation motions relative to those in shorter structures. This occurs because tall, heavy structures develop more inertia during earthquake shaking than short, light structures, and because foundation damping effects decrease with increasing aspect ratio (i.e. Fig. 2.10).

(d) *Large de-amplification of foundation-level accelerations at particular sites*

The de-amplification of foundation-level accelerations relative to the free-field was particularly significant for sites A3 and A9 and for several data sets from the Upland Earthquake (at sites A35-37). The structure at site A3 is an 86-foot deep caisson with a 30-foot radius ($e/r = 86/30 = 2.9$), and hence the embedment effect is unusually pronounced. At site A9, the structure and free-field accelerograph are at the foot and top, respectively, of a 3H:1V, 84-foot tall slope. Hence, topographic effects, which would tend to amplify the free-field motions and de-amplify the structural motions by as much as 20% at this slope angle (Ashford and Sitar, 1994), may have contributed to the large de-amplification at this site.

Data pairs from sites A35-37 in the Upland earthquake indicated unusually de-amplified foundation accelerations in the structures' longitudinal direction. These structures have basements, and a pronounced embedment effect may have resulted from the free-field motions having high predominant frequencies (f_{eq} ~ 6 to 7 Hz) in the structure's longitudinal directions. These high frequencies give rise to short wavelengths (about 140 feet based on V_S ~ 800 to 1000 fps at these sites) which have a node (at 1/4 of the wavelength) near the embedment depth (10 to 20 feet). In contrast, the predominant frequency of the transverse free-field motions was lower (f_{eq} ~ 2 to 4 Hz), and the attenuation of foundation motions relative to the free-field was less significant.

(e) *Amplification of foundation-level motions*

As can be seen from Figs. 5.1 to 5.3, amplification of foundation motions relative to the free-field was unusual. Where it occurred (e.g. sites A12, A42-tr), amplification was generally most pronounced in acceleration data, and hence appears to be a high frequency effect. In the case of site A42-tr, the foundation instrument is located adjacent to a 6 to 8-foot deep pit, and a reinforced concrete retaining wall separates the pit from the floor where the instrument is located (the transverse direction of the structure is normal to the alignment of the retaining wall). The high frequency amplification in this case may have resulted from local topographic amplification near the wall. In the case of site A12, further study is required to determine the cause of the amplification of foundation-level accelerations. The behavior of the soil-foundation-structure system is relatively complex in this case as the structure was severely damaged by the earthquake shaking and was subsequently razed.

5.2.2 Spectral Accelerations

Spectral accelerations at the first-mode flexible-base period of the structures ($\tilde{T}$) for foundation and free-field motions are compared in Fig. 5.4. The contributions of inertial interaction to foundation motion are most pronounced at $\tilde{T}$, and a comparison of Figs. 5.1 and 5.4 confirms that less de-amplification of foundation motion occurred in spectral accelerations at $\tilde{T}$ than in peak accelerations (which are the spectral acceleration at T=0). Relative trends in the data for the various conditions in plots (a) to (d) are similar to those noted for peak accelerations. No significant differences in spectral accelerations are observed for rock/soil sites or structures with shallow/deep foundations, but the attenuation of foundation motions is notably more pronounced for "short" than "tall" and for embedded than surface foundations. In fact, no de-amplification of spectral accelerations at $\tilde{T}$ occurred on average for either "tall" or surface structures.

Spectral accelerations from foundation and free-field motions are also compared at the fundamental period of earthquake shaking (T_{eq}) in Fig. 5.5. This comparison shows significant de-amplification of these foundation spectral accelerations. The same relative trends noted above for conditions in plots (a) through (d) are observed again in Fig. 5.5.

Some of the outliers in the spectral acceleration comparisons are labeled in Figs. 5.4 and 5.5. Explanations for the large de-amplifications at sites A3, A9, and A35-37 (up) were discussed in Section 5.2.1. Foundation spectral accelerations at sites A12 and A42-

tr were not amplified (except at site A42-tr, minor amplification at the low T_{eq} value), which contrasts with the amplification of peak accelerations in Fig. 5.1. Amplified foundation spectral accelerations at site A22 may be unreliable due to potentially large spatial incoherence effects (the free-field and structure are separated by about 1700 feet).

5.3 Empirical Evaluation of the Effects of Inertial Interaction

5.3.1 Evaluation of Modal Parameters: Overview

For the investigation of inertial interaction effects in this study, modal parameters were evaluated for two cases of base fixity: (1) a "fixed-base" case in which the system flexibility is associated entirely with the structure (i.e. no SSI effects), and (2) a "flexible-base" case in which the system flexibility is associated with foundation translation and rocking as well as structural deformations. Inertial interaction effects are quantified by the first-mode period lengthening ratio ($\tilde{T} / T$) and the foundation damping factor ($\tilde{\zeta}_0$).

Modal parameters were evaluated using the system identification procedures described in Sections 3.1 to 3.5. As described in Section 3.6, the fixed- and flexible-base parameters were directly evaluated using system identification procedures when the site instrumentation included a free-field accelerograph, a structure with foundation- and roof-level lateral sensors, and foundation-level vertical sensors capable of measuring base rocking. However, the instrumentation at many sites lacked foundation sensors for measuring base rocking (many 'A' sites) or free-field accelerographs (all 'B' sites). For these cases, the fixed- or flexible-base parameters were estimated using procedures in Section 3.6.2. These procedures require that modal parameters be evaluated for a third “pseudo flexible-base” case. Hence, modal parameters identified for each structure included fixed-base (T, ζ), flexible-base ($\tilde{T}, \tilde{\zeta}$), and pseudo flexible-base ($\tilde{T}^*, \tilde{\zeta}^*$).

5.3.2 Verification of Estimated First-Mode Periods and Damping Ratios

Analytical procedures were developed in Section 3.6.2 to estimate fixed- or flexible-base parameters for sites with inadequate instrumentation for direct identifications. For sites where these parameters can be evaluated directly, verification of the estimation procedures against identified parameters is possible. Results for eleven such sites, with 19 data sets, are evaluated in this section. The results are summarized in Table 5.2.

The conditions necessary to apply the parameter estimation procedures are that $\tilde{f} < \tilde{f}^*$ for estimating fixed-base parameters and $\tilde{f}^* < f$ for estimating flexible-base parameters. For the 11 sites with complete instrumentation sets, these conditions were met for 11 of the 19 data sets for estimating fixed-base parameters, and in 17 of 19 data sets for estimating flexible-base parameters. Each site which failed the $\tilde{f} < \tilde{f}^*$ or $\tilde{f}^* < f$ criteria had negligible period lengthening, and the criteria were not met as a result of small numerical errors inherent to all system identification results. These errors can be associated with inadequate model structure and random disturbance errors in the output data, as discussed below in Section 5.3.3(b).

Based on the results in Table 5.2, the parameter estimation procedures appear to provide good estimates of fixed- and flexible-base periods both at sites where inertial interaction effects are significant (e.g. A46) as well as sites where these effects are minor (e.g. A8).

Table 5.2: Comparison of system identification results (mean and standard deviation) and estimated fixed- and flexible-base fundamental-mode parameters at 11 sites

				Pseudo Flex.-base		Fixed-base (Sys. ID)		Fixed-base (estimated)		Flex.-base (Sys. ID)		Flex.-base (estimated)	
Site	e/r_1	EQ[1]	dir	$\tilde{f}^*$ (Hz)	$\tilde{\zeta}^*$ (%)	f (Hz)	ζ (%)	f (Hz)	ζ (%)	$\tilde{f}$ (Hz)	$\tilde{\zeta}$ (%)	$\tilde{f}$ (Hz)	$\tilde{\zeta}$ (%)
A4	0	LP	TR	0.41±0.01	7.5±2.2	0.41±0.02	7.4±7.3	0.44	0	0.40±0.02	13.0±4.4	0.41	7.6
			L	0.37±0.01	7.1±2.0	0.38±0.01	5.9±1.7	--	--	0.39±0.02	12.8±4.9	0.37	8.1
A8	0	LP	TR	6.07±0.01	2.9±0.1	6.32±0.02	2.2±0.1	6.42	3.2	5.44±0.02	4.8±0.1	5.60	15.2
A23	0.65	NR	TR	1.11±0.01	6.6±0.4	1.21±0.01	6.9±0.5	--	--	1.12±0.01	5.5±0.5	1.10	6.9
A24	0	NR	L	2.50±0.1	5.4±0.1	3.63±0.02	6.5±0.2	2.87	5.2	2.27±0.01	6.1±0.3	2.06	4.3
A25	0	NR	TR	0.79±0.02	31.1±6.4	0.79±0.02	29.3±6.0	--	--	0.84±0.03	27.1±6.6	0.79	72
A31	0	NR	TR	1.18±0.00	4.9±0.2	1.34±0.01	8.5±0.5	1.27	7.1	1.16±0.01	3.2±0.2	1.15	3.0
A33	0.11	WT	L	0.82±0.01	2.8±0.3	0.82±0.01	3.0±0.3	--	--	0.83±0.02	3.5±0.7	--	--
		NR	L	0.82±0.01	3.1±0.5	0.82±0.01	3.4±0.5	--	--	0.82±0.02	4.6±0.6	--	--
A37	0.12	RD	TR	1.68±0.01	4.2±0.3	1.71±0.01	3.7±0.3	1.70	4.3	1.66±0.02	4.3±0.5	1.64	10.9
		WT	TR	1.57±0.01	4.9±0.2	1.58±0.01	5.0±0.2	1.58	5.0	1.55±0.02	4.4±0.4	1.54	5.4
		UP	TR	1.28±0.01	7.3±0.4	1.29±0.01	7.8±0.4	--	--	1.31±0.02	4.7±0.6	1.26	4.7
		LD	TR	1.16±0.01	12.7±1.3	1.17±0.02	12.5±1.3	1.17	12.9	1.16±0.02	11.2±1.4	1.15	17.8
		NR	TR	1.32±0.01	6.4±0.2	1.34±0.01	6.9±0.2	1.32	6.5	1.32±0.01	4.6±0.4	1.29	2.9
A43	0.16	LD	TR	0.78±0.01	12.6±0.9	0.80±0.01	13.2±1.0	--	--	0.78±0.01	11.5±1.0	0.76	13.3
		NR	TR	0.82±0.01	7.1±0.5	0.85±0.01	7.1±0.5	--	--	0.83±0.01	6.6±0.5	0.80	12.3
A45	0	NR	TR	1.49±0.02	3.7±0.5	1.88±0.02	5.7±0.7	1.86	6.6	1.41±0.02	4.0±0.4	1.41	5.2
A46	0.92	LT7	TR	2.37±0.02	16.7±1.1	8.5	3	*	*	2.04±0.03	30.6±2.8	2.19	30.2
			L	2.42±0.02	12.9±0.8	9.0	3	*	*	2.25±0.03	31.0±3.0	2.24	30.0

-- no solution possible as $\tilde{f} > \tilde{f}^*$ for fixed-base, or $\tilde{f}^* > f$ for flexible-base

* No solution

[1] Earthquakes: 1985 Redlands (RD), 1987 Whittier (WT), 1989 Loma Prieta (LP), 1990 Upland (UP), 1992 Landers (LD), 1994 Northridge (NR), Lotung event LSST07 (LT7).

Estimates of fixed-base damping (ζ) differed from identified values by absolute differences of about 1 to 2% (except at site A4, where random disturbance errors in ζ are large). At several sites with significant interaction, estimated ζ values are closer to "known" ζ values than are the pseudo flexible-base damping ($\tilde{\zeta}^*$) values (e.g. A31, A45). By contrast, the estimation of flexible-base damping ($\tilde{\zeta}$) is highly sensitive to differences between ζ and $\tilde{\zeta}^*$ values, and where such differences are small (i.e. within the range of uncertainty of the system identification results), $\tilde{\zeta}$ values can be significantly overestimated [e.g. A8, A25, A37 (rd), A37 (up), A43(nr)]. However, when the difference between ζ and $\tilde{\zeta}^*$ values is large (e.g. A24, A31, A45, A46), the flexible-base damping is generally well predicted. Overestimated $\tilde{\zeta}$ values are usually fairly obvious from comparisons with $\tilde{\zeta}^*$ values. For such cases, the results in Table 5.2 indicate that flexible-base damping is generally better estimated by $\tilde{\zeta}^*$ values.

The fixed-base parameters could not be estimated for site A46. A large increase in f relative to $\tilde{f}$ is predicted by the procedure (which is consistent with the unusually large SSI effect at this site), but the estimate is undefined because $\tilde{\omega}_\theta < \tilde{\omega}^*$ (i.e. see Eq. 3.57). In this case, the estimation of f is highly sensitive to the relatively small difference between $\tilde{f}$ and $\tilde{f}^*$, and the instability of the estimate is likely associated with small numerical identification errors. Errors associated with model structure are unusually large at this site due to the stiff structural response (i.e. the system identification results in this case were sensitive to the order of the model, *J*). In contrast, the flexible-base parameters were accurately estimated because the estimate is based on the relatively large differences between the fixed and pseudo flexible-base parameters.

In summary, the estimation procedures generally provide reasonable estimates of system identification results at eleven sites where complete instrumentation sets are available. Comparisons of estimated and "known" first-mode parameters show that (1) fixed- and flexible-base frequencies are reliably predicted by the parameter estimation procedures, (2) estimated fixed-base damping ratios are fairly accurate (absolute difference between estimated and actual values of about 1 to 2%), and (3) flexible-base damping is generally well predicted when SSI effects are significant, but can be overpredicted when SSI effects are modest. For cases with modest SSI effects but large differences between estimated flexible-base damping and identified fixed-base damping, the flexible-base damping is better estimated by the pseudo flexible-base damping.

5.3.3 Interpretation of Modal Parameters

System identification analyses for the 57 sites considered in this study were performed according to the procedures in Chapter 3. Modal vibration periods and damping ratios were evaluated for the fixed-base (T, ζ) and flexible-base ($\tilde{T}, \tilde{\zeta}$) cases, and are listed in Table 5.3. This section will describe the assignment of relative confidence levels to these parameters, and the assessment of numerical errors and system nonlinearities in the identification results.

Table 5.3: Compilation of first-mode parameters for 'A' and 'B' sites

								Transverse									Longitudinal									
Site	Station	Eqk.	MHA (g)	h (ft)	e (ft)	Vs (fps)	β(%)	r_1 (ft.)	r_2 (ft.)	$\tilde{T}$ (sec.)	T (sec.)	$\tilde{\zeta}$ (%)	ζ (%)	$\frac{1}{\sigma}$	$\tilde{T}/T$	$\tilde{\zeta}_0$	r_1 (ft.)	r_2 (ft.)	$\tilde{T}$ (sec.)	T (sec.)	$\tilde{\zeta}$ (%)	ζ (%)	$\frac{1}{\sigma}$	$\tilde{T}/T$	$\tilde{\zeta}_0$	Conf.
'A' Sites																										
1	Eureka Apts.	PT	0.18	31	0	701	5.1	57	42	0.24	0.15	19.6	15.9	0.29	1.57	15.4	57	77	0.25	0.22	12.8	5.5	0.20	1.09	8.6	A
2	Fortuna Market	PT	0.12	22	0	772	5.6	115	112	0.37	0.36	34.0	26.0	0.08	1.04	11.2	115	122	0.31	0.29	39.4	18.0	0.10	1.08	25.1	L
		PTA	0.19			786	5.8			0.35	0.34	17.2	15.0	0.08	1.05	4.1			0.29	0.28	25.6	17.6	0.10	1.03	9.6	L
4	Emeryville PPP	LP	0.25	218	0	448	6.8	87	94	2.50	2.45	13.0	7.4	0.20	1.02	6.1	87	94	2.58	2.65	12.8	5.9	0.18	1.00	6.9	A
5	Hayward City Hall	LP	0.05	84	0	2210	0.8	66	54	1.16	1.11	3.8	3.5	0.03	1.04	0.7	66	82	0.87	0.85	3.2	4.2	0.04	1.03	0.0	A
6	Hayward 13-St.	LP	0.09	141	0			63	64	U3	U3	U3	U3	U3	U3	U3	63	64	U3	U3	U3	U3	U3	U3	U3	
7	Hollister 1-St.	LP	0.36	30	0	502	7.7	97	75	0.73	0.71	26.9	19.0	0.08	1.03	9.3	97	130	U2	U2	U2	U2	U2	U2	U2	A
8	Piedmont Jr. HS	LP	0.08	25	0	1820	1.3	52	46	0.18	0.16	4.8	2.2	0.09	1.16	3.4	52	59	0.17	0.17	7.0	5.1	0.08	1.00	2.0	A
9	PVPP	CGA	0.21	48	32	970	3.2	53	37	0.53	0.53	8.2	5.2	0.09	1.00	3.0	53	77	U2	U2	U2	U2	U2	U2	U2	L
10	Richmond CH	LP	0.13	33	10	768	3.7	75	54	0.30	0.28	9.2	3.9	0.16	1.08	6.1	75	106	0.27	0.26	14.4	1.4	0.16	1.03	13.1	A
11	San Jose 3-St.	LP	0.27	35	0	2642	0.9	86	68	0.64	0.67	20.6	24.8	0.02	1.00	0.0	86	111	0.60	0.66	20.3	23.6	0.02	1.00	0.0	A
12	El Centro Bldg.	IMP	0.24	54	0	464	6.6	61	55	0.74	0.50	16.0	23.4	0.23	1.47	8.8	61	69	1.23	1.25	33.9	36.6	0.09	1.00	0.0	A
13	Indio 4-St.	LD	0.09	56	15.5	695	4.1	69	58	0.71	0.67	10.3	7.5	0.12	1.05	3.8	69	85	0.66	0.64	10.9	10.9	0.13	1.03	1.0	A
14	Lancaster 3-St.	WT	0.07	26	0	908	2.1	54	47	0.20	0.20	13.4	12.4	0.14	1.00	1.1	54	63	U2	U2	U2	U2	U2	U2	U2	A
15	Lancaster 5-St.	NR	0.07	40	0	1001	2.5	99	83	0.73	0.69	10.0	7.5	0.06	1.06	3.6	99	121	0.72	0.71	8.2	9.1	0.06	1.02	0.0	A
16	Lancaster Airfield	NR	0.08	45	6	953	1.7	11.9	11.9	0.34	0.27	9.9	24.5	0.18	1.28	0.0	11.9	11.9	0.33	0.24	8.9	13.6	0.20	1.34	3.3	L
17	Loma Linda VA	NR	0.06	50	0	1415	3.4	246	248	0.29	0.25	15.0	5.8	0.14	1.17	11.3	246	250	0.32	0.29	10.1	5.6	0.12	1.09	5.7	A
18	Long Beach 7-St.	WT	0.07	58	0	615	3.5	49	46	U3	U3	U3	U3	U3	U3	U3	49	53	1.12	1.14	5.5	6.5	0.08	1.00	0.0	A
20	Long Beach VA	NR	0.07	98	23	1143	2.9	84	83	0.58	0.51	3.1	4.6	0.17	1.13	0.0	84	87	0.58	0.55	4.5	4.1	0.16	1.05	1.0	A
21	LA 2-St. FCCB	SM	0.11	22	0	1006	1.3	71	59	0.79	0.79	9.4	13.3	0.03	1.01	0.0	71	88	0.79	0.82	21.5	17.7	0.03	1.00	3.9	L
		LD	0.05			1010	1.2			0.97	0.98	14.2	14.9	0.02	1.00	0.0			0.90	0.90	18.4	18.9	0.02	1.00	0.0	L
		NR	0.32			981	1.7			0.92	0.95	34.4	40.1	0.02	1.00	0.0			0.83	0.84	33.4	39.5	0.03	1.00	0.0	L
22	LA 3-St. Bldg.	NR	0.28	46	22.5	980	5.9	130	128	U1	U1	U1	U1	U1	U1	U1	130	134	U1	U1	U1	U1	U1	U1	U1	L
23	LA 6-St. Bldg.	NR	0.25	56	14	630	5.2	21.4	20.6	0.89	0.82	5.5	6.9	0.11	1.08	0.0	21.4	22.7	U3	U3	U3	U3	U3	U3	U3	A
24	LA 6-St. Garage	NR	0.22	40	0	870 (tr) 640 (L)	7.3 (tr) 6.2 (L)	159	154	0.52	0.51	6.6	6.1	0.09	1.04	1.1	54	47	0.44	0.28	6.1	6.5	0.23	1.60	4.5	A
25	LA 7-St. Hos.	LD	0.04	68	0	1148	1.2	110	110	1.14	1.18	11.8	12.1	0.05	1.00	0.0	110	110	1.09	1.11	10.1	13.1	0.05	1.00	0.0	A
		NR	0.49			1065	2.5			1.19	1.27	27.1	29.3	0.05	1.00	0.0			1.21	1.19	21.1	28.0	0.05	1.01	0.0	A
26	LA 7-St. Bldg.	NR	0.47	66	13.5	548	7.6	33	30	0.66	0.63	9.2	16.1	0.19	1.04	0.0	33	37	1.04	1.09	7.0	11.5	0.11	1.00	0.0	L
27	LA 15-St. Bldg.	LD	0.03	174	0	1161	1.2	131	110	3.15	3.20	3.9	3.0	0.05	1.00	1.0	131	161	3.09	3.10	2.1	1.8	0.05	1.00	0.3	A
		NR	0.19			1120	2.0			3.12	3.20	8.5	2.8	0.05	1.00	5.6			3.07	3.09	8.8	2.0	0.05	1.00	6.8	A
28	LA 19-St. Bldg.	NR	0.28	220	38	980	5.9	92	76	3.24	3.45	U1	U1	0.07	1.00	U1	92	113	3.72	3.89	U1	U1	0.06	1.00	U1	A
29	LA Hollywood SB	WT	0.21	96	9	930	2.8	59	42	1.80	1.77	9.1	5.4	0.06	1.01	3.9	59	86	U4	U4	U4	U4	U4	U4	U4	L
		NR	0.39			879	4.4			2.10	2.05	18.3	15.4	0.05	1.02	3.9			0.80	0.75	8.0	8.5	0.15	1.06	0.9	L
30	LA Wadsworth	NR	0.25	78	17	981	6.3	189	199	1.00	0.92	9.3	9.3	0.09	1.08	1.9	189	199	U3	U3	U3	U3	U3	U3	U3	A
31	Newport Beach	LD	0.04	94	0	1009	2.3	61	52	0.84	0.70	4.7	2.9	0.13	1.19	3.0	61	74								A
		NR	0.11			969	3.2			0.86	0.75	3.2	8.5	0.13	1.16	0.0			0.77	0.67	3.9	4.4	0.14	1.14	0.9	A
32	Norwalk 12400	WT	0.23	70	13.5	730	6.8	93	83	U3	U3	U3	U3	U3	U3	U3	93	106	1.48	1.54	9.6	8.5	0.06	1.00	1.1	A

33	Norwalk 12440	WT	0.23	72	15	794	7.3	142	105	1.32	1.32	2.0	1.8	0.07	1.00	0.2	142	195	1.20	1.22	3.5	3.0	0.07	1.00	0.5	A
		NR	0.08			906	4.0			1.28	1.30	6.3	4.9	0.06	1.00	1.4			1.20	1.22	4.6	3.4	0.07	1.00	1.2	A
34	Palmdale 4-St.	NR	0.08	24	0	1575	1.7	69	49	0.20	0.12	18.5	24.1	0.12	1.66	13.1	69	100	0.20	0.16	12.4	4.9	0.09	1.22	9.7	A
35	Pomona 2-St.	WT	0.06	28	10.5	1246	1.6	59	57	0.26	0.25	8.7	5.5	0.09	1.02	3.6	59	63	0.27	0.26	5.8	8.6	0.09	1.02	0.0	A
		UP	0.21			1178	3.2			0.29	0.29	9.2	4.9	0.08	1.01	4.4			0.30	0.30	11.2	12.1	0.08	1.00	0.0	A
36	Pomona 6-St.	UP	0.21	53	12.5	1148	3.1	50	43	U1	U1	U1	U1	U1	U1	U1	50	59	U1	U1	U1	U1	U1	U1	U1	L
		LD	0.07			1188	2.2			1.26	1.07	9.3	13.4	0.04	1.17	1.0			1.20	0.87	9.8	9.5	0.05	1.39	6.2	L
37	Rancho Cuc. LJC	RD	0.04	56	14	1172	1.4	120	87	0.60	0.59	4.3	3.7	0.08	1.03	0.9	120	170	0.60	0.60	5.6	4.2	0.08	1.00	1.4	A
		WT	0.06			1157	1.7			0.65	0.63	4.4	5.0	0.08	1.02	0.0			0.66	0.65	8.4	6.1	0.07	1.01	2.5	A
		UP	0.24			1060	4.5			0.76	0.77	4.7	7.8	0.07	1.00	0.0			0.75	0.77	6.0	6.7	0.07	1.00	0.0	A
		LD	0.11			1039	4.4			0.87	0.85	11.2	12.5	0.06	1.01	0.0			0.89	0.87	17.2	17.4	0.06	1.02	0.9	A
		NR	0.07			1114	2.8			0.76	0.75	4.6	6.9	0.07	1.02	0.0			0.81	0.79	7.5	8.9	0.06	1.02	0.0	A
38	San Bern. 3-St.	LD	0.09	29	0	883	3.8	78	77	0.56	0.52	6.2	7.2	0.06	1.07	0.4	78	80	0.57	0.55	7.6	10.9	0.06	1.03	0.0	L
39	San Bern. 5-St.	NR	0.07	52	13	1233	2.6	95	86	0.63	0.65	9.1	5.2	0.06	1.00	3.9	95	107	0.50	0.51	7.5	6.2	0.08	1.00	1.3	L
40	San Bern. 9-St.	LD	0.10	74	0	848	3.4	55	52	2.01	2.01	5.0	6.8	0.04	1.00	0.0	55	59	2.05	2.08	7.4	6.0	0.04	1.00	1.3	A
41	San Bern. CGC	NR	0.04	38	0	1011	2.4	114	114	0.51	0.51	2.6	3.4	0.07	1.01	0.0	114	114	0.93	0.91	4.5	4.0	0.04	1.02	0.7	A
42	Santa Susana	NR	0.28	91	0	4460	1.0	23.5	20.5	0.54	0.53	19.1	15.1	0.04	1.02	4.9	23.5	27.6	0.54	0.55	11.4	8.3	0.04	1.00	3.1	L
43	Seal Beach 8-St.	LD	0.05	83	16	933	2.6	103	90	1.28	1.26	11.5	13.2	0.07	1.02	0.0	103	121	1.16	1.12	13.7	16.2	0.08	1.04	0.0	A
		NR	0.08			911	3.3			1.21	1.18	6.6	7.1	0.08	1.03	0.0			1.09	1.06	9.1	8.7	0.09	1.03	1.1	A
44	Sylmar Hos.	WT	0.05	63	0	1506	1.9	126	132	0.30	0.27	9.1	9.9	0.16	1.10	1.7	126	132	0.29	0.25	9.5	8.6	0.17	1.17	4.1	A
		NR	0.84			1119	9.1			0.38	0.37	18.9	19.4	0.15	1.04	1.7			0.34	0.26	23.4	17.5	0.21	1.29	15.2	A
45	Ventura 12-St.	NR	0.06	69	0	886	2.8	62	47	0.71	0.53	4.0	5.7	0.15	1.34	1.6	62	83								A
46	Lotung Reactor	L07	0.11	47	15	275	9.7	16.3	16.3	0.49	0.12	30.6	3.0	1.45	4.14	30.6	16.3	16.3	0.45	0.11	31.0	3.0	1.54	4.01	31.0	A
'B' Sites																										
1	Milpitas 2-St.	LP	0.14	26	0	649	4.1	6.4	10.9	0.25	0.24	15.3	21.9	0.17	1.06	0.0										A
2	San Bruno 9-St.	LP	0.11	66	0	916	3.6	72	59	1.10	0.97	12.5	11.4	0.07	1.13	4.7										A
3	San Fran. 47-St.	LP	0.16	414	27	478	4.3	86	80	5.16	5.03	U4	U4	0.17	1.03	U4										A
4	San Fran. Trans.	LP	0.12	475	51	801	5.9	98	99	U3	U3	U3	U3	U3	U3	U3										A
5	San Jose 10-St.	LP	0.12	61	0	768	4.1	65	49	0.48	0.29	6.7	18.6	0.27	1.64	2.5										A
6	San Jose 13-St.	LP	0.10	109	13.5	725	3.5	83	84	2.16	2.13	1.0	1.3	0.07	1.01	0.0	83	84	2.19	2.17	2.8	2.2	0.07	1.01	0.6	A
7	Walnut Crk 10-St	LP	0.10	89	14	1405	1.2	32	26	0.77	0.66	6.6	13.3	0.10	1.17	0.0										A
9	El Segundo 14-St.	NR	0.13	114	0	899	4.1	69	64	U3	U3	U3	U3	U3	U3	U3										A
10	LA 9-St.	NR	0.16	89	13	878	3.7	50	38	1.25	1.25	10.3	7.8	0.08	1.00	2.5	65	67	1.06	1.04	11.5	13.0	0.10	1.03	0.0	A
11	LA 17-St.	LD	0.04	91	0	1190	0.9	76	35.2	0.96	0.85	4.1	3.4	0.09	1.13	1.7										A
		NR	0.26			1140	1.4			1.05	0.90	4.9	3.9	0.09	1.17	2.5										A
12	LA 32-St.	NR	0.11	300	54	1339	1.2	93	91	1.94	1.84	7.6	7.1	0.12	1.06	1.7	93	97	U3	U3	U3	U3	U3	U3	U3	A
13	LA 54-St.	NR	0.14	414	57.5	1317	3.4	96	87	5.81	5.70	7.7	15.0	0.06	1.02	0.0										A
14	Whittier 8-St.	NR	0.17	48	0	842	3.2	64	28.5	0.56	0.49	12.1	12.9	0.12	1.14	3.4										A

h= effective structure height ≈ 0.7 · full height
e= embedment depth
Vs= soil shear wave velocity
β = soil hysteretic damping
Vs and β evaluated from soil profiles in Stewart (1997)

U1-U4 denote unacceptably low confidence results that are unreported
A, L denote acceptable and low confidence in results, respectively
blank entries = insuffiencient strong motion data to evaluate modal parameters
r_u, r_θ =foundation radii matching area and moment of inertia of actual foundation
$1/\sigma = h / (V_s \cdot T)$

* Lateral force resisting systems:
SW = shear wall, masonry or conc.
DWF = dual wall/frame system
CF = concrete frame
SF = steel frame
BI = base isolated

Earthquakes: CGA=Coalinga Aftershock, IMP=Imperial Valley, LD=Landers, LP=Loma Prieta, L07=Lotung Event 7, NR=Northridge, PT=Petrolia, PTA=Petrolia Aftershock, RD=Redlands, SM=Sierra Madre, UP=Upland, WT=Whittier

(a) *Confidence levels*

System identification results for each site were assigned one of three possible confidence levels: A = acceptable confidence, L = low confidence, and U = unacceptable confidence. Unacceptable confidence is associated with one of the following situations:

- U1: Reliable flexible-base parameters could not be developed due to significant incoherence between foundation and free-field motions.
- U2: The structure and foundation were so stiff that the roof and foundation level motions were essentially identical, and hence the response could not be established by system identification.
- U3: At 'A' sites, fixed-base parameters could not be obtained directly by system identification, and also could not be estimated because (1) $\tilde{T} < \tilde{T}^*$ and (2) base rocking effects were evident from comparisons of vertical foundation and free-field motions. Evidence of base rocking suggests that SSI effects are significant, and that fixed-base period will differ substantially from flexible- and pseudo flexible-base period. Hence, the inability to estimate fixed-base period necessarily terminates the analysis. At 'B' sites, the U3 error indicates that flexible-base parameters could not be estimated because $T > \tilde{T}^*$.
- U4: Reliable parametric models of structural response could not be developed for unknown reasons. This occurred at site A29-L (wt) and B3, and may have resulted in part from contamination of ground motions from vibrations of nearby structures.

Low confidence levels occur most often because of poor characterization of geotechnical conditions (i.e., insufficient data to evaluate stratigraphy and shear wave velocities to depths of about one foundation radius). Although geotechnical data have no direct effect on vibration parameters evaluated with system identification, V_S affects the manner in which SSI results are interpreted relative to other sites through the parameter $\sigma = V_S \cdot T/h$. Other reasons for low confidence in the results include contamination of free-field data from vibrations of nearby structures (A26 and A29), moderately incoherent foundation and free-field motions (A22 and A36), and short duration strong motion data [A2 (pta) and A9 (cga)].

(b) *Errors in first-mode parameters*

As noted in Section 3.4.3(d), there is always uncertainty in models identified from parametric analyses due to imperfect model structures and disturbances in the output data (Ljung, 1995). Systematic errors can result from inadequate model structure (i.e. non-optimal selection of the *d* or *J* parameters) which cannot be readily quantified. A second type of error results from random disturbances in the output data. This error quantifies how the model would change if the identification were repeated with the same model structure and input, but with a different realization of the output. This uncertainty can be readily computed from the least-squares solution for the model parameters. The coefficients of variation associated with random disturbance errors are generally about 0.5 to 1.5% for frequency and 5 to 15% for damping.

Errors associated with inadequate model structure are controlled by selecting *J* so as to minimize deviations between the model output and roof recording, while not over-parameterizing the model in such a way as to cause pole-zero cancellation in the transfer function. However, an additional constraint is to maintain the same value of *J* for all output/input pairs in a given direction. This is enforced to maximize the likelihood that variations between modal parameters for different conditions of base fixity are reflective of true SSI effects and are not by-products of the analyses. As a result of this constraint on *J*, models for some output/input pairs may not be optimally parameterized with respect to the minimization of model error.

Despite these efforts to develop consistent model structures for different output/input pairs, numerical errors can still occur which result in conditions such as $\tilde{T} < \tilde{T}^*$, $T > \tilde{T}^*$, or $\tilde{\zeta}_0 < 0$. Such errors are generally small (i.e. within the range of the "random" errors noted above), and only become apparent at sites where inertial interaction effects are small. Nonetheless, the $\tilde{T} < \tilde{T}^*$ and $T > \tilde{T}^*$ conditions make impossible the implementation of fixed- and flexible-base parameter estimation procedures, respectively. If $T > \tilde{T}^*$ at a 'B' site, a U3 error is assigned. If $\tilde{T} < \tilde{T}^*$, the significance of base rocking is evaluated using foundation-level and free-field vertical motions, and one of the following is done: (a) if rocking is evident from amplification of foundation-level vertical motions at the fundamental mode of the structure, a U3 error is assigned, or (b) if no rocking is evident, fixed-base parameters are approximated by pseudo flexible-base parameters. Hence, the final results for some sites indicate $\tilde{T} < T$, despite the obvious error associated with such a finding. Similarly, there were cases of $\tilde{\zeta}_0 < 0$. Such results are interpreted as indicative of small SSI effects, and are taken as $\tilde{T} / T = 1$ or $\tilde{\zeta}_0 = 0$.

(c) *System nonlinearities*

Modal parameters are generally developed from CEM parametric system identification analyses, and hence are based on the assumption of linear, time invariant behavior. As a check of this assumption, the time dependence of first-mode parameters is also evaluated by recursive techniques (i.e. RPEM).

An example of essentially linear, time invariant response was previously provided in Fig. 3.2. An illustration of nonlinear structural response is provided by the six-story Imperial County Services Building (site A12) which partially collapsed during the 1979 Imperial Valley Earthquake. As shown in Fig. 5.6, reductions in first-mode frequency and high damping are evident during the first 20 seconds of strong shaking. A nonlinear structural response such as this can lead to significant differences between RPEM modal parameters at a given time and CEM modal parameters evaluated across the duration of the time history. What is important from the standpoint of evaluating inertial interaction effects is that differences between CEM parameters for different cases of base fixity are consistent with differences in RPEM parameters during times when the identification is stable. For example, at site A12, differences between fixed- and pseudo flexible-base frequencies were generally consistent with the difference in CEM frequencies throughout the duration of strong shaking (CEM results were $\tilde{f} = 1.36$, $\tilde{f}^* = 1.54$ Hz). Conversely, differences between damping values were strongly time-dependent, with $\tilde{\zeta}$ significantly exceeding $\tilde{\zeta}^*$ for t < 20 sec. and the opposite trend subsequently. The corresponding CEM results are $\tilde{\zeta} = 16.0\%$ and $\tilde{\zeta}^* = 13.5\%$, which is reasonably representative of RPEM results during early portions of the time history. Recursive results for t < 20

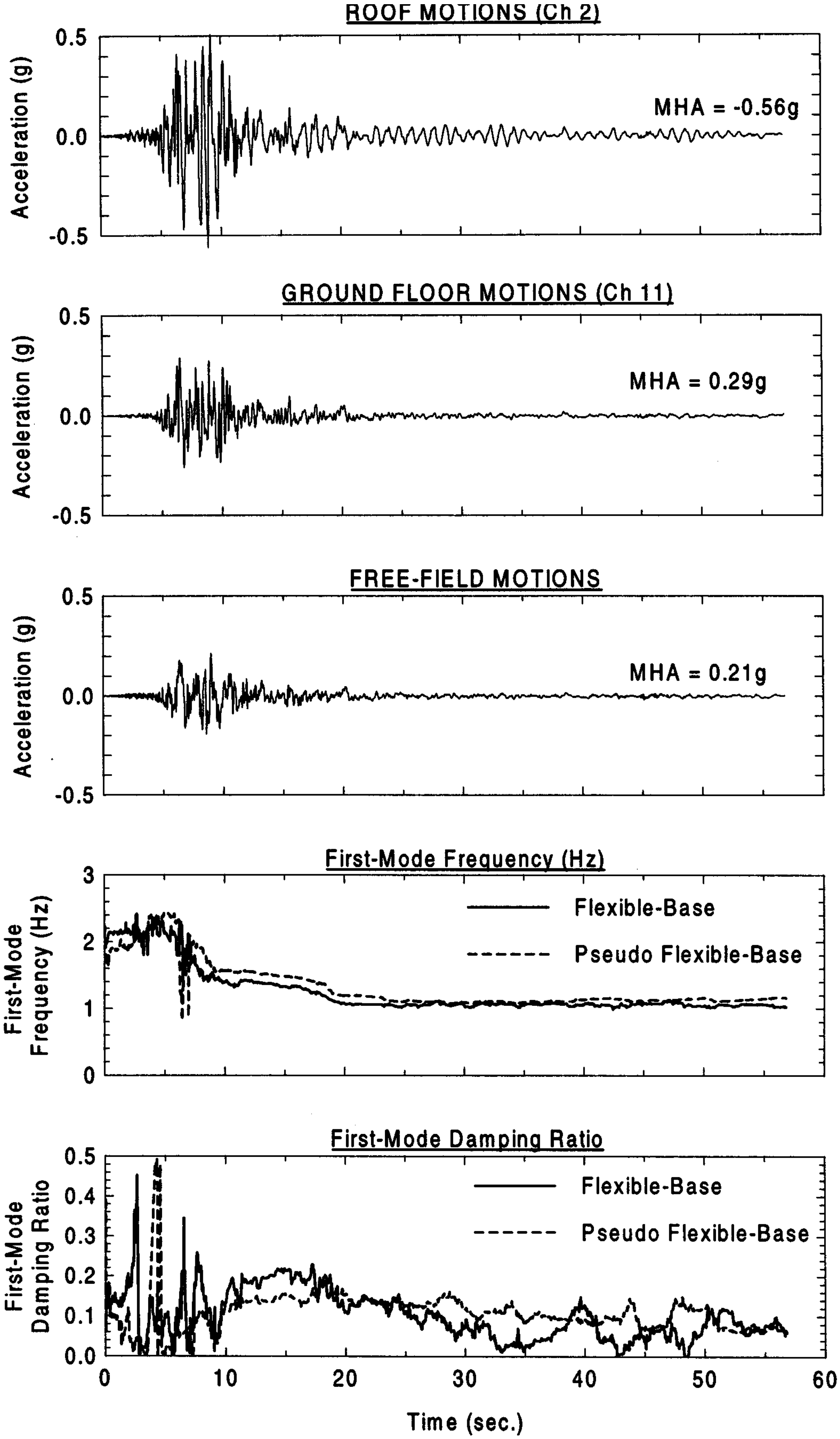

Fig. 5.6: Transverse acceleration time histories and time variation of first-mode parameters, Imperial County Services Building, 1979 Imperial Valley Earthquake

seconds are likely more stable than subsequent results due to the much reduced amplitude of shaking for t > 20 seconds. Hence, the CEM damping results were consistent with recursive results from the most stable portion of the time history in this case, and the CEM results were used for final characterization of SSI effects at the site.

Occasionally, differences between modal parameters from CEM and RPEM analyses are inconsistent. In such cases, average differences between parameters for different base fixity conditions computed from RPEM analyses over times of stable identification can be used for evaluating SSI effects. Such usage of recursive results was seldom necessary, but was more common for evaluating $\tilde{\zeta}_0$ than $\tilde{T}/T$. Where made, these corrections are indicated in Stewart (1997).

5.3.4 Evaluation of Period Lengthening and Foundation Damping Factors

(a) *Definition of soil and structure parameters*

The data presented in Table 5.3 is used to illustrate the inertial interaction effects of $\tilde{T}/T$ and $\tilde{\zeta}_0$. These data are plotted against the ratio of structure-to-soil stiffness as expressed by the parameter $1/\sigma = h/(V_S \cdot T)$, where *h*, V_S, and T are defined as follows:

- *h* is the distance above the foundation level at which the building's mass can be concentrated to yield the same base moment that would occur in the actual structure assuming a linear first-mode shape. For many low- to mid-height structures, it was found than $h \approx 0.7 \times H$ (H = full structure height, from foundation level to roof).
- V_S is the effective shear wave velocity of either a halfspace or a finite soil layer overlying a rigid base (all sites except A24-L were characterized as a halfspace). V_S

and hysteretic soil damping (β) are stain-dependent material properties calculated with the aid of deconvolution analyses [details presented in Stewart (1997) and Section 2.2.2 (b)].

- T is the fixed-base period of the structure.

(b) *General trends*

Presented in Fig. 5.7 are the variations of $\tilde{T}/T$ and $\tilde{\zeta}_0$ with $1/\sigma$ for sites where there is an "acceptable" or "low" confidence level in the modal parameters. Also shown are second-order polynomials fit to the acceptable confidence data by linear regression analysis, and analytical results by Veletsos and Nair (1975) for h/r = 1 and 2. Both $\tilde{T}/T$ and $\tilde{\zeta}_0$ are seen to increase with $1/\sigma$, and the best fit lines through the data are similar to the Veletsos and Nair curves. The Veletsos and Nair curves are only shown to provide a benchmark against which the empirical results can be compared. Detailed comparisons of $\tilde{T}/T$ and $\tilde{\zeta}_0$ values with predictions by the "modified Veletsos" and "modified Bielak" procedures are presented in Section 5.4.

There is significant scatter in the data in Fig. 5.7, although much of this results from systematic variations in $\tilde{T}/T$ and $\tilde{\zeta}_0$ associated with factors such as structure aspect ratio and foundation embedment, type, shape, and flexibility effects. In addition, $\tilde{\zeta}_0$ is influenced by the hysteretic soil damping (β), which varies with soil type.

Results from several sites help to illustrate the strong influence of $1/\sigma$ on inertial interaction effects. The most significant inertial interaction occurred at site A46

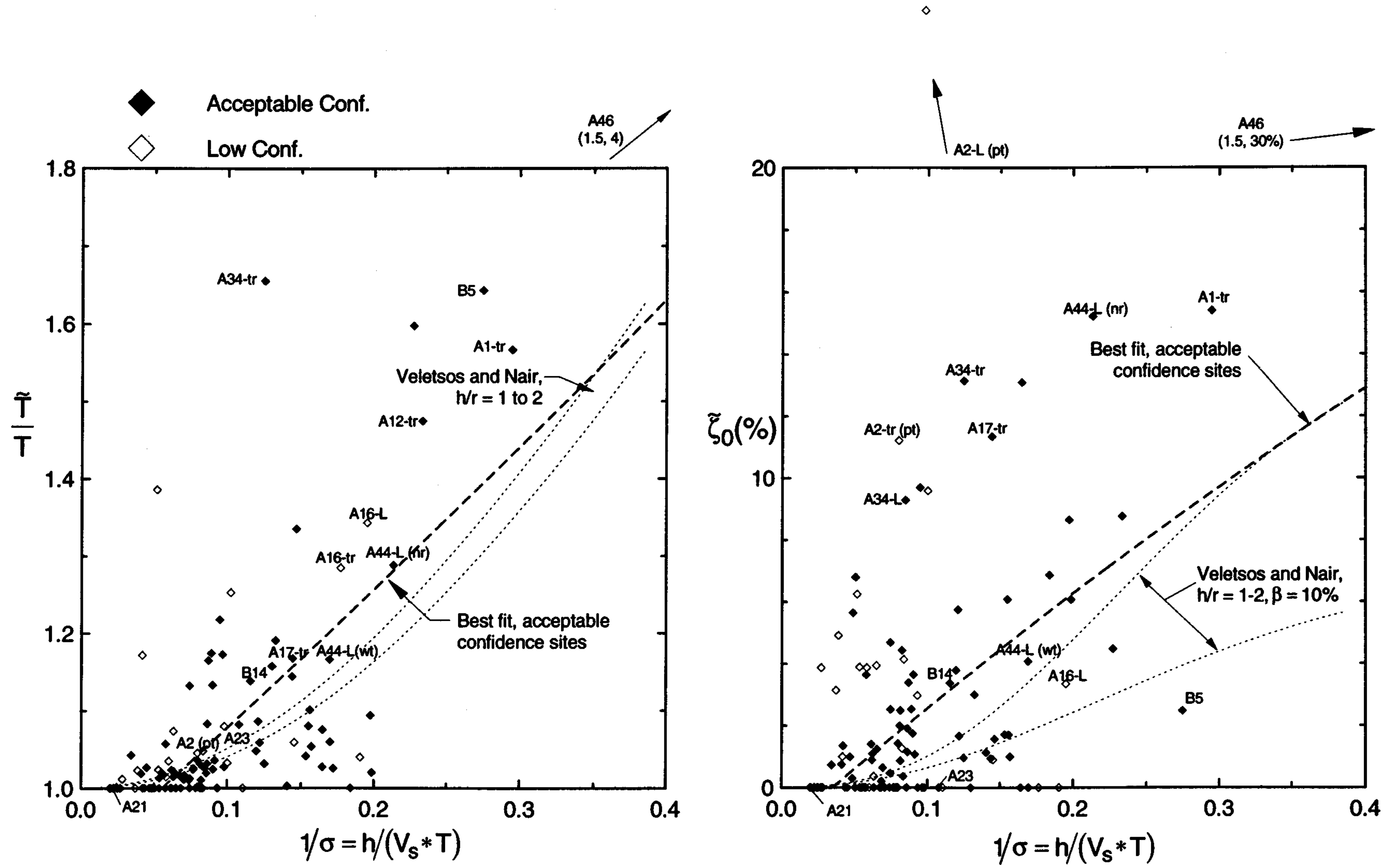

Fig. 5.7: Period lengthening ratio and foundation damping factor for sites sorted by confidence level, and analytical results from Veletsos and Nair (1975). (tr=transverse, L=longitudinal direction)

($\tilde{T}/T \approx 4$ and $\tilde{\zeta}_0 \approx 30\%$), which has a stiff ($T \approx 0.1$ sec) cylindrical concrete structure (h=47 feet, r=16 feet) and relatively soft foundation soils ($V_S \approx 275$ fps), giving a large $1/\sigma$ of about 1.5. Conversely, the inertial interaction effects are negligible at site A21 ($\tilde{T}/T \approx 1$ and $\tilde{\zeta}_0 \approx 0\%$), which has a relatively flexible ($T \approx 0.8$-1.0 sec) base-isolated structure (h=21 feet, r_1=71 feet) that is founded on rock ($V_S \approx 1000$ fps), giving a much smaller $1/\sigma$ value of 0.02-0.03. These two sites represent the extremes of inertial interaction. More typical SSI effects occur at sites B14 ($\tilde{T}/T = 1.14$ and $\tilde{\zeta}_0 \approx 3.4\%$) and A1-tr ($\tilde{T}/T = 1.57$ and $\tilde{\zeta}_0 \approx 15.4\%$). The structures at both sites are shear wall buildings with periods of T = 0.49 and 0.15 sec, respectively, and are founded on medium-stiff soils (V_S = 840 and 700 fps), combining to give $1/\sigma \approx 0.12$ at B14 and $1/\sigma \approx 0.29$ at A1-tr. The results from these four sites indicate that both $\tilde{T}/T$ and $\tilde{\zeta}_0$ increase with increasing $1/\sigma$.

Several sites appear to be significant outliers with respect to the database. Site A34-tr is a stiff ($T \approx 0.12$ sec.) shear wall structure founded on soil that has pronounced period lengthening relative to the general trend as well as unusually high damping in both directions. Several sites with small aspect ratios ($h/r_2 \approx 0.5$) had pronounced damping without unusually large period lengthening [A2 (pt) and A17-tr], while some high aspect ratio structures ($h/r_2 > 2.5$) had little foundation damping but significant period lengthening (A16, A23). Many of these outlying results are explained to a large extent by factors other than $1/\sigma$ which are not incorporated into Fig. 5.7. A discussion of “true” outliers that remain after correction for these effects is deferred to Section 5.4.2(h).

(c) *Effect of aspect ratio*

The data in Table 5.3 is plotted in Fig. 5.8 to illustrate the influence of aspect ratio (h/r_2) on $\tilde{T}/T$ and $\tilde{\zeta}_0$. For these plots, the data was sorted into aspect ratios $h/r_2 < 1$ and $h/r_2 > 1$. Second-order polynomials fit to the data using linear regression analyses are plotted through both data sets in Fig. 5.8. Though the overall range of aspect ratios was 0.18 to 5.2, separate regressions for smaller discretizations of aspect ratio were not justified as only 16% of the data has $h/r_2 > 2$, and many of these are long period structures with essentially negligible $\tilde{T}/T$ and $\tilde{\zeta}_0$ (see Part f).

A trend of increasing period lengthening and decreasing foundation damping with increasing h/r_2 is evident in Fig. 5.8. These findings are consistent with aspect ratio effects predicted by theoretical formulations such as Veletsos and Nair, 1975 (i.e. Figs. 2.9 and 2.10).

In order to more rationally evaluate the influence of aspect ratio on inertial interaction effects, it is necessary to compare results for pairs of sites with similar $1/\sigma$, embedment, and structure type, but different h/r_2. Few such pairs are present in the database, but two that are suitable are A1-tr/B5 and A8-tr/B7. Sites A1-tr and B5 have stiff shear wall structures on moderately stiff soil ($1/\sigma$ = 0.28 and 0.25, respectively), but different aspect ratios of h/r_2 = 0.74 and 1.24, respectively. Sites A8-tr and B7 have shear wall structures founded on bedrock materials ($1/\sigma$ = 0.087 and 0.096, respectively), but have significantly different aspect ratios of 0.5 and 3.4, respectively. As shown in Fig.

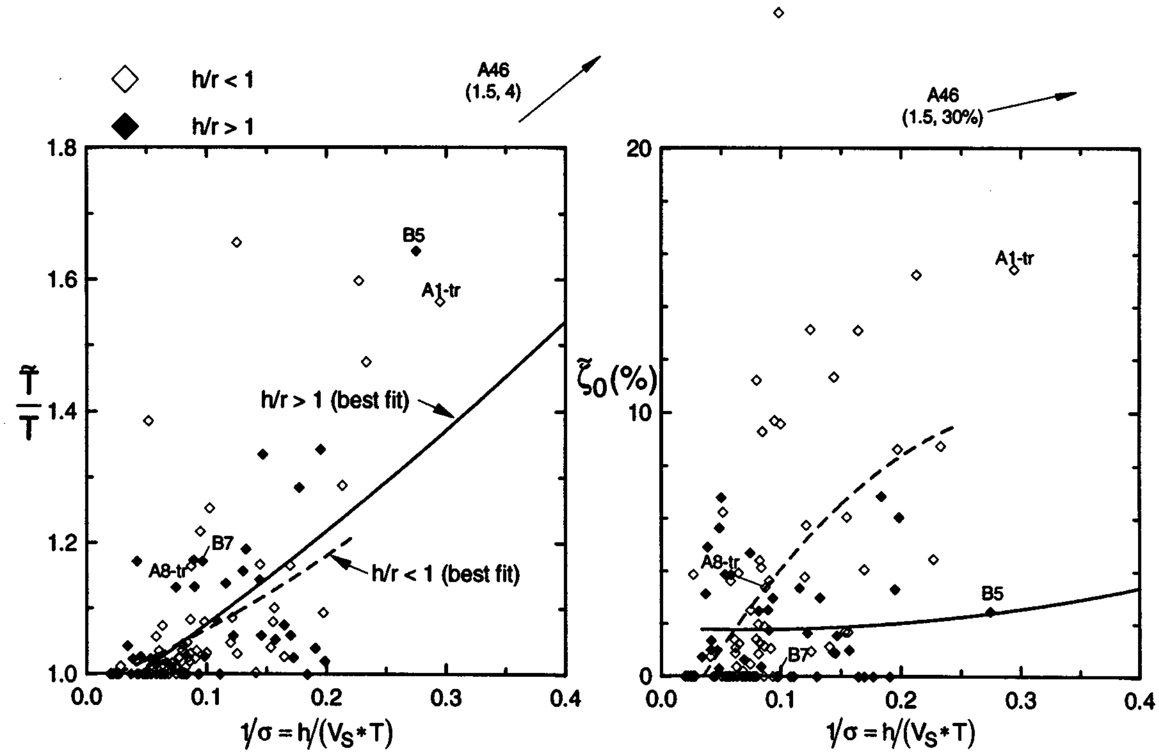

Fig. 5.8: Effect of aspect ratio on period lengthening ratio and foundation damping factor

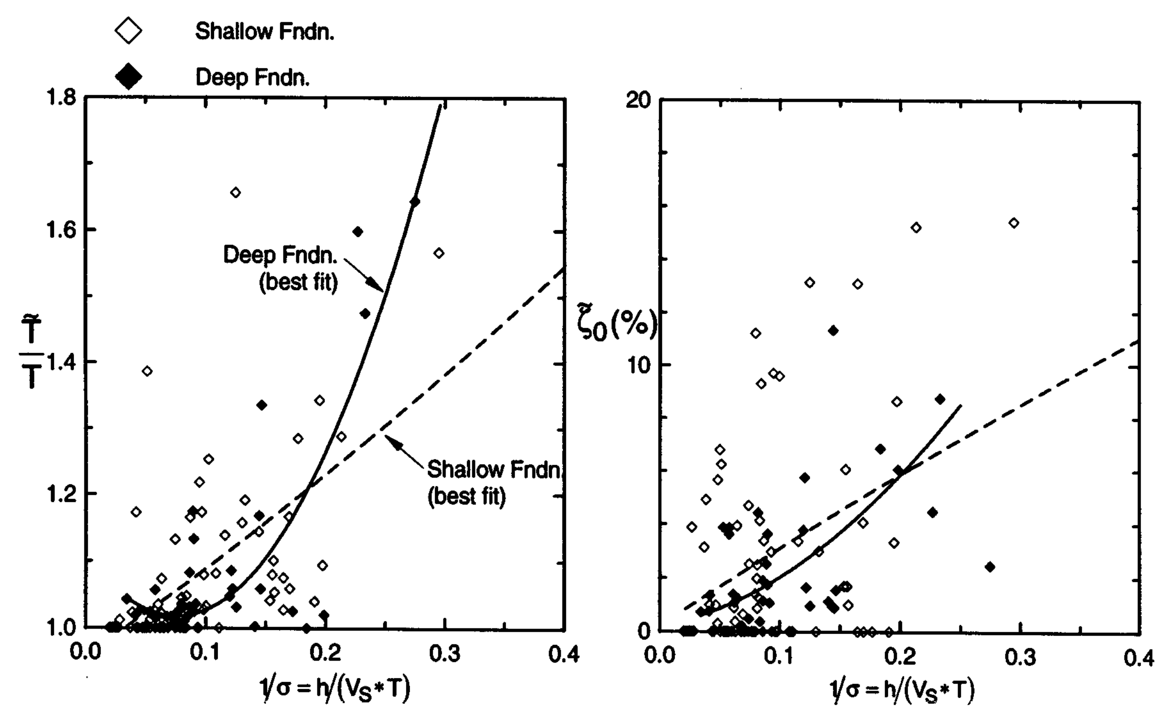

Fig. 5.9: Effect of foundation type on period lengthening ratio and foundation damping factor

5.8, B5 and B7 have higher $\tilde{T}/T$ and smaller $\tilde{\zeta}_0$ than A1-tr and A8-tr, respectively (though the differences in $\tilde{T}/T$ are small).

(d) *Effect of foundation type*

The database was separated according to foundation type (i.e. deep foundations such as piles or piers and shallow foundations such as footings or mats) for the plots in Fig. 5.9. Regression curves were calculated for each data set and are plotted in the figure.

For values of $1/\sigma > 0.15$ to 0.20, the period lengthening and damping for deep foundations exceed that for shallow foundations, though it is noted that the data are sparse in this range. The opposite trend is present for $1/\sigma < 0.15$, where the bulk of the data resides, indicating that it would be tenuous to draw firm conclusions from these data. In general, these results do not clearly indicate a strong effect of foundation type on $\tilde{T}/T$ or $\tilde{\zeta}_0$.

These data should not be interpreted to imply that foundation type cannot be a potentially important factor in inertial interaction processes. Presented in this form, the data are simply unable to illustrate the relatively modest influences of deep foundations on these inertial interaction effects. Deep foundations are addressed in more detail in Section 5.4.2 (d) where analytical formulations for shallow foundations are examined for their ability to predict $\tilde{T}/T$ and $\tilde{\zeta}_0$ values for sites with deep foundations.

(e) *Effect of embedment*

The database was separated into embedded and surface structures for the plots in Fig. 5.10. A majority of the structures with basements are shallowly embedded (e/r = 0.1 to 0.5), and of the deeply embedded structures, many have long periods and negligible inertial interaction effects (see Part f). Hence, the data for embedded structures was not discretized into subsets of embedment ratio (e/r).

The regression curves in Fig. 5.10 indicate greater period lengthening for surface than embedded structures, which is consistent with the analytical findings of Bielak (1975) and Aviles and Perez-Rocha (1996) (i.e. Fig. 2.11). Empirical results for $\tilde{\zeta}_0$ indicate larger damping for surface structures than embedded structures, which counters the analytical findings. The empirical trend in this case may be misleading, and highlights the difficulty of evaluating subtle influences (such as embedment) on $\tilde{T}/T$ and $\tilde{\zeta}_0$ when other, potentially more significant effects (such as aspect ratio) cannot readily be controlled for in the regression.

A more detailed analysis of embedment effects is provided in Section 5.4.2(b), where empirical inertial interaction effects for embedded structures are compared to predictions from the "modified Veletsos" and "modified Bielak" analytical formulations.

(f) *Effect of structure type*

Five different types of lateral load resisting systems are represented in the database: shear walls, dual wall/frame systems, concrete frames, steel frames, and base-isolation systems. For plots of $\tilde{T}/T$ and $\tilde{\zeta}_0$ in Figs 5.11 to 5.13, these are grouped as: (1) base

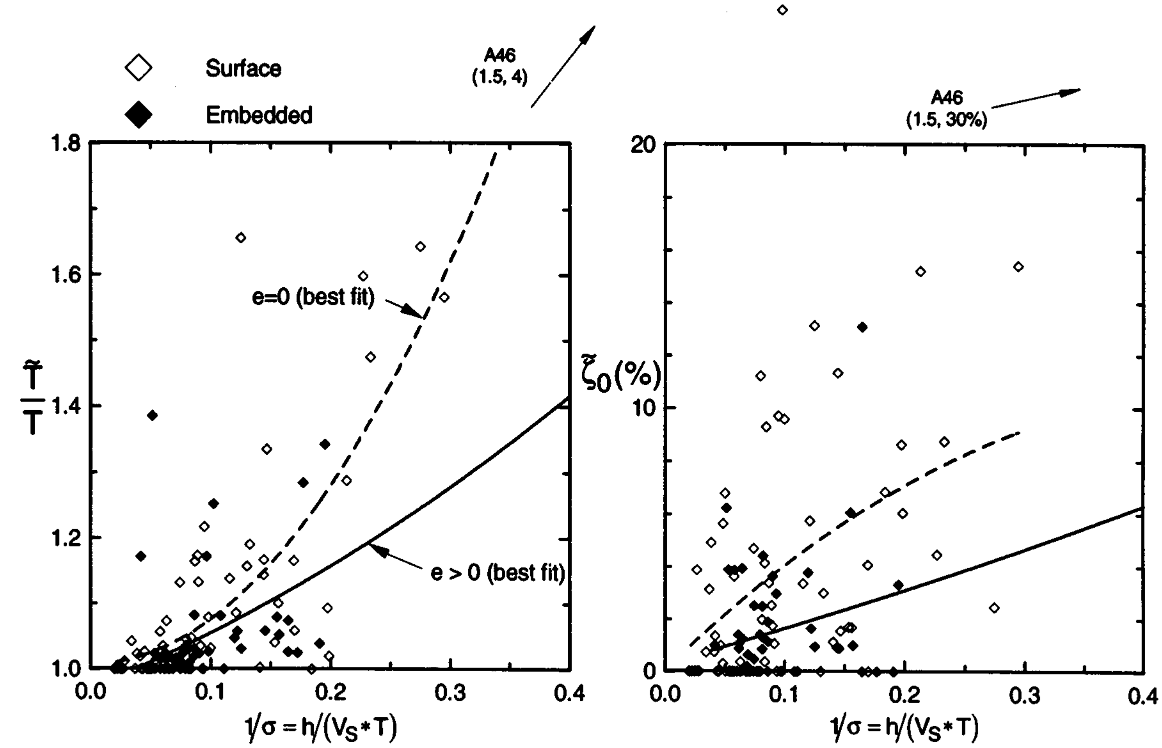

Fig. 5.10: Effect of embedment on period lengthening ratio and foundation damping factor

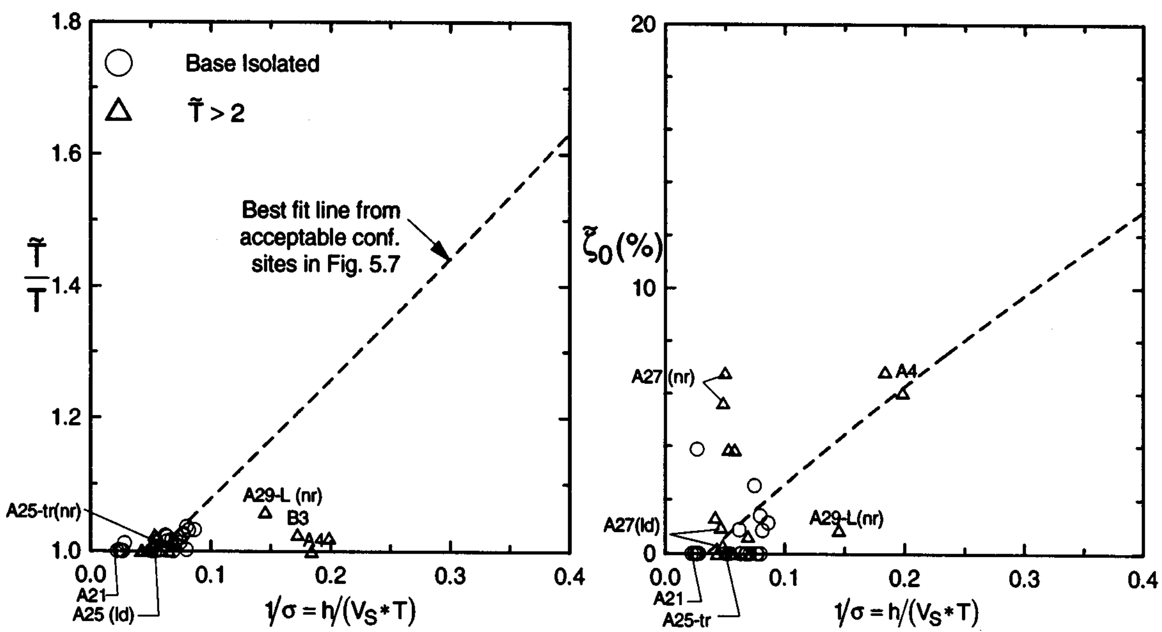

Fig. 5.11: Period lengthening ratios and foundation damping factors for base isolated and long-period structures compared to the best fit line from acceptable confidence sites

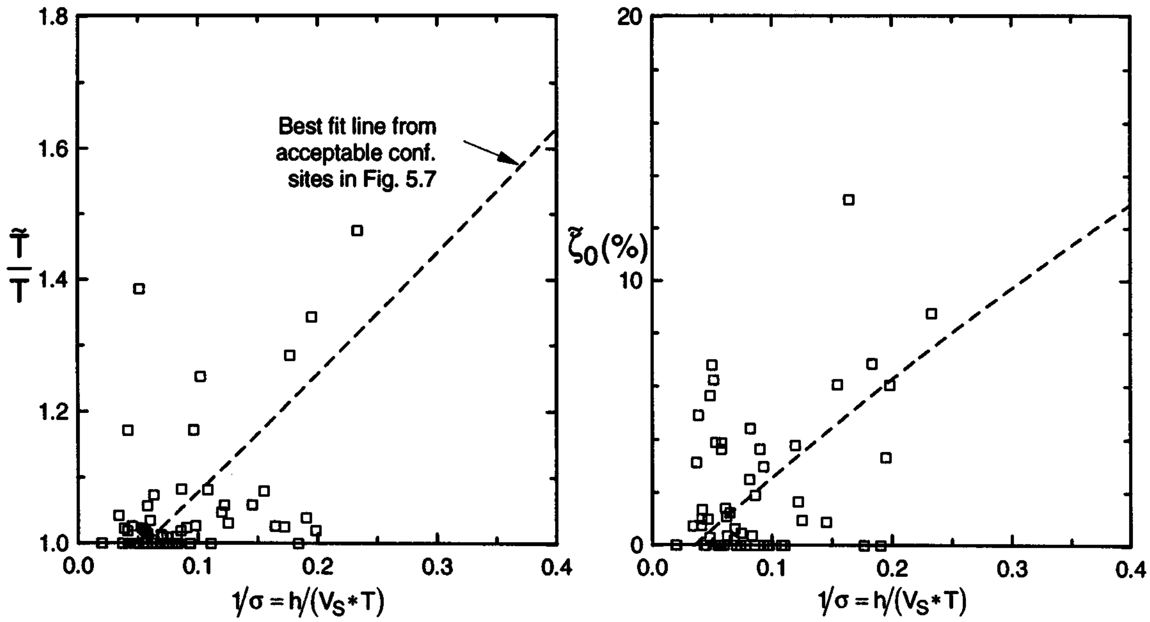

Fig. 5.12: Period lengthening ratios and foundation damping factors for moment frame and dual wall/frame buildings

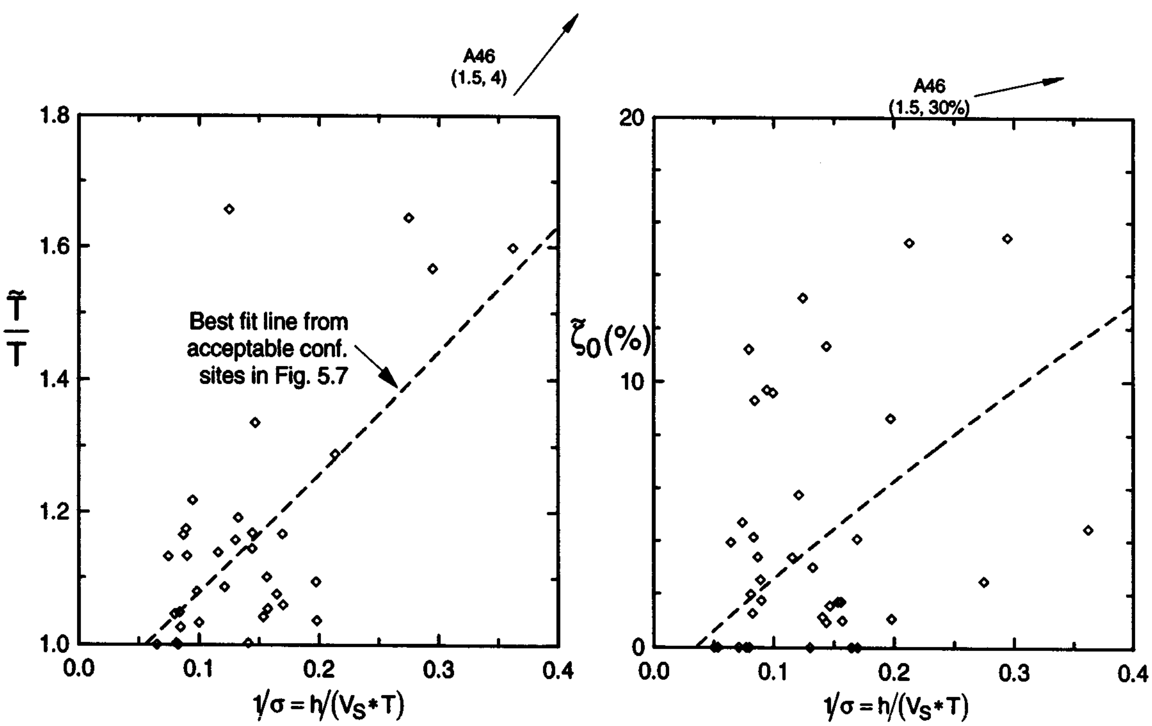

Fig. 5.13: Period lengthening ratios and foundation damping factors for shear wall buildings

isolated buildings, (2) frame and dual wall/frame buildings, and (3) shear wall buildings. Also shown in Fig. 5.11 are $\tilde{T}/T$ and $\tilde{\zeta}_0$ values for long period ($\tilde{T} > 2$ sec.) structures having lateral load resisting systems such as base isolation or frames.

The database contains four base-isolated structures, two on rock (A21, A25) and two on stiff soils with V_S > 900 fps (A37, A43). Modal parameters for these structures include isolator flexibility, and the structures have fairly long periods of 0.6 to 1.2 sec. These relatively long structure periods and stiff ground conditions combine to yield low 1/σ values of 0.02 to 0.08. Accordingly, as seen in Fig. 5.11, $\tilde{T}/T$ and $\tilde{\zeta}_0$ values are small (< 1.04 and 4%, respectively), which is consistent with the general trends in the overall database.

Results for ten long-period structures are also presented in Fig. 5.11 [A4, A27-28, A29-tr (nr), A40, B3, B6, B9, B13]. As with base-isolated structures, the long periods of these buildings generally result in low 1/σ values (< 0.06), though two buildings on soft soils (A4, B3) have 1/σ = 0.17-0.20. These structures characteristically have little period lengthening ($\tilde{T}/T < 103$), which is consistent with trends from the overall database except at sites A4 and B3. Further discussion on the performance of these structures is deferred to Sections 5.4.2(d) and (e). Damping values for long period structures are generally consistent with the best fit curve for acceptable confidence sites.

Period lengthening and damping for frame and dual wall/frame buildings (Fig. 5.12) and shear wall buildings (Fig. 5.13) are consistent with the general trends for acceptable confidence sites. These results are not surprising, as the primary difference between these types of structures is their height-to-stiffness ratio, which is accounted for in 1/σ.

(g) *Effect of ground shaking intensity*

At several sites with multiple earthquake recordings, the magnitude of inertial interaction effects increased with the severity of ground shaking. For example, peak ground accelerations at site A44-L were about 0.05-0.06g during the M_W 6.0 Whittier Earthquake and 0.60-0.84g during the M_W 6.7 Northridge Earthquake, and as shown in Fig. 5.7, $\tilde{T}/T$ and $\tilde{\zeta}_0$ values were significantly larger during the Northridge event. Similarly, as shown in Fig. 5.11, the long period structure at site A27 ($T \approx 3$ to 3.5 sec) and the base-isolated structure at site A25 had larger $\tilde{\zeta}_0$ values during the Northridge (0.19g and 0.49g, respectively) than the Landers events (0.03g and 0.04g, respectively); significant period lengthening was observed at neither sites A27 nor A25.

Inertial interaction effects increase with ground motion amplitude due to strain softening of foundation soils, which decreases the shear modulus and increases the hysteretic damping. These effects are approximately captured by the strain-dependent V_S and β terms used in the development of impedance functions. Fixed-base structural period T can increase with shaking amplitude, but the soil degradation effect is typically greater so that $1/\sigma = h/(V_S \cdot T)$ has a net decrease.

5.4 Calibration of Predictive Analytical Formulations for Inertial Interaction Effects

5.4.1 Overview of Analysis Procedures and Required Input

Simplified analyses for inertial interaction estimate the first-mode period lengthening ratio ($\tilde{T}/T$) and foundation damping factor ($\tilde{\zeta}_0$) given the fixed-base properties of the structure (T, ζ) and parameters describing foundation and site conditions. One methodology is termed the "modified Veletsos" (MV) formulation, because it is based on the impedance function developed by Veletsos and Verbic (1973) and the evaluations of $\tilde{T}/T$ and $\tilde{\zeta}_0$ by Veletsos and Nair (1975). The basic model considered in the MV formulation is a single degree-of-freedom structure supported on a rigid circular foundation resting on the surface of a homogeneous visco-elastic halfspace. The "modified" term refers to adjustments to the impedance function required to account for the effects of nonuniform soil profiles and foundation embedment, shape, and non-rigidity. Due to shortcomings in the impedance function adjustments for foundation embedment effects, a second analysis procedure adapted from Bielak (1975) is used for embedded structures. This "modified Bielak" (MB) formulation utilizes the same procedures for characterizing non-uniform soil profiles and foundation shape and flexibility effects as are used in the MV approach.

Input parameters used in the MV or MB formulations are as follows:

- Soil conditions: shear wave velocity V_S and hysteretic damping ratio β, both of which should be representative of the site stratigraphy and the severity of ground shaking; Poisson's ratio ν.

- Structure/Foundation Characteristics: effective height of structure above foundation level, h; foundation embedment, e; foundation radii which match the area and moment of inertia of the actual foundation, r_1 and r_2; appropriate corrections to the foundation impedance for embedment, shape, and non-rigidity effects.
- Fixed-Base 1st Mode Parameters: period and damping ratio, T and ζ.

These parameters are listed in Table 5.3 for the sites considered in this study.

Using these input parameters, $\tilde{T}/T$ and $\tilde{\zeta}_0$ were predicted using the MV formulation for each site. For sites with embedded structures, $\tilde{T}/T$ and $\tilde{\zeta}_0$ were also predicted using the MB formulation. The empirical and predicted values of $\tilde{T}/T$ and $\tilde{\zeta}_0$ are listed in Table 5.4.

5.4.2 Assessment of Predicted Period Lengthening and Foundation Damping Factors

(a) *General trends*

Deviations in MV predictions of $\tilde{T}/T$ and $\tilde{\zeta}_0$ relative to empirical values are shown in Fig. 5.14(a) for sites with acceptable and low confidence designations. Also plotted are best fit second-order polynomials established from linear regression analyses on data from acceptable confidence sites. For most sites, the predictions were found to be accurate to within absolute errors of about ±0.1 in $\tilde{T}/T$ and ±3% damping in $\tilde{\zeta}_0$ for $1/\sigma$ = 0 to 0.4. The regression curves indicate no significant systematic bias in predictions of either $\tilde{T}/T$ and $\tilde{\zeta}_0$ up to $1/\sigma = 0.4$. However, there is a significant downward trend in the best fit curve for damping for $1/\sigma > 0.5$ due to a large underprediction of $\tilde{\zeta}_0$ at site

Table 5.4: Inertial interaction effects evaluated from system identification analyses and predicted by "modified Veletsos" and "modified Bielak" formulations

		Transverse							Longitudinal						
			Obs.		Veletsos		Bielak			Obs.		Veletsos		Bielak	
Site	Eqk.	$\frac{1}{\sigma}$	$\tilde{T}/T$	$\tilde{\zeta}_0$	$\tilde{T}/T$	$\tilde{\zeta}_0$	$\tilde{T}/T$	$\tilde{\zeta}_0$	$\frac{1}{\sigma}$	$\tilde{T}/T$	$\tilde{\zeta}_0$	$\tilde{T}/T$	$\tilde{\zeta}_0$	$\tilde{T}/T$	$\tilde{\zeta}_0$
'A' Sites															
1	PT	0.27	1.57	15.4	1.51	10.6			0.20	1.09	8.6	1.17	11.6		
2	PT	0.08	1.04	11.2	1.07	4.9			0.10	1.08	25.1	1.10	7.4		
	PTA	0.09	1.05	4.1	1.07	5.3			0.10	1.03	9.6	1.11	7.7		
4	LP	0.20	1.02	6.1	1.17	1.7			0.18	1.00	6.9	1.15	1.4		
5	LP	0.03	1.04	0.7	1.01	0.0			0.05	1.03	0.0	1.01	0.1		
6	LP		U3	U3						U3	U3				
7	LP	0.09	1.03	9.3	1.06	3.1				U2	U2				
8	LP	0.09	1.16	3.4	1.04	1.5			0.08	1.00	2.0	1.03	1.5		
9	CGA	0.09	1.00	3.0	1.03	1.5	1.03	2.4		U2	U2				
10	LP	0.15	1.08	6.1	1.14	6.3	1.11	12.1	0.17	1.00	13.0	1.12	10.3	1.12	21.3
11	LP	0.02	1.00	0.0	1.00	0.1			0.02	1.00	0.0	1.00	0.0		
12	IMP	0.19	1.47	8.8	1.26	6.1			0.10	1.00	0.0	1.03	0.9		
13	LD	0.12	1.05	3.8	1.05	1.6	1.05	2.8	0.12	1.03	1.0	1.04	2.1	1.06	3.4
14	WT	0.14	1.00	1.1	1.11	4.8				U2	U2				
15	NR	0.06	1.06	3.6	1.02	0.8			0.06	1.02	0.0	1.02	0.8		
16	NR	0.18	1.28	0.0	1.14	0.2	1.21	1.6	0.17	1.34	3.3	1.17	0.3	1.26	2.1
17	NR	0.14	1.17	11.3	1.21	12.5			0.12	1.09	5.7	1.15	9.9		
18	WT		U3	U3					0.08	1.00	0.0	1.02	0.3		
20	NR	0.17	1.13	0.0	1.09	1.6	1.11	4.3	0.16	1.05	1.0	1.08	1.5	1.1	3.8
21	SM	0.03	1.01	0.0	1.01	0.2			0.03	1.00	3.9	1.00	0.1		
	LD	0.02	1.00	0.0	1	0.1			0.02	1.00	0.0	1.00	0.1		
	NR	0.02	1.00	0.0	1.01	0.2			0.03	1.00	0.0	1.01	0.2		
22	NR	0.09	U1	U1					0.10	U1	U1				
23	NR	0.11	1.08	0.0	1.04	0.5	1.06	1.2		U3	U3				
24	NR	0.09	1.04	1.1	1.08	5.1			0.23	1.60	4.5	1.28	7.2		
25	LD	0.05	1.00	0.0	1.01	0.2			0.05	1.00	0.0	1.01	0.3		
	NR	0.06	1.00	0.0	1.01	0.3			0.06	1.01	0.0	1.01	0.3		
26	NR	0.20	1.04	0.0	1.13	2.2	1.16	4.2	0.12	1.00	0.0	1.03	0.6	1.05	1.3
27	LD	0.05	1.00	1.0	1.01	0.1			0.05	1.00	0.3	1.01	0.1		
	NR	0.05	1.00	5.6	1.01	0.1			0.05	1.00	6.8	1.01	0.1		
28	NR	0.07	1.00		1.02		1.02		0.06	1.00		1.01		1.02	
29	WT	0.06	1.01	3.9	1.03	0.1	1.02	0.1							
	NR	0.05	1.02	3.9	1.02	0.1	1.01	0.2	0.15	1.06	0.9	1.04	1.4	1.09	1.8
30	NR	0.09	1.08	1.9	1.04	2.1	1.04	3.5		U3	U3				
31	LD	0.13	1.19	3.0	1.11	0.7									
	NR	0.13	1.16	0.0	1.11	0.7			0.14	1.14	0.9	1.06	1.2		
32	WT		U3	U3					0.06	1.00	1.1	1.01	0.4	1.02	0.6
33	WT	0.07	1.00	0.2	1.03	0.8	1.02	1.4	0.07	1.00	0.5	1.02	1.3	1.03	2.1
	NR	0.06	1.00	1.4	1.02	0.6	1.02	0.9	0.07	1.00	1.2	1.02	0.8	1.02	1.3
34	NR	0.11	1.66	13.1	1.13	5.8			0.10	1.22	9.7	1.05	3.8		
35	WT	0.09	1.02	3.6	1.04	2.0	1.04	3.2	0.09	1.02	0.0	1.03	1.8	1.04	3.1
	UP	0.08	1.01	4.4	1.03	1.6	1.03	2.6	0.08	1.00	0.0	1.03	1.5	1.03	2.5
36	UP	0.05	U1	U1					0.05	U1	U1				

	LD	0.04	1.17	1.0	1.01	0.1	1.01	0.1		1.39	6.2	1.01	0.2	1.01	0.2
37	RD	0.08	1.03	0.9	1.04	1.5	1.03	2.3	0.08	1.00	1.4	1.03	1.7	1.04	2.6
	WT	0.08	1.02	0.0	1.04	1.7	1.03	2.3	0.07	1.01	2.5	1.02	1.4	1.03	2.2
	UP	0.07	1.00	0.0	1.03	0.9	1.02	1.4	0.07	1.00	0.0	1.02	1.2	1.03	1.9
	LD	0.06	1.01	0.0	1.03	2.2	1.02	2.6	0.06	1.02	0.9	1.02	0.9	1.02	1.4
	NR	0.07	1.02	0.0	1.03	0.2	1.02	0.7	0.06	1.02	0.0	1.02	0.9	1.02	1.4
38	LD	0.06	1.07	0.4	1.03	1.2			0.06	1.03	0.0	1.02	1.1		
39	NR	0.06	1.00	3.9	1.02	0.7	1.02	0.7	0.08	1.00	1.3	1.03	1.4	1.03	2.1
40	LD	0.04	1.00	0.0	1.01	0.1			0.04	1.00	1.3	1.01	0.1		
41	NR	0.07	1.01	0.0	1.03	1.8			0.04	1.02	0.7	1.01	0.4		
42	NR	0.07	1.02	4.9	1.02	0.0			0.07	1.00	3.1	1.01	0.0		
43	LD	0.07	1.02	0.0	1.02	0.3	1.02	0.6	0.08	1.04	0.0	1.02	0.6	1.02	0.9
	NR	0.08	1.03	0.0	1.02	0.4	1.02	0.7	0.08	1.03	1.1	1.02	0.6	1.03	1.0
44	WT	0.16	1.10	1.7	1.12	6.4			0.17	1.17	4.1	1.14	7.6		
	NR	0.15	1.04	1.7	1.12	6.7			0.21	1.29	15.2	1.23	12.2		
45	NR	0.15	1.34	1.6	1.14	1.4									
46	L07	1.45	4.14	30.6	3.76	17.0	4.94	26.7	1.54	4.01	31.0	3.97	16.9	5.21	26.8
'B' Sites															
1	LP	0.17	1.06	0.0	1.06	3.4									
2	LP	0.08	1.13	4.7	1.17	3.4									
3	LP	0.17	1.03	U4	1.20		1.24								
4	LP	0.17	U3	U3											
5	LP	0.28	1.64	2.5	1.44	5.2									
6	LP	0.07	1.01	0.0	1.02	0.2	1.02	0.3	0.07	1.01	0.6	1.02	0.2	1.02	0.3
7	LP	0.10	1.17	0.0	1.05	0.2	1.05	0.4							
9	NR	0.06	U3	U3											
10	NR	0.08	1.00	2.5	1.04	0.3	1.03	0.4	0.10	1.03	0.0	1.03	0.5	1.04	0.8
11	LD	0.09	1.13	1.7	1.20	0.2									
	NR	0.09	1.17	2.5	1.19	0.3									
12	NR	0.12	1.06	1.7	1.05	0.2	1.1	1.0							
13	NR	0.05	1.02	0.0	1.02	0.1	1.02	0.2							
14	NR	0.12	1.14	3.4	1.25	1.1									

Sites A19 and B8 omitted

Earthquakes: CGA=Coalinga Aftershock, IMP=Imperial Valley, LD=Landers, LP=Loma Prieta, L07=Lotung Event 7, NR=Northridge, PT=Petrolia, PTA=Petrolia Aftershock, RD=Redlands, SM=Sierra Madre, UP=Upland, WT=Whittier

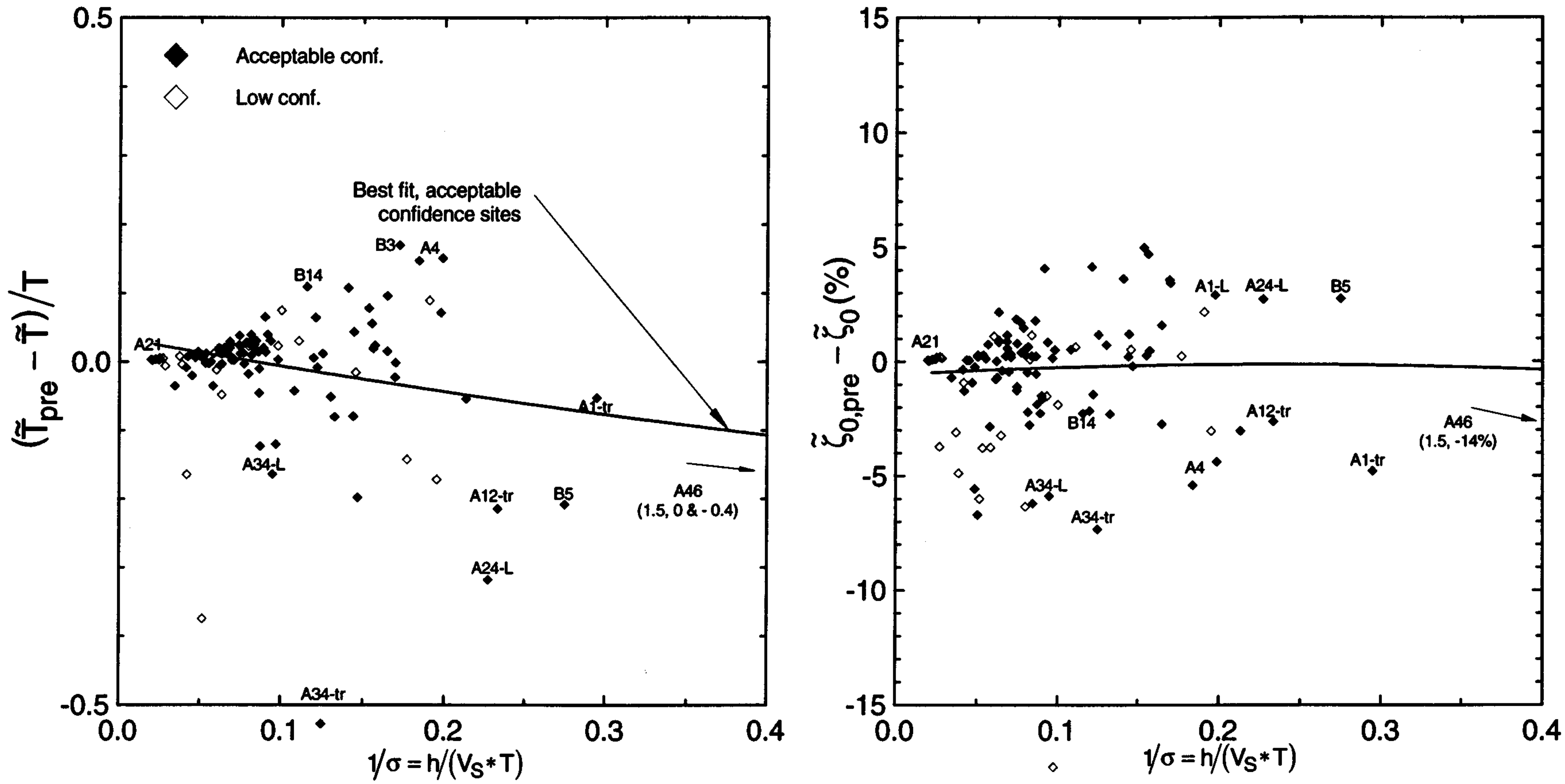

Fig. 5.14(a): Errors in "modified Veletsos" formulation for sites sorted by confidence level (tr=transverse, L=longitudinal direction)

A46 (at which 1/σ = 1.5). As noted below in Part (b), this underprediction of $\tilde{\zeta}_0$ is associated with a pronounced embedment effect at site A46.

Results from several sites help illustrate the general findings of Fig. 5.14(a). The minimal inertial interaction effects at site A21 (1/σ = 0.02 to 0.03, $\tilde{T}/T \approx 1$ and $\tilde{\zeta}_0 \approx 0\%$) were well predicted by the MV analyses, as was typical of sites with 1/σ < 0.1. Satisfactory predictions were generally also obtained for sites with intermediate 1/σ values such as B14 and A1-tr (1/σ = 0.12, 1/σ = 0.29). At these sites, period lengthening values of 1.14 and 1.57 are over- and under-predicted by absolute differences of about 0.11 and 0.06, respectively, while foundation dampings of 3.4 and 15.4% are underpredicted by absolute differences of 2.3 and 4.8%, respectively. The large inertial interaction effects at site A46 (1/σ = 1.5, $\tilde{T}/T \approx 4.0$ and $\tilde{\zeta}_0 \approx 30\%$) are predicted to within an absolute difference of about 0.4 for period lengthening, but damping was underpredicted by an absolute difference of 14%. With the exception of the damping results at site A46 (where there is a significant embedment effect), these results indicate that predictions of $\tilde{T}/T$ and $\tilde{\zeta}_0$ by the MV procedure are generally reasonably good considering the breadth of conditions represented in the database.

There are several noteworthy outliers in Fig. 5.14(a). The significance of these outliers is clarified by normalizing differences between empirical and predicted SSI effects by the magnitude of the SSI effect. In Fig. 5.14(b), errors in period lengthening ratio are normalized by empirical period lengthening, while errors in foundation damping factors are normalized by empirical flexible-base damping (normalization by empirical

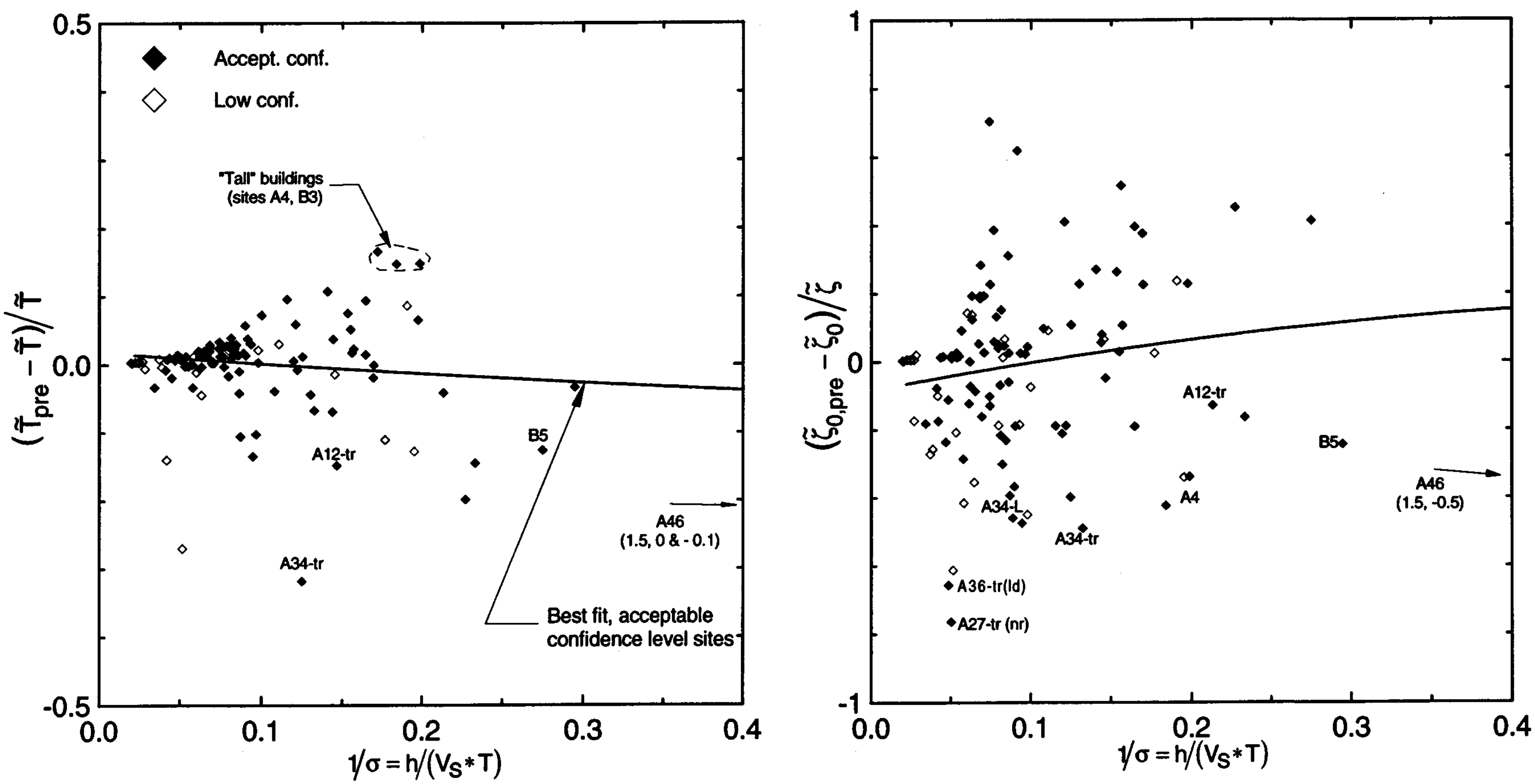

Fig. 5.14(b): Errors in "modified Veletsos" formulation for acceptable and low confidence level sites with normalization by flexible-base parameters

$\tilde{\zeta}_0$ was not practical, as some values of $\tilde{\zeta}_0$ are nearly zero). Based on Fig. 5.14(b), the most significant outliers for period lengthening are seen to be site A34 and several long period structures (A4, B3). Long period structures are discussed in Part (e). The unusual results at site A34 are discussed in Part (h).

Parts (b) to (g) below focus on the effects of embedment, aspect ratio, foundation type, structure type, and foundation shape and non-rigidity on the accuracy of the predicted inertial interaction effects.

(b) *Effect of embedment: comparison of "modified Veletsos" (MV) and "modified Bielak" (MB) methodologies*

Plotted in Fig. 5.15 are deviations between predicted and empirical results for three data sets, (1) MV predictions for buildings with surface foundations, (2) MV predictions for buildings with embedded foundations, and (3) MB predictions for buildings with embedded foundations. As before, the best fit curves are second-order polynomials established from linear regression analyses.

The regression curves in Fig. 5.15 suggest that $\tilde{T}/T$ is slightly overpredicted for embedded structures (by either MV or MB), and fairly well-predicted for surface structures. The differences between MV and MB predictions are generally minor (e.g. absolute differences of about 0.02 at A20-tr, 0.02 at A23) for common values of $1/\sigma$ (i.e. < 0.4). At site A46 ($1/\sigma = 1.5$), the absolute difference between the predictions is about 1.2, which is modest compared to the empirical value of $\tilde{T}/T \approx 4.0$.

The accuracy of $\tilde{\zeta}_0$ predictions in Fig. 5.15 by the MV methodology are comparable for surface and embedded structures. However, there are disparities between the MB and

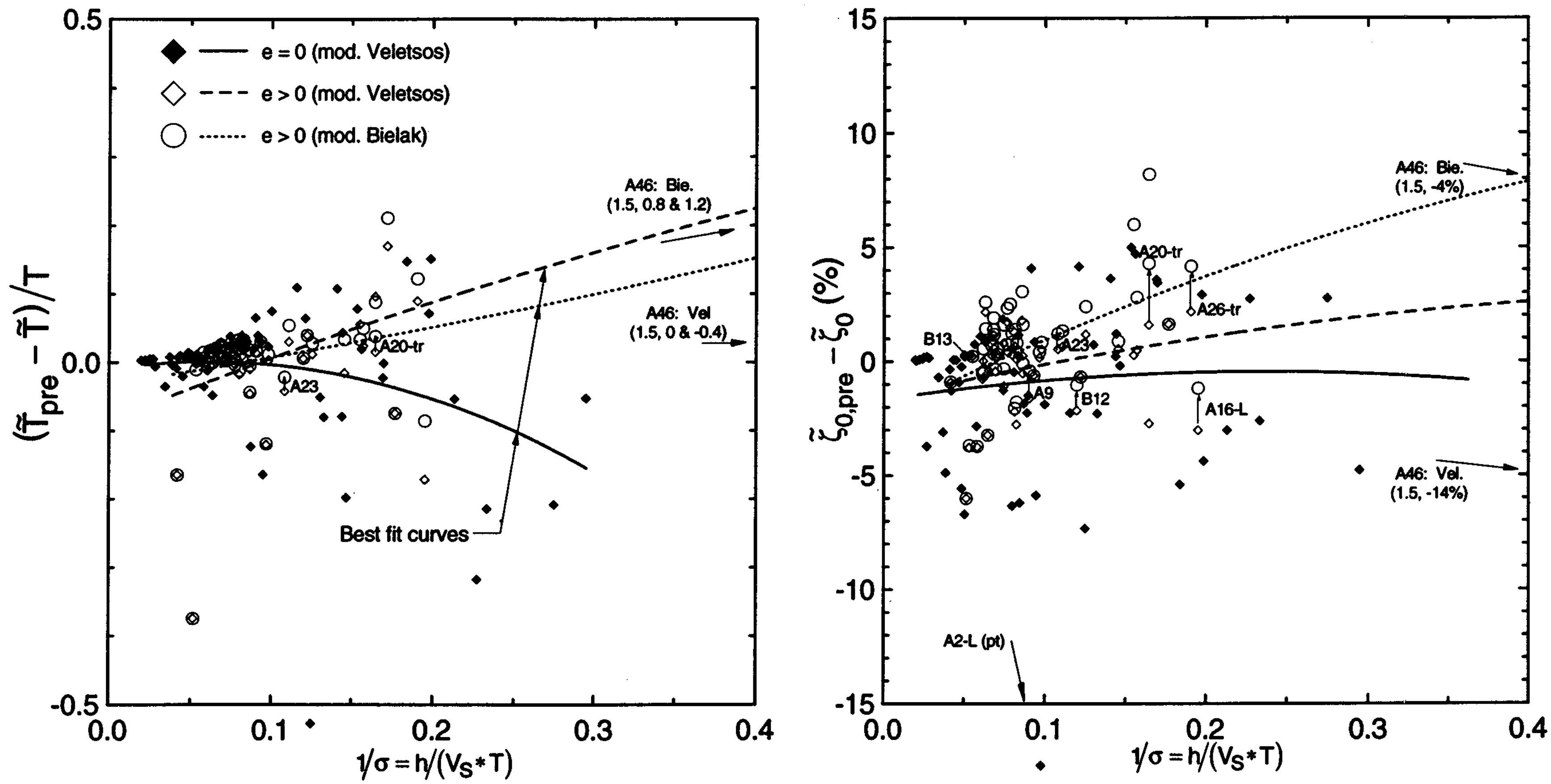

Fig. 5.15: Errors in "modified Veletsos" and "modified Bielak" formulations for surface and embedded structures

MV $\tilde{\zeta}_0$ predictions for embedded structures which increase with 1/σ (e.g. absolute differences of 0.7% at A23, 1/σ = 0.11; 2.7% at A20-tr, 1/σ = 0.17; 10% at A46, 1/σ = 1.5). The regression curves are principally controlled by the shallowly embedded foundations (e/r < 0.5), which are the most numerous in the database. For such cases, MV predictions are typically more accurate than MB predictions, as shown by the regression curves in Fig. 5.15, and as illustrated by sites A20 (e/r = 0.27) and A26 (e/r = 0.41). However, there are systematic errors in MV predictions for more deeply embedded foundations. These errors are not surprising because only the MB formulation incorporates dynamic basement wall/soil interaction effects into the foundation impedance function. As shown by individual labeled sites in Fig. 5.15, MV predictions of $\tilde{\zeta}_0$ are generally too low for structures with relatively deeply embedded foundations with continuous basement walls around the building perimeter such as A46 (e/r = 0.92) as well as A9, B12, and A16-L (e/r > 0.5). Other structures in the database with e/r > 0.5 had negligible foundation damping (i.e. $\tilde{\zeta}_0$ < 1%) which was overestimated by both the MV and MB predictions (i.e. A16-tr and B13). Hence, it appears that MB predictions of $\tilde{\zeta}_0$ are generally more accurate than MV predictions for structures with e/r > 0.5 and significant SSI effects. These differences are most pronounced at site A46, where the MB prediction of $\tilde{\zeta}_0 = 27\%$ matches the empirical value of 30% better than the MV prediction of 17%.

In summary, the accuracy of period lengthening predictions by the MV methodology are reasonably good for surface and embedded structures, and differences between the MV and MB predictions are generally minor for 1/σ values of common engineering interest ($1/\sigma < 0.4$). Accuracies of MV damping predictions are generally acceptable for surface and shallowly embedded structures ($e/r < 0.5$). For deeper embedment ($e/r > 0.5$), MB damping predictions are generally more accurate. These results suggest that dynamic basement-wall/soil interaction modeled by the MB procedure can be important for deeply embedded foundations.

Recognizing the limitations of the MV methodology for high embedment ratios, the data in Fig. 5.14(a) were re-plotted in Fig. 5.16 using MV predictions for $e/r < 0.5$ and MB predictions for $e/r > 0.5$. Subsequent plots in Figs. 5.17 to 5.19 are based on these mixed MV/MB predictions.

(c) *Effect of aspect ratio*

The results from Fig. 5.16 are re-plotted in Fig. 5.17 for aspect ratios of $h/r_2 < 1$ and $h/r_2 > 1$. Differences in the average errors of $\tilde{T}/T$ and $\tilde{\zeta}_0$ predictions for structures in both ranges are modest and not statistically significant. Hence, the effects of aspect ratio appear to be reasonably well captured by the analytical formulations.

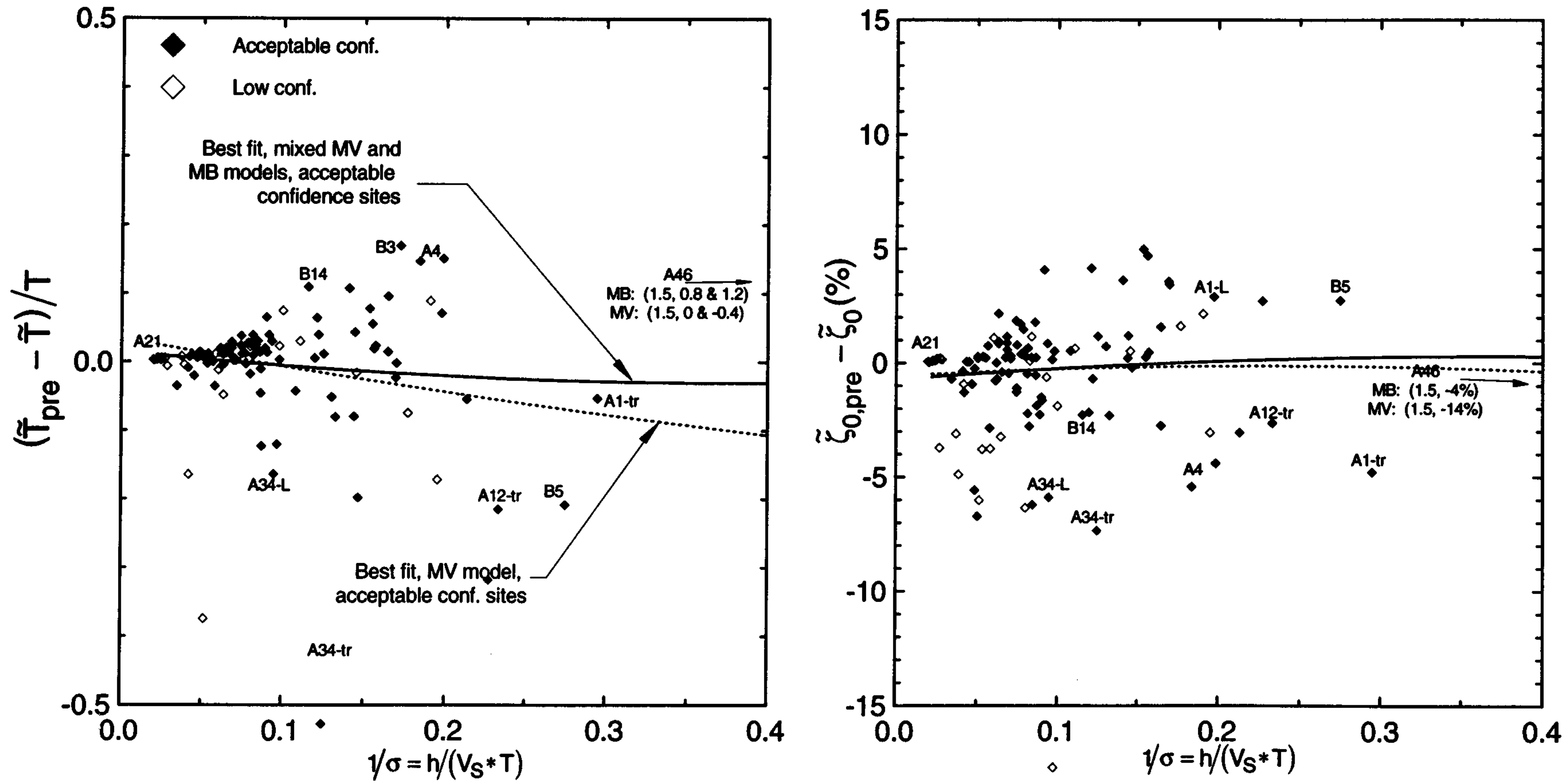

Fig. 5.16: Errors in predicted period lengthening ratios and foundation damping factors optimized for different embedment ratios [based on "modified Bielak" (MB) methodology for e/r > 0.5, "modified Veletsos" (MV) otherwise]

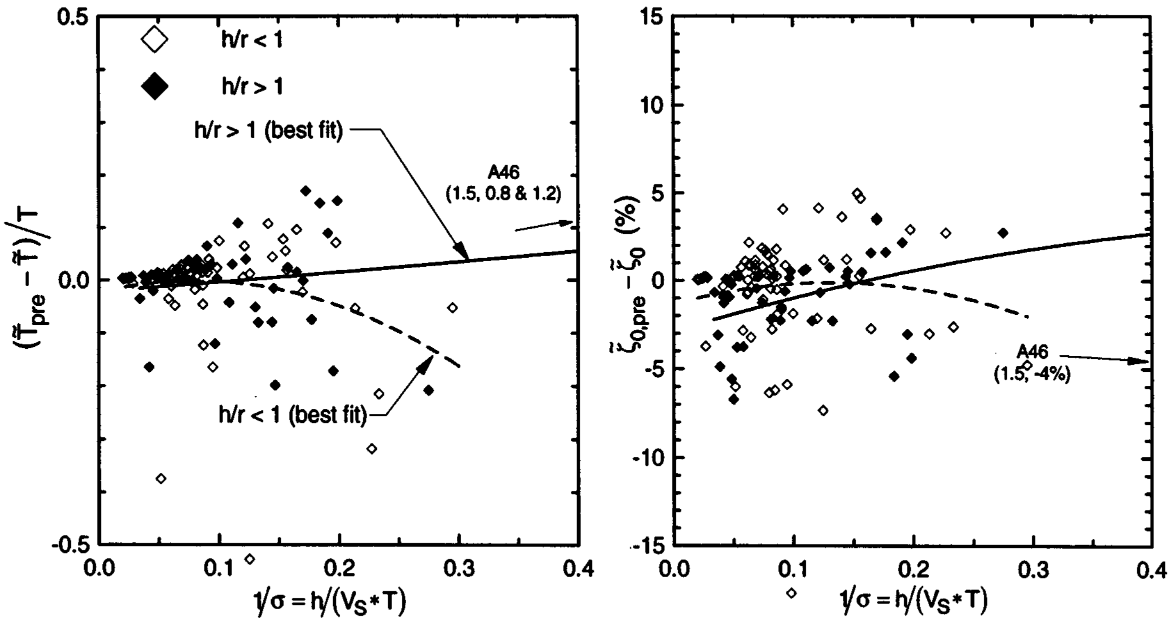

Fig. 5.17: Errors in predicted period lengthening ratios and foundation damping factors for sites sorted according to aspect ratio

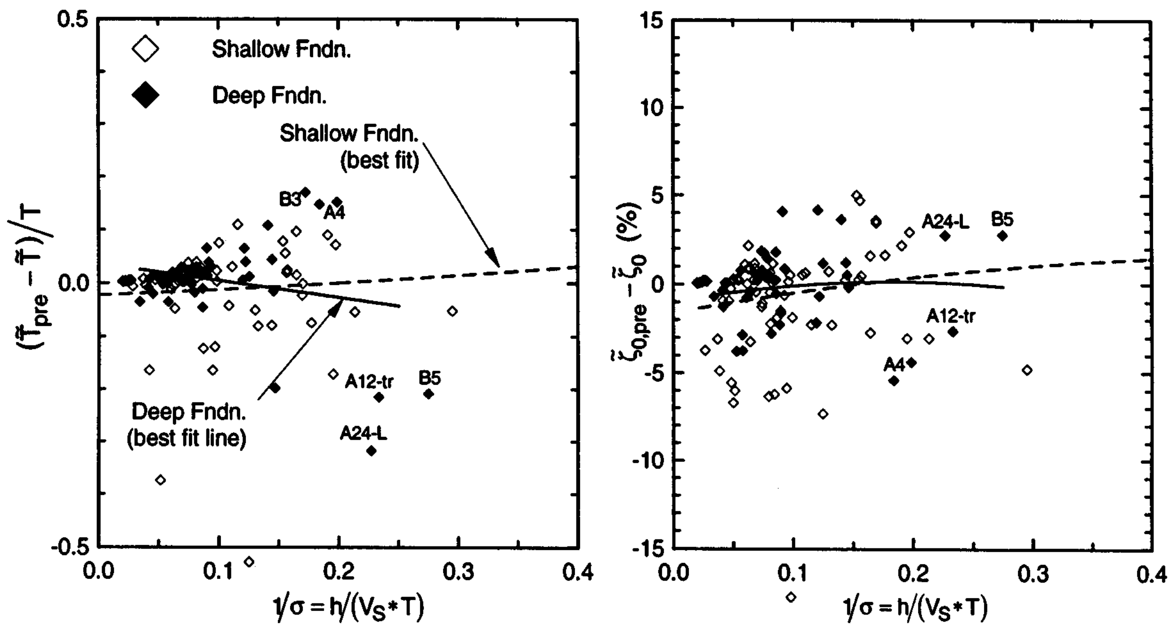

Fig. 5.18: Errors in predicted period lengthening ratios and foundation damping factors for sites sorted according to foundation type

(d) *Effect of foundation type*

The results from Fig. 5.16 are re-plotted in Fig. 5.18 for structures with shallow foundations (i.e. footings, grade beams, and mats) and deep foundations (i.e. piles and piers). Across the range of 1/σ strongly represented in the database (0 to 0.2), the average errors in predictions of $\tilde{T}/T$ and $\tilde{\zeta}_0$ are comparable for structures with either foundation type, suggesting that the influence of deep foundations on inertial interaction effects is small within this range. However, many of the deep foundation sites for which this trend was established have fairly stiff surficial soils and no marked increase in stiffness across the depth of the foundation elements. For such cases, it is reasonable that dynamic foundation behavior would be strongly influenced by the interaction of surface foundation elements (e.g. pile caps, base mats, footings) with soil. For example, sites B5 and A24 have 44-foot long friction piles and 15- to 25-foot deep belled piers, respectively, with $V_S \approx 650$ to 1000 fps across the foundation depth (in both cases). Large inertial interaction effects occurred at both sites which are slightly under-predicted by the MV procedure, indicating that the deep foundations were unlikely to have contributed significant rocking stiffness or radiation damping to the foundation impedance.

A limited number of sites have foundation piles which pass through relatively soft surficial soils (e.g. $V_S < 500$ fps) into stiffer underlying materials (A4, A12, B3). Period lengthening ratio is overpredicted at sites A4 and B3, which are pile supported high-rise structures in the San Francisco Bay Area underlain by soft cohesive Holocene sediments. In contrast, period lengthening is underpredicted at site A12, which is a mid-height shear wall structure supported by piles and underlain by soft clays. The contrast in results for these sites suggests that the errors in $\tilde{T}/T$ for these pile supported structures may be associated with factors other than foundation type. With regard to damping, $\tilde{\zeta}_0$ was underestimated at A4 and A12 ($\tilde{\zeta}_0$ not estimated at B3), suggesting that soil-pile interaction may have contributed to the foundation damping in these structures.

(e) *Effect of structure type*

The results from Fig. 5.16 are re-plotted in Fig. 5.19 and 5.20 for structures with lateral force resisting systems comprised of base isolation, frames and dual wall/frames, and shear walls. Also shown in Fig. 5.19 are results for long period ($\tilde{T} > 2$ sec.) structures. The average errors in predictions of $\tilde{T}/T$ and $\tilde{\zeta}_0$ are comparable for structures with the above lateral force resisting systems, suggesting that the influence of structure type on inertial interaction effects is generally small.

As shown in Fig. 5.19 and previously noted in Part (d), differences between empirical and predicted inertial interaction effects are significant for two high-rise structures on soft soils (sites A4 and B3). An examination of system identification results for long period structures ($\tilde{T} > 2$ sec.) in Table 5.3 indicates $\tilde{T}/T$ values near unity. Most of these are founded on relatively stiff soils and have $1/\sigma < 0.06$ [i.e. A27, A28, A29-tr(nr), A40, B6, B9, B13], so predictions of $\tilde{T}/T$ are near unity. However, predicted $\tilde{T}/T$ for sites A4 and B3 are about 1.17 to 1.24 due to the soft soils and associated large $1/\sigma$ values (0.17-0.20). The cause of the poor predictions at these sites may be associated with limitations of the MV and MB single degree-of-freedom models for structures with significant

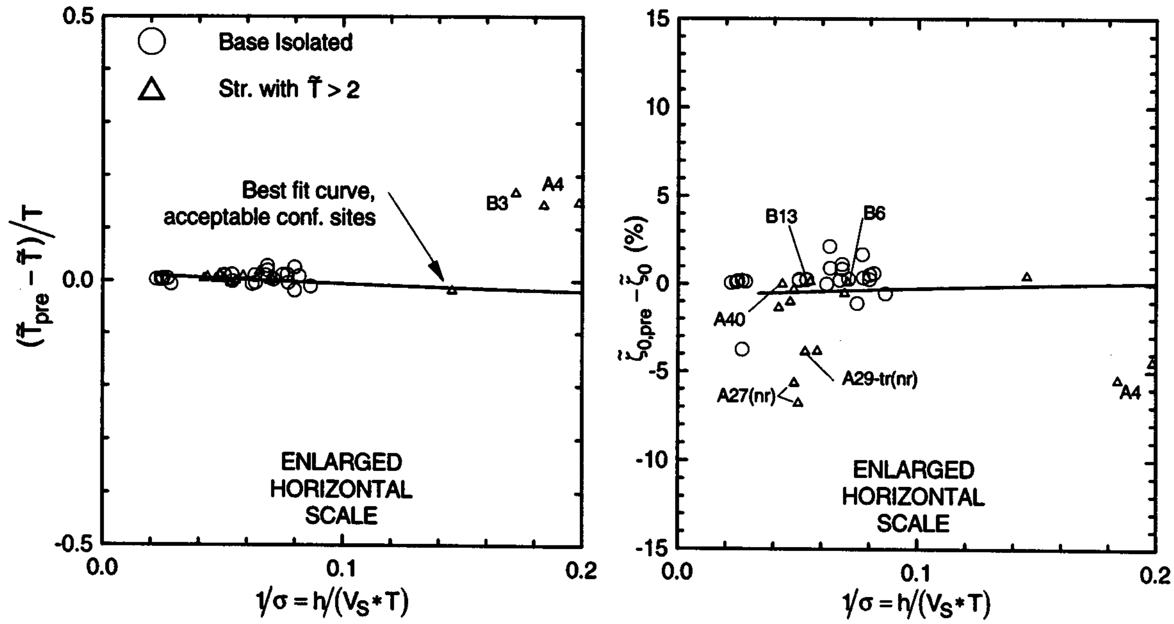

Fig. 5.19: Errors in predicted period lengthening ratios and foundation damping factors for sites with base isolated and long period structures

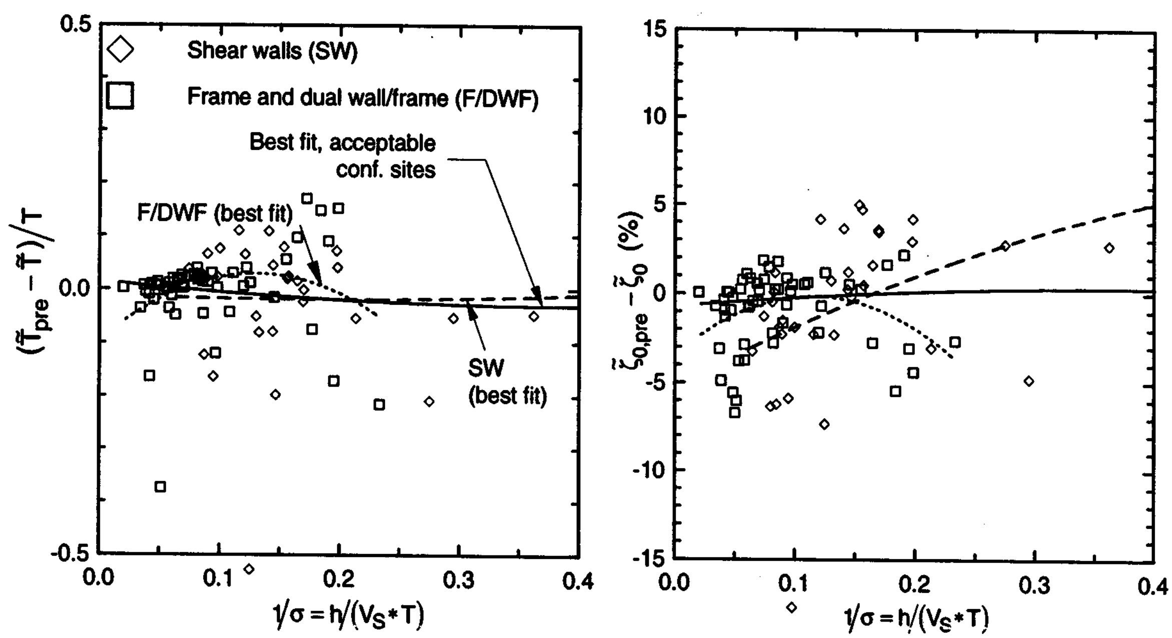

Fig. 5.20: Errors in predicted period lengthening ratios and foundation damping factors for sites with (a) shear wall structures and (b) frame and dual wall/frame structures

higher-mode responses. As noted in Part (d), the errors of $\tilde{\zeta}_0$ predictions for long-period structures (A4 and B3) appear to relate to foundation type. As shown in Fig. 5.19, the underprediction of $\tilde{\zeta}_0$ is not as clear in long-period structures with lower $1/\sigma$ values.

(f) *Effect of foundation shape*

The evaluation of foundation impedance for both the MV and MB methodologies is based on a circular foundation shape. Different foundation radii are used for translation and rocking deformation modes to match the area and moment of inertia, respectively, of the actual foundation (Eq. 2.3). However, Dobry and Gazetas (1986) found that a non-circular foundation can have a greater radiation damping effect in the rocking mode than a circular foundation with equivalent moment of inertia. Hence, rocking radiation damping values are increased for non-circular foundations according to the criteria in Section 2.2.2(d) in calculating the MV and MB predictions of $\tilde{\zeta}_0$ reported in Table 5.4. This section evaluates the significance of shape effects by comparing predicted $\tilde{\zeta}_0$ values developed with and without the corrections to empirical $\tilde{\zeta}_0$ values.

Shape effect corrections to rocking radiation damping were made in the prediction of $\tilde{\zeta}_0$ values at 31 sites (A1, 5, 7-13, 15, 21, 27-29, 31-34, 36-37, 39, 42-43, 45, B1-2, 5, 7, 10-11, 14). For 23 sites, the absolute difference in damping associated with the correction was less than 0.05%. These corrections were small because the radiation damping effect for the rocking deformation mode is small for structures with low fundamental mode frequencies. For the remaining eight sites, Table 5.5 lists empirical

$\tilde{\zeta}_0$ values along with predictions made with and without shape effect corrections. The empirical values are dependent on whether the shape effect correction was made because this correction affects the estimated fixed- or flexible-base parameters. The predictions are based on the MV and MB methodologies for e/r < 0.5 and e/r > 0.5, respectively.

Table 5.5: Empirical and predicted values of foundation damping factor $\tilde{\zeta}_0$ developed with and without corrections for shape effects (S indicates shape correction made, S=1 indicates no correction)

	Empirical		Predicted	
	S	S=1	S	S=1
A1-tr	15.4	14.9	10.6	10.3
A10-tr	6.05	5.90	6.33	6.17
A13-L	0.93	0.89	2.11	1.99
A31-L (nr)	0.93	0.89	1.15	1.08
A34-tr	12.8	12.0	5.79	5.49
A45-tr	1.55	1.55	1.37	1.31
B2-tr	4.67	4.70	3.40	3.28
B5-tr	2.56	3.14	5.22	4.84

The data in Table 5.5 indicate no significant improvement in $\tilde{\zeta}_0$ predictions with the shape correction, suggesting that foundation shape effects on rocking radiation damping are minor for the structures in this database.

(g) *Effect of foundation flexibility*

Both the MV and MB methodologies use the assumption of rigid foundations. As discussed in Section 2.2.2(e), foundation flexibility can significantly reduce the rocking stiffness and damping of foundations with continuous base-slabs loaded only through rigid central core walls. Three structures in this study have central core shear walls which are designed to resist the bulk of the structure's lateral loads in at least one direction: A24-L, B2, and B7. The foundation for the central core walls at site B7 is independent of the foundations for the remainder of the structure. Hence, the effects of foundation non-rigidity could only be assessed at sites A24-L and B2.

The base slab in both of these structures is loaded both through a stiff central core and through vertical load bearing elements outside of the core. Hence, the assumption in the theoretical formulations of a flexible base slab loaded only through a rigid core is not satisfied. The suitability of the theoretical corrections for foundation flexibility (which were adapted from Iguchi and Luco, 1982) are investigated by repeating the predictive analyses for four conditions: (1) rigid foundation, (2) flexible foundation with corrections to foundation rocking impedance (both stiffness and damping), (3) flexible foundation with corrections to foundation rocking impedance for stiffness only, and (4) rigid foundation beneath central core, but perfect flexibility outside of the core (i.e. only the core area is considered in calculating foundation impedance). Shown in Table 5.6 are the empirical $\tilde{T}/T$ and $\tilde{\zeta}_0$ values along with predictions for the four sets of conditions. At site B2, it was necessary to estimate flexible-base parameters using the procedures in Section 3.6.2, so the empirical $\tilde{T}/T$ and $\tilde{\zeta}_0$ values depend on the assumed foundation flexibility. At site A24, both flexible- and fixed-base parameters are obtained from system identification, and hence are unaffected by assumptions about foundation flexibility.

Table 5.6: Comparisons of empirical period lengthenings and foundation damping factors for sites A24-L and B2 with MV predictions for different assumed conditions of foundation non-rigidity

		A24-L		B2	
		$\tilde{T}/T$	$\tilde{\zeta}_0$ (%)	$\tilde{T}/T$	$\tilde{\zeta}_0$ (%)
1. Rigid fndn.	Empirical	1.60	4.5	1.19	20.0
	Prediction	1.25	13.5	1.03	0.3
2. Flexible fndn.	Empirical	1.60	4.5	1.13	7.2
	Prediction	1.30	13.3	1.17	0.5
3. Mixed	Empirical	1.60	4.5	1.13	4.6
	Prediction	1.30	14.7	1.17	3.4
4. Rigid core	Empirical	1.60	4.5	1.13	5.0
	Prediction	1.28	7.2	1.09	0.2

These results indicate that foundation flexibility significantly affects interaction phenomena for these structures. The predictions are poor for the rigid foundation assumption (Condition 1). When corrections to the stiffness and damping components of rocking impedance are made (Condition 2), $\tilde{T}/T$ values improve, but $\tilde{\zeta}_0$ predictions are erroneous. For site A24-L, the best overall results for $\tilde{T}/T$ and $\tilde{\zeta}_0$ are obtained when the foundation area beyond the core is neglected (Condition 4), implying that the pier and grade beam foundation is sufficiently flexible outside of the core that it effectively does not participate in the structural response of the core. For site B2, the best results are achieved when corrections for foundation flexibility are only made for stiffness (Condition 3). This result implies that the 2.5 to 5-foot thick foundation slab for this building is unaffected by the vertical load bearing columns outside of the core from the standpoint of rocking stiffness, but that the restraint on the foundation provided by these columns effectively eliminates any reduced damping effect that might otherwise be expected from foundation flexibility.

(h) *Discussion of site A34*

As shown in Figs. 5.7, 5.14(b) and 5.16, $\tilde{T}/T$ and $\tilde{\zeta}_0$ values at A34 were unusually large for the value of $1/\sigma \approx 0.1$ at this site. The site was given an "acceptable" confidence designation based on the criteria in Section 5.3.3. As shown in Fig. 5.21(a), the structure at site A34 is a four-story concrete block shear wall building with no basement. The foundation consists of 2.3-foot deep footings beneath the walls. The free-field instrument is located in a parking lot about 240 feet from the structure. As shown in Fig. 5.21(b), soil conditions consist of sands and silty sands with V_S values ranging from 1000 to 2500 fps, as established by downhole measurements by Fumal et al. (1982).

The most likely cause of the unusual result at site A34 is shear wave velocities which are too high. Generally, when both shear and compression wave velocities are measured, V_S is found to be about one-half of V_P in unsaturated cohesionless soils (implying that $\nu = 0.33$). For this site, however, V_S/V_P ratios were in the range of about 0.7 to 0.8, which is not possible, as this condition would require $\nu > 0.5$ for the sandy soils at the site. Hence, there is an error in the measured velocities, but it is not known if the error is in V_S or V_P (Gibbs, *pers. communication*, 1996). Thus, a conclusive determination of the source of the unusual results at site A34 cannot be made. However, it is interesting to note that if V_S is lowered so that the $V_S/V_P = 0.5$, $1/\sigma$ increases to about 0.16, and $\tilde{T}/T$ and $\tilde{\zeta}_0$ predictions are increased such that the absolute differences with empirical values are about -0.3 and -5% in the transverse direction and -0.05 and -4% in the longitudinal direction. Such underpredictions would not be particularly significant outliers relative to results for other sites.

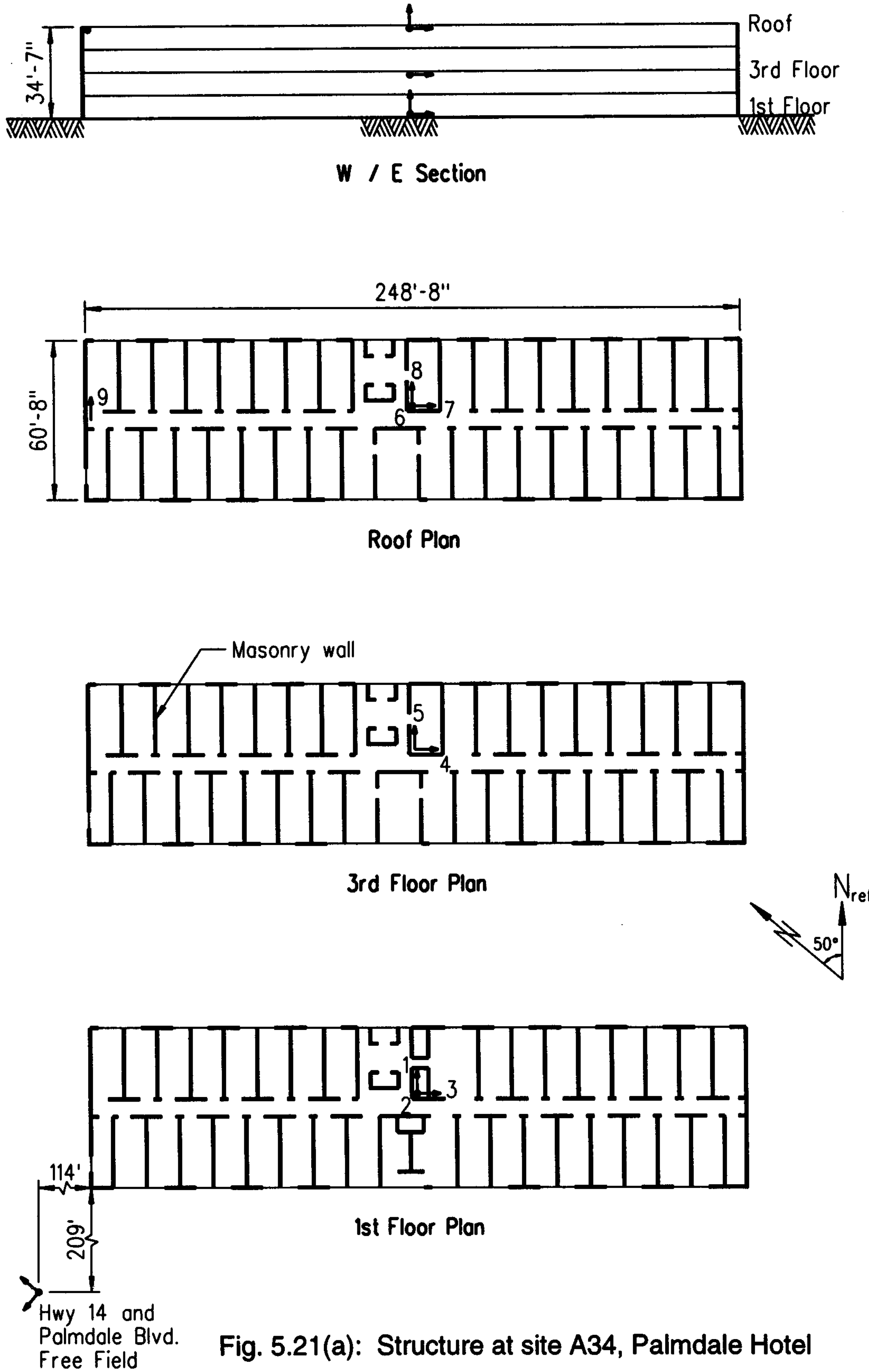

Fig. 5.21(a): Structure at site A34, Palmdale Hotel

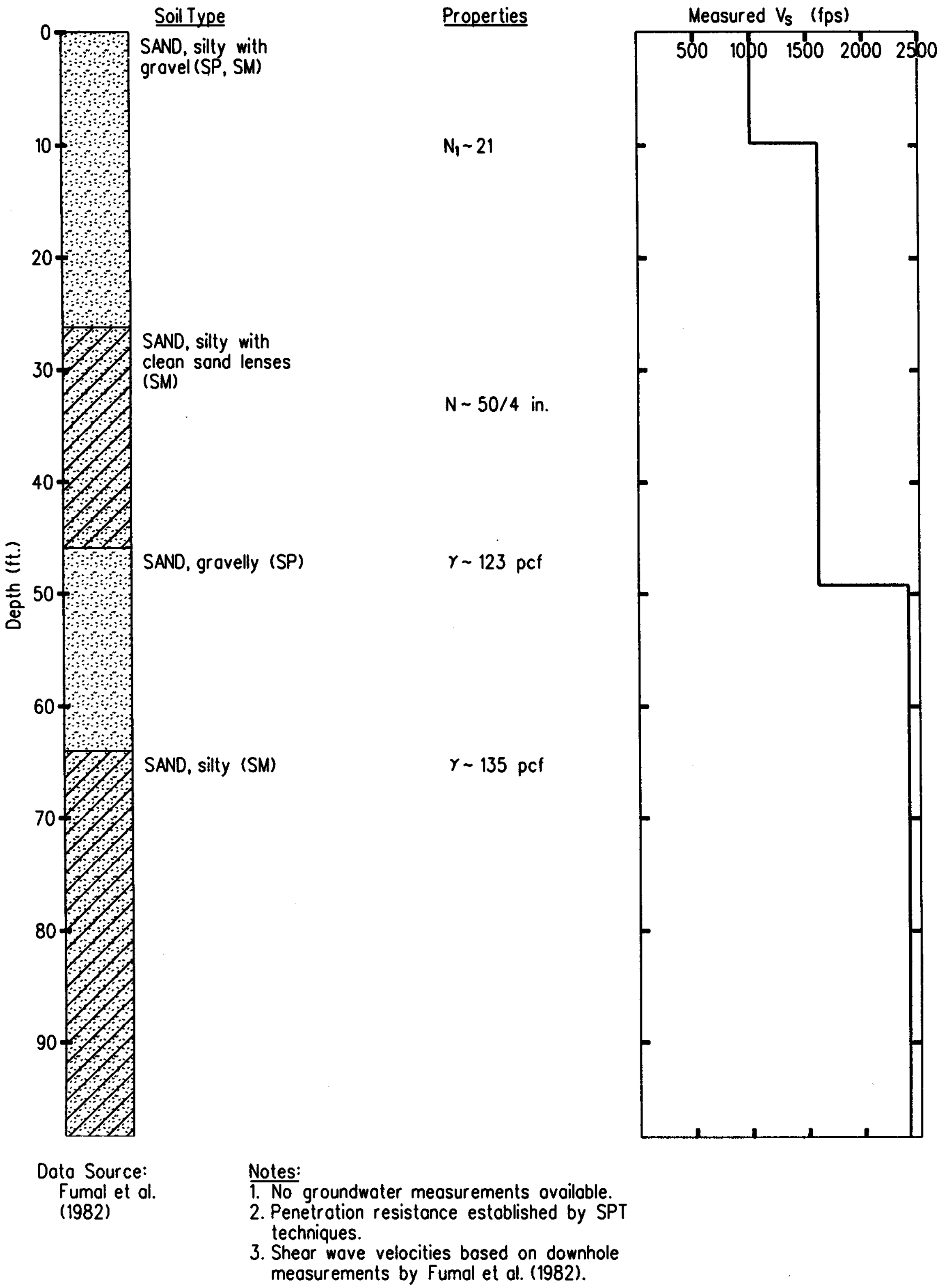

Fig. 5.21(b): Soil column at site A34, Palmdale Hotel

5.5 Verification of Code Provisions for Inertial Interaction

5.5.1 Overview of Analysis Procedures and Required Input

In this section, current SSI provisions in two U.S. building codes (BSSC, 1997 and ATC, 1978) are examined relative to the database of "observed" SSI effects. The code procedures are based on the framework developed by Veletsos and Nair (1975) and Bielak (1975) wherein inertial soil-structure interaction effects are described in terms of period lengthening ratio $\tilde{T}/T$ and foundation damping factor $\tilde{\zeta}_0$. These provisions incorporate inertial SSI effects into evaluations of seismic base shear forces in structures, but are "optional" in the current versions of these codes, and are commonly neglected in practice. Kinematic interaction effects are neglected in current code provisions, consequently the focus here is on inertial interaction.

The code provisions are based on a single degree-of-freedom structure model with a rigid disk foundation resting on the surface of a visco-elastic halfspace. Parameters needed to evaluate the system response to a given ground motion include: (1) fundamental-mode fixed-base period (T) and damping ratio (ζ), as well as effective structure height (h), (2) foundation radii for rocking (r_1) and translation (r_2), and (3) soil shear wave velocity (V_S) and hysteretic damping ratio (β).

The single degree-of-freedom model is extended to multi-story structures by taking height (h) as the distance from the base to the centroid of the inertial forces associated with the first mode. This effective height is taken as 70% of the total structure height. Higher modes are not considered to be affected by SSI, hence only fundamental-mode structural parameters are required as input.

The foundation geometry is represented by equivalent disk radii so that closed-form solutions for the static impedance of a rigid disk foundation (Eq. 2.5) can be used. Eq. 2.3 is used to compute foundation radii which match the area (A_f) and moment of inertia (I_f) of the actual foundation (i.e. $r_u = \sqrt{A_f/\pi}$ and $r_\theta = \sqrt[4]{4I_f/\pi}$). Eq. 2.7 is used to extend the analysis to embedded foundations and soil conditions more appropriately modeled as a finite soil layer over a rigid base. The real part of the foundation impedance function is taken as the static value (i.e. the α factors defined in Eq. 2.4 are taken as 1.0). The imaginary part is not directly computed, rather the graphical solution in Fig. 5.22 is used to evaluate $\tilde{\zeta}_0$ from $\tilde{T}/T$. This relationship, which was modified from Veletsos (1977), was derived for rigid disk foundations on a homogeneous halfspace, and no corrections for conditions such as foundation embedment, shape, or flexibility are suggested in the code provisions or commentary.

For non-uniform soil profiles, effective shear moduli (or shear wave velocities, V_S) are derived from irregular V_S profiles by taking the ratio of profile depth to travel time through the profile. The code commentary recommends effective profile depths of $1.5 \times r_2$ for rocking, and $4 \times r_1$ for translations. The strain-dependence of the V_S profile is correlated with the effective long-period ground motion parameter A_v using Table 5.7.

Other soil parameters needed in the analysis are Poisson's ratio (υ) and strain-dependent hysteretic damping ratio (β). The BSSC code commentary recommends υ=0.33 for clean sands and gravels, υ=0.40 for stiff clays and cohesive soils, and υ=0.45 for soft clays. Soil damping ratio β is correlated to ground motion parameter A_v in Fig. 5.22, and does not directly enter the analysis.

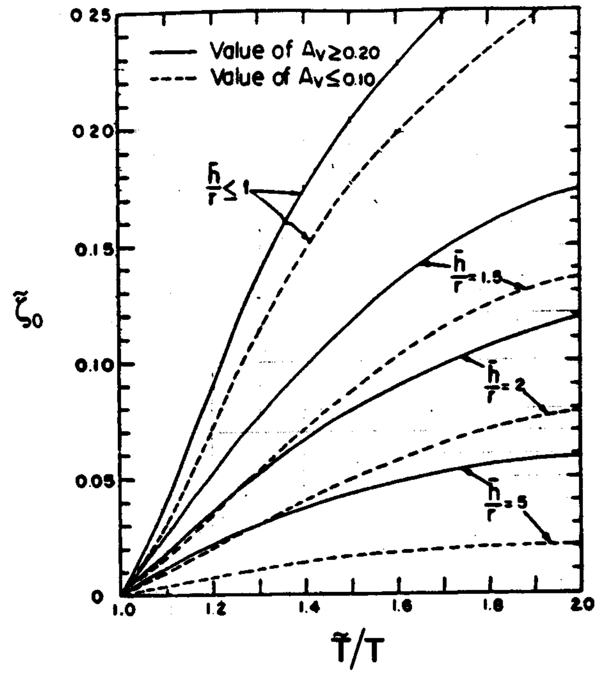

Fig. 5.22: Relationship between foundation damping factor ($\tilde{\zeta}_0$) and period lengthening ratio for rigid disk foundation on homogeneous halfspace (BSSC, 1995; ATC, 1978)

Table 5.7: Code-prescribed values of soil modulus and V_S degradation with effective long period ground acceleration, A_v (BSSC, 1995)

	Ground Acceleration Coefficient, A_v			
	≤ 0.10	≤ 0.10	≤ 0.20	≥ 0.30
G/G_{max}	0.81	0.64	0.49	0.42
$V_s/(V_s)_{max}$	0.90	0.80	0.70	0.65

5.5.2 Verification Analyses

(a) *Database*

The empirical database used for the verification studies was presented in Section 4.2. Period lengthening ratios and foundation damping factors are presented in Table 5.8 for sites in which the confidence level in the result accuracy is “acceptable” or “low” based on the criteria in Section 5.3.3(a).

(b) *Analysis procedures*

Several suites of analyses were performed to evaluate period lengthening and foundation damping for comparison with the system identification results. These are summarized as:

- *Method 1*: Code procedures (ATC, 1978 and BSSC, 1997) as described in 5.5.1. Period lengthening is computed as,

  $$\frac{\tilde{T}}{T} = \sqrt{1 + 25\frac{\gamma r_1 h}{V_{S1}^2 T^2}\left(1 + 112\frac{r_1 h^2 V_{SI}^2}{r_2^3 V_{S2}^2}\right)}$$

  where γ is a dimensionless structure-to-soil mass ratio (Eq. 2.13) and is usually taken as 0.15, and V_{S1} and V_{S2} are defined for profiles of depth $4 \times r_1$ for translations and $1.5 \times r_2$ for rocking, respectively. Foundation damping is evaluated from $\tilde{T}/T$ using Fig. 5.22.

- *Method 2*: Same as Method 1, except the strain-dependence of V_S is evaluated from deconvolution analyses with the program SHAKE (Schnabel et al., 1972). These analyses made use of recorded free-field motions, as well as modulus degradation and damping curves by Seed et al. (1986) for sands, Vucetic and Dobry (1991) for clays, and

Table 5.8: Inertial interaction effects evaluated from system identification and various design procedures

Transverse

Site	Eqk.	Cont.	$\frac{1}{\sigma_{1,4,5}}$	$\frac{1}{\sigma_2}$	$\frac{1}{\sigma_{3,6}}$	Obs. $\tilde{T}/T$	Obs. $\tilde{\zeta}_0$	Meth. 1 $\tilde{T}/T$	Meth. 1 $\tilde{\zeta}_0$	Meth. 2 $\tilde{T}/T$	Meth. 2 $\tilde{\zeta}_0$	Meth. 3 $\tilde{T}/T$	Meth. 3 $\tilde{\zeta}_0$	Meth. 4 $\tilde{T}/T$	Meth. 4 $\tilde{\zeta}_0$	Meth. 5 $\tilde{T}/T$	Meth. 5 $\tilde{\zeta}_0$	Meth. 6 $\tilde{T}/T$	Meth. 6 $\tilde{\zeta}_0$
'A' Sites																			
1	PT	A	0.36	0.3	0.29	1.57	15.4	1.32	13.5	1.30	12.6	1.40	16	1.47	18.3	1.30	12.5	1.51	10.6
2	PT	L	0.08	0.08	0.08	1.04	11.2	1.06	2.0	1.07	2.5	1.06	2.1	1.07	2.2	1.06	2	1.07	4.9
	PTA	L	0.09	0.08	0.08	1.05	4.1	1.07	2.5	1.07	2.3	1.07	2.4	1.08	2.8	1.07	2.5	1.07	5.3
4	LP	A	0.18	0.16	0.20	1.02	6.1	1.13	2.4	1.10	1.9	1.17	2.8	1.14	2.4	1.13	2.4	1.17	1.7
5	LP	A	0.04	0.03	0.03	1.04	0.7	1.01	0.0	1.01	0	1.01	0	1.01	0	1.01	0	1.01	0.0
7	LP	A	0.09	0.08	0.08	1.03	9.3	1.03	0.9	1.03	0.8	1.06	1.7	1.04	1	1.03	0.9	1.06	3.1
8	LP	A	0.08	0.08	0.09	1.16	3.4	1.02	0.6	1.02	0.4	1.04	1.2	1.02	0.6	1.02	0.7	1.04	1.5
9	CGA	L	0.1	0.09	0.09	1.00	3.0	1.06	1.7	1.06	1.5	1.06	1.6	1.07	1.8	1.06	1.7	1.03	2.4
10	LP	A	0.22	0.16	0.16	1.08	6.1	1.19	8.5	1.10	4	1.14	6.5	1.23	11.5	1.18	8	1.14	6.3
11	LP	A	0.03	0.02	0.02	1.00	0.0	1.00	0.0	1.00	0	1.00	0	1.00	0	1.00	0	1.00	0.1
12	IMP	A	0.27	0.23	0.23	1.47	8.8	1.19	8.8	1.14	6.5	1.18	8.5	1.21	9.3	1.17	7.8	1.26	6.1
13	LD	A	0.13	0.12	0.12	1.05	3.8	1.07	2.3	1.07	2	1.07	2.2	1.07	2.4	1.07	2	1.05	1.6
14	WT	A	0.15	0.13	0.14	1.00	1.1	1.10	2.9	1.08	2.4	1.11	3.2	1.11	3.4	1.10	3.1	1.11	4.8
15	NR	A	0.07	0.06	0.06	1.06	3.6	1.03	0.7	1.02	0.6	1.03	0.8	1.03	0.8	1.02	0.5	1.02	0.8
16	NR	L	0.21	0.18	0.18	1.28	0.0	1.28	1.9	1.25	1.8	1.25	1.8	1.28	2	1.22	1.5	1.14	0.2
17	NR	A	0.11	0.11	0.14	1.17	11.3	1.05	1.5	1.05	1.4	1.18	6.6	1.06	1.8	1.05	1.5	1.21	12.5
18	WT	A																	
20	NR	A	0.15	0.15	0.16	1.13	0.0	1.11	3.3	1.10	3.5	1.13	4.5	1.11	3.6	1.09	3.4	1.09	1.6
21	SM	L	0.03	0.03	0.03	1.01	0.0	1.00	0.0	1.00	0	1.01	0	1.00	0	1.00	0	1.01	0.2
	LD	L	0.02	0.02	0.02	1.00	0.0	1.00	0.0	1.00	0	1.00	0	1.00	0	1.00	0	1.00	0.1
	NR	L	0.02	0.02	0.02	1.00	0.0	1.00	0.0	1.00	0	1.00	0	1.00	0	1.00	0	1.01	0.2
23	NR	A	0.13	0.11	0.11	1.08	0.0	1.13	2.0	1.10	1.9	1.10	1.9	1.13	2	1.10	1.9	1.06	1.2
24	NR	A	0.1	0.09	0.12	1.04	1.1	1.07	3.0	1.06	2.5	1.07	2.7	1.08	3.2	1.07	2.7	1.08	5.1
25	LD	A	0.05	0.05	0.05	1.00	0.0	1.01	0.2	1.01	0.1	1.01	0.3	1.01	0.2	1.01	0	1.01	0.2
	NR	A	0.05	0.05	0.05	1.00	0.0	1.01	0.2	1.01	0.1	1.02	0.4	1.01	0.2	1.01	0	1.01	0.3
26	NR	L	0.19	0.17	0.19	1.04	0.0	1.21	3.6	1.16	2.9	1.23	3.7	1.22	3.6	1.2	3.5	1.13	2.2
27	LD	A	0.05	0.04	0.05	1.00	1.0	1.02	0.2	1.01	0.1	1.02	0.2	1.02	0.1	1.01	0.1	1.01	0.1
	NR	A	0.05	0.05	0.05	1.00	5.6	1.01	0.1	1.01	0.1	1.02	0.2	1.01	0.1	1.01	0.1	1.01	0.1
28	NR	A	0.09	0.07	0.07	1.00		1.07	1.3	1.04	0.8	1.04	0.7	1.07	1.3	1.05	0.9	1.02	
29	WT	L	0.07	0.06	0.06	1.01	3.9	1.06	1.7	1.04	1.2	1.04	1.2	1.06	1.7	1.04	1.3	1.03	0.1
	NR	L	0.06	0.05	0.05	1.02	3.9	1.04	1.3	1.03	0.9	1.03	0.9	1.04	1.3	1.03	0.9	1.02	0.1
30	NR	A	0.09	0.07	0.09	1.08	1.9	1.03	0.8	1.02	0.5	1.04	1.5	1.03	0.9	1.02	0.7	1.04	2.1
31	LD	A	0.13	0.12	0.13	1.19	3.0	1.12	1.2	1.1	1	1.13	1.3	1.12	1.2	1.09	1	1.11	0.7
	NR	A	0.14	0.12	0.13	1.16	0.0	1.11	1.2	1.1	1	1.13	1.3	1.11	1.2	1.09	1	1.11	0.7
32	WT	A																	
33	WT	A	0.08	0.07	0.07	1.00	0.2	1.04	1.4	1.04	1.2	1.04	1.4	1.04	1.5	1.04	1.2	1.03	0.8
	NR	A	0.08	0.06	0.06	1.00	1.4	1.04	1.4	1.03	0.9	1.03	1	1.04	1.5	1.03	1.2	1.02	0.6
34	NR	A	0.17	0.12	0.12	1.66	13.1	1.12	5.0	1.06	2.3	1.09	3.6	1.14	6	1.12	5	1.13	5.8
35	WT	A	0.09	0.09	0.09	1.02	3.6	1.04	1.2	1.03	1.1	1.04	1.2	1.04	1.3	1.04	1.3	1.04	2.0
	UP	A	0.08	0.08	0.08	1.01	4.4	1.03	1.0	1.03	0.9	1.04	1	1.03	1	1.03	1	1.03	1.6
36	LD	L	0.04	0.04	0.04	1.17	1.0	1.01	0.1	1.01	0.1	1.01	0.1	1.01	0.1	1.01	0.1	1.01	0.1
37	RD	A	0.09	0.08	0.08	1.03	0.9	1.04	1.2	1.03	1	1.04	1.3	1.04	1.3	1.04	1.1	1.04	1.5

Longitudinal

Site	Eqk.	Cont.	$\frac{1}{\sigma_{1,4,5}}$	$\frac{1}{\sigma_2}$	$\frac{1}{\sigma_{3,6}}$	Obs. $\tilde{T}/T$	Obs. $\tilde{\zeta}_0$	Meth. 1 $\tilde{T}/T$	Meth. 1 $\tilde{\zeta}_0$	Meth. 2 $\tilde{T}/T$	Meth. 2 $\tilde{\zeta}_0$	Meth. 3 $\tilde{T}/T$	Meth. 3 $\tilde{\zeta}_0$	Meth. 4 $\tilde{T}/T$	Meth. 4 $\tilde{\zeta}_0$	Meth. 5 $\tilde{T}/T$	Meth. 5 $\tilde{\zeta}_0$	Meth. 6 $\tilde{T}/T$	Meth. 6 $\tilde{\zeta}_0$
'A' Sites																			
1	PT	A	0.20	0.18	0.20	1.09	8.6	1.10	4	1.08	2.8	1.14	6.4	1.12	4.5	1.09	3.8	1.17	11.6
2	PT	L	0.10	0.10	0.10	1.08	25.1	1.09	3.1	1.10	3.5	1.09	3.2	1.10	3.3	1.09	3.1	1.10	7.4
	PTA	L	0.10	0.10	0.10	1.03	9.6	1.10	3.5	1.09	3.2	1.10	3.5	1.11	3.6	1.10	3.5	1.11	7.7
4	LP	A	0.17	0.14	0.18	1.00	6.9	1.12	1.9	1.09	1.7	1.15	2.7	1.12	2	1.12	1.9	1.15	1.4
5	LP	A	0.04	0.04	0.04	1.03	0.0	1.01	0.1	1.00	0	1.01	0.1	1.01	0.1	1.01	0.1	1.01	0.1
7	LP	A																	
8	LP	A	0.07	0.06	0.08	1.00	2.0	1.01	0.3	1.01	0.1	1.03	0.9	1.01	0.3	1.02	0.4	1.03	1.5
9	CGA	L																	
10	LP	A	0.20	0.14	0.16	1.00	13.0	1.10	4	1.06	2.2	1.12	4.5	1.12	4.5	1.10	3.8	1.12	10.3
11	LP	A	0.03	0.02	0.02	1.00	0.0	1.00	0.1	1.00	0	1.00	0.1	1.00	0.1	1.00	0.1	1.00	0.0
12	IMP	A	0.10	0.09	0.09	1.00	0.0	1.03	1	1.02	0.9	1.03	1.1	1.03	1	1.03	0.8	1.03	0.9
13	LD	A	0.13	0.12	0.13	1.03	1.0	1.06	2	1.05	1.7	1.05	1.7	1.06	2.1	1.06	1.8	1.04	2.1
14	WT	A																	
15	NR	A	0.06	0.05	0.06	1.02	0.0	1.02	0.8	1.02	0.4	1.02	0.6	1.03	0.8	1.02	0.5	1.02	0.8
16	NR	L	0.23	0.20	0.20	1.34	3.3	1.31	3.1	1.23	2.7	1.23	2.7	1.31	3.2	1.24	2.8	1.26	2.1
17	NR	A	0.10	0.09	0.12	1.09	5.7	1.04	1.1	1.03	1	1.13	4.2	1.04	1.3	1.04	1.1	1.15	9.9
18	WT	A	0.07	0.08	0.08	1.00	0.0	1.02	0.4	1.02	0.4	1.03	0.7	1.02	0.4	1.02	0.3	1.02	0.3
20	NR	A	0.14	0.14	0.16	1.05	1.0	1.08	2.3	1.08	2.1	1.11	2.5	1.09	2.4	1.07	1.8	1.08	1.5
21	SM	L	0.02	0.02	0.03	1.00	3.9	1.00	0	1.00	0	1.00	0	1.00	0	1.00	0	1.00	0.1
	LD	L	0.02	0.02	0.02	1.00	0.0	1.00	0	1.00	0	1.00	0	1.00	0	1.00	0	1.00	0.1
	NR	L	0.02	0.02	0.03	1.00	0.0	1.00	0	1.00	0	1.00	0	1.00	0	1.00	0	1.01	0.2
23	NR	A																	
24	NR	A	0.23	0.21	0.23	1.60	4.5	1.22	10	1.18	8.5	1.26	12	1.35	15	1.19	9.0	1.28	7.2
25	LD	A	0.05	0.05	0.05	1.00	0.0	1.01	0.2	1.01	0.1	1.02	0.4	1.01	0.3	1.01	0.1	1.01	0.3
	NR	A	0.05	0.05	0.05	1.01	0.0	1.01	0.2	1.01	0.2	1.02	0.4	1.01	0.2	1.01	0.1	1.01	0.3
26	NR	L	0.10	0.09	0.11	1.00	0.0	1.04	0.8	1.03	0.6	1.05	1	1.04	0.8	1.04	0.7	1.03	0.6
27	LD	A	0.05	0.04	0.05	1.00	0.3	1.01	0	1.00	0	1.01	0	1.01	0	1.00	0	1.01	0.1
	NR	A	0.05	0.04	0.05	1.00	6.8	1.00	0	1.00	0	1.01	0	1.00	0.1	1.00	0	1.01	0.1
28	NR	A	0.07	0.05	0.06	1.00		1.01		1.01		1.01		1.01		1.01		1.01	
29	WT	L																	
	NR	L	0.14	0.13	0.15	1.06	0.9	1.05	1.2	1.04	0.9	1.06	1.5	1.05	1.1	1.04	0.9	1.04	1.4
30	NR	A																	
31	LD	A																	
	NR	A	0.14	0.11	0.14	1.14	0.9	1.05	0.8	1.04	0.7	1.07	1.2	1.05	0.8	1.04	0.6	1.06	1.2
32	WT	A	0.06	0.06	0.06	1.00	1.1	1.01	0.2	1.01	0.2	1.02	0.3	1.01	0.2	1.01	0.2	1.01	0.4
33	WT	A	0.08	0.07	0.07	1.00	0.5	1.02	0.5	1.02	0.6	1.03	0.7	1.02	0.6	1.02	0.5	1.02	1.3
	NR	A	0.08	0.06	0.07	1.00	1.2	1.03	0.7	1.02	0.5	1.02	0.6	1.03	0.8	1.02	0.7	1.02	0.8
34	NR	A	0.11	0.08	0.09	1.22	9.7	1.06	2	1.03	1	1.05	1.8	1.06	2.1	1.06	2	1.05	3.8
35	WT	A	0.09	0.08	0.09	1.02	0.0	1.03	1	1.03	0.9	1.04	1.1	1.04	1.1	1.04	1.1	1.03	1.8
	UP	A	0.08	0.07	0.08	1.00	0.0	1.03	0.8	1.03	0.8	1.03	0.9	1.03	0.8	1.03	0.9	1.03	1.5
36	LD	L	0.05	0.05	0.05	1.39	6.2	1.01	0.1	1.01	0.1	1.01	0.1	1.01	0.1	1.01	0.1	1.01	0.2
37	RD	A	0.08	0.07	0.08	1.00	1.4	1.02	0.5	1.02	0.4	1.03	0.8	1.02	0.6	1.02	0.5	1.03	1.7

	WT	A	0.08	0.08	0.08	1.02	0.0	1.03	1.0	1.03	0.9	1.04	1.2	1.04	1.1	1.03	1	1.04	1.7	0.07	0.06	0.07	1.01	2.5	1.02	0.4	1.02	0.3	1.02	0.7	1.02	0.5	1.02	0.4	1.02	1.4
	UP	A	0.07	0.07	0.07	1.00	0.0	1.02	0.6	1.02	0.6	1.03	0.9	1.02	0.7	1.02	0.6	1.03	0.9	0.06	0.06	0.07	1.00	0.0	1.01	0.2	1.01	0.2	1.02	0.5	1.01	0.2	1.01	0.2	1.02	1.2
	LD	A	0.06	0.06	0.06	1.01	0.0	1.02	0.5	1.02	0.5	1.03	0.8	1.02	0.5	1.02	0.4	1.03	2.2	0.05	0.05	0.06	1.02	0.9	1.01	0.1	1.01	0.1	1.02	0.3	1.01	0.1	1.01	0.1	1.02	0.9
	NR	A	0.07	0.07	0.07	1.02	0.0	1.02	0.7	1.02	0.6	1.03	0.9	1.01	0.2	1.02	0.6	1.03	0.2	0.06	0.05	0.06	1.02	0.0	1.01	0.2	1.01	0.1	1.02	0.4	1.01	0.2	1.01	0.2	1.02	0.9
38	LD	L	0.08	0.06	0.06	1.07	0.4	1.03	1.0	1.02	0.6	1.02	0.6	1.03	1	1.03	1	1.03	1.2	0.07	0.06	0.06	1.03	0.0	1.03	0.8	1.02	0.8	1.02	0.7	1.03	0.8	1.03	0.9	1.02	1.1
39	NR	L	0.06	0.06	0.06	1.00	3.9	1.02	0.5	1.02	0.5	1.02	0.6	1.02	0.5	1.02	0.4	1.02	0.7	0.08	0.08	0.08	1.00	1.3	1.03	0.7	1.03	0.7	1.03	0.9	1.03	0.8	1.02	0.6	1.03	1.4
40	LD	A	0.05	0.04	0.04	1.00	0.0	1.01	0.2	1.01	0.1	1.01	0.2	1.01	0.2	1.01	0.1	1.01	0.1	0.04	0.04	0.04	1.00	1.3	1.01	0.1	1.01	0	1.01	0.1	1.01	0.1	1.01	0	1.01	0.1
41	NR	A	0.08	0.07	0.07	1.01	0.0	1.04	1.2	1.04	1.1	1.04	1.3	1.04	1.3	1.03	0.9	1.03	1.8	0.04	0.04	0.04	1.02	0.7	1.01	0.2	1.01	0.1	1.01	0.3	1.01	0.2	1.01	0.1	1.01	0.4
42	NR	L	0.05	0.04	0.04	1.02	4.9	1.02	0.3	1.01	0.1	1.01	0.1	1.02	0.3	1.03	0.4	1.02	0.0	0.05	0.03	0.04	1.00	3.1	1.01	0.2	1.00	0	1.01	0.1	1.01	0.2	1.01	0.2	1.01	0.0
43	LD	A	0.08	0.07	0.07	1.02	0.0	1.03	0.7	1.02	0.6	1.03	0.9	1.03	0.8	1.02	0.5	1.02	0.3	0.08	0.07	0.08	1.04	0.0	1.03	0.8	1.02	0.5	1.03	0.8	1.03	0.8	1.02	0.6	1.02	0.6
	NR	A	0.08	0.07	0.08	1.03	0.0	1.03	0.9	1.03	0.8	1.03	1	1.03	0.9	1.02	0.6	1.02	0.4	0.08	0.08	0.09	1.03	1.1	1.02	0.5	1.02	0.5	1.03	0.8	1.02	0.6	1.02	0.4	1.02	0.6
44	WT	A	0.16	0.15	0.16	1.10	1.7	1.09	2.6	1.07	2.2	1.12	3.9	1.11	3.4	1.08	2.3	1.12	6.4	0.17	0.16	0.17	1.17	4.1	1.10	3	1.09	2.6	1.14	4.5	1.13	4.3	1.09	2.7	1.14	7.6
	NR	A	0.16	0.16	0.15	1.04	1.7	1.09	3.5	1.08	2.9	1.12	5	1.11	4.5	1.08	3.2	1.12	6.7	0.22	0.22	0.21	1.29	15.2	1.18	8.1	1.16	7	1.24	11.3	1.26	12	1.17	7.5	1.23	12.2
45	NR	A	0.19	0.14	0.15	1.34	1.6	1.17	3.5	1.12	2.4	1.14	2.9	1.18	3.7	1.17	3.5	1.14	1.4																	
46	L07	A	1.32	1.47	1.45	4.14	30.6	4.86		5.4		5.42		6.41		4.86		4.94	26.7	1.40	1.56	1.54	4.01	31.0	5.13		5.70		5.73		7.00		5.13		5.21	26.8
'B' Sites																																				
1	LP	A	0.21	0.16	0.17	1.06	0.0	1.12	3.8	1.12	3.5	1.18	6.1	1.16	5.3	1.12	3.8	1.06	3.4																	
2	LP	A	0.07	0.07	0.07	1.13	4.7	1.04	0.9	1.04	1.1	1.04	1	1.04	1	1.03	0.8	1.17	3.4																	
3	LP	A	0.16	0.19	0.17	1.03		1.29		1.37		1.33		1.29		1.29		1.2																		
5	LP	A	0.31	0.27	0.27	1.64	2.5	1.56	15.2	1.46	13.9	1.51	15	1.67	17.5	1.46	13.8	1.44	5.2																	
6	LP	A	0.07	0.06	0.07	1.01	0.0	1.03	0.7	1.02	0.5	1.03	0.7	1.03	0.8	1.02	0.4	1.02	0.2	0.07	0.06	0.07	1.01	0.6	1.03	0.6	1.02	0.5	1.03	0.6	1.03	0.7	1.02	0.4	1.02	0.2
7	LP	A	0.11	0.1	0.10	1.17	0.0	1.12	0.9	1.1	0.7	1.10	0.7	1.13	1	1.12	0.9	1.05	0.2																	
10	NR	A	0.11	0.08	0.08	1.00	2.5	1.13	2.0	1.08	1.8	1.08	1.8	1.13	2	1.09	1.9	1.04	0.3	0.12	0.09	0.10	1.03	0.0	1.07	1.9	1.04	1.2	1.05	1.4	1.07	1.9	1.05	1.5	1.03	0.5
11	LD	A	0.1	0.09	0.09	1.13	1.7	1.09	0.9	1.08	0.7	1.08	0.8	1.09	0.9	1.06	0.6	1.2	0.2																	
	NR	A	0.12	0.09	0.09	1.17	2.5	1.13	2.4	1.08	1.5	1.08	1.5	1.13	2.4	1.09	1.8	1.19	0.3																	
12	NR	A	0.13	0.12	0.12	1.06	1.7	1.17	1.3	1.15	1.1	1.15	1.1	1.2	1.3	1.1	0.9	1.1	1.0																	
13	NR	A	0.08	0.06	0.06	1.02	0.0	1.07	0.9	1.04	0.6	1.04	0.5	1.1	0.9	1.1	0.9	1.02	0.1																	
14	NR	A	0.14	0.11	0.12	1.14	3.4	1.11	3.7	1.08	2.8	1.10	3.5	1.1	3.8	1.1	3.2	1.25	1.1																	

Results for sites A6, A19, A22, B4, B8, B9, B30 omitted due to lack of strong motion data or system id. results of low reliability.

Values of $1/\sigma$ established from V_S values approrpriate for analysis methods 1 to 6

Earthquakes:

IMP = 1979 Imperial Valley
L07 = Lotung event LSST 07
CGA = 1983 Coalinga aftershock
WT = 1987 Whittier
LP = 1989 Loma Prieta
SM = 1991 Sierra Madre
LD = 1992 Landers
PT = 1992 Petrolia, PTA = aftershock
NR = 1994 Northridge

Schnabel (1973) for rock. The deconvolution was taken to the code-recommended profile depths of $1.5 \times r_2$ for rocking and $4 \times r_1$ for translations.

- *Method 3*: Same as Method 2, except the effective profile depth is taken as r_1 for rocking and translation (similar to the MV and MB procedures).
- *Method 4*: The code procedures are implemented as in Method 1, with the exception that the frequency dependence of the real part of the foundation impedance function is accounted for using the relations by Veletsos and Verbic (1973). In Method 1, it was assumed that the real part of the foundation impedance function was independent of frequency.
- *Method 5*: The code procedure is implemented as in Method 1, with the exception that the effective structure height (h) is taken as the distance from the base to the centroid of the inertia forces associated with the first mode (assuming triangular distribution of inertial force across height of structure, unless structure-specific data suggested otherwise). In the code procedure, h was taken as 70% of the total structural height.
- *Method 6*: MV procedures are used for shallow foundations ($e/r_1 < 0.5$) and MB procedures for deeper embedment ($e/r_2 > 0.5$). The predictions by Method 6 are identical to those shown in Fig. 5.16.

(c) *Results*

Deviations in Method 1 predictions of $\tilde{T}/T$ and $\tilde{\zeta}_0$ relative to "observed" values from the system identification are shown in Fig. 5.23 for all sites with acceptable and low confidence designations. Also plotted are best fit second order polynomials established from regression analyses on data from acceptable confidence sites. For most sites, the predictions are accurate to within absolute errors of about ±0.2 in $\tilde{T}/T$ and ±5% in $\tilde{\zeta}_0$. The regression curves indicate no significant systematic bias in predictions of $\tilde{T}/T$ or $\tilde{\zeta}_0$ for the range of $1/\sigma$ which is substantially represented in the database (about 0 to 0.2).

Small inertial interaction effects for long-period structures on stiff soil or rock (e.g. A21 and B6, $1/\sigma \approx 0.02$ to 0.03) are well predicted by the Method 1 analyses. Period lengthening and damping estimates for structures with intermediate $1/\sigma$ (about 0.1 to 0.2) can be significantly in error (e.g. A17, A45), but do not appear to be systematically biased. An exception is long-period structures (T > 2 sec.) on soft clay soils (e.g. A4, B3; $1/\sigma \approx 0.2$), for which period lengthening is consistently overpredicted.

Eight "high confidence" level sites in the database have $1/\sigma_1$ (based on Method 1 velocities) > 0.2: A1-tr, A10-tr, A12-tr, A24-L, A44-L, A46, B1 and B5. When normalized by $\tilde{T}/T$, errors in Method 1 period lengthening predictions for these sites were less than 20%. Damping was reasonably accurately predicted for A1, A10-tr, A12-tr, and A44-L, significantly overpredicted for A24-L, B1, and B5, and could not be evaluated for A46 (the $\tilde{T}/T$ is beyond the range of Fig. 5.22).

Best fit second order polynomials for the deviations between Method 1 through 5 predictions and the empirical data are presented in Fig. 5.24. It can be seen that when

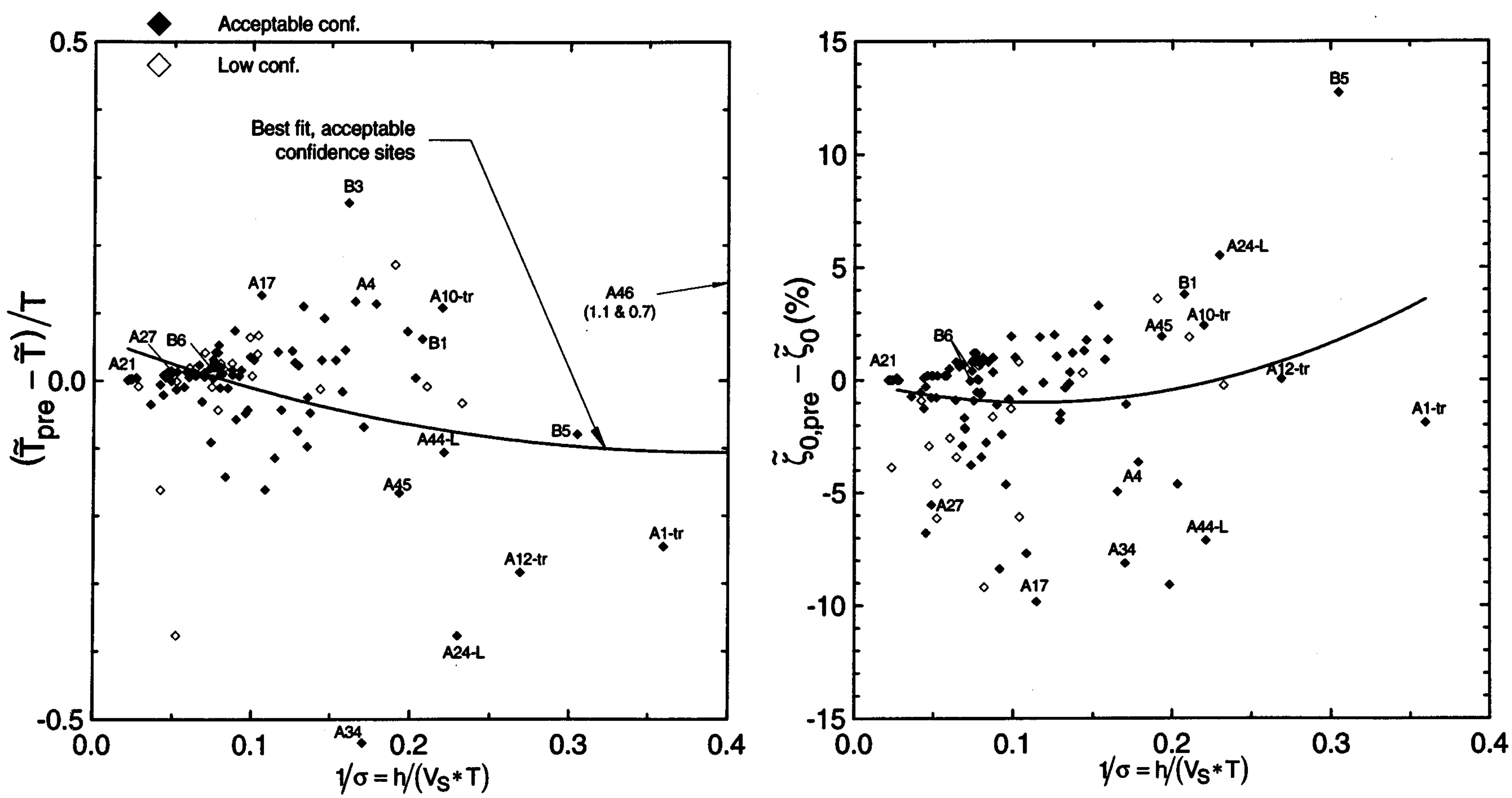

Fig. 5.23: Errors in Method 1 design procedure for sites sorted by confidence level

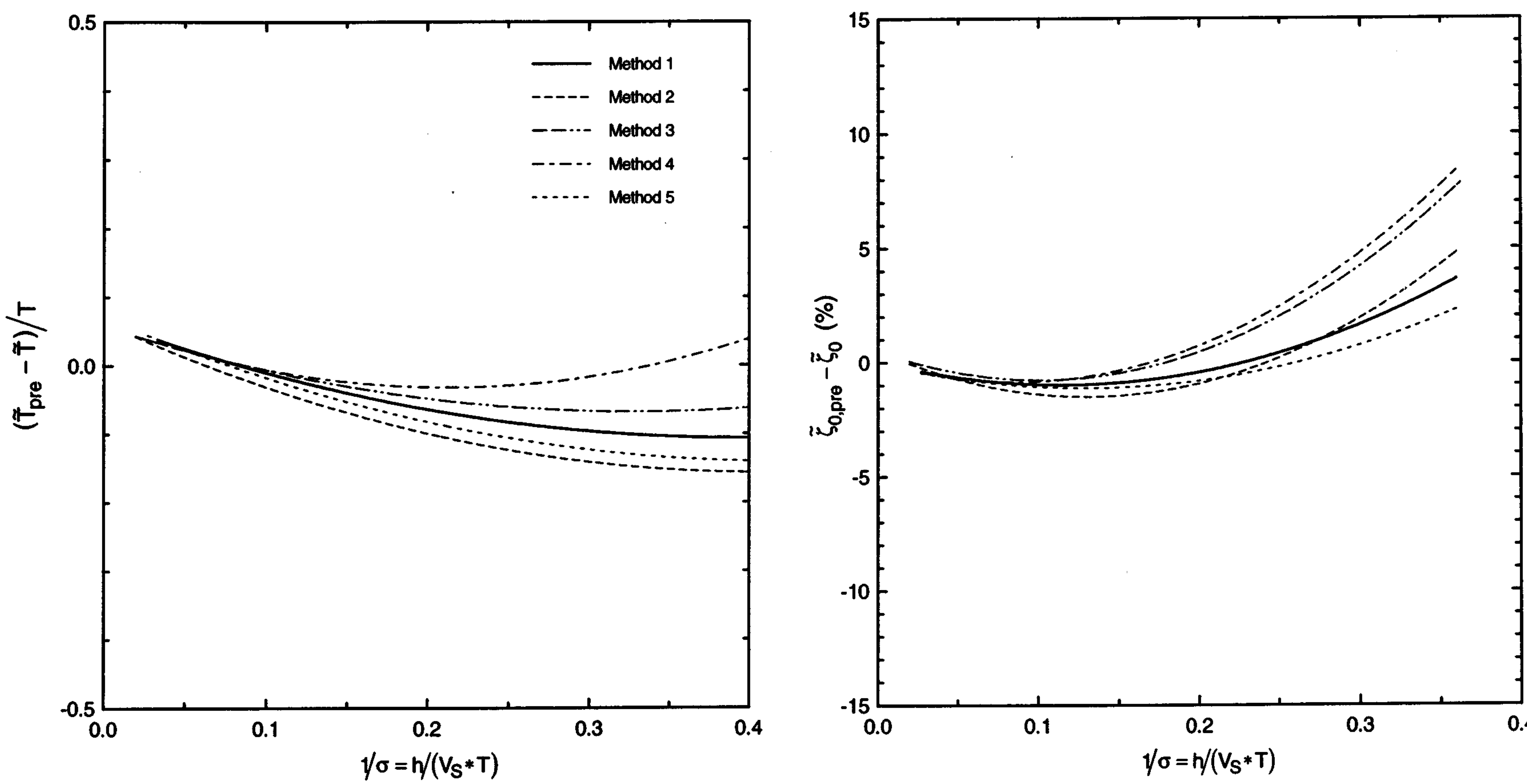

Fig. 5.24: Errors in predicted period lengthening ratios and foundation damping factors for design Methods 1 to 5

averaged over a large number of sites, the accuracy of period lengthening predictions by the different methods does not vary significantly. Damping is shown as being overpredicted at $1/\sigma > 0.2$ by each method, but this is primarily a product of consistent overprediction at site B5. Further insight into distinctions between methods can be gained through examination of results for six sites with $1/\sigma_6 > 0.2$ which experienced the most significant SSI [A1, A12, A24-L, A44-L, A46, and B5]:

- Of the four modifications to the Method 1 procedure, the use of frequency-dependent foundation stiffness with Method 4 generally had the most significant effect on $\tilde{T}/T$. This influence of frequency on impedance increases with structural stiffness, and is most pronounced at sites A1 and A46, which have high fundamental-mode, fixed-base frequencies ($f_1 > 6$ Hz). Inclusion of the frequency effect improved the predictions at each of the six sites except A46, where overpredictions of $\tilde{T}/T$ were increased.
- For all sites except A46, use of a shallower soil profile for calculating V_S (Method 3) improved the $\tilde{T}/T$ analysis results. These sites generally have only moderate increases in soil stiffness with depth, and hence the effect of profile depth is of modest importance.
- More precise definitions of soil modulus degradation (from deconvolution analysis, Method 2) or effective building height (Method 5) appear to only modestly affect average $\tilde{T}/T$ analysis results.

Deviations between Method 6 analysis results and the empirical data were presented in Fig. 5.16. Many of the general trends from Fig. 5.23 are also present in Fig. 5.16. The small SSI effects for structures with $1/\sigma < 0.1$ are well predicted by both methods. However, the more rational modeling of the soil-foundation-structure system in Method 6 can reduce prediction errors for structures with intermediate $1/\sigma$ (e.g. sites A17 and A45). Similarly, predictions for structures with large $1/\sigma$ were significantly improved in several cases (e.g. A1 for $\tilde{T}/T$; B5 for $\tilde{\zeta}_0$). Based on the findings from the analyses by Methods 2 to 5, the principal contributors to these improvements are incorporation of dynamic effects in analysis of the impedance function and evaluation of V_S across a shallower profile depth.

For several sites, large errors from Method 1 are also observed with Method 6 for reasons such as possible system identification errors associated with incoherent ground motions, poor geotechnical site characterization (A34), or the inadequacy of single-mode modeling procedures for long-period structures (A4, A27, B3).

It may also be noted that $\tilde{T}/T$ and $\tilde{\zeta}_0$ for site A46 were accurately estimated by Method 6 (no analysis was possible by Method 1). The foundation at site A46 is relatively deeply embedded ($e/r_u = 0.92$), and inclusion of embedment effects in the analysis of the impedance function is critical to obtaining reasonable estimates of $\tilde{\zeta}_0$.

CHAPTER 6

SUMMARY AND CONCLUSIONS

6.1 Scope of Research

A wealth of strong motion data has become available over the last decade from sites with instrumented structures and free-field accelerographs which has provided an opportunity to evaluate empirically the effects of soil-structure interaction (SSI) on the seismic response of structures. Prior to the availability of this data, insights into inertial and kinematic interaction processes were generally drawn only from analytical studies or low-amplitude forced and ambient vibration testing. While these studies were helpful in establishing the framework within which SSI analyses are performed, the paucity of strong motion data has contributed to the widely held belief among practicing engineers that SSI effects are unimportant and that to ignore them is conservative.

In this study, strong motion data were used in system identification analyses to quantify the effects of SSI on modal parameters of structures and the motions which occur at the base of structures. From these results, the conditions under which SSI effects are significant were determined, and the reliability of simplified analytical techniques intended to predict these effects was evaluated.

Simplified analytical methodologies to predict inertial interaction effects such as period lengthening ratio ($\tilde{T} / T$) and soil/foundation damping factor ($\tilde{\zeta}_0$) have been available for over twenty years (e.g. Veletsos and Nair, 1975, Bielak, 1975, Jennings and Bielak, 1973). These formulations are for a single degree-of-freedom structure with a rigid circular foundation resting on (Veletsos and Nair), or embedded into (Bielak), a uniform visco-elastic halfspace. Design code provisions by the Applied Technology Council (ATC, 1978) and National Earthquake Hazards Reduction Program (NEHRP) (BSSC, 1997) are based on an adaptation of the approach by Veletsos and Nair. To apply these procedures to structures in this study, guidelines were developed for modeling within these simplified frameworks "realistic" conditions such as nonuniform soil profiles, embedded structures, and foundations which are non-circular in shape or non-rigid. The guidelines and models were combined to form unified analytical procedures termed the "modified Veletsos" (MV) and "modified Bielak" (MB) methodologies. The principle difference between the two is that the MB methodology is expected to simulate more accurately embedment effects such as dynamic basement wall-soil interaction.

The analysis of recorded data was performed using system identification techniques. By repeating the analyses for a given site with different output/input data pairs, it was possible to determine modal parameters for different conditions of base fixity. What was sought for each site were first-mode periods and damping ratios for the flexible-base case (which includes SSI effects) and a fictional fixed-base case in which SSI effects are "removed" and the results reflect only the flexibility of the structure. With the limited instrumentation available at many sites, it was not always possible to evaluate directly one set of either the fixed- or the flexible-base parameters. For these situations, it was necessary to consider a third condition of base fixity (pseudo flexible-base) which incorporates the effects of structural deformations and base rocking, but not relative foundation/free-field translations, into the overall system flexibility. Using the pseudo flexible-base parameters in conjunction with either the fixed- or flexible-base parameters (whichever was available), the unknown set of modal parameters could be estimated using analytical techniques developed as part of this research.

For each of the 58 sites considered in this study, system identification analyses and related parameter estimation procedures were performed to evaluate the fixed- and flexible-base modal parameters. To aide in the interpretation of these results, data on structural and geotechnical conditions at each site were compiled such as foundation radii, effective structure height, type of lateral force resisting system, soil stratigraphy and type, and shear wave velocity profiles. Using these data, $\tilde{T}/T$ and $\tilde{\zeta}_0$ values at the sites were evaluated as functions of various factors including structure-to-soil stiffness ratio, structure type and aspect ratio, foundation type and embedment ratio, and the amplitude of ground motion. These empirical results were then compared to predictions from the MV and MB methodologies, as well as more simplified code-based procedures, to evaluate the accuracy of these analytical formulations. Collectively, these empirical and analytical results provided significant insights into inertial interaction phenomena.

6.2 Research Findings and Recommendations

Inertial interaction effects for buildings can be expressed in terms of the lengthening of first-mode period ($\tilde{T}/T$) and the damping associated with soil-foundation interaction ($\tilde{\zeta}_0$). The motivation for characterizing these effects is that they can be used to estimate flexible-base vibration parameters ($\tilde{T}, \tilde{\zeta}$), which in turn are used in response spectrum-based approaches for evaluating design-level seismic base shear forces and deformations in structures. As shown in Fig. 6.1, whether SSI increases or decreases the base shear force is a function of the period lengthening, the change in damping between the fixed- and flexible-base cases, and the shape of the design spectra.

Kinematic interaction effects were interpreted in an approximate manner from variations between free-field and foundation-level ground motion indices, although both inertial and kinematic interaction were found to affect foundation motions.

6.2.1 Interaction Effects as Quantified from Foundation/Free-Field Ground Motion Indices

Available strong motion data suggests that foundation-level and free-field spectral accelerations at the period of principal interest in structural design (i.e. the first-mode flexible-base period, $\tilde{T}$) are similar for structures with surface foundations, and that foundation-level spectral accelerations are generally only modestly de-amplified (averaging about 20%) for embedded foundations. Since the free-field and foundation level ground motions therefore appeared to be comparable for most of the structures in this study, the focus of this research was primarily on evaluating the effects of inertial interaction on structural response.

6.2.2 Inertial Interaction Effects as Quantified by Variations between Fixed- and Flexible-Base First-Mode Parameters

The factor found to exert the greatest influence on $\tilde{T}/T$ and $\tilde{\zeta}_0$ was the ratio of structure-to-soil stiffness as quantified by the parameter $1/\sigma = h/(V_S \cdot T)$. When $1/\sigma$ was nearly zero, $\tilde{T}/T$ and $\tilde{\zeta}_0$ values were about unity and zero, respectively, whereas at the

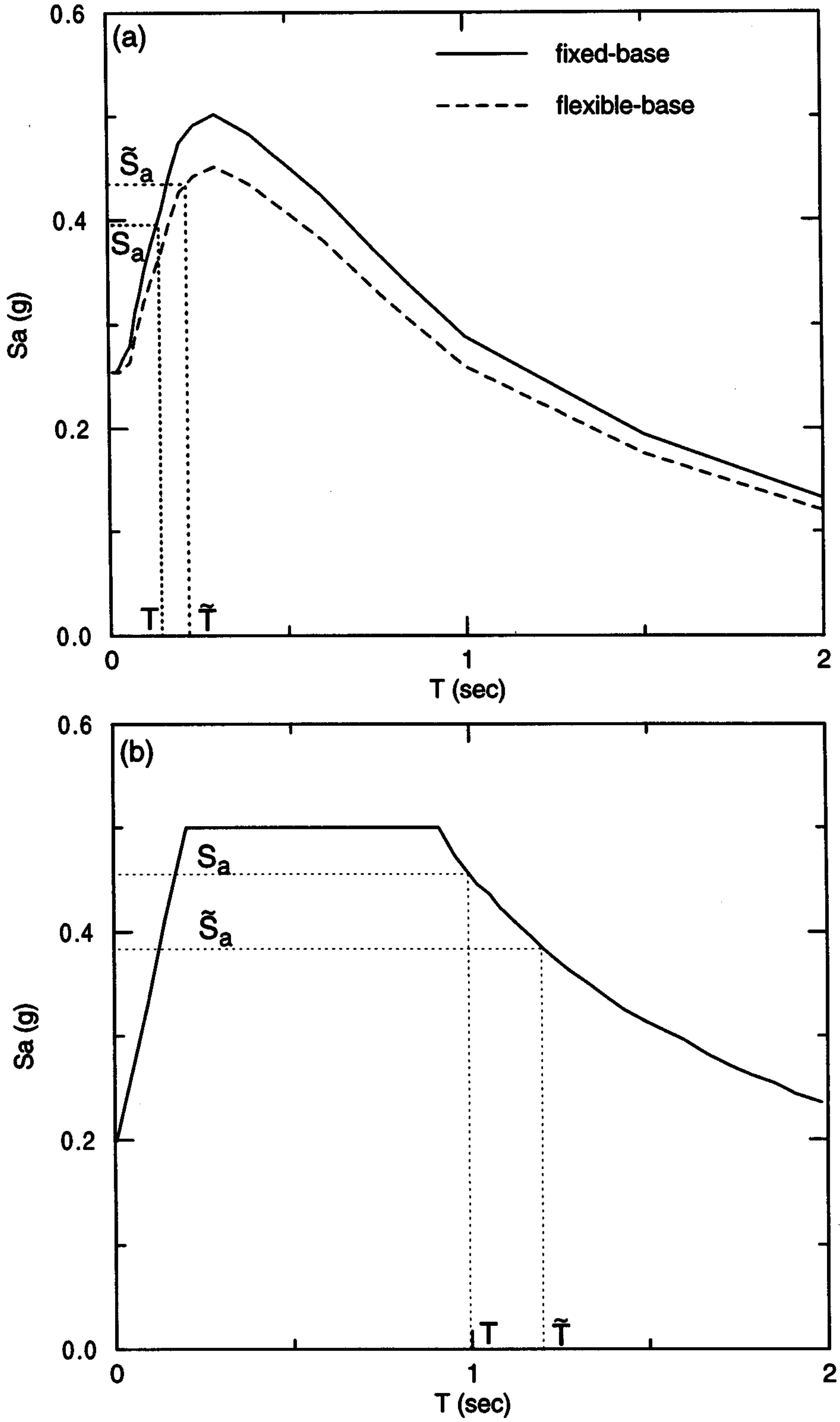

Fig. 6.1: (a) Example of increased spectral acceleration resulting from consideration of inertial interaction effects with smoothed site-specific spectra, and (b) example of reduced spectral acceleration resulting from consideration of inertial interaction effects with code-based spectra with no damping correction

maximum observed value of $1/\sigma = 1.5$ at site A46, interaction effects dominated the structural response ($\tilde{T}/T \approx 4$ and $\tilde{\zeta}_0 \approx 30\%$). Additional factors of secondary importance which affect the inertial interaction process include:

1. *Structure aspect ratio (h/r_2).* The data indicate an increase in period lengthening and a decrease in foundation damping factor with increasing h/r_2. These effects are adequately captured by the analysis procedures.
2. *Foundation embedment*. No significant differences are observed between $\tilde{T}/T$ and $\tilde{\zeta}_0$ values for surface and shallowly embedded structures ($e/r < 0.5$). However, more deeply embedded structures can have significant additional damping as a result of dynamic soil/basement-wall interaction. The MV predictive analyses are sufficiently accurate for surface and shallowly embedded structures ($e/r < 0.5$), whereas the MB approach provides superior results for cases of deeper embedment.
3. *Foundation type*. No significant differences are observed between $\tilde{T}/T$ or $\tilde{\zeta}_0$ values for structures with deep foundations (piles and piers) and shallow foundations (footings, grade beams, or mats). Further, the accuracy of predicted $\tilde{T}/T$ or $\tilde{\zeta}_0$ values by the MV or MB methodologies (which assume shallow foundations) is on average equally good for both foundation types. However, these results from deep foundation sites are strongly influenced by a large number of sites with fairly stiff surficial soils ($V_S > 500$ fps) and no marked increase in soil stiffness across the depth of the foundation elements. For such cases, the dynamic foundation behavior appears to be dominated by the interaction of near-surface foundation elements with soil. For a limited number of cases where piles pass through soft surficial soils and bottom out

in stiffer underlying materials, there is pronounced additional damping in the system that may be associated with radiation damping from soil-pile interaction. This damping is not captured by the MV or MB procedures.

4. *Foundation shape effects*. Non-circular foundation shapes can have a higher level of radiation damping in the rocking mode than circular foundations with equivalent moment of inertia. However, this was generally a small effect (absolute difference of < 0.5% damping) for the structures considered in this study.
5. *Foundation flexibility effects*. Based on analyses from a single site (B2), it appears that continuous flexible foundations supporting a stiff central core of shear walls and gravity loading bearing columns outside the core can exhibit a marked decrease in rocking stiffness relative to a rigid foundation. Foundation damping in the rocking mode is not similarly decreased in the case history, although a decrease is predicted by theoretical studies by Iguchi and Luco (1982) for a flexible foundation loaded only through a central core.
6. *Structure type*. The effect of the type of lateral force resisting system appears to be adequately captured by the ratio of fixed-base structural period to height that is incorporated into the $1/\sigma$ parameter. However, the period lengthening is surprisingly small in several tall, long-period structures ($T > 2$ sec.) founded on soft soils, which may result from significant higher-mode responses in these buildings.

SSI design provisions in the BSSC (1997) and ATC (1978) codes are able to capture gross increases in period lengthening ratio and foundation damping factor with increasing $1/\sigma$, but generally these procedures replicate the observed SSI effects less accurately than the MV or MB procedures. These errors appear to be associated with several simplifying assumptions made in the development of the code provisions. In particular, neglecting of the frequency-dependence of the real part of the foundation impedance function leads to significant errors for high frequency structures. Further, the response of deeply embedded foundations is poorly modeled by the rigid disk on halfspace foundation model. Finally, the code-prescribed profile depths of $1.5r_2$ and $4.0r_1$ do not appear to improve estimates of effective soil shear stiffness for analyses of foundation impedance functions relative to the r_1 depth employed in the MV and MB procedures.

6.2.3 Recommendations and Considerations for Design

As previously noted, the key SSI effects for an engineering design are the period lengthening ratio ($\tilde{T}/T$) and foundation damping factor ($\tilde{\zeta}_0$). The foundation damping factor is combined with the fixed-base damping and period lengthening as per Eq. 2.11 to evaluate the flexible-base damping ratio. Based on this study, it appears that these inertial interaction effects can generally be reliably predicted by the MV methodology for many types of buildings (including base-isolated buildings). However, several caveats to this basic recommendation are appropriate:

1. Inertial interaction effects were generally observed to be small for $1/\sigma < 0.1$ (i.e. $\tilde{T}/T < 1.1$ and $\tilde{\zeta}_0 < 4\%$), and for practical purposes could be neglected in such cases.
2. For structures with foundations having embedment ratios greater than 0.5, the MB methodology should be used in lieu of MV to appropriately model the extra damping contributed by dynamic soil/basement-wall interaction.

3. Damping results for pile supported structures on relatively soft foundation soils (V_S < 500 fps) should be interpreted with caution, as the damping is likely to exceed the values predicted from simplified analyses (which assume shallow foundations) due to soil-pile interaction effects.
4. Period lengthening for tall (T > 2 sec.) structures with significant higher-mode responses should be neglected.
5. Corrections to rocking damping values for foundation shape effects are generally small and can be neglected without introducing significant errors.

Kinematic interaction effects are often neglected in SSI analyses for earthquake loading conditions. Additional study of free-field and foundation-level ground motions is needed to evaluate the potential significance of these effects.

REFERENCES

Abrahamson, N.A. (1988). “Empirical models of spatial coherency of strong ground motion,” *Proc. 2nd Workshop on Strong Motion Arrays*, Institute of Earth Sciences, Taipei, Taiwan, 65-92.

Abrahamson, N.A. (1992). “Spatial variation of earthquake ground motion for application to soil-structure interaction,” *Rpt. No. EPRI TR-100463*, Electrical Power Research Institute, Palo Alto, CA, March.

Abrahamson, N.A., Schneider, J.F., and Stepp, J.C. (1991). “Empirical spatial coherency functions for application to soil-structure interaction analyses,” *Earthquake Spectra*, EERI, 7(1), 1-27.

Applied Technology Council (1978). “Tentative provisions for the development of seismic regulations for buildings: a cooperative effort with the design profession, building code interests, and the research community,” *Rpt. No. ATC 3-06*, U.S. Dept. of Commerce, National Bur. of Standards, Washington DC.

Apsel, R.J. and Luco, J.E. (1987). “Impedance functions for foundations embedded in a layered medium: an integral equation approach,” *J. Earthquake Engrg. Struct. Dynamics*, 15(2), 213-231.

Ashford, S.A. and Sitar, N. (1994). "Seismic Response of Steep Natural Slopes," *Rpt. No. UCB/EERC-94/05*, Earthquake Engrg. Research Ctr., Univ. of California, Berkeley, May.

Åström, K.J. and Wittenmark B. (1984). *Computer Controlled Systems*, Prentice-Hall, Englewood Cliffs, NJ.

Aviles, J. and Perez-Rocha, L.E. (1996). “Evaluation of interaction effects on the system period and the system damping due to foundation embedment and layer depth,” *Soil Dynamics and Earthquake Engrg.*, 15(1), 11-27.

Bard, P.-Y., Gueguen, P., and Wirgin, A. (1996). “A note on the seismic wavefield radiated from large building structures into soft soils,” *Proc. 11th World Conf. Earthquake Engrg.*, Paper No. 1838.

Bechtel Power Corporation (1991). “A synthesis of predictions and correlation studies of the Lotung soil-structure interaction experiment,” *Rpt. No. EPRI NP-7307-M*, Electrical Power Research Institute, Palo Alto, CA, October.

Bielak, J. (1975). “Dynamic behavior of structures with embedded foundations,” *J. Earthquake Engrg. Struct. Dynamics*, 3(3), 259-274.

Borcherdt, R.D. (1994). "Estimates of site dependent response spectra for design (methodology and justification)," *Earthquake Spectra*, EERI, 10(4), 617-653.

Borja, R.I., Smith, H.A., Wu, W-H., and Amies, A.P. (1992). "A methodology for nonlinear soil-structure interaction effects using time-domain analysis techniques," *Rpt. No. 101*, Blume Earthquake Engrg. Ctr., Stanford Univ., June.

Building Seismic Safety Council, BSSC (1997). "NEHRP Recommended provisions for seismic regulations for new buildings, Part 1, Provisions and Part 2, Commentary" *Rpt. No. FEMA 302 & 303*, Federal Emergency Management Agency, Washington D.C.

Celebi, M. (1995). "Free-field motions near buildings," *Proc. 10th European Conf. Earthquake Engrg.*, 215-221.

Chang, C.-Y., Power, M.S., Idriss, I.M., Somerville, P.G., Silva, W., and Chen, P.C. (1985). "Engineering characterization of ground motion. Task 2: Observational data on spatial variations of earthquake ground motion," *Rpt. No. NUREG/CR-3805*, U.S. Nuclear Regulatory Commission, Washington DC, February.

Chen, J-C., Lysmer, J., and Seed, H.B. (1981). "Analysis of local variations in free-field seismic ground motions," *Rpt. No. UCB/EERC 81-03*, Earthquake Engrg. Research Ctr., Univ. of California, Berkeley.

Chopra, A.K. and Gutierrez, J.A. (1973). "Earthquake analysis of multistory buildings including foundation interaction," *Rpt. No. EERC 73-13*, Earthquake Engrg. Research Ctr., Univ. of California, Berkeley.

Clough, R.W. and Penzien, J. (1993). *Dynamics of Structures*, 2nd ed., McGraw Hill, New York, NY.

Crouse, C.B., Hushmand, B., Luco, J.E., and Wong, H.L. (1990). "Foundation impedance functions: theory versus experiment," *J. Geotech. Engrg.*, ASCE, 116(3), 432-449.

Day, S.M. (1977). "Finite element analysis of seismic scattering problems," *Ph.D. Dissertation*, Univ. of California, San Diego.

Dobry, R. and Gazetas, G (1986). "Dynamic response of arbitrarily shaped foundations," *J. Geotech. Engrg.*, ASCE, 112(2), 109-135.

Elsabee, F. and Morray, J.P. (1977). "Dynamic behavior of embedded foundations," *Rpt. No. R77-33*, Dept. of Civil Engrg., MIT, Cambridge, Mass.

Fenves, G.L. and DesRoches, R. (1994). "Response of the northwest connector in the Landers and Big Bear Earthquakes," *Rpt No. UCB/EERC-94/12*, Earthquake Engrg Research Ctr., Univ. of California, Berkeley.

Fenves, G.L. and Serino, G. (1992). "Evaluation of soil-structure interaction in buildings during earthquakes," *Data Utilization Rpt. CSMIP/92-01*, California Strong Motion Instrumentation Program, Sacramento, CA, June.

Franklin, G.F. and Powell, J.D. (1980). *Digital Control of Dynamic Systems*, Addison-Wiley, Reading, MA.

Fumal, T.E., Gibbs, J.F., and Roth, E.F. (1982). "In-situ measurements of seismic velocity at 22 locations in the Los Angeles, California Region," *Open File Rpt. 82-833,* U.S. Geological Survey, Menlo Park, CA.

Ganev, T., Yamazaki, F., and Katayama, T. (1994). "Soil-structure interaction of a reinforced concrete tower based on earthquake and microtremor observations," *5th U.S. National Conf. on Earthquake Engrg.*, Vol. 4, 35-44.

Geomatrix Consultants (1991). "Analysis of ground response data at Lotung large-scale soil-structure interaction experiment site," *Rpt. No. EPRI NP-7306-M*, Electrical Power Research Institute, Palo Alto, CA, December.

Ghanem, R.G., Gavin, H., and Shinozuka, M. (1991). "Experimental verification of a number of structural system identification algorithms," *Rpt. No. NCEER-91-0024*, National Ctr. for Earthquake Engrg. Research, State Univ. of New York, Buffalo.

Gohl, W.B. (1993). "Response of pile foundations to earthquake shaking - general aspects of behavior and design methodologies," *Seismic soil/struct. interaction seminar*, Vancouver, Canada.

Hanada, K., Iwatate, T., Sawada, Y., and Ezure, H. (1988). "Soil-structure interaction of 'JPDR' based on earthquake observations and forced vibration tests," *Nuclear Engrg. and Design*, 105(2), 173-183.

Iguchi, M. and Luco, J.E. (1982). "Vibration of flexible plate on viscoelastic medium," *J. Engrg. Mech.*, ASCE, 108(6), 1103-1120.

International Conference of Building Officials, ICBO (1997). *Uniform Building Code, 1997 Edition*.

Ishii, K., Itoh, T., and Suhara, J. (1984). "Kinematic interaction of soil-structure system based on observed data," *Proc. 8th World Conf. Earthquake Engrg.*, Vol. 3, 1017-1024.

Jennings, P.C. (1970). "Distant motions from a building vibration test," *Bull. Seism. Soc. Am.*, 60(6), 2037-2043.

Jennings, P.C. and Bielak, J. (1973). "Dynamics of building-soil interaction," *Bull. Seism. Soc. Am.*, 63, 9-48.

Johnson, J.J. and Asfura, A.P. (1993). "Soil-structure interaction: observations, data, and correlative analysis," *in* Developments in Dynamic Soil-Structure Interaction, P. Gülkan and R.W. Clough, eds., Kluwer Academic Publishers, 219-258.

Kausel, E. (1974). "Forced vibrations of circular foundations on layered media," *Rpt. No. R74-11*, Dept. of Civil Engrg., MIT, Cambridge, Mass.

Kobori, T. and Shinozaki, Y. (1982). "Ground motion of surface and subsurface irregular site excited by forced vibration generator," *J. Seism. Soc. Japan*, 35(2), 259-281 (in Japanese).

Krauss, T.P., Shure, L., and Little, J.N. (1994). *Signal Processing Toolbox, Users Guide*, The Math Works, Inc., Natick, Mass.

Lin, A.N. and Jennings, P.C. (1984). "Effect of embedment on foundation-soil impedances," *J. Engrg. Mech.*, ASCE, 110(7), 1060-1075.

Liou, G.-S. and Huang, P.-H. (1994). "Effect of flexibility on impedance functions for circular foundations," *J. Engrg. Mech.*, ASCE, 120(7), 1429-1446.

Ljung, L. (1987). *System Identification: Theory for the User*, Prentice Hall, Englewood Cliffs, NJ.

Ljung, L. (1995). *System Identification Toolbox, Users Guide*, The Math Works, Inc., Natick, Mass.

Luco, J.E. (1980a). "Soil-structure interaction and identification of structural models," *Proc. 2nd ASCE Conf. on Civil Engrg. and Nuclear Power*, Vol. 2, 10/1/1-10/1/31.

Luco, J.E. (1980b). "Linear soil-structure interaction," *in Soil-structure interaction: The status of current analysis methods and research*, J.J. Johnson, ed., Rpt. No. NUREG/CR-1780 and UCRL-53011, U.S. Nuclear Regulatory Com., Washington DC and Lawrence Livermore Lab., Livermore, CA

Luco, J.E. and Mita, A. (1987). "Response of circular foundation to spatially random ground motions," *J. Engrg. Mech.*, ASCE, 113(1), 1-15.

Luco, J.E. and Westmann, R.A. (1971). "Dynamic response of circular footings," *J. Engrg. Mech.*, ASCE, 97(5), 1381-1395.

Luco, J.E. and Wong, H.L. (1986). "Response of a rigid foundation to a spatially random ground motion," *J. Earthquake Engrg. Struct. Dynamics*, 14(6), 891-908.

Lysmer, J., Tabatabaie-Raissi, M., Tajirian, F., Vahdani, S., and Ostadan, F. (1981). "SASSI: A system for analysis of soil-structure interaction", *Rpt. No. UCB/GT-81/02*, Geotech. Engrg., Univ. of California, Berkeley, April.

Lysmer, J., Udaka, T., Tsai, C-F., and Seed, H.B. (1975). "FLUSH - A computer program for approximate 3-D analysis of soil structure interaction problems", *Rpt. No. UCB/EERC-75/30*, Earthquake Engrg. Research Ctr., Univ. of California, Berkeley.

Mita, A. and Luco, J.E. (1989). "Dynamic response of a square foundation embedded in an elastic halfspace," *Soil Dynamics and Earthquake Engrg.*, 8(2), 54-67.

Novak, M. (1987). discussion on "Stochastic variation of earthquake ground motion in space and time," by R.S. Harichandran and E. Vanmarcke, *J. Engrg. Mech.*, ASCE, 112 (4), 1267-1270.

Novak, M. (1991). "Piles under dynamic loads," *Proc. 2nd Int. Conf. on Recent Advances in Geotech. Engrg. and Soil Dynamics*, St. Louis, MO, 2433-2456.

Oppenheim, A.V. and Schafer, R.W. (1989). *Discrete-Time Signal Processing*, Prentice Hall, Englewood Cliffs, NJ.

Pandit, S.M. (1991). *Modal and Spectrum Analysis*, John Wiley, New York, NY.

Poland, C.D., Soulages, J.R., Sun, J., and Mejia, L.H. (1994). "Quantifying the effect of soil-structure interaction for use in building design", Rpt. to Offc. of Strong Motion Studies, Div. of Mines and Geology, California Dept. of Conservation, Sacramento, CA, May.

Priestly, M.B. (1980). "State dependent models: a general approach to nonlinear time series analysis," *Time Series Analysis*, 1(1), 47-73.

Riggs, H.R. and Waas, G. (1985). "Influence of foundation flexibility on soil-structure interaction," *J. Earthquake Engrg. Struct. Dynamics*, 13(5), 597-615.

Roesset, J.M. (1980). "A review of soil-structure interaction," in *Soil-structure interaction: The status of current analysis methods and research*, J.J. Johnson, ed., Rpt. No. NUREG/CR-1780 and UCRL-53011, U.S. Nuclear Regulatory Com., Washington DC, and Lawrence Livermore Lab., Livermore, CA.

Safak, E. (1988). "Analysis of recordings in structural engineering: adaptive filtering, prediction, and control," *Open File Rpt. 88-647*, U.S. Geological Survey, Menlo Park, CA.

Safak, E. (1991). "Identification of linear structures using discrete-time filters," *J. Struct. Engrg.*, ASCE, 117(10), 3064-3085.

Schnabel, P.B., Lysmer, J., and Seed, H.B. (1972). "SHAKE: A Computer Program for Earthquake Response Analysis of Horizontally Layered Soil Deposits", *Rpt. No. UCB/EERC-72/12*, Earthquake Engrg. Research Ctr., Univ. of California; 1991 modifications by Idriss, I.M. and Sun, J.I.

Schneider, J.F., Abrahamson, N.A., Somerville, P.G., and Stepp, J.C. (1990). "Spatial variation of ground motion from EPRI's dense accelerograph array at Parkfield, California," *Proc. 4th U.S. National Conf. Earthquake Engrg.*, EERI, Vol. 1, 375-384.

Seed, H.B. and Lysmer, J. (1980). "The seismic soil-structure interaction problem for nuclear facilities," *in* Soil-structure interaction: the status of current analysis methods and research, J.J. Johnson, ed., *Rpt. No. NUREG/CR-1780 and UCRL-53011*, U.S. Nuclear Regulatory Com., Washington DC and Lawrence Livermore Lab., Livermore, CA.

Seed, H.B., Romo, M.P., Sun, J.I., Jaime, A., and Lysmer, J. (1988). "The Mexico Earthquake of September 19, 1985 - relationships between soil conditions and earthquake ground motions," *Earthquake Spectra*, EERI, 4(4), 687-729.

Seed, R.B., Dickenson, S.E., and Mok, C.M. (1992). "Recent lessons regarding seismic response analyses of soft and deep clay sites," *Proc. Seminar on Seismic Design and Retrofit of Bridges*, Earthquake Engrg. Research Ctr., Univ. of California, Berkeley and Div. of Structures, California Dept. of Transportation, 18-39.

Seed, R.B., Dickenson, S.E., Riemer, M.F., Bray, J.D., Sitar, N., Mitchell, J.K., Idriss, I.M., Kayen, R.E., Kropp, A.K., Harder, L.F. Jr., and Power, M.S. (1990). "Preliminary report on the principal geotechnical aspects of the October 17, 1989 Loma Prieta Earthquake", *Rpt. No. UCB/EERC-90/05*, Earthquake Engrg. Research Ctr., Univ. of California, Berkeley.

Smith, S.W., Ehrenberg, J.E., and Hernandez, E.N. (1982). "Analysis of the El Centro differential array for the 1979 Imperial Valley Earthquake," *Bull. Seism. Soc. Am.*, 72(1), 237-258.

Somerville, P.G., McLaren, J.P., Sen, M.K., and Helmberger, D.V. (1991). "The influence of site conditions on the spatial incoherence of ground motions," *Struct. Safety*, 10(1-3), 1-13.

Stewart, J.P. and Stewart, A.F. (1997). "Analysis of soil-structure interaction effects on building response from earthquake strong motion recordings at 58 sites," *Rpt. No. UCB/EERC-97/01*, Earthquake Engrg. Research Ctr., Univ. of California, Berkeley.

Trifunac, M.D. (1972). "Interaction of a shear wall with the soil for incident plane SH waves," *Bull. Seism. Soc. Am.*, 62(1), 63-83.

Valera, J.E., Seed, H.B., Tsai, C.F., and Lysmer, J. (1977). "Seismic soil-structure interaction effects at Humboldt Bay Power Plant," *J. Geotech. Engrg.*, ASCE, 103(10), 1143-1161.

Veletsos, A.S. (1977). "Dynamics of structure-foundation systems," *Structural and Geotechnical Mechanics*, Prentice-Hall, Inc., Englewood Cliffs, N.J., 333-361.

Veletsos, A.S. and Meek, J.W. (1974). "Dynamic behavior of building-foundation systems," *J. Earthquake Engrg. Struct. Dynamics*, 3(2), 121-138.

Veletsos, A.S. and Nair V.V. (1975). "Seismic interaction of structures on hysteretic foundations," *J. Struct. Engrg.*, ASCE 101(1), 109-129.

Veletsos, A.S. and Prasad, A.M. (1989). "Seismic interaction of structures and soils: stochastic approach," *J. Struct. Engrg.*, ASCE, 115(4), 935-956.

Veletsos, A.S., Prasad, A.M., and Wu, W.H. (1997). "Transfer functions for rigid rectangular foundations," *J. Earthquake Engrg. Struct. Dynamics*, 26 (1), 5-17.

Veletsos, A.S. and Verbic, B. (1973). "Vibration of viscoelastic foundations," *J. Earthquake Engrg. Struct. Dynamics*, 2(1), 87-102.

Veletsos, A.S. and Wei, Y.T. (1971). "Lateral and rocking vibrations of footings," *J. Soil Mech. and Foundations Div.*, ASCE, 97(9), 1227-1248.

Wallace, J.W. and Moehle, J.P. (1990). "Evaluation of ATC requirements for soil-structure interaction using data from the 3 March 1985 Chile Earthquake," *Earthquake Spectra*, EERI, 6(3), 593-611.

Weidlinger Associates (1978). "Nonlinear soil-structure interaction," *Rpt. No. EPRI NP-945*, Electrical Power Research Institute, Palo Alto, CA, December.

Welch, P.D. (1967). "The use of Fast Fourier Transform for the estimation of power spectra: a method based on time averaging over short, modified periodograms," *Transactions on Audio and Electroacoustics*, IEEE, AU-15(2), 70-73.

Wirgin, A. and Bard, P.-Y. (1996). "Effects of buildings on the duration and amplitude of ground motion in Mexico City," *Bull. Seism. Soc. Am.*, 86(3), 914-920.

Wong, H.L., Trifunac, M.D., and Luco, J.E. (1988). "A comparison of soil-structure interaction calculations with results of full-scale forced vibration tests," *Soil Dynamics and Earthquake Engrg.*, 7(1), 22-31.